AD_____

Award Number: W81XWH-12-2-0013

TITLE: Locomotion With Loads: Practical Techniques for Predicting Performance Outcomes

PRINCIPAL INVESTIGATOR: Peter Weyand

CONTRACTING ORGANIZATION: Southern Methodist University

Dallas, TX 75205

REPORT DATE: July 2019

TYPE OF REPORT: Final

PREPARED FOR: U.S. Army Medical Research and Materiel Command
Fort Detrick, Maryland 21702-5012

DISTRIBUTION STATEMENT: Approved for Public Release; Distribution Unlimited

REPORT DOCUMENTATION PAGE

Form Approved
OMB No. 0704-0188

1. REPORT DATE	**2. REPORT TYPE**	**3. DATES COVERED**
July 2019	Final	5 Apr 2012 - 14 Apr 2019

4. TITLE AND SUBTITLE
Locomotion with loads: practical techniques for predicting performance outcomes

5a. CONTRACT NUMBER
W81XWH-12-2-0013

5b. GRANT NUMBER
W81XWH-12-2-0013

5c. PROGRAM ELEMENT NUMBER

6. AUTHOR(S)

Peter Weyand

E-Mail: pweyand@smu.edu

5d. PROJECT NUMBER

5e. TASK NUMBER

5f. WORK UNIT NUMBER

7. PERFORMING ORGANIZATION NAME(S) AND ADDRESS(ES)

Southern Methodist University, Office of Research Administration, 6425 Boaz Lane, Suite 103, Dallas, TX 75205

8. PERFORMING ORGANIZATION REPORT NUMBER

9. SPONSORING / MONITORING AGENCY NAME(S) AND ADDRESS(ES)
U.S. Army Medical Research and Materiel Command
Fort Detrick, Maryland 21702-5012

10. SPONSOR/MONITOR'S ACRONYM(S)

11. SPONSOR/MONITOR'S REPORT NUMBER(S)

12. DISTRIBUTION / AVAILABILITY STATEMENT
Approved for Public Release; Distribution Unlimited

13. SUPPLEMENTARY NOTES

14. ABSTRACT

Here, load carriage interventions for walking *energy expenditure* and *running speed* have been designed to: 1) advance existing models and 2) contribute needed data to the broader effort to develop load-carriage decision-aid tools for modern soldiers. We hypothesize first that our height, weight (including load), speed, and grade algorithms proposed will allow walking metabolic rates to be predicted to within 6.0 and 12.0% in laboratory and field settings, respectively. We hypothesize second that the speed-load carriage algorithms will allow load-induced decrements in all-out sprint running speeds to be predicted to within 6.0% in both laboratory and field settings. Respective load-carriage algorithms for *walking energy expenditure* and *running speed* will be developed and tested (Technical Objectives 1.0 and 2.0) in the laboratory and the field.

15. SUBJECT TERMS
gait, metabolism, performance, load carriage

16. SECURITY CLASSIFICATION OF: Unclassified			**17. LIMITATION OF ABSTRACT**	**18. NUMBER OF PAGES**	**19a. NAME OF RESPONSIBLE PERSON**
a. REPORT	**b. ABSTRACT**	**c. THIS PAGE**			USAMRMC
U	U	U	UU	19	**19b. TELEPHONE NUMBER** *(include area code)*

Table of Contents

INTRODUCTION

The Need for Load Carriage Decision-Aid Tools

Load carriage is a foot-soldier requirement with direct consequences for a broad array of physiological, performance and health outcomes. Metabolic energy expenditure, heat production, macronutrient requirements, water requirements, and injury risks are all directly elevated by the weight of the equipment soldiers carry while both short- and long-term mobility are substantially reduced (Knapik et al., 1996; Knapik et al., 2004). Clearly, the physiological stresses and mobility losses induced by load carriage do not constitute desirable field outcomes. Indeed, anecdotal (Knapik & Reynolds, 2010) and formal (Dean, 2004) accounts of the negative consequences of pack overloads are readily available from a multitude of field combat situations. In both modern and historical warfare environments alike, the physiological status and mobility of foot soldiers influence combat performance, wound and survival rates. Accordingly, exacting considerations of the value of carried equipment evaluated against the negative performance, wound and mortality consequences of added weight are a matter of vital military importance.

A priori, one might expect that the major advances in both material science and electronics in the modern era would provide soldiers with more effective equipment while simultaneously reducing the loads soldiers carry. However, the historical record indicates a marked trend in the opposite direction. During the 150-year period from the Civil War through the present day, the pack weights of American foot soldiers have *increased* by a factor of approximately 3-fold, from 15 kg during the Civil War to 35 kg in World War II to approximately to 45 kg in Desert Shield (Knapik & Reynolds, 2010), and 45 kg or above in Afghanistan (Dean, 2004). For an average-sized male US soldier, a load of 45 kg constitutes well over 50% of the body's weight. Thus, the theoretical potential for technological advances in equipment and materials to lighten the pack and total body loads carried by modern foot soldiers has not been realized.

This brief consideration of the historical trends for the loads carried by US soldiers across different eras begs two immediate questions: are the loads carried by modern soldiers excessive? And if so, how harmful is the additional weight carried to warfighter performance?

This answer depends on a fundamental and long-standing load carriage trade-off assessment that balances the *benefits of the equipment carried* vs. the *detrimental performance consequences* imposed by carrying additional weight. On a qualitative level, the benefits of modern body armor, firepower, and communication equipment are relatively obvious, as are the negative physiological and mobility consequences of carrying heavy loads. However, at present, the data needed for quantitative, evidence-based considerations are unavailable. Consequently, well-informed decisions about the pack and total body loads that will be most effective for soldiers in operational environments are not possible.

Given that warfighter field effectiveness is crucial to the efforts of the US military, moving beyond qualitative considerations of the load carriage cost-benefit trade-offs constitutes minimum due diligence to the soldiers in the field as well as to the enormous national investment in our military initiatives. The work proposed here will contribute to a broader experimental work effort to develop **load-carriage, decision aid tools** that take an evidence-based approach to determining loads for foot-soldiers. The specific experimental work we propose focuses on the cost, or detriment side of the load carriage trade-off equation. This work is expected to provide

data that are currently lacking, but necessary for informing strategic decisions regarding pack and total load carriage weights.

We present a series of experiments designed to quantify the negative physiological and performance consequences of the loads modern soldiers carry. The work has been formulated using two promising physiological-mechanical models: 1) a stature-based model to explain walking energy expenditure, and 2) a ground force model to explain brief, all-out running speeds. Fulfilling our experimental objectives should allow predictions of the specific physiological, performance and mobility decrements that would be expected across a broad continuum of potential loads.

Objective One: Walking Energy Expenditure

Previous Scientific Efforts of Direct Military Relevance: Because metabolic rates are so fundamentally related to physiological status and sustained performance capabilities, the Army has a long-standing interest in developing techniques to predict and monitor the metabolic rates of soldiers walking in the field. As with most efforts to acquire or predict physiological data in field environments, this has proven to be a challenging undertaking. However, modern monitoring capabilities and improved predictive modeling should allow for meaningful progress.

The pioneering efforts of Pandolf and others in the 1970's (Givoni & Goldman, 1971; Pandolf et al., 1977) established generalized equations that predict the metabolic rates of walking soldiers from total weight (i.e. body weight + load), speed and grade. However, the utility of these equations depends heavily on the ability to acquire walking speed and grade data in the field. This ability was formerly quite limited, but in recent decades has become fully feasible and highly accurate.

In part, because the ability to monitor speed and distance in field environments limited the original applicability of the Pandolf et al. equations, other approaches were pursued. In the 1990's, Hoyt and colleagues (Hoyt et al., 1994; Hoyt & Weyand, 1996; Hoyt et al., 2004; Weyand et al., 2001) adopted an innovative technological approach that, in contrast to the Pandolf approach, did not require speed and distance data. Hoyt devised a bio-monitoring strategy to predict locomotor metabolic rates from the body's weight and the periods of foot-ground contact. This approach was inspired by algorithms (Kram & Taylor, 1990) that explained the metabolic rates of different-sized terrestrial running and hopping animals. Hoyt and colleagues successfully developed biosensors that accurately monitored ambulatory foot-ground contact times and predicted metabolic rates under some conditions (Hoyt et al., 1994; Hoyt et al., 2004; Weyand et al., 2001). However, this approach was not without limitations. Foot-ground contact monitoring requires a functioning sensor and a wireless network, and current monitors cannot detect the surface inclinations that have a substantial effect on walking energy expenditure (Margaria et al., 1968; Minetti et al., 1994; Minetti et al., 2002).

Modeling Walking Metabolism: Recently, we have developed a promising model for predicting walking metabolic rates that combines the strengths of the Pandolf and Hoyt approaches that can be readily implemented in the field using the accurate geo-location systems now available.

Our model may advance predictive accuracy beyond that provided by the two generalized models most commonly used to estimate the metabolic rates of human walkers at present: the Pandolf

and American College of Sports Medicine (ACSM) equations. Both use *body weight* and *walking speed*, but not *stature* to predict metabolic rates. Although comparative physiologists have long recognized (Alexander, 1976; Taylor et al., 1982; Kram & Taylor, 1990) that the mass-specific metabolic cost of locomotion varies in a systematic manner with the linear dimensions of the body, the leading models for predicting locomotor costs of humans have not incorporated body or leg lengths. The inverse relationship between the body's length (i.e., height) and the mass-specific metabolic rates of individual human walkers has been recently demonstrated (Weyand et al., 2010)

The Stature-Based Model of Walking Metabolism: Our new stature-based model of walking energy expenditure (Weyand et al., 2010) includes three fully independent variables: body mass, stature and walking speed. The quantitative form of the model is as follows:

$$E_{metab} = RMR + C_1 \bullet RMR + C_2 \bullet V^e/Ht \qquad \text{(eq. 1)}$$

where E_{metab} is the body's total metabolic rate, RMR is resting metabolic rate, V is the velocity of walking, and Ht is height. C_1 and C_2 are empirically derived coefficients, and e is an exponent that quantifies equivalent walking velocities for individuals who differ in height. All metabolic rates in the equation are expressed in mass-specific terms.

In our model, RMR is the body's minimum or baseline rate of energy expenditure, the quantity ($C_1 \bullet RMR$) represents the factorial increase above resting metabolic rate needed to maintain a walking posture (i.e. a postural metabolic rate, or PMR), and the term ($C_2 \bullet V^e/Ht$) describes the curvilinear, or exponential, increase in mass-specific metabolic rates that occurs with increases in walking velocities standardized to height in accordance with the original suggestion of Alexander (Alexander, 1976; Alexander, 2003) to use the Froude Number ($= V^2/\text{gravity} \bullet \text{leg length}$). The product of our slightly modified (for utility and convenience) model term V^e/Ht, and the coefficient C_2, represents the metabolic energy expended to lift, support and accelerate the body's center of mass with each step as walking speed is increased.

Two critical assumptions were involved in our development of the stature-based model to predict walking metabolic rates. First, we assumed that the mass-specific **metabolic energy expended per stride is the same at equivalent walking speeds** regardless of the height and weight of the individual. Second, we assumed that individuals who differ in stature **walk in a mechanically similar way at equivalent walking speeds** (i.e. the same Froude Number or value of V^2/Ht). Here, mechanical similarity is defined as stride lengths and times being related by a constant proportion across individuals of different heights.

Extending the Stature-Based Model to Load Carriage and Graded Walking:

Load Carriage: Two aspects of the model seem promising with respect to extending the stature-based model to the load carriage conditions: the predictive accuracy of the model on the independent and heterogeneous subjects evaluated so far, and a clear conceptual and quantitative basis from which to predict the effect that loading will have. Per below, our stature-based model breaks total walking metabolism into resting and walking components.

$$\dot{E}_{metab} = \underbrace{RMR}_{\text{Resting}} + \underbrace{C_1 \cdot RMR + C_2 \cdot V^e / Ht}_{\text{Walking}}$$

Because the relationship between the weight supported and both of the walking, or non-resting component of our model is 1:1, the predictions of the model for the effect of loading are straightforward: loading will increase the *walking* portion of the total metabolic rate in direct proportion to the load added. Thus, a load equal to 10% body's weight will increase walking metabolic rates by 10%; a load equal to 20% of body's weight will increase walking metabolic rates 20%, etc.

While there is a relatively large body of literature on the consequences of loading for walking metabolism (Bastien et al., 2003; Das & Saha, 1966; Duggan & Haisman, 1992; Falola et al., 2000; Griffin et al., 2003; Holewijn, 1990; Martin & Nelson, 1986; Pimental & Pandolf, 1979), none of the studies available provide the data needed to evaluate the predictive accuracy of the stature-based model under these conditions. Two quantitative issues prevent this: existing data sets and models have not included the influence of stature on walking metabolism, and previous studies have not quantified or reported resting metabolic rates that can be quantitatively related to the resting and postural terms in our model. However, the best data available for evaluating our model (Griffin et al., 2003) indicate that loading results in gross walking metabolic rates being elevated slightly less than in direct proportion to load, while net walking rates (subtracting a standing value) are elevated in slightly greater than 1:1 proportion are consistent with our model predictions.

Graded Walking: Similarly, our expectation is that our model will also apply to graded walking, although per above, quantitative evaluations of our model using the existing literature (Margaria, 1968; Minetti et al., 1994; Minetti et al., 2002; Wanta et al., 1993) are not possible. For graded walking, our approach will be to extend our findings of a constant metabolic cost per stride at equivalent speeds for different individuals to inclined and declined conditions. Under level walking conditions, we found that the lower mass-specific metabolic rates of taller vs. shorter individuals are fully explained by differences in body lengths (i.e. height) and proportional differences in the horizontal distance traveled with each stride (i.e. stride length). Extending our stature-based model to explain metabolic rates during inclined and declined walking involves similar quantification of the distance traveled by the body during each stride. During horizontal walking, including only the horizontal displacements is sufficient. During graded walking, our stature-based model predicts metabolic rates will be a function of both the *horizontal* and *vertical* displacements of the body over the course of each stride. Stride lengths during graded walking are expected to be proportional to stature at equivalent walking speeds as during horizontal walking. However, the vertical displacements of the body over the course of each stride will be a function of both the surface grade and stature. Per intuition, the vertical distance per stride traveled will be greater on any inclined or declined walking surface for taller vs. shorter individuals. Accordingly, metabolic rate deviations from the level condition for taller vs. shorter individuals are also expected to be greater on any given incline or decline. Mechanically, this is most easily conceptualized as the metabolic cost per stride increasing and decreasing in accordance with the positive and negative displacements of the body during each stride. This metabolic pattern is well described in the comparative literature for large and small animals (Taylor et al., 1972), but the data needed to assess humans of different statures is unavailable.

Our expectation is that we can use stature and percent grade to quantify this effect. In the specific terms of our model, our expectation is that our coefficient, C_2 that describes the increases in metabolic rate in relation to increases in equivalent walking speeds, will have the same value for any given positive or negative vertical displacements of the body per stride. Although this relationship will need to be determined empirically, we can make the simple prediction that the value of C_2 during inclined and declined walking will be proportional to the product of the stature of the individual and the percent grade of the surface (i.e. $C_2 \propto$ Ht • % grade).

The experiments proposed here represent the most fundamental empirical steps needed to extend and validate our stature-based model. Once the basic work needed to develop algorithms including load, incline and decline conditions has been completed, additional work to incorporate the effects of fatigue (Epstein et al., 1988; Patton et al., 1991), terrain (Pandolf et al., 1977) and very steep downhill grades (Margaria, 1968; Santee et al., 2001) may then be explored in the context of the model.

Objective Two: Sprint Running Speed

Previous Scientific Efforts: The scientific literature on the basis of brief, all-out running performance is far less extensive than that devoted to the energy cost of walking. Early efforts focused primarily on explaining performance in terms of the metabolic power available for these events (Hill, 1925; Hill, 1950; Ward-Smith, 1985; Ward-Smith, 1999; Ward-Smith, 2000). While some investigators have continued to use metabolic models to explain these performances (Rittweger et al., 2009), the predominant scientific focus has shifted to mechanical models (Bundle et al., 2006; Usherwood & Wilson, 2005; Usherwood & Wilson, 2006, Chang & Kram, 2007; Weyand et al. 2000; Weyand et al., 20006; Weyand et al., 2010) to explain sprint exercise performances. In our view, this shift is scientifically warranted as mechanical approaches can directly explain the motion of the body and promising force models using this approach are being developed (Weyand et al., 2006; Weyand et al., 2010). In contrast, metabolic models continue to be difficult to validate at present due to the ongoing inability to quantify the whole-body anaerobic and total metabolic energy released during sprinting (Bangsbo, 1998; Van Pragh, 2007).

For the purposes of predicting sprint exercise performance here, we have opted to quantify load-induced decrements in speed as fractional decrements from the unloaded condition. Our interpretation of the existing literature indicates that this approach is likely to provide the greatest predictive accuracy from a simple, practical model. There are at least two sound, literature-based reasons for adopting this approach. First, maximal sprint performances vary considerably between individuals for physiological and mechanical reasons that are incompletely understood and likely cannot be modeled simply. Second, the relationship between all-out sprint running speeds and the average ground forces applied during each step, both within and across individuals, is reasonably linear during sprint running (Weyand et al., 2000; Weyand et al., 2010) which simplifies model predictions.

We expect to be able to predict load-induced decrements in speed with a high degree of accuracy because loads are not likely to alter the maximum forces runners can apply to the ground, but will predictably increase the ground force required to run at any speed. Accordingly, we should be able to use a runner's force maximum at his or her unloaded sprinting speed maximum, load-

induced increases in the ground forces required, and the general force-speed relationship to predict load-induced decrements in all-out speed.

Our speed model takes the simple following form:

$$V_L = C_1 \bullet (L/W_b) \bullet V_{UL} \qquad \text{(eq. 2)}$$

where V_L is the maximum velocity of loaded running for all-out runs of brief duration, W_b is body weight, L is the weight of the load carried, C_1 is the coefficient describing the load-induced decrements in speed resulting from fractional additions to the body's weight (L/W_b) via loading, and V_{UL} is the maximum velocity of running in the unloaded condition.

Our force-speed model has its basis in both basic Newtonian mechanics and the ground force capabilities of individual runners. An extensive body of scientific evidence supports the view that a primary mechanical requirement of running is supporting the body's weight against gravity. Successful characterizations of running energetics and even speed and distance monitoring have been realized from this conceptual starting point (Kram & Taylor, 1990; Weyand et al., 2001). Our force-speed model also begins with this basic recognition.

The mechanical basis of our empirically-formulated force model of sprint running is most easily understood by considering how the ground contact and aerial phases of a running stride change across speed for individual runners. The relative durations of the aerial and foot-ground contact phases of a running stride vary with speed. As runners increase their speeds, they spend relatively more time in the air and relatively less time on the ground. Consequently, the ground support forces that runners apply increase in an approximately linear fashion with speed and are set by body mass. For runners regardless of ability, stance-averaged ground support forces are 1.5 times the body's weight while jogging, and increase to 2.0 times the body's weight or more when running at sprinting speeds.

Here, we expect that loading will result in proportional increases in the stance-average ground reaction forces required with little effect on the time course of ground force application. This result has also been reported from studies examining loaded running at slower speeds (Chang & Kram, 2000). The consistency observed in the foot-ground contact times at any given speed across different loads suggests that our general approach is sound

Beyond this, we have found that the limit to running speed occurs when runners reach that speed at which they are repositioning their limbs as quickly as possible while simultaneously applying maximum ground forces. Contrary to intuition, the minimum times runners require to reposition their limbs at their top running speeds does not vary in relation to how fast they can run. Consequently, individual differences in speed are explained all but entirely by the mechanics of the stance phase. These mechanical observations support a modeling approach that focuses on the ground force required and available for speed.

At present, firm predictions of the decrements in brief, all-out running speeds that will occur with loading and that will be quantified by the coefficient C_1 in our force-running speed model are difficult. This is the case because only small number of studies to date have examined the effects of loading on sprint running performance (Alcaraz et al., 2008; Cronin et al., 2008; Holewijn & Lotens, 1992). The few studies that do present loaded and unloaded all-out sprinting speed data

do so under conditions that make more generalized predictions difficult, and none of these studies include the ground reaction force data. The most informative study with respect to our experimental objectives here is that of Holewijn & Lotens (1992) who reported that a load equal to 21% of body weight reduced all-out running velocities by 13 and 18% for all-out 80- and 400-meter runs. More recently, Alcaraz et al. (2008) reported only 3% reductions in brief, all-out running speeds with loads equal to 9% of the body's mass, while Cronin et al. reported fractional reductions in all-out loaded sprinting speeds that were approximately half as large as the fractional increases in load/body weight ratios. The disparity in the different results reported to date could result from a large number of factors, and is therefore difficult to interpret. These empirical results project a C_1 value in our model somewhere between 0.4 and 1.0.

Fractional reductions in brief, all-out running speeds that are, in some cases only half as large as the fractional loading of the body's weight reported are surprising. The relatively shallow slope of the force-speed relationship portends a much greater sensitivity. The mechanistic factors that explain a much more limited effect than would be theoretically expected from unloaded force-speed data only are almost certainly rooted in the mechanics of the stance phase ground force application that occurs under loaded conditions. These likely involve mechanical adaptations to loading that improve the leverage of the limb (Biewener et al., 2004) and thereby reduce the muscle forces required in relation to the load being carried.

However, in the complete absence of ground reaction force data or the accompanying video data to determine limb leverage, speculating about the adjustments that may constrain load-induced decrements in speed is difficult. The limited existing data available point to a critical need to acquire ground reaction force and video data under a variety of load and duration conditions to develop a robust predictive model. These data should provide the key to understanding how musculoskeletal mechanics, loading strategies, training and conditioning strategies, and conceivably external aids like exoskeletons, may be utilized to minimize detrimental losses in the short-term mobility of soldiers that result from carrying heavy loads.

BODY

The majority of the calendar year has been devoted to analysis, synthesis and report and manuscript writing. Individuals receiving support from the award during the last calendar year were: Jennifer Nollkamper, Lindsay Ludlow and Peter Weyand.

The load carriage experiments have two specific objectives: 1) to develop and validate algorithms that predict walking metabolic rates from height, weight (including load), speed and grade, and 2) to develop and validate algorithms that predict brief, all-out running speeds from the body and pack weights of the individual. These objectives will be pursued in parallel per the following experimental timeline.

<u>Objective 1 – Walking Energy Expenditure</u>:

We intend to acquire energy expenditure data in the laboratory on those subjects on whom our predictive metabolic equations will be developed using our stature-based model. Subjects will

complete walking trials at a number of different walking speeds treadmill grades while their rates of oxygen uptake and energy expenditure are measured.

We will also complete the aforementioned laboratory walking trials across speed and grade needed for our original subjects as needed for algorithm development. In addition, we will undertake field data acquisition by having subjects will undergo a field march on a surveyed field course of known elevations and grades while instrumented to acquire the metabolic and position data.

Objective 2 – Sprint Running Speed:

We will first conduct high-speed running tests in the laboratory on subjects under three different loading conditions: unloaded, +15% body weight, and +30% body weight. Subjects will complete protocols to determine their maximum speeds for efforts ranging from 2 to 90 s while force and video data are acquired.

Next, we will acquire all-out overground running data in both indoor and outdoor settings on subjects. These subjects will complete 25 meter runs indoors and 60 meter runs outdoors under four different loading conditions: unloaded, +15% body weight, +30% body weight, and +45% body weight. Simultaneous force and video data will be acquired during the indoor 25-meter running trials.

KEY RESEARCH ACCOMPLISHMENTS

Key accomplishments over the reporting period of the grant were as follows:

April 2012 – April 2013

1) Set up experimental protocols and facilities to conduct work
2) Filed applications for approvals to do research on human subjects
3) HRPO approval granted in December 2012
4) Experiments commenced in early 2013

April - June of 2013

1) Finalized the testing set-ups and protocols for both the loaded walking and running objectives. This included augmenting the treadmill frame with scaffolding to accommodate the downhill conditions.
2) The protocol for unloaded walking across speed and incline for algorithm development was tested and refined.
3) Weighting material, packaging, load distribution and related logistics were developed.
4) Back-pack modifications were made for subject comfort. These included switching backpack type for subject comfort and safety. The newer version identified provided greater shoulder padding and comfort.

5) Standardized footwear was purchased to accommodate research subjects.

The pilot data available for guiding our walking protocol development at this juncture appears in Figure 1 below.

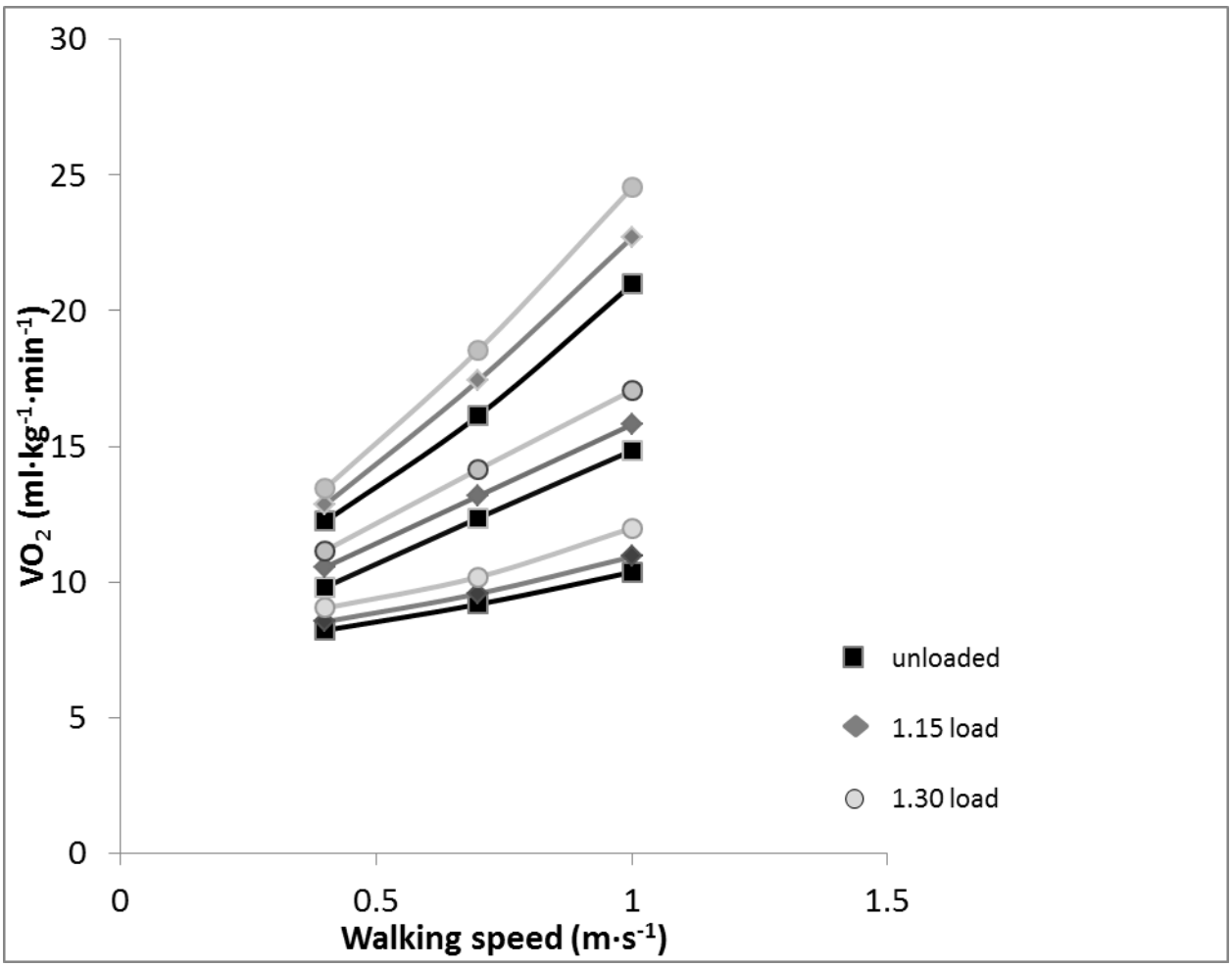

Figure 1. *Walking rates of oxygen uptake as a function of speed on three treadmill inclinations and under three loading conditions for one subject. All measures were taken under steady-state conditions.*

The vest and backpack selection were finalized in the latter portion of the prior reporting year once human subjects testing authorization had been acquired. The specific gear and loading schemes are illustrated in the pictures appearing in Figure 2:

Panel A

Panel B

Figure 2. *The vest and backpack used to add loads to subjects from lateral (A) and front (B) views. Yoga blocks and sealed bags of shot are used to add the condition-specific weight needed for protocol administration for subjects who differ in body mass.*

In the first quarter, we also acquired initial data from our loaded running protocol for both the areobic demands of running under load and the performance-duration relationship for all-out runs of brief duration. Representative data from individual subjects appears below in Figure 3

Panel A

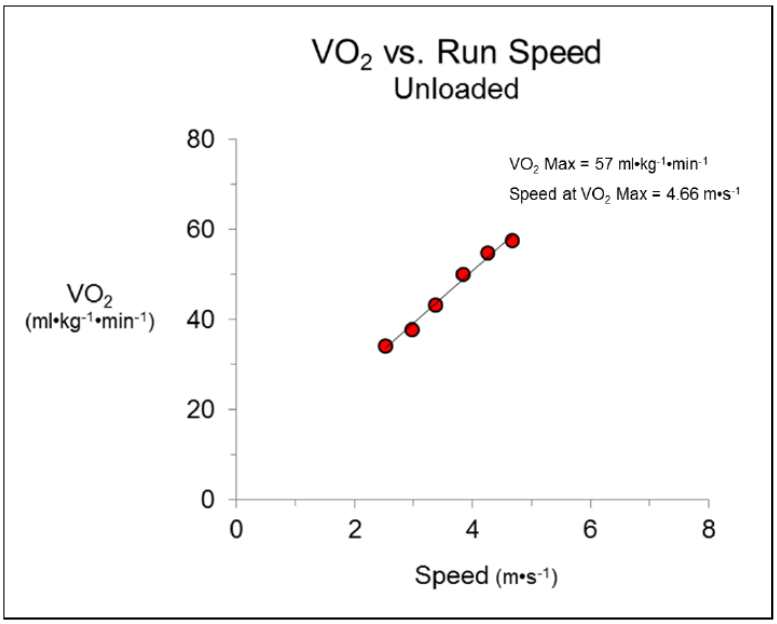

Panel B

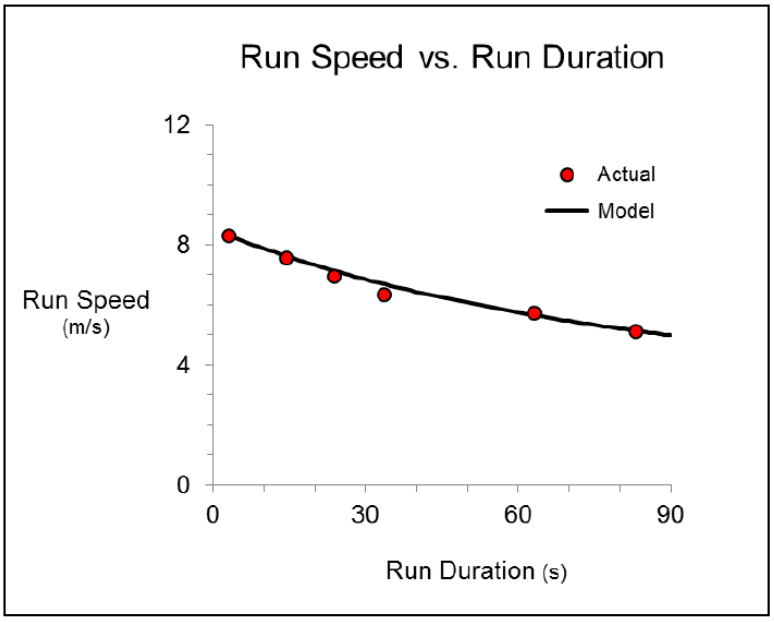

Figure 3. *Steady-state rates of oxygen uptake measured during a progressive, discontinuous treadmill test up to the individual's aerobic maximum in the unloaded condition (A) and all-out running speeds as a*

function of run duration while running also in the unloaded condition. The line depicts the predictions of the speed reserve model for performance under these conditions.

July - September 2013

1) Efforts were devoted primarily to testing and data acquisition, particularly to meet the very heavy testing and data acquisition requirements of objective 1 for predicting walking metabolic rates.
2) Testing protocols, weighting schemes and general logistics for the laboratory testing protocols were largely finalized. This included finalizing the protocol for the unloaded treadmill walking tests. Some modifications for the treadmill running tests came under consideration for refinement due to the rigor and number of test sessions involved for individual subjects.
3) Minor modifications were made to provide better padding of the backpacks for the walking sessions to make the subjects more comfortable during testing.
4) In preparation for the running biomechanics testing for objective 2, we purchased a motion capture system which has been delivered and is now up and running in our main laboratory. We prepared to begin validation of the new system against our existing system to ensure data validity.
5) Software programming to precisely locate the center of pressure on the force platforms to be used to running data acquisition was also initiated. The goal of these efforts was to resolve the location of the center of pressure on the force plates to within 1.0 millimeter or less. The estimated programming time requirement at this juncture was 80 hours.
6) We moved forward with site location and logistical preparations for the field test of the walking model.
7) We revised our running force model paper that was in review at the *Journal of Experimental Biology*.
8) Our manuscript that introduced a new generalized equation to predict walking metabolic rates was accepted and moved toward publication at the *Journal of Applied Physiology*.
9) We began an effort to digitize a literature data set to test and refine the walking metabolism model introduced in the paper currently in press.

Representative data for objective 2 on running metabolism are provided below in Figures 4 and 5 for both steady-state running at speeds below the aerobic maximum and for all-out running as a function of run duration on both the weighted and un-weighted conditions.

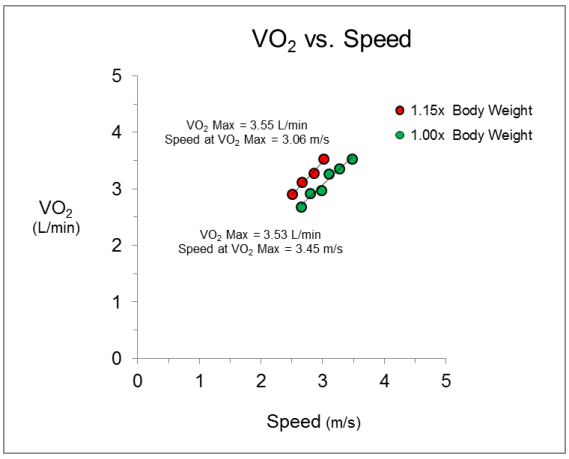

Figure 4. *Rates of oxygen uptake vs. speed during unloaded and loaded running.*

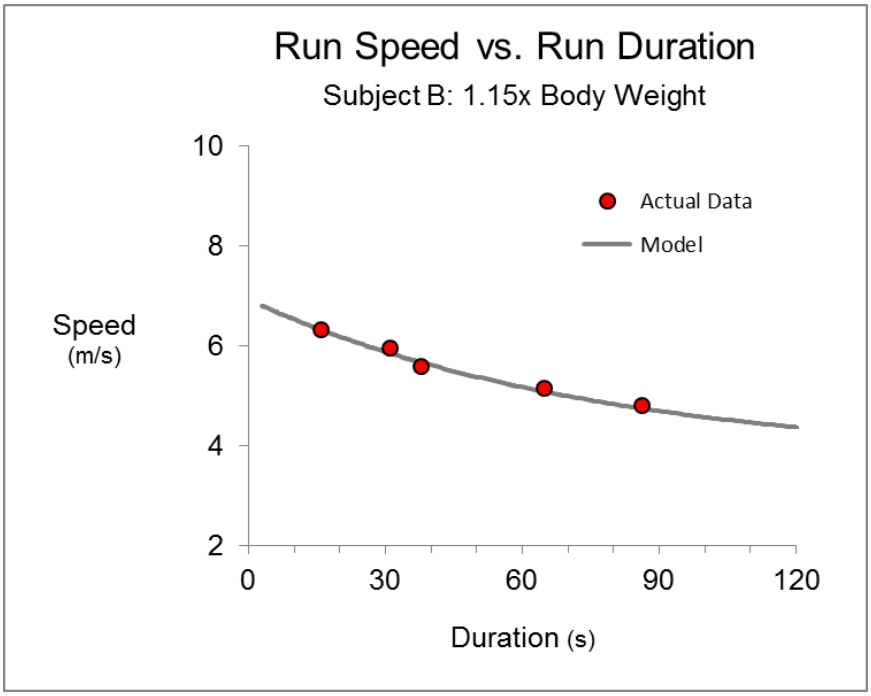

Figure 5, *All-out running speeds as a function of run duration during loaded running. The solid indicates the speeds predicted by the force-based speed reserve model as detailed in the grant proposal.*

<u>October 2013 - January 2014</u>

1) Continued testing and data acquisition, and technical efforts to set up data acquisition systems for objective two.
2) We also organized our efforts to organize and reduce data and conduct data analysis for both the walking (1) and running (2) objectives of the project.
3) Analysis and manuscript work continued in both the walking and running objectives.

4) Planning all aspects of the walking field tests also began. These include equipment, data acquisition systems, site planning and preparation, tec.
5) We made some modifications on specific test protocols for objective two on running mechanics to improve subject comfort.
6) Considerable effort was devoted to the technical work needed to ensure high quality mechanics data for grant objective two. These efforts included approximately 100 hours of software programming for precision location of the center of pressure on our contiguous in-ground force plates. This work was successfully completed. Per our last report, the resolution of the center of pressure on the force plates is 1.0 millimeter as anticipated. These efforts also included approximately 80 hours of system set-up and data acquisition testing using a new Opti-Track Motion Capture System procured to execute the experimental work on objective two.
7) We devised data reduction and organization systems for objective one on walking metabolism in order to allow for quick screening of the data upon acquisition. We also implemented a data organization system that will allow for rapid analysis and modeling with the large and unique metabolic data set we are in the process of acquiring.
8) We continued to refine our walking metabolism and running mechanics models with original and literature data. Several hundred person hours were devoted to both efforts in the last quarter. These efforts resulted in the submission of a revised manuscript on running mechanics to the *Journal of Experimental Biology* and a walking metabolism manuscript that is in preparation for submission to the *Journal of Applied Physiology*.

Per the report details presented in the report from January of 2014, we presented some of the data set and analysis of our digitized literature data set that was acquired to provide a robust, valid, level walking data set spanning a broad range of body sizes and a broad range of walking speeds. This data set includes original and literature data selected to maximize the natural biological variability present. The data set is comprised of mean data, with the subjects within each group being similar in stature, but with substantial height differences being present across groups. These data and preliminary analyses appear below in Figures 6 and 7.

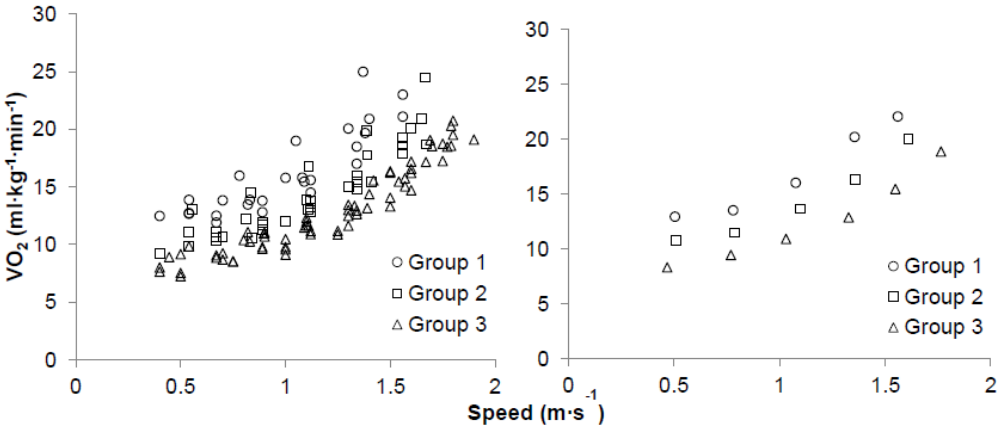

Figure 6. *Rates of oxygen uptake vs. speed during unloaded walking (panel A, n=129). Each data point represents the mean value acquired from a population of subjects walking on a firm*

level surface. The data set includes both over-ground and treadmill data. The three symbol types for group 1 (circles), group 2 (squares) and group 3 (triangles) are for short, medium and tall subjects. The overall mean values for all the subject groups within the three respective height ranges appear in panel B.

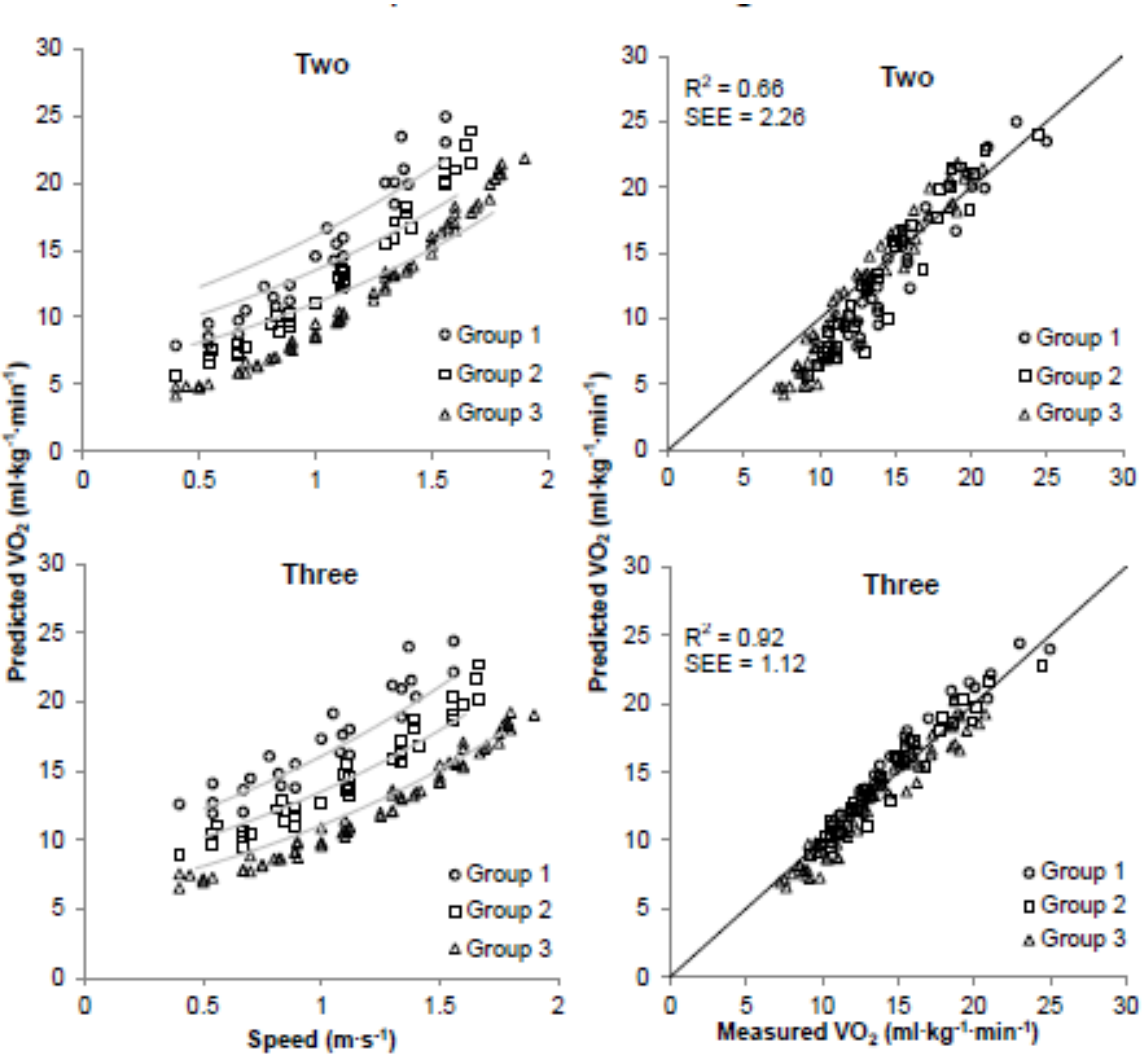

Figure 7. *Predicted rates of oxygen uptake vs. speed during level walking for groups of individuals who differ in height (left-hand upper and lower panels; circles- short, squares – average height, triangles – tall. The gray lines show the mean fits to the original data for each of the three height categories). The predictions are best-fit based on two iterations of our walking metabolism model, one with two metabolic components (upper left panel) and one with three metabolic components (lower left panel).*

Measured vs. model predicted values for these data points appear on the right-hand upper and lower panels labeled for two and three components, respectively. The proportion of variance

accounted for has increased from prior reports, the predictive error has decreased and the error in the direction of prediction has become less sensitive to the absolute oxygen uptake values. [Note: the data points appearing correspond to the original data points from Figure 1, left-hand panel above].

In the final quarter of the reporting year (January through March of 2014), as detailed in our April 2014 reports, our efforts were as follows:

1) We nearly finished the data acquisition for the loaded portion of the treadmill walking protocol.
2) We began recruiting for the unloaded portion of the laboratory walking protocol.
3) Data analysis and manuscript preparation using a combined literature plus original data approach detailed in the last report continued. The objective of this effort has been to refine our height-weight-speed model of walking metabolism on level surfaces.
4) Preliminary modeling of the loaded treadmill walking data has begun.
5) Experimental planning and preparations for the field testing portion of objective 1 has continued. Refurbishing of our portable metabolic system was completed. A vertical and horizontal GPS system was purchased and acquired.
6) We completed preparations and begun pilot testing the biomechanics data acquisition system for objective 2. These efforts included force plate and motion capture data acquisition systems as detailed previously. These efforts required several hundred person hours during the last quarter. Briefly, the overground running mechanics technical efforts included custom programming of the force plate data acquisition system using LabView, configuring the OptiTrack motion capture system, establishing the marker set to be used for the testing (which would not interfere with the vest/backpack system), developing a custom start trigger method and pilot testing two subjects.
7) The treadmill running testing for objective 2 has continued.

Pilot and technical data from the extensive work done in the fourth quarter to set up, validate and pilot test the laboratory overground running data acquisition system t meet objective 2 apopears below in Figures 8 and 9.

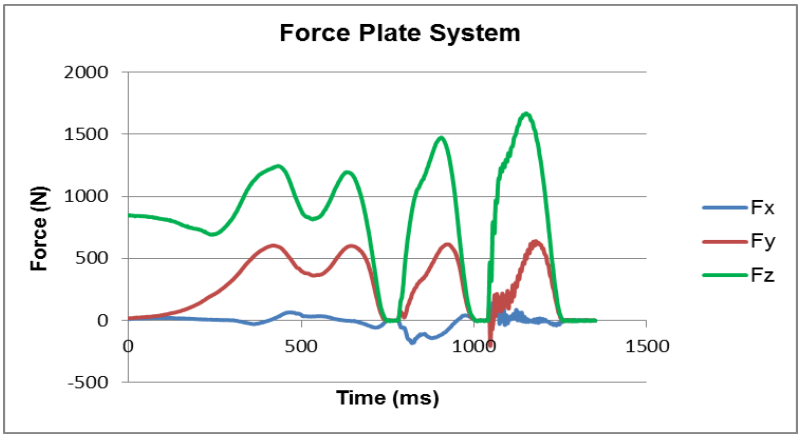

Figure 8. *Lateral (blue), horizontal (red) and vertical (green) ground reaction forces during an all-out run from a standing start through the second step two of a 10-meter running trial.*

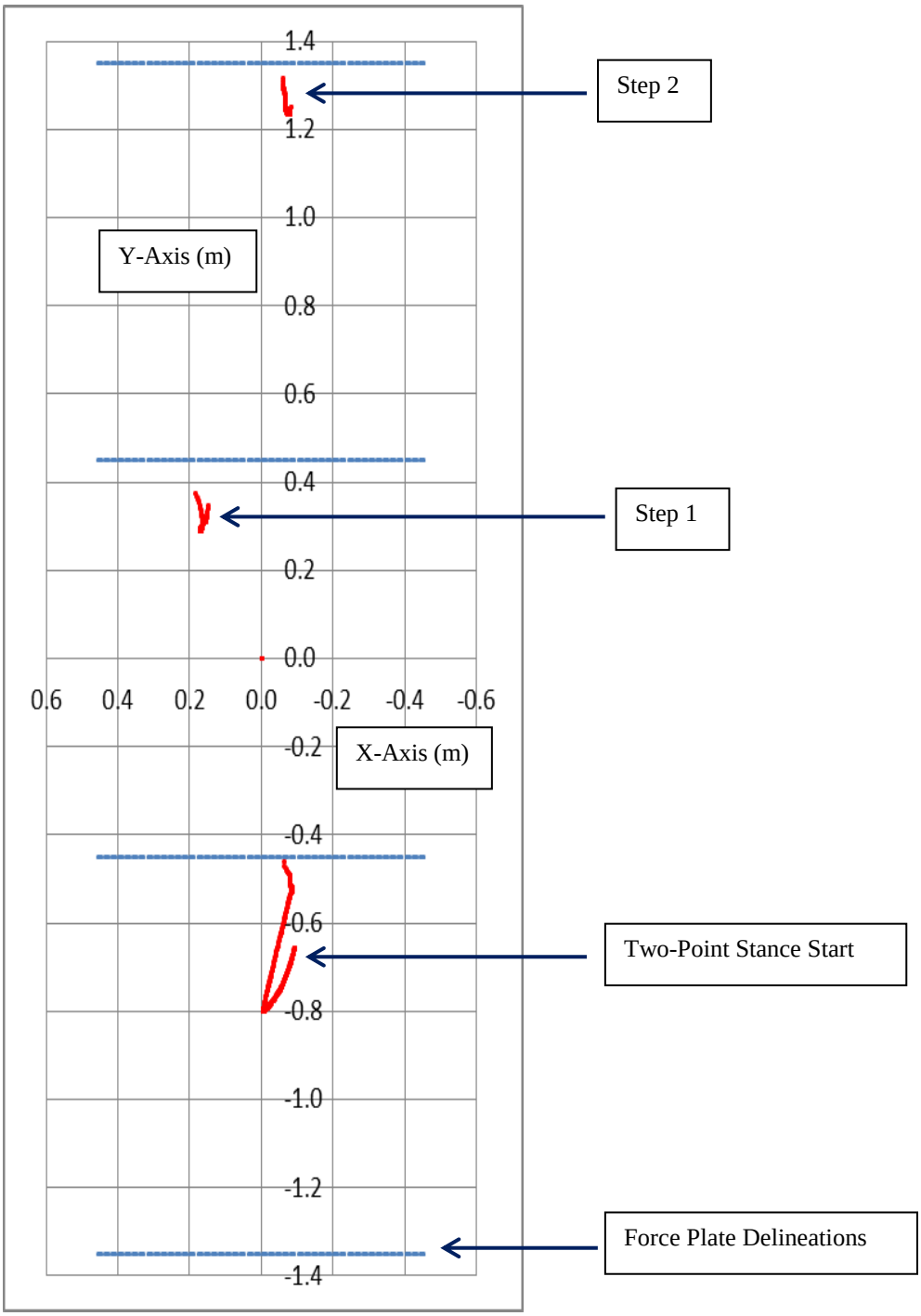

Figure 9. *Center of foot-ground pressure data from a standing start and the first two steps of a brief all-out run from our custom three-force plate system.*

April - June of 2014

6) The loaded portion of the laboratory testing for objective 1 is essentially complete. One subject has not been able to schedule his last remaining tests, but 19 subjects have finished the protocol.
7) The unloaded portion of the laboratory testing for objective 1 is well underway. We expect the majority of the laboratory experimental work unloaded walking to be completed in the coming quarter. With good fortune, the unloaded testing will be finished before the end of the next quarter.
8) Modeling efforts have been a primary focus in the past quarter. These occurred in parallel with two data sets: a) a literature compiled data set that is being used to refine our level walking model of walking energetics, and b) the newly acquired walking metabolism data across speed and loaded conditions. Our level model is now being extended to include both incline and load.
9) Manuscript preparation for modeling the level walking data has move forward and remains in progress.
10) Preparations for field testing have continued. These include the acquisition of a GPS unit for the field testing, an on-site demo/training session from the GPS representative and plotting of potential courses for the field testing.
11) Technical and validation work on our instrumentation for the overground portion of objective has also continued. These efforts have included: a) validating the center of mass motion form our newly acquired OptiTrack motion capture system vs. force plate data and instrumented push bars for an independent test.
12) Treadmill testing for objective 2 has continued.
13) Modeling of the determining factors of running ground reaction forces which are critical for performance has continued.

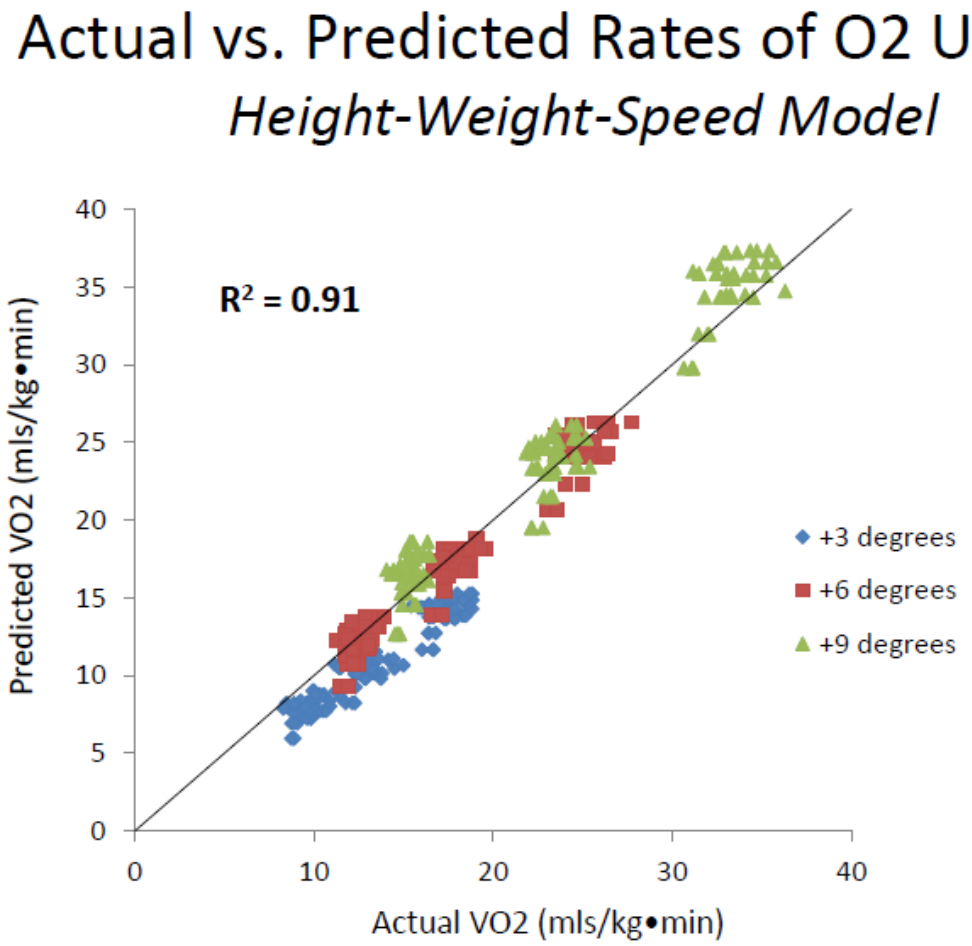

Figure 1. Actual rates of oxygen uptake vs. those predicted by the Height-Weight-Speed model as currently adapted to inclined and loaded walking at different speeds (as of June 2014).

July - September of 2014

1) The loaded portion of the laboratory testing for objective 1 is complete.
2) The unloaded portion of the treadmill walking tests is nearing completion. The unloaded portion of the protocol involves walking across a range of speed at a series of different treadmill grades.
3) Modeling efforts of the walk model in general and specific modeling of the now available incline and loaded walking data continue. Our initial efforts have been reasonably positive for the prospect of successful extension of our height-weight-speed model to graded and loaded conditions.
4) Significant progress has been made on a new manuscript involving a rigorous test of the height-weight-speed model.
5) Preparations for field testing have progressed. These include a site visit by Project Officer William Santee in August during which the course was visited and evaluated. Plans for a minor protocol adjustment were also discussed.
6) A protocol amendment involving a slight modification of the field test was submitted for and approved by the SMU IRB.

7) The approved amendment was provided to HRPO from whom we received notification that no further action on the protocol adjustment is needed.
8) The treadmill running tests to meet grant objective 2 were also modified to require fewer sessions.
9) A new motion capture system was implemented and integrated with the force treadmill for simultaneous force and motion data acquisition.
10) Work has continued on our mechanics model that links running ground reaction forces and motion.

October 2014 - January 2015

1) The unloaded portion of the laboratory testing for objective 1 was completed during the last quarterly period.
2) Modeling efforts are now being extended to include the unloaded treadmill walking data which are being screened and finalized as incorporated into our modeling spreadsheets.
3) Technical work to introduce and validate a new motion capture data acquisition system into our existing force treadmill was completed to support objective 2. Some custom programming was necessary to avoid marker occlusion under loaded conditions.
4) Technical work was conducted on our in-ground force-motion data system.
5) Objective 2 treadmill testing has continued.
6) Preparations for field testing for objective 1 also continue.
7) Manuscript preparation of our most recent level walking metabolism modeling effort continues.
8) Work has continued on our mechanics model that links running ground reaction forces and motion.

January - March 2015

1) The laboratory portion of the objective 1 work has been completed Modeling of the data for algorithm determination has begun.
2) Specific modeling to extend the level algorithm to include load and grade is underway.
3) Field testing preparations have continued. Pilot testing of the walking course has begun. GPS survey and course data has been acquired.
4) Testing on objective 2, loaded running has continued.
5) Manuscript preparations of our most recent level walking metabolism modeling effort have continued. Two manuscripts were submitted
6) Work has continued on our mechanics model that links running ground reaction forces and motion.

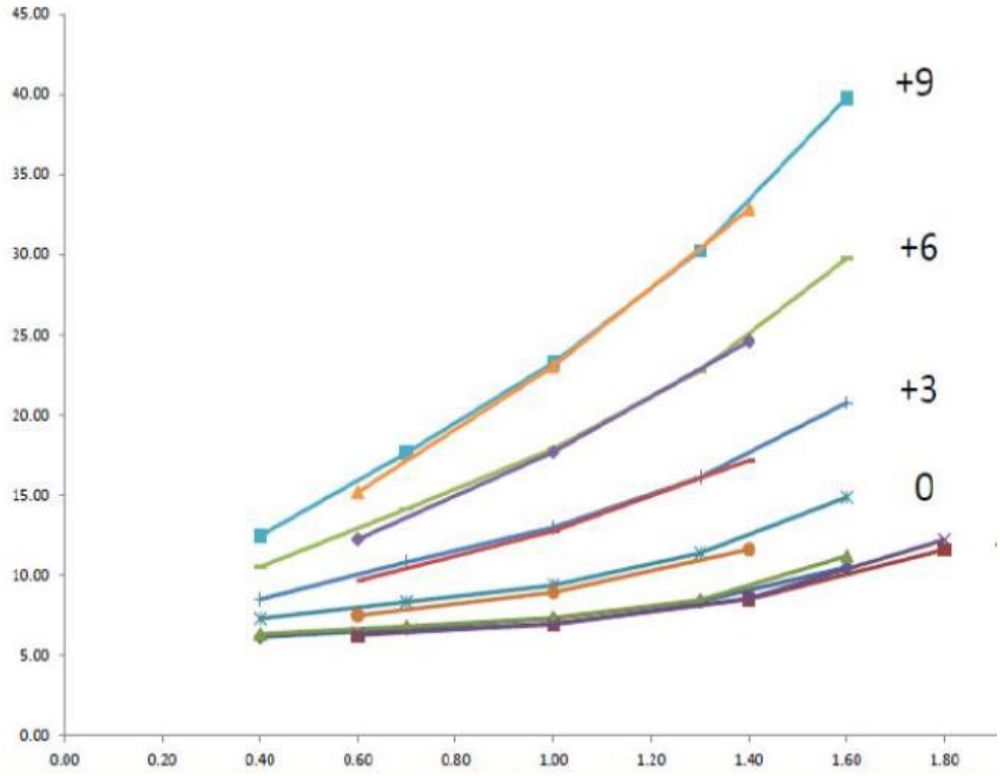

Figure 2. Mass-specific rates of O2 uptake (mls/kg •min) vs. walking speed (m/s) on different grades with and without load.

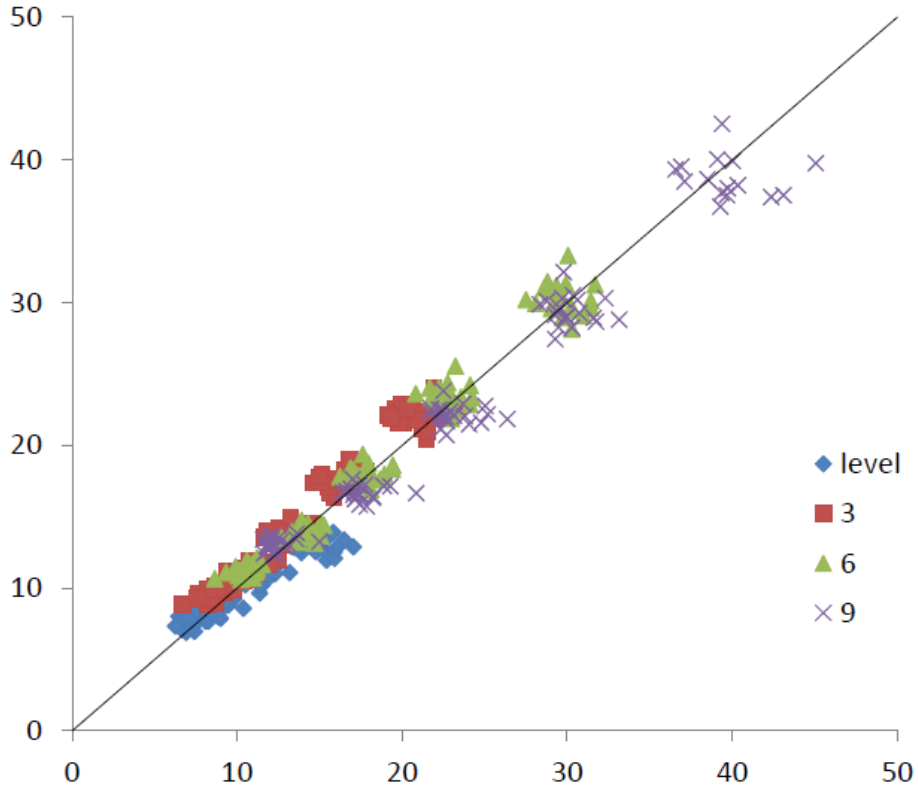

Figure 3. Mass-specific rates of O2 uptake (mls/kg •min) vs. walking speed (m/s) on different grades with and without load (as of April 2015).

April 2015 - July 2015

1) Modeling of the data for algorithm determination for objective 1 continued. Specific modeling to extend the level algorithm to include load and grade began.
2) Field testing of the algorithm for objective 1 began. We completed 4 unloaded field trials and one pilot loaded trial. The course was finalized and includes varied terrain as well as up and downhill slopes of consistent grade.
3) Testing on objective 2, loaded running continued. The treadmill portion of the testing was nearly completed. Field tests of overground acceleration testing commenced and were nearly completed.
4) Two manuscripts are in press, a third was revised for submission to a new journal.
5) Work has continued on our mechanics model that links running ground reaction forces and motion. Substantial progress has been made on the mechanical basis of the horizontal component of the ground reaction force.

July 2015 – October 2015

1) Modeling of the data for algorithm determination for objective 1 continued. Specific modeling to extend the level algorithm to include load and grade was underway.
2) Our large laboratory data sets have been organized to allow both best-fit and cross-validation modeling of speed, load, and grade.

3) Field testing of the algorithms developed for objective 1 began. We enrolled and tested subjects to complete the lab and field testing needed for algorithm validation.
4) As part of object the field testing, we tested our portable vs. laboratory metabolic units to be sure we have accurately quantified any system differences that will directly influence field validations.
5) Testing on objective 2, loaded running was completed. In the last quarter, both the treadmill and overground running tests were finished.
6) An editorial manuscript on sprint running acceleration published.
7) Our manuscript which further developed our level walking metabolism algorithms was prepared for submission to the Journal of Applied Physiology.
8) Work has continued on our mechanics model that links running ground reaction forces and motion. Substantial progress was made on the mechanical basis of the horizontal component of the ground reaction force.
9) With the running load data now fully acquired, we began using the load condition to test our existing model.

Oct 2015 – Jan 2016

1) Modeling of the data for algorithm determination for objective 1 continued after finalization and organization of the data in the prior quarter. Specific modeling to extend the level algorithm to include load and grade began.
2) Modeling objectives include expanding our Height-Weight-Speed algorithms to load, grade and terrain. We are also testing the expanded version vs. other predictive models.
3) Field testing of the algorithms developed for objective 1 continued.
4) As part of object the field testing, we tested our portable vs. laboratory metabolic units to be sure we have accurately quantified any system differences that will directly influence field validations.
5) Our annual service calibration of our portable metabolic system was completed at the end of the end of the quarter.
6) Testing on objective 2, loaded running was completed in the 4th quarter of 2015. Analysis of the data began.
7) A manuscript on loaded running mechanics was prepared for the upcoming Body Sensor Network conference.
8) Work has continued on our mechanics model that links running ground reaction forces and motion.
9) With the running load data now fully acquired, we began using the load condition to test our existing model.

Jan 2016 – April 2016

1) Field testing of loaded and unloaded walking metabolism continued.
2) Modeling of the laboratory data base for walking metabolism for objective 1 continued
3) Modeling efforts on our loaded running mechanics data for objective 2 continued
4) Two manuscripts were prepared and submitted for the upcoming IEEE Body Sensor Network conference in June.

5) An original manuscript on the relationship between running force and motion was prepared and submitted to the Journal of Experimental Biology.

April 2016 - July 2016

1) Field testing of loaded and unloaded walking metabolism continued.
2) Modeling of the laboratory data base for walking metabolism for objective 1 continued
3) Modeling efforts on our loaded running mechanics data for objective 2 continued
4) Two manuscripts were prepared for the upcoming IEEE Body Sensor Network conference in June.
5) An original manuscript on the relationship between running force and motion was prepared and submitted to the Journal of Experimental Biology.
6) A new version of our level walking metabolic model published in the Journal of Applied Physiology.
7) Scientific American visited for the laboratory for two days to shoot and interview for an upcoming feature story on running performance to appear in a summer issue of the magazine.

July 2016 – October 2016

1) Field testing of loaded and unloaded walking metabolism continued.
2) Additional laboratory testing for declined surfaces was undertaken. Field tests for quantifying the influence of terrain were planned.
3) Modeling of the laboratory data base for walking metabolism for objective 1 continued.
4) Modeling efforts on our loaded running mechanics data for objective 2 continued.
5) Two manuscripts from the upcoming IEEE Body Sensor Network conference in June were accepted for publication.
6) An original manuscript on the relationship between running force and motion was revised for imminent resubmission to the Journal of Experimental Biology.
7) Our new level walking metabolic model that published in the Journal of Applied Physiology received media coverage from a number of media outlets.
8) Scientific American visited for the laboratory for two days to shoot and interview for an upcoming feature story on running performance to appear in a summer issue of the magazine.
9) Two subjects were tested during the last quarter, undergoing the complementary field and lab testing protocol.
10) Objective 2 testing on loaded running continues in the analysis phase.
11) Two IEEE manuscripts were presented at the Body Sensor Network Conference in San Francisco in June in preparation: one on loaded running and one on the metabolic cost of loaded walking.
12) Two manuscripts were accepted for publication in IEEE Engineering and Medicine in Biology.
13) One manuscript was revised for resubmission to the Journal of Experimental Biology.

Oct 2016 – Jan 2017

1) Laboratory testing for extreme declines on a subset of subjects was completed.
2) Analysis of field testing of loaded and unloaded walking metabolism continued.
3) Additional field sites for field testing for terrain and flatter surface trials have been identified.
4) Modeling of the laboratory data base for walking metabolism for objective 1 continued.
5) Modeling efforts on our loaded running mechanics data for objective 2 continued.
6) An original manuscript on the relationship between running force and motion was resubmitted and accepted at the Journal of Experimental Biology
7) Preparation of a manuscript that presents our expanded, generalized model of walking metabolism has continued.
8) An analysis of standing metabolism is underway for a more in-depth understanding of the metabolic requirements for postural support.

January 2017 - April 2017

1) Manuscript preparation with ongoing analysis of the laboratory algorithm for walking metabolism took place.
2) Continued analysis of field data trials continued. This included smoothing of the GPS data and interpretation of the Cosmed portable metabolic system data.
3) Declined metabolic efforts continued.
4) Analysis of loaded running continued.

April 2017 - July 2017

1) Laboratory testing for extreme declines on an expanded subset of subjects has been identified as a need. Recruiting has commenced.
2) Analysis of field testing of loaded and unloaded walking metabolism has continued.
3) Modeling of the laboratory data base for walking metabolism for objective 1 continued.
4) Modeling efforts on our loaded running mechanics data for objective 2 continued.
5) Preparation of a manuscript that presents our expanded, generalized model of walking metabolism has continued and continued.
6) An analysis of standing metabolism is underway for a more in-depth understanding of the metabolic requirements for postural support continues.

July 2017 – October 2017

1) Analysis of field testing of loaded and unloaded walking metabolism has continued.
2) Modeling efforts on our loaded running mechanics data for objective 2 continued.
3) Preparation of a manuscript that presents our expanded, generalized model of walking metabolism has continued and continued.
4) Revision of our manuscript on predicting walking metabolism commenced after receiving reviews of the first submission.

5) Preparation of a provisional patent on our method of predicting walking energy expenditure is also in progress.

Oct 2017 – Jan 2018

1) Analysis of field testing of loaded and unloaded walking metabolism has continued.
2) Modeling efforts on our loaded running mechanics data for objective 2 continued.
3) A manuscript reporting our field testing of our walking metabolic model is in progress.
4) Analysis of stride mechanics data to assess the mechanical basis of our walking model has been engaged as a first part of a comprehensive evaluation.
5) A footwear test of our running mechanics model is being analyzed.
6) A video abstract of our November J Applied Physiology manuscript was completed and published online.

January 2018 - April 2018

1) Analysis of field testing of loaded and unloaded walking metabolism has continued.
2) Modeling efforts on our loaded running mechanics data for objective 2 continued.
3) A short manuscript using our running mechanics model to predict impact forces has been prepared, submitted and accepted at *Current Issues in Sport Sciences.*
4) A manuscript reporting our field testing of our walking metabolic model is in progress.
5) Reduction of stride mechanics data to assess the mechanical basis of our walking model has been completed. This required time-extensive quantification of foot-ground contact and stride times from 21 subjects on six grades under three load conditions. This will allow the mechanical basis of our model predicting walking metabolic rates to be assessed via ongoing analysis.
6) A footwear test of our running mechanics model is being analyzed.
7) A manuscript modeling the mechanics of maximal acceleration during running is now in progress.

April 2018 - July 2018

In the last quarterly period:

1) Analysis of field testing of loaded and unloaded walking metabolism has continued.
2) Modeling efforts on our loaded running mechanics data for objective 2 continued.
3) A manuscript reporting our field testing of our walking metabolic model is in progress.
4) Reduction of stride mechanics data to assess the mechanical basis of our walking model has been completed. This required time-extensive quantification of foot-ground contact and stride times from 21 subjects on six grades under three load conditions. This will allow the mechanical basis of our model predicting walking metabolic rates to be assessed via ongoing analysis.
5) A footwear test of our running mechanics model has been submitted to the journal of Royal Society Interface.
6) A manuscript modeling the mechanics of maximal acceleration during running has been submitted to the journal of biomechanics.

August 2018 – April 2019

In the last quarterly period:

1) Analysis and modeling of loaded and unloaded walking metabolism has continued.
2) Modeling efforts on our loaded running mechanics data for objective 2 continued. We are currently analyzing the effect of loading condition on ground force application to identify the determinants of the mechanics runners adopt under load conditions.
3) A manuscript reporting our field testing of our walking metabolic model continues to progress.
4) Analysis of our walking stride mechanics data for integration with our metabolic model has also continued.
5) A footwear test of our running mechanics model has been revised and resubmitted to the Journal of Applied Physiology.
6) A manuscript modeling the mechanics of maximal acceleration during running is being revised for resubmission to the journal of biomechanics and is currently in revision.

REPORTABLE OUTCOMES

Reportable outcomes follow directly from the key accomplishments listed for each quarter above. These were:

April 2014 – April 2015

1. We enrolled and tested 43 research subjects. Of these, 14 withdrew. Eleven of the withdrawals were voluntary, three were screen failures.
2. One hundred and eighty-eight test sessions were completed.
3. Nearly all of the loaded laboratory data acquisition for loaded walking was completed.
4. A portion of the loaded treadmill running data acquisition has been completed.
5. We have begun recruiting subjects for the unloaded portion of the treadmill walking protocol.
6. The data acquisition systems for the over-ground loaded running tests were set-up and validated. These preparations required hundreds of hours of technical work on force plate systems, motion capture systems, and timing systems.
7. The protocol for the loaded treadmill running tests has been modified to reduce the number of test sessions required.

8. The elaborate preparations needed to undertake the field walking studies were begun. These have included the refurbishing of our portable metabolic unit, the identification of field site, the identification of a GPS system that provides both vertical and horizontal position data.
9. Two manuscripts were accepted for publication: one each in the *Journal of Applied Physiology* and *Journal of Experimental Biology*.
10. An additional manuscript on our walking metabolism is in progress.

April 2015 – April 2016

1. We enrolled and tested 68 research subjects. Of these, 16 withdrew. Thirteen of the withdrawals were voluntary, three were screen failures.
2. Three hundred and thirty-two test sessions have completed to date.
3. All of the loaded laboratory data acquisition for loaded and unloaded walking has been completed.
4. Most of the loaded treadmill running data acquisition has been completed.
5. Overground running testing has been scheduled.
6. The preparations needed to undertake the field walking studies have been completed. Preliminary field testing has begun.
7. One manuscript has been accepted for publication in the *IEEE Biology and Medicine* section. One was accepted and was published in the *Journal of Experimental Biology*.
8. One manuscript has been submitted to the *American Journal of Physiology*.
9. An additional editorial manuscript has been submitted to the *Scandinavian Journal of Medicine and Science in Sports*.
10. Supported Personnel: Lindsay Ludlow, Jennifer Nollkamper, Kenneth Clark and Peter Weyand.

April 2016 – April 2017

1. Two subjects and ten field trials were tested during the last quarter. Eighteen test sessions were completed on the subjects enrolled.
2. Objective 2 testing on loaded running is no in the analysis phase.
3. Our level walking model manuscript published in the March issue of the Journal of Applied Physiology.
4. Two IEEE manuscripts are in preparation: one on loaded running, one of walking energy expenditure.
5. Two manuscripts were accepted for publication in IEEE Engineering and Medicine in Biology.
6. One manuscript was submitted to IEEE Journal of Biomedical and Health Informatics
7. Two subjects were tested during the last quarter, undergoing the complementary field and lab testing protocol.
8. Objective 2 testing on loaded running continues in the analysis phase.

9. Two IEEE manuscripts were presented at the Body Sensor Network Conference in San Francisco in June in preparation: one on loaded running and one on the metabolic cost of loaded walking.
10. Two manuscripts were accepted for publication in IEEE Engineering and Medicine in Biology.
11. One manuscript was revised for resubmission to the Journal of Experimental Biology.
12. Two subjects were tested to measure the metabolic requirements of walking on a series of steep declines.
13. Objective 2 testing on loaded running continues in the analysis phase.
14. Experimental plans and field sites have been identified to evaluate terrain influences and for field validations for loaded and unloaded trials on relatively flatter courses.
15. Two invention disclosures were submitted to SMU's Office of Research Administration.
16. One manuscript was accepted and is now in press at the Journal of Experimental Biology.
17. One manuscript is in preparation for submission to the Journal of Applied Physiology.
18. The laboratory work and algorithm continued in preparation for manuscript submission.
19. Analysis of loaded running data continued.
20. Analysis of field data and early stages of manuscript preparation began.
21. One invited lecture was delivered at the American College of Sports Medicine national conference in May.

<u>April 2017 - July 2017</u>

1. A manuscript introducing our multi-conditional model of walking metabolism was revised and re-submitted to the Journal of Applied Physiology.
2. Objective 2 testing on loaded running continues in the analysis phase.
3. Two invention disclosures were submitted to SMU's Office of Research Administration.
4. A provisional patent for a method for predicting walking metabolism continues to be prepared.
5. An invited keynote lecture on locomotor performance was delivered at the meeting of the International Society for Biomechanics in Sports.
6. Our walking metabolism manuscript was accepted and is in press at the *Journal of Applied Physiology*. A copy of the manuscript has been submitted with this report.

<u>April 2017 – April 2018</u>

1. A manuscript introducing our multi-conditional model of walking metabolism was accepted and has published at the Journal of Applied Physiology.
2. Objective 2 testing on loaded running continues in the analysis phase.
3. Two invention disclosures were submitted to SMU's Office of Research Administration.
4. A provisional patent for a method for predicting walking metabolism has been submitted.
5. Work on our running mechanics model has continued.
6. Data acquisition for downhill walking metabolism has continued to support our field validation effort.
7. Objective 2 testing on loaded running continues in the analysis phase.
8. Kinematic data analysis of our loaded walking data set has been completed.

9. Work on our running mechanics model has continued.
10. Model comparisons for our field walking trials are being implemented and analyzed as part of our manuscript preparation process.
11. Some acquisition of downhill walking data continues to finalize recommendations for field uses of our walking model.

April 2018 – April 2019

1. Objective 2 testing on loaded running continues in the analysis phase.
2. Kinematic data analysis of our loaded walking data set has been completed allowing integration of the stride mechanics data with our walking metabolic rate model (see Figure 1 below for data from one subject).
3. Work on our running mechanics model has continued.
4. Model comparisons for our field walking trials are being implemented and analyzed as part of our manuscript preparation process.
5. Some acquisition of downhill walking data continues to finalize recommendations for field uses of our walking model.

PUBLICATIONS, ABSTRACTS, PPRESENTATIONS

- Weyand P, Ryan L, Clark K (2014), Gait modification to increase sprint running speeds: acute, cross-sectional, and artificial considerations. World Congress of Biomechanics, Boston, MA.
- Clark K, Weyand P (2014), Is running speed maximized with spring-like stance mechanics, World Congress of Biomechanics, Boston, MA.
- Clark K, Ryan L, Weyand P. (2014), Foot-speed, fot-strike and footwear: linking gait mechanics and running ground reaction forces, Journal of Experimental Biology,
- Ludlow L & Weyand P, Energetics of level walking: a half century of literature data modeled for predictive accuracy, *American Journal of Physiology*, submitted.
- Ludlow L & Weyand P (2015), Energetics of walking: a loaded approach. *IEEE Biology & Medicine.* accepted/in press.
- Clark K, Weyand P, Sprint running research speeds up: a first look at the mechanic of elite acceleration, *Scandinavian Journal of Medicine and Science in Sports*, in review.
- Udofa A, Ryan L, Weyand P, Impact forces during running: loaded questions, sensible outcomes. *IEEE Body Sensor Network*, 2016.
- Ludlow L, Weyand P. Inclined walking energetics: body mass, loaded mass and predictability. *IEEE Body Sensor Network*, 2016.
- Ludlow L, Weyand P. Energy expenditure during level human walking: seeking a simple and accurate predictive solution, *Journal of Applied Physiology*, 120: 481-494.

- Ludlow L, Weyand P. Locomotor energy expenditure: a single algorithm for level walking with and without torso loads, *IEEE Journal of Biomedical and Health Informatics*, in revision.
- Clark K, Ryan L, Weyand P. A general relationship links gait mechanics and ground reaction forces, *Journal of Experimental Biology*, in revision.
- Calrk K, Weyand P. Sprint acceleration research speeds up: a first look at the mechanics of elite acceleration, *Scandinavian Journal of Medicine and Science in Sports*, 25(5): 581-582, 2015.
- Ludlow L, Weyand P. Predicting level walking energy expenditure, Oral Presentation at the Body Sensor Network Conference, June 2016, Cambridge, MA
- Udofa A, Ryan L, Weyand P, Impact forces during running: loaded questions, sensible outcomes. *IEEE Body Sensor Network*, pp 371-376, 2016.
- Ludlow L, Weyand P. Ludlow L, Weyand P. Estimating loaded, inclined loaded walking energetics: no functional difference between loaded mass and body mass, IEEE Body Sensor Network Conference, pp 306-311, 2016.
- Clark K, Ryan L, Weyand P. A general relationship links gait mechanics and ground reaction forces, *Journal of Experimental Biology*, published Vol 220: 347-258, 2017.
- Ludlow L, Weyand P. Estimating loaded, inclined loaded walking energetics: no functional difference between loaded mass and body mass, Oral Presentation at the Body Sensor Network Conference, June 2016, San Francisco, CA
- Udofa A, Ryan L, Weyand P, Impact forces during running: loaded questions, sensible outcomes. *IEEE Body Sensor Network*, pp 371-376, 2016.
- American College of Sports Medicine Annual National Meeting, May 31st, 2017, Denver, Colorado, *invited lecture*: "New insights into the limits of sprint running performance".
- Michael Johnson Performance Center, McKinney, TX, April 7th, 2017, *invited lecture*: "The mechanical basis of sprint running performance".
- Sloan School of Management Sports Analytics Conference, National Annual Meeting, Boston, MA, March 2nd, 2017, *invited lecture*: "Marathons, milestones, and moon shots: the science of human performance in the era of cheating".
- US Army Research Institute for Environmental Medicine Jan 27th, 2017, Natick MA, *invited lecture*: "Walking metabolism, from low to high to loaded".
- Running Summit Southwest, Dallas TX, December 16th, 2017, *invited lecture*: "Running performance from the ground up: a mechanical perspective."
- University of Texas Southwestern, School of Health Professions, November 16th 2016, *invited lecture*: "Artificial running performance from artificial limbs"
- Ludlow LW, Weyand PG. Walking economy is predictably determined by speed, grade and gravitational load, Journal of Applied Physiology, 123(5): 1288-1302.
- Clark K, Udofa A, Ryan L, Weyand P. Running impact forces: from half a leg to holistic understanding. *Current Issues in Sport Sciences*, in press.
- Weyand P. Force, motion, speed: a grounded perspective on human running performance. Proceedings of the International Conference on Biomechanics in Sports, July, 2017.

- Udofa A, Ryan L, Clark K, Weyand P. Ground reaction forces during competitive track events: a motion-based assessment method. *Proceedings of the International Conference on Biomechanics in Sports.* July, 2017.
- From Muybridge to Motion: The Physics of running ground force application. Invited lecture, Dickinson College, October, 2017.
- Weyand P. New insights into Sprint Running Performance, invited lecture, American College of Sports Medicine, National Meeting, Denver, may, 2017.
- Weyand, P. The mechanical basis of sprint running performance, Keynote address, International Conference of Biomechanics in Sports, Cologne, Germany, June, 2017.

CONCLUSIONS

Per the above reporting on outcomes and publication, we have met the objectives of the grant to develop and validate a new walking energy expenditure model that predicts walking metabolic rates across a broad range of speed, grade and load conditions. We have also developed and tested our running gait mechanics model that predicts all-out running speeds on the basis gait mechanics and ground force as well as duration. The work published has received significant international attention in the scholarly literature and popular media as well.

REFERENCES

Knapik, J.J., Harman, E. and Reynolds, K. (1996). Load carriage using packs: a review of physiological, biomechanical and medical aspects. *Appl Ergon*. **27**, 207–216.

Knapik, J.J., Reynolds, K.L. and Harman, E. (2004). Soldier load carriage: historical, physiological, biomechanical, and medical aspects. *Mil Med*. **169**, 45–56.

Knapik, J.J. and Reynolds, K. (2010). Load Carriage in Military Operations. Walter Reed Army Medical Center: *Borden Institute Monograph Series*, pp. 1-78.

Dean, C.E. (2004). *The Modern Warrior's Combat Load. Dismounted Operations in Afghanistan, April–May 2003*. Fort Leavenworth, Kansas: Army Center for Lessons Learned.

Givoni, B. and Goldman, R.F. (1971). Predicting metabolic energy cost. *J Appl Physiol*. **30**, 429–433.

Pandolf, K.B., Givoni, B. and Goldman, R.F. (1977). Predicting energy expenditure with loads while standing or walking very slowly. *J Appl Physiol*. **43**, 577–581.

Hoyt, R.W., Knapik, J.J., Lanza, J.F., Jones, B.H. and Staab, J.S. (1994). Ambulatory foot contact monitor to estimate metabolic cost of human locomotion *J Appl Physiol.* **76**, 1818-1822.

Hoyt, R.W. and Weyand, P.G. (1996). Advances in ambulatory monitoring: using foot contact time to estimate the metabolic cost of locomotion. In: *Emerging Technologies for Nutrition Research: Potential for Assessing Military Performance Capability,* edited by Mariott, B.M. and Carlson, S.J. Washington, DC: National Academy of Sciences, National Academy Press, pp. 315–343.

Hoyt, R.W., Buller, M., Santee, W., Yokota, M., Weyand, P. and Delany, J. (2004). Total Energy Expenditure Estimated Using Foot-Ground Contact Pedometry. *Diabetes Technol Ther*., **6**, 71-81.

Weyand, P.G., Kelly, M., Blackadar, T., Darley, J.C., Oliver, S.R., Ohlenbusch, N.E., Joffe, S.W and Hoyt, R.W. (2001). Ambulatory estimates of maximal aerobic power from foot -ground contact times and heart rates in running humans. *J Appl Physiol.* **91**, 451-458.

Kram, R. and Taylor, C.R. (1990). The energetics of running: a new perspective. *Nature* **346**, 2265–2267.

Margaria, R. (1968). Positive and negative work performances and their efficiencies in human locomotion. *Int Z Angew Physiol*. **25**, 339–351.

Minetti, A. E., Ardigo, L. P. and Saibene, F. (1994). Mechanical determinants of the minimum energy cost of gradient running in humans. *J. Exp Biol.* **195**, 211–225.

Minetti, A.E., Moia, C., Roi, G.S., Susta, D., and Ferretti, G. (2002). Energy cost of walking and running at extreme uphill and downhill slopes. *J Appl Physiol.* **93**, 1039-1046.

American College of Sports Medicine. (2006). *American College of Sports Medicine Guidelines for Graded Exercise testing and Prescription, 7th edition* (Lippincott, Williams & Wilkins, Philadelphia).

Alexander, R.M. (1976). Estimates of the speeds of dinosaurs. *Nature* **261**, 129-130.

Taylor, C.R., Heglund, N.C. and Maloiy, G.M. (1982). Energetics and mechanics of terrestrial locomotion. I. Metabolic energy consumption as a function of speed and body size in birds and mammals. *J Exp Biol.* **97**, 1-21.

Weyand, P., Smith, B., Puyau, M. and Butte, N. (2010). The mass-specific energy cost of human walking is set by stature. *J Exp Biol.* **213**, 3972-3979.

Alexander, R. M. (2003). *Principles of Animal Locomotion.* Princeton: Princeton University Press.

Bastien, G. J., Heglund N. C. and Schepens, B. (2003). The double contact phase in walking children. *J. Exp. Biol.* **206,** 2967-2978.

Das, S.K. and Saha, H. (1966). Climbing efficiency with different modes of load carriage. *Indian J Med Res* **54**, 866–871.

Duggan, A. and Haisman, M.F. (1992). Prediction of the metabolic cost of walking with and without loads. *Ergonomics* **35**, 417–426.

Falola, J.M., Delpech, N., Brisswalter, J. (2000). Optimization characteristics of walking with and without a load on the trunk of the body. *Percept Mot Skills* **91**, 261–272.

Griffin, T., Roberts, T.J. and Kram R. (2003). Metabolic cost of generating muscular force in human walking: insights from load-carrying and speed experiments. *J Appl Physiol.* **95**, 172-183.

Holewijn, M. (1990). Physiological strain due to load carrying. *Eur J Appl Physiol Occup Physiol* **61**, 237–245.

Martin, P.E. and Nelson, R.C. (1986). The effect of carried loads on the walking patterns of men and women. *Ergonomics* **29**, 1191–1202.

Pimental, N.A. and Pandolf, K.B. (1979). Energy expenditure while standing or walking slowly uphill or downhill with loads. *Ergonomics* **22**, 963–973.

Wanta, D.M., Nagle, F.J. and Webb, O. (1993). Metabolic response to graded downhill walking. *Med Sci Sport Exerc.* **25**, 159-162.

Taylor, C. R., Caldwell, S.L. and Rowntree, V.J. (1972). Running up and down hills: some consequences of size. *Science* **178**, 1096-1097.

Epstein, Y., Rosenblum, J., Burstein, R. and Sawka, M.N. (1988). External load can alter the energy cost of prolonged exercise. *Eur J Appl Physiol*. **57**, 243–247.

Patton, J.F., Kaszuba, J., Mello, R.P. and Reynolds, K.L. (1991). Physiological responses to prolonged treadmill walking with external loads. *Eur J Appl Physiol*. **63**, 89–93.

Santee, W.R., Allison, W.F., Blanchard, L.A. and Small, M.G. (2001). A proposed model for load carriage on sloped terrain. *Aviat Space Environ Med*. **72**, 562–566.

Hill, A.V. The physiological basis of athletic records. In: British Association for the Advancement of Science: Report of the 93rd Meeting, 1925, p. 156-173.

Rittweger, J., di Prampero, P.E., Maffulli, N. and Narici, M.V. (2009). Sprint and endurance power and ageing: and analysis of master athletic world records. *Proc Biol Sci.* **276**, 683- 689.

Bundle, M., Ernst, C., Bellizzi, M., Wright, S. and Weyand, P. (2006). A metabolic basis for impaired muscle force production and neuromuscular compensation during sprint cycling. *Am J Physiol Regul Integr Comp Physiol.*, **291**: R1457-R1464.

Usherwood, J.R. and Wilson, A.M. (2005). No force limit on greyhound sprint speed. *Nature* **438**, 753-754.

Usherwood, J.R. and Wilson, A.M. (2006). Accounting for elite indoor 200 m sprint results *Biol Lett* **2**, 47-50.

Chang, Y.H. and Kram, R. (2007). Limitations to maximum running speed on flat curves. *J Exp Biol* **210**, 971-982.

Weyand, P., Sternlight, D., Bellizzi, M. and Wright, S. (2000). Faster top running speeds are achieved with greater ground forces not more rapid leg movements. *J Appl Physiol.* **89**, 1991-2000.

Weyand, P., Lin, J. and Bundle, M. (2006). Sprint performance-duration relationships are set by the fractional duration of external force application. *Am J Physiol Regul Integr Comp Physiol.*, **290**, R758-R765.

Weyand, P., Sandell, R., Prime, D. and Bundle, M. (2010). The biological limits to running speed are imposed from the ground up. *J Appl Physiol.* **108**, 950-961.

Bangsbo, J. (1998). Quantification of anaerobic energy production during intense exercise. *Med Sci Sport Exerc* 30, 47-52.

Van Pragh, E. (2007). Anaerobic fitness tests: what are we measuring? *Med Sport Sci*, **50**, 26- 45.

Chang, Y., Huang, H. C., Hamerski, C. M. and Kram, R. (2000). The independent effects of gravity and inertia on running mechanics. *J. Exp. Biol.* **203**, 229-238.

Alcaraz, P. E., Palao, J. M., Elvira, J. L. and Linthorne, N. P. (2008). Effects of three types of resisted sprint training devices on the kinematics of sprinting at maximum velocity. *J Strength Cond Res*, **22**, 890-897.

Cronin, J. B., Hansen, K., Kawamori, N. and McNair, P. (2008). Effects of weighted vests and sled towing on sprint kinematics. *Sports Biomech*, **7**, 160-172.

Holewijn, M. and Lotens ,W.A. (1992). The influence of backpack design on physical performance. *Ergonomics*. **35**, 149–157.

Biewener A.A., Farley, C.T., Roberts, T.J. and Temanar, M. (2004). Muscle mechanical advantage of human walking and running: implications for energy cost. *J Appl Physiol.* **97**, 2266–2274.

APPENDICES

Please see the submitted manuscripts that follow.

Udofa A, Clark K, Ryan L, Weyand P. Running ground reaction forces across footwear conditions are predicted by the motion of two body mass components. *Journal of Applied Physiology*, 2019, **26**(5): 1315-1325, 2019.

Clark K, Udofa A, Ryan L, Weyand P. Impact forces during running: from half a leg to holistic understanding. *Current Issues in Sport Sciences*, **3**, 10711-10714, 2018.

Ludlow L, Weyand P. Walking economy is predictably determined by speed, grade and gravitational load. *Journal of Applied Physiology*, **123,** 1288-1302, 2017.

Clark K, Ryan L, Weyand P. A general relationship links gait mechanics and running ground reaction forces. *Journal of Experimental Biology*, **220**, 2: 247-258, 2017.

Udofa A, Ryan L, Weyand P. Impact forces: loaded questions, sensible outcomes, *IEEE Engineering and Medicine in Biology, Wearable and Implantable Body Sensor Networks*, July, 2016.

Ludlow L, Weyand P. Estimating loaded, inclined walking energetics: No functional difference between added and body mass. *IEEE Engineering and Medicine in Biology, Wearable and Implantable Body Sensor Networks*, July, 2016.

Ludlow L, Weyand P. Energy expenditure during level human walking: seeking a simple and accurate predictive solution, *Journal of Applied Physiology*, **120**, 5: 481-494, March, 2016.

Ludlow L, Weyand P. Walking energy expenditure: a loaded approach to predictive modeling. *IEEE, Wearable and Implantable Body Sensor Networks*, October, 2015.

Clark K, Weyand P. Sprint running research speeds up: a first look at the mechanics of elite acceleration. *Scandinavian Journal of Medicine and Science in Sports*, **25**(5): 581-582, 2015.

Clark K, Weyand P. Are sprint running speeds maximized with simple-spring stance mechanics? *Journal of Applied Physiology*, **117:** 604-615, 2014.

Clark K, Ryan L, Weyand P. Foot speed, foot-strike and footwear: linking gait mechanics to running ground reaction forces. *Journal of Experimental Biology*, **217:** 2037-2030, 2014.

Walking energy expenditure: a loaded approach to algorithm development

Lindsay W. Ludlow and Peter G. Weyand
Department of Applied Physiology and Wellness
Southern Methodist University
Dallas, TX, USA
pweyand@smu.edu

Sensor-based predictions for walking energy expenditure require sufficiently versatile algorithms to generalize to a variety of conditions. Here we test whether our height-weight-speed (HWS) model validated across speed under level conditions is similarly accurate for loaded walking. We hypothesized that increases in walking energy expenditure would be proportional to added load when resting metabolism was subtracted from gross walking metabolism. After subtracting resting metabolic rate, walking energy expenditure was found to increase in direct proportion to load at walking speeds of 0.6, 1.0, and 1.4 $m \cdot s^{-1}$. With load carriage treated as body weight, the predictive algorithms derived using the HWS model were similar for loaded and unloaded conditions. Determination of the direct relationship between load and energy expenditure for level walking provides insight which may be used to refine algorithms, such as the HWS model, for use in body sensors to monitor physiological status in the field.

Keywords—load carriage, sensors, generalized equation, algorithm, metabolism

I. INTRODUCTION

Prediction and monitoring of whole-body energy expenditure depends heavily on the accuracy of the algorithms utilized. For individuals at rest, algorithms that accurately predict metabolic rates from body size, sex, and age have been established for decades [1]. For individuals during locomotion, however, the algorithms currently available are not equivalently accurate [2,3]. Prediction of the latter is considerably more difficult because of the many factors that influence the extent to which whole-body metabolism is elevated during locomotion. These include but are not limited to: height, weight, speed, grade, terrain, and load carriage.

Recent work indicates that whole-body locomotor metabolism can be predicted accurately under certain controlled conditions. Specifically, we found that walking metabolic rates on firm, level surfaces could be predicted to within 8% if the height, weight, and speed of the walker are known. Thus, under these controlled conditions, sensors capable of [4,5] providing walking speed could be used in conjunction with height and weight to accurately estimate whole-body metabolic rates. Here, under the same conditions, we test whether our existing HWS algorithm can similarly describe walking metabolic rates when torso loads are carried.

Theoretically, the existing HWS model might accurately account for loaded metabolic rates if the added load is treated as additional body weight in the existing equation. A critical issue for considering this possibility is the method used to partition the body's total metabolic rate into resting vs. walking portions. A common approach has been to subtract a standing metabolic rate to represent the resting component [7,8]. However, during quiet standing, metabolic rates have been reported to be 1.15 – 1.5 times greater than those obtained during a traditional supine resting measurement (RMR) [8,9,10,11,12,13]. The variability in standing metabolic rates may explain some of the inconsistency thus far reported in the metabolic responses to walking with loads when the former is the baseline quantity subtracted. While the general consensus has been that metabolic rates increase in proportion to the load carried, results have been somewhat variable [12,14,15].

Here, we used the elevations in locomotor metabolic rates introduced by load carriage as an experimental tool for two purposes. Our first objective was to investigate whether the elevations in locomotor metabolic rates (gross – supine rest) would be directly proportional to loads added to the torso. A direct relationship would allow the influence of added loads on locomotor metabolism to be more easily predicted and modeled. After quantifying the relationship between walking energy expenditure and load, our second objective was to determine if the HWS model would accurately predict unloaded and loaded metabolic rates. If so, the HWS model would provide a robust algorithm for sensor development with potential to determine walking metabolic rate under multiple conditions. We specifically tested the following corresponding hypotheses. First, we hypothesized that the net energy expended while walking (gross – supine rest) would increase in direct proportion to the load carried. Second, we hypothesized that the independent equations derived in the form of the HWS model would be similar for loaded and unloaded conditions.

II. METHODS

A. Experimental Design

To test whether locomotor energy expenditure increases in proportion to added torso load we measured metabolic rate under three conditions: unloaded (i.e. body weight only, W_b), and two added load conditions equaling 1.17 W_b, and 1.31 W_b. We utilized metabolic data acquired from all three load conditions, as well as metabolic rates during supine rest and quiet standing, to assess the influence of the baseline quantity subtracted. Using supine rest as our baseline subtraction

This work was made possible by grant DAMD17-03-2-005 and award W81XWH-12-2-0013 from the Medical and Materiel command of the United States DOD.

978-1-4673-7201-5/15/$31.00 ©2015 IEEE

quantity, we assessed whether walking metabolic rates increased in direct proportion to the loads carried.

B. Subjects

Ten volunteer subjects, 5 male and 5 female (means ± SEM, age = 29.6 ± 1.4 years, height = 171.6 ± 2.2 cm, mass = 67.0 ± 2.9 kg) participated in the study after providing written informed consent in accordance with the Institutional Review Board of Southern Methodist University. All subjects were healthy and did not have cardiovascular risk factors as a contraindication for exercise according to the guidelines set forth by the American College of Sports Medicine. Subjects reported to the laboratory on eight different days for testing sessions consisting of a VO_{2max} test, 6 sessions of loaded and unloaded walking, and a final session for measurement of metabolic rate during supine rest, and quiet standing. For the final session, subjects were instructed to arrive at the laboratory immediately after waking, to avoid exercise prior to testing and refrain from eating and caffeine use for eight hours prior.

C. Gross Metabolic Rates

Metabolic rates were determined from indirect calorimetry through the measurement of expired gases during supine resting, quiet standing, and walking at three different treadmill speeds and under three different load conditions (no load, ~15% of body weight, ~30% of body weight) using a computerized metabolic system (Parvo Medics TrueOne 2400, Sandy, UT, USA). A one-way breathing valve and tubing were used to collect expired gases and direct flow through a pneumotach, which measured volume flow rates, and into a mixing chamber. Aliquots of expired air were sampled from the mixing chamber and analyzed for O_2 and CO_2 fractions using paramagnetic and infrared gas analyzers, respectively. Data were collected continuously, with rates of oxygen uptake averaged over a two minute period under steady-state conditions. Resting metabolic rates were determined from the lowest 10-minute average during a 30-minute, supine resting trial. The lowest five minute average during the final 10 minutes of a 15-minute trial was used to determine standing metabolic rate.

D. Treadmill Testing Protocol

Walking bouts were conducted on a level treadmill at speeds of 0.6, 1.0, and 1.4 $m \cdot s^{-1}$. All speeds were completed under the following loaded conditions: unloaded, carrying ~15% body weight, and carrying ~30% bodyweight. Subjects were weighed on their first visit to the laboratory and assigned a loading scheme based on their weight rounded to the nearest ten pound increment. Therefore the exact percentage of body weight carried varied slightly from 15% and 30% for some subjects, with the average actual percent body weight across the 10 subjects coming out to 17% and 31% for the two different load carriage conditions. For the loaded trials, weight was carried both on the front in a vest and on the back in a backpack and was symmetrically distributed about the torso. For each condition, walking trials lasted for five minutes to ensure that the final two minutes were under steady-state conditions. All loaded conditions and walking speeds were repeated on two separate days, and the average of the steady-state values from the two trials was taken to determine gross energy expenditure.

E. Relationship Between Load and Metabolic Rate

Net metabolic rate was calculated by subtracting supine resting energy expenditure from gross energy expenditure while walking. In order to determine whether metabolic rate increases in direct proportion to the mass of the load carried we calculated the ratio of energy expenditure while loaded ($E_{metab\ L}$) to energy expenditure unloaded ($E_{metab\ U}$) at all walking speeds for both gross and net metabolic rates. We then plotted these values against the ratio of total mass (M_{Total}) to body mass (M_{Body}) for each walking speed.

F. Height-Weight-Speed Model Equation Derivations

Walking metabolic rates were estimated using the previously published HWS model [6]. The HWS model is comprised of three components: a resting metabolic rate (RMR), a minimum walking metabolic rate which is modeled as a multiple of RMR, and a speed-dependent metabolic rate, as shown by equation 1 below.

$$VO_2 = RMR + C_1 \cdot RMR + C_2 \cdot V^2 \cdot height^{-1} \quad \text{(eq. 1)}$$

All of the terms for the HWS model were derived and are reported in mass-specific units of oxygen uptake in $ml \cdot kg^{-1} \cdot min^{-1}$. However, illustrated metabolic rates are presented in SI units ($W \cdot kg^{-1}$).

For the present study, the coefficients C_1 and C_2 were derived to obtain a best fit to the data set. Optimized coefficients were obtained for the unloaded and loaded conditions alone, as well as with the unloaded and loaded conditions combined. The optimizer function in Excel was used to determine the values of C_1 and C_2 such that the sum squared error was minimized. The Excel optimizer (Microsoft Excel Solver, Excel 2010 version) was chosen due to its ability to optimize a coefficient while holding other values (resting metabolic rate, walking speed, and subject height) constant [16]. Once the forms of the equations were derived they were used to describe walking metabolic rates for each subject across all walking speeds and load conditions. The R^2 values for measured versus predicted values, as well as the standard error of estimate (SEE) were calculated for each equation. An accurate model fit was evaluated using the criteria of a value for SEE of less than 10% of the grand mean.

III. Results

A. Gross Metabolic Rates

The mean standing metabolic rate was 1.1 times greater than the mean for supine rest (1.16 ± 0.03 vs. 1.27 ± 0.04 $W \cdot kg^{-1}$; Fig. 1). Between-subject variability was appreciable, with standing values ranging from 1.03 to 1.19 times greater than respective supine resting values. The difference between metabolic rate during supine rest and during quiet standing varied for most, but not all subjects, as several subjects had essentially the same values under the two conditions (Fig. 2).

Walking metabolic rates increased across walking speeds under all three load conditions (Fig. 1). Further, load carriage resulted in an increase in walking energy expenditure at all walking speeds that was in direct proportion to the load carried (Fig. 1).

978-1-4673-7201-5/15/$31.00 ©2015 IEEE

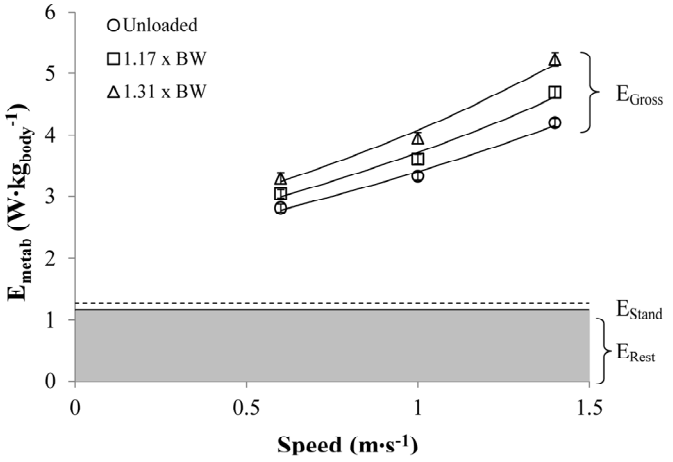

Fig. 1. Mass-specific gross metabolic rate (E_{metab}) increases with walking speed under all three load conditions. E_{metab} is plotted for walking without load, walking with a load equal to ~17% of body weight, and with a load of ~31% of body weight. On the y-axis, the value for kilograms includes the weight of the subject plus the weight of the load carried (kg_{total}^{-1}). Metabolic rate during quiet standing and during supine rest are depicted as constants.

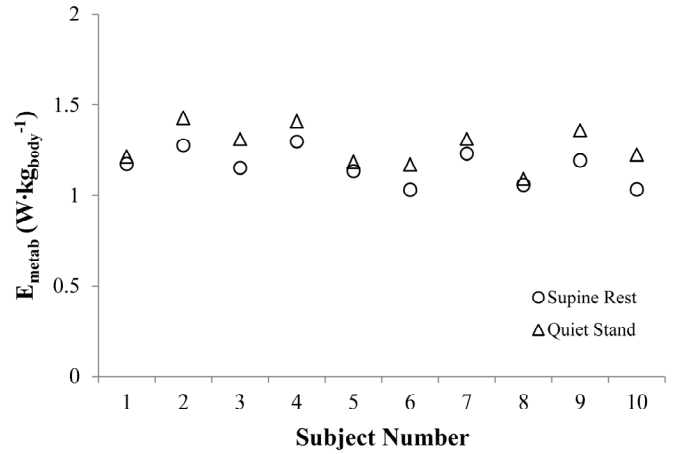

Fig. 2. Individual mass-specific gross metabolic rates (E_{metab}) during supine rest and quiet standing. Subjects are represented on the graph in ascending order of body mass from 52.2 to 82.8 kg.

B. Relationship Between Load and Metabolic Rate

Across all walking speeds, increases in gross metabolic rates in the loaded conditions were not proportional to the loads carried (Fig. 3). However, increases in net walking metabolic rates under loaded conditions were almost exactly proportional to the load carried as hypothesized. When subtracting energy expenditure for supine rest to calculate net metabolic rate, we found that walking energy expenditure increased in proportion to load carried across all three walking speeds (Fig. 3). For example, at 1 $m \cdot s^{-1}$, when subjects carried a load that was 31% greater than their body weight, gross metabolic rate only increased by 19%, whereas net metabolic rate increased by 29%.

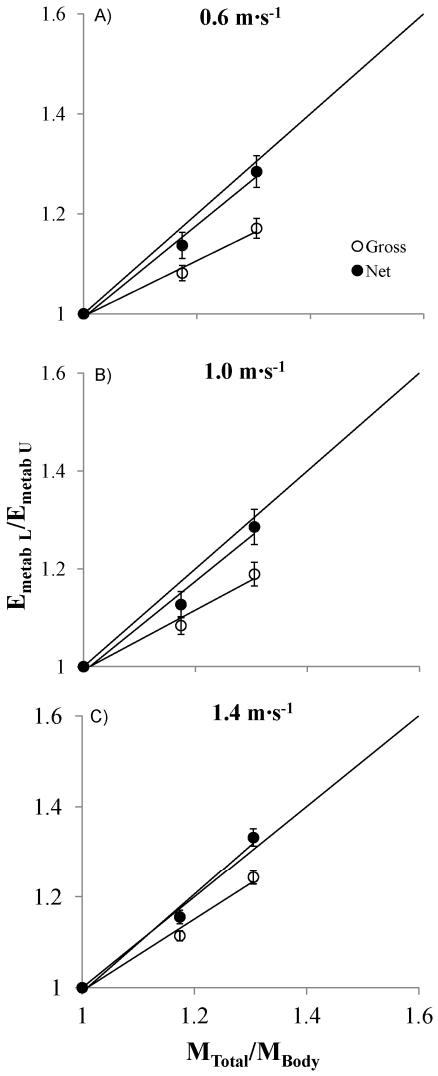

Fig 3. Net metabolic rate increases in direct proportion to load carried. Panels A-C depict the ratio of metabolic rate while carrying load ($E_{metab\ L}$) to metabolic rate while unloaded ($E_{metab\ U}$) plotted against the ratio of total mass (body mass + load; M_{Total}) to body mass (M_{body}). Gross metabolic rate and net metabolic rate are plotted for walking speeds of 0.6 (Panel A), 1.0 (Panel B), and 1.4 $m \cdot s^{-1}$ (Panel C). The diagonal line indicates direct proportionality between the X and Y values such that metabolic rate is proportional to the mass of the load carried.

C. HWS Model Predictions of Walking Energy Expenditure

The optimized HWS model coefficients for the unloaded, loaded, and all three load conditions combined appear in Table 1. The unloaded, loaded, and combined loaded and unloaded model derivations produced similar values for both coefficients in the HWS model equation. Further, using the three optimized equations to provide best fits of the data produced similar values for R^2 and standard error of estimate (SEE). For the optimized HWS model on the unloaded data, an R^2 of 0.91 and SEE of 0.52 mls $O_2 \cdot kg^{-1} \cdot min^{-1}$ were attained (Table 1). For the loaded data, the optimized equation resulted in a best fit with an R^2 of 0.85 and SEE of 0.72 mls $O_2 \cdot kg^{-1} \cdot min^{-1}$ (Table 1). When loaded and unloaded conditions were combined, the optimized HWS model fits produced an R^2 of 0.84 and SEE of 0.74 mls $O_2 \cdot kg^{-1} \cdot min^{-1}$ (Table 1). For all three equations, the

978-1-4673-7201-5/15/$31.00 ©2015 IEEE

SEE was less than 10% of the grand mean, thus meeting our criteria for model accuracy,

Model	C_1	C_2	exponent	R^2	SEE
Unloaded	1.00	4.37	2	0.91	0.52
Loaded	0.76	4.56	2	0.85	0.72
Unloaded + Loaded	0.84	4.49	2	0.84	0.74

Table 1. Empirical Derivations of the Height-Weight-Speed Model Equation with all metabolic units, including SEE, expressed in mls $O_2 \cdot kg^{-1} \cdot min^{-1}$.

IV. Discussion

Our first finding was that the energy expended for level walking, when determined as the quantity: (gross – supine rest), increases in direct proportion to the load carried. We found direct proportionality across all three speeds and the two load conditions we tested. This finding is of particular importance as it allows for added torso load to be directly incorporated into predictive algorithms for walking metabolism. Second, as hypothesized, we found that the HWS model provided accurate descriptions of walking metabolic rate both with and without load. The independent equations derived in the form of the HWS model for loaded and unloaded conditions (Table 1) were nearly identical.

A. Baseline Subtractions

Metabolic rates measured during quiet standing are commonly utilized as a baseline subtraction quantity in order to determine net walking metabolic rates. However, the typical elevations observed in the energy expended in the standing vs. supine resting condition (Fig. 1) seem likely to result from the muscular activation required for postural support [17,18,19]. Accordingly, standing metabolism seems unlikely to generally represent the body's true resting metabolic rate. Moreover, subtracting standing rates from the gross metabolic rates measured during walking risks subtracting out a portion of the metabolic energy expended to support the body's weight against gravity while walking. In light of the substantial evidence of a relationship between weight supported and walking energy expenditure across studies of load carriage [12,14,15], obesity [11], and weight loss [20] the use of standing metabolic rate as a standard baseline subtraction measure should be carefully considered in accordance with experimental objectives. If the objective is the most valid partitioning of the resting vs. walking portions of the body's gross locomotor metabolic rates, our results suggest supine resting values are likely to provide a more valid baseline quantity than quiet standing for doing so.

The above conclusion is based in part upon the individual variability observed in standing metabolic rate values. When our measured standing values were expressed in relation to supine resting values, the elevations observed for different individuals ranged from 1.03 to 1.19 times the latter value. The variability observed raises the possibility that quiet standing may include a skill component that influences the extent of the elevations observed above supine rest. At present, the correct interpretations of measured standing metabolic rates, both in general and as a baseline subtraction quantity, are not fully clear.

B. Load Carriage and Energy Expenditure

As hypothesized, we found that walking metabolic rates (gross - supine rest) increased in close proportion to the loads carried and regardless of speed. Across the three speeds and two loading conditions included here, the mean deviation from the direct proportionality expected was 1.6 ± 0.85%. Others have reported previously that when net metabolic rates are determined by subtracting standing metabolism from gross walking metabolism, metabolic rate to increase in a fashion that is greater than proportional to load carriage [12]. We found the standing metabolic rate values to be larger than resting metabolic rate, thus load-induced increases in metabolic rate would also be greater than the added load using the standing metabolic rate subtraction. Our data are consistent with a multitude of prior experimental results indicating that the primary determinant of locomotor metabolic rates is the weight that must be supported against gravity, whether the body's weight only or the body's weight plus an external load [21,22].

C. Estimating Walking Energy Expenditure

While numerous equations have been derived to predict walking energy expenditure, the accuracy many of these equations under conditions such as load carriage is not known [6]. Predictive accuracy is of critical importance in order for algorithms for walking energy expenditure to be incorporated into sensor technologies. In the set of ten subjects presented here, the optimized HWS model provides accurate (SEE < 10% of grand mean) descriptions of walking metabolism across a range of walking speeds both with and without load carriage. Our data indicate that the HWS model is an attractive candidate for use in body sensor devices to estimate walking energy expenditure.

D. Conclusions and Recommendations

Our results indicate that level walking metabolic rates increase in close proportion to added torso loads across a range of speeds and loads up to nearly one-third of the body's weight. This finding should simplify the incorporation of torso loads into predictive equations for sensor-based and other field applications. Accurate determination of the relationship between load carriage and energy expenditure is of particular military importance to predicting and monitoring the performance of soldiers in the field, and also for the general population seeking accurate methods for quantifying energy expenditure during exercise that involves load carriage (e.g. weighted vest, backpacking). Additional efforts will be needed to expand predictive capabilities to include additional load, grade and terrain conditions.

Acknowledgments

We thank Jennifer Nollkamper and Emily Field for their help in subject recruitment and data collection.

References

[1] W.N. Schofield. "Predicting basal metabolic rate, new standards and review of previous work," Hum. Nutr. Clin. Nutr., vol. 39, Supp. 1, pp. 5-41, 1985.

[2] American College of Sports Medicine Guide to Exercise Testing and Prescription, 6th edition, Lippincott, Williams & Wilkins, 2000.

[3] K. Pandolf, B. Givoni, and R.K. Goldman, "Predicting energy expenditure with loads while standing or walking very slowly," J. Appl. Physiol., vol. 43, pp. 577-581, 1977.

[4] R.W. Hoyt, J.J. Knapik, J.F. Lanza, B.H. Jones, and J.S. Staab. "Ambulatory foot contact monitor to estimate metabolic cost of human locomotion," J. Appl. Physiol., vol. 76, pp. 1818-1822, 1994.

[5] P.G. Weyand et al. "Ambulatory estimates of maximal aerobic power from foot-ground contact times and heart rates in running humans," J. Appl. Physiol., vol. 91, pp. 451-458, 2001.

[6] P.G. Weyand, B.R. Smith, N.S Schultz, L.W. Ludlow, M.R. Puyau, and N.F. Butte. "Predicting metabolic rate across walking speed: one fit for all body sizes?," J. Appl. Physiol., vol. 115, pp. 1332-1342, 2013.

[7] J.M. Donelan, R. Kram, and A.D. Kuo. "Mechanical work for step to step transitions is a major determinant of the metabolic cost of human walking," J. Exp. Biol., vol. 205, pp. 3717-3727, 2002.

[8] D.J. McCann and W.C. Adams. "A dimensional paradigm for identifying the size-independent cost of walking," Med Sci. Sports Exerc., vol. 34, pp 1009-1017, 2002.

[9] V.T. Inman, H.J. Ralston, and F. Todd, Human Walking. Baltimore, MD, Williams & Wilkins, 1981.

[10] D. DeJaeger, P.A. Willems, and N.C. Heglund, "The energy cost of walking in children," Pflügers Arch. Eur. J. Physiol., vol. 441, pp. 538-543, 2001.

[11] R. C. Browning, E. A. Baker, J. A. Herron, and R. Kram, "Effects of obesity and sex on the energetic cost and preferred speed of walking," J. Appl. Physiol., vol. 100, pp. 390-398, 2006.

[12] T.M. Griffin, T.J. Roberts, and R. Kram, "Metabolic cost of generating muscular force in human walking: insights from load-carrying and speed experiments," J. Appl. Physiol., vol. 95, pp. 172-183, 2003.

[13] P.G. Weyand, B.R. Smith, and R.F. Sandell. "Assessing the metabolic cost of walking: the influence of baseline subtractions," Conf. Proc. IEEE Eng. Med. Biol. Soc., pp. 6878-6881, 2009.

[14] R.F. Goldman, and P.F. Iampietro. "Energy cost of load carriage," J. Appl. Physiol., vol. 17, pp. 675-676

[15] G. J. Bastien, P.A. Willems, B. Schepens, and N.C. Heglund, "Effect of load and speed on the energetic cost of human walking," Eur J. Appl. Physiol. vol. 94, pp. 76-83, 2005.

[16] D. Fylstra, L. Lasdon, J. Watson, and A. Waren. "Design and Use of the Microsoft Excel Solver," Interfaces. vol. 28, pp. 29-55, 1998.

[17] J.V. Basmajian and C. De Luca, "Muscles Alive: Their Functions Revealed by Electromyography," Williams & Wilkins, Baltimore, 1985.

[18] J. Joseph and A. Nightingale, "Electromyography of posture: leg muscles in males," J. Physiol. vol. 117, pp. 484-491, 1952.

[19] I .D. Loram, C.N. Maganaris and M. Lakie, "The passive, human calf muscles in relation to standing: the non-linear decrease from short range to long range stiffness," J. Physiol., vol. 584, pp. 661-675, 2007.

[20] G. R. Hunter, J. P. McCarthy, D.R. Bryan, P.A. Zuckerman, M.M. Bamman, and N.M. Byrne, "Increased strength and decreased flexibility are related to reduced oxygen cost of walking," Eur. J. Appl. Physiol., vol. 104, pp. 895-901, 2008.

[21] R. Kram, and C.R. Taylor. "Energetics of running: a new perspective," Nature, vol. 346, pp. 265-267, 1990.

[22] C.R. Taylor. "Relating mechanics and energetics during exercise," Adv. Vet. Sci. Comp. Med., vol. 38A, pp. 181-215, 1994.

978-1-4673-7201-5/15/$31.00 ©2015 IEEE

J Appl Physiol 120: 481–494, 2016.
First published December 17, 2015; doi:10.1152/japplphysiol.00864.2015.

Energy expenditure during level human walking: seeking a simple and accurate predictive solution

Lindsay W. Ludlow and Peter G. Weyand

Southern Methodist University, Locomotor Performance Laboratory, Department of Applied Physiology and Wellness, Dallas, Texas

Submitted 9 October 2015; accepted in final form 7 December 2015

Ludlow LW, Weyand PG. Energy expenditure during level human walking: seeking a simple and accurate predictive solution. *J Appl Physiol* 120: 481–494, 2016. First published December 17, 2015; doi:10.1152/japplphysiol.00864.2015.—Accurate prediction of the metabolic energy that walking requires can inform numerous health, bodily status, and fitness outcomes. We adopted a two-step approach to identifying a concise, generalized equation for predicting level human walking metabolism. Using literature-aggregated values we compared *1*) the predictive accuracy of three literature equations: American College of Sports Medicine (ACSM), Pandolf et al., and Height-Weight-Speed (HWS); and *2*) the goodness-of-fit possible from one- vs. two-component descriptions of walking metabolism. Literature metabolic rate values (n = 127; speed range = 0.4 to 1.9 m/s) were aggregated from 25 subject populations (n = 5-42) whose means spanned a 1.8-fold range of heights and a 4.2-fold range of weights. Population-specific resting metabolic rates ($\dot{V}O_{2rest}$) were determined using standardized equations. Our first finding was that the ACSM and Pandolf et al. equations underpredicted nearly all 127 literature-aggregated values. Consequently, their standard errors of estimate (SEE) were nearly four times greater than those of the HWS equation (4.51 and 4.39 vs. 1.13 ml $O_2 \cdot kg^{-1} \cdot min^{-1}$, respectively). For our second comparison, empirical best-fit relationships for walking metabolism were derived from the data set in one- and two-component forms for three $\dot{V}O_2$-speed model types: linear ($\propto V^{1.0}$), exponential ($\propto V^{2.0}$), and exponential/height ($\propto V^{2.0}/Ht$). We found that the proportion of variance (R^2) accounted for, when averaged across the three model types, was substantially lower for one- vs. two-component versions (0.63 ± 0.1 vs. 0.90 ± 0.03) and the predictive errors were nearly twice as great (SEE = 2.22 vs. 1.21 ml $O_2 \cdot kg^{-1} \cdot min^{-1}$). Our final analysis identified the following concise, generalized equation for predicting level human walking metabolism: $\dot{V}O_{2total} = \dot{V}O_{2rest} + 3.85 + 5.97 \cdot V^2/Ht$ (where V is measured in m/s, Ht in meters, and $\dot{V}O_2$ in ml $O_2 \cdot kg^{-1} \cdot min^{-1}$).

walking economy; generalized equation; algorithm; exercise metabolism; wearable sensors

THE METABOLIC ENERGY THAT WALKING requires can be accurately measured, but it is difficult to predict in the absence of direct measurement. Two factors have prompted extensive efforts to develop predictive equations: the fundamental importance of walking metabolism to the body's health, fitness, and physiological status, and the impracticality of direct measurement under most circumstances. The large majority of the many predictive equations that currently exist were developed on small, homogeneous populations using best-fit approaches. This includes the two leading standardized equations (3, 36) that have been heavily used since their original formulations decades ago. Accordingly, the large majority of existing equations have not been validated beyond the test populations on whom they were developed, and many have not been validated at all. With the advent of affordable, wearable sensors capable of incorporating predictive algorithms, the importance and potential application of these algorithms have arguably never been greater. Nonetheless, a comprehensive assessment of the relative accuracy, or lack thereof, of the algorithms that currently exist is largely unavailable.

The two most established and commonly used predictive equations, the American College of Sports Medicine (ACSM) (3) and Pandolf et al. (36) equations, respectively, were developed using very small, homogeneous populations of adult men. Each partitions the body's total or gross, mass-specific metabolic rate during walking into resting and nonresting components, quantifying the latter as a single, speed-dependent component. However, they differ formulaically in how they do so: the ACSM equation quantifies the relationship between walking speed and metabolic rate as a linear function, whereas the Pandolf et al. equation uses an exponential description. The former equation is heavily used throughout health, fitness, and clinical communities; the latter is heavily used for military purposes. To date, independent assessments of the accuracy of these standard equations have been surprisingly limited given their broad acceptance and widespread use. Consequently, their general accuracy, the predictive consequences of their different mathematical forms, and their ability to generalize to populations other than adult men of average stature are largely unknown.

We recently formulated a model with potentially broader applicability to human walking metabolism. Our approach deviated from the long-standing practice of testing populations that are homogeneous with respect to both age and body size (3, 9, 16, 36, 48). We did so because our earlier work indicated that age, long considered to be a factor explaining the elevated metabolic requirements of children, has no quantifiable effect when body size and related gait mechanics are taken into account (49). Hence we used body size stratification as an experimental tool for model development to maximize the generalizability of our model. Formulaically, the Height-Weight-Speed (HWS) model that resulted, like the Pandolf et al. model, describes the metabolic rate vs. speed relationship as exponential, but it does so with two features that differ from literature norms (Fig. 1). The first is that walking metabolism is partitioned into two components: one that is primarily postural and constant across speed, and a second that is speed-dependent. The second differentiating feature is that the term describing speed-dependent increases in walking metabolic rates includes an inverse relationship to stature (V^{exp}/Ht).

Address for reprint requests and other correspondence: P. Weyand, Locomotor Performance Laboratory, Dept. of Applied Physiology and Wellness, Southern Methodist Univ., 5538 Dyer St., Dallas, TX 75206 (e-mail: pweyand@smu.edu).

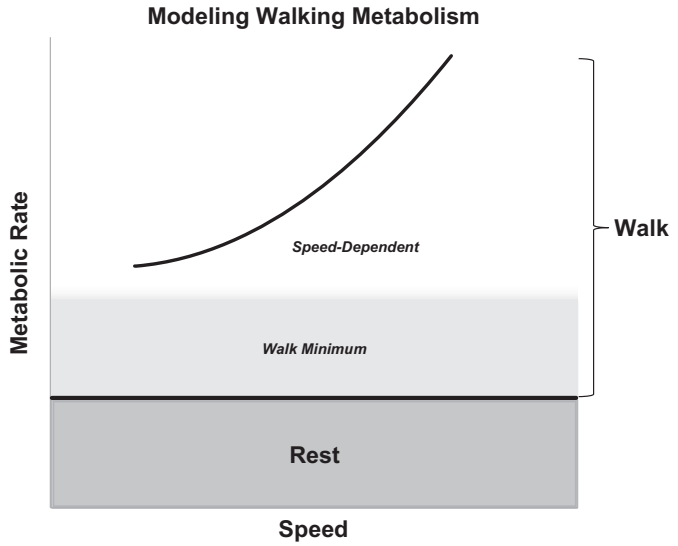

Fig. 1. A schematic representation of the metabolic rate vs. walking speed relationship illustrating how the body's total metabolic rate can be partitioned into one resting ($\dot{V}O_{2rest}$), and two walking components per the Height-Weight-Speed (HWS) model [according to (51)]. In the HWS model, walking metabolic rates are the sum of a minimum walking rate ($\dot{V}O_{2Walk\ Minimum}$) and a speed-dependent walking rate ($\dot{V}O_{2Speed\text{-}Dependent}$). Alternatively, the walking portion of the body's total metabolic rate can be modeled as a single metabolic component. Per physiological convention, metabolic rates are presented as rates of oxygen uptake throughout the manuscript.

This second feature quantifies the economizing influence of stature on walking metabolism (15, 18, 31, 33, 49, 51).

In our original study, these features apparently allowed our HWS model to achieve greater overall accuracy than either the ACSM or Pandolf et al. models for the level condition investigated. For our sample of 78 subjects who varied substantially in body size (derivation group, $n = 39$; validation group, $n = 39$), the HWS model was able to predict measured metabolic rates to within an average of 8.1 ± 6.7%. Additionally, we found the predictive error of the HWS model to be one-third that of the two older standardized equations on our validation-group subjects, and less than half that when only larger or adult subjects were assessed. These results raised several questions regarding the basis of the predictive accuracy originally observed for our HWS model. First, from a technical standpoint, the relative accuracy of the HWS model was likely overrepresented because we evaluated our own model, but not the other two, with data acquired under identical conditions with the same instrumentation. Second, from a scientific standpoint, our original study did not reveal the extent to which the largely distinct features of the HWS model were responsible for the greater predictive accuracy achieved. Specifically, we did not know the predictive importance of *1*) the addition of a second metabolic component for walking metabolism, and *2*) the incorporation of height into predictions of speed-dependent increases in walking metabolic rates.

Our overall goal was to identify a concise, broadly accurate equation for predicting metabolic rates during level human walking. For this purpose, we used the existing literature to compile a data set that was well-stratified with respect to both the walking speeds and body sizes of the subject populations included. We used this data set to pursue our overall objective in two analytical steps. First, we assessed how accurately the aforementioned three equations were able to predict the fully independent metabolic rate values in the literature data set. Second, we used the different mathematical forms of these three equations to identify the elements that are essential for broad, accurate prediction. This included specifically evaluating whether the total or gross walking metabolic rates in the data set would be more accurately described when the walking, or nonresting portion, of the body's total metabolic rate consisted of two components rather than one. Accordingly, we formulated both one- and two-component versions of three $\dot{V}O_2$-speed model types: linear ($\propto V^{1.0}$), exponential ($\propto V^{2.0}$), and exponential with an inverse relationship to height ($\propto V^{2.0}/Ht$).

Our first hypothesis was that the error of the HWS model equation in predicting the literature data set values would be less than half that of both the ACSM and Pandolf et al. equations. Our second hypothesis was that accounting for 90% of the total data set variability would be possible when walking metabolism was quantified with two components, but not possible when quantified with only one.

METHODS

Experimental Design

We adopted a literature compilation approach to evaluating the relative accuracy with which formulaically different models predict human walking metabolism for several reasons. First, the existing literature is now sufficiently expansive to comprehensively incorporate the influences of height, weight, and speed on level walking metabolic rates. Second, the aggregation of means from many studies should mitigate measurement or condition-specific error from individual studies. Finally, contemporary digitizing techniques allow data published in graphic form to be extracted with a high degree of accuracy (21, 43). Collectively, these factors should allow for the aggregation of a robust, powerful data set for investigating our two hypotheses regarding energy cost of level human walking.

Hypothesis Tests One and Two

Based largely on the prior results reported on 78 individuals who spanned a broad range of body sizes (51), we expected two hypothesis test outcomes. First, we expected that the error with which the aggregated literature means would be predicted by the ACSM and Pandolf et al. equations would be at least two times larger than the corresponding error of prediction of the HWS model equation using the standard error of estimate (SEE) as our evaluative standard. Second, we expected that the SEE would, on average, be at least twice as large when the walking portion of the body's total metabolic rate was modeled with one component rather than two. Furthermore, as general evaluative standards for whether each model was able to fit to the aggregated data set well, we set a priori thresholds of ≥90% of the total data set variance explained and ≤10% error in the accuracy of the estimates of individual data set values. These thresholds were set in accordance with our expectation that an accurate model should *1*) account for 90% of the total variability in the data set and *2*) have a predictive error of less than 10% of the grand mean of the 127 values in the data set. The first threshold was quantified using the R^2 statistic, the second using the coefficient of variation, here calculated using the SEE divided by the grand mean of the values ($n = 127$) in the data set (i.e., SEE/grand mean × 100).

Data Set Criteria

Our literature data set was strategically aggregated to broadly encompass the influences of height, weight, and speed on human walking metabolism. However, we did not seek to acquire all the valid

data available from the literature. We avoided this because doing so would have skewed the data set toward the adult populations that are overrepresented in the literature. Accordingly, nearly all of the suitable literature data from subadult populations was included, whereas much of the data available from adult populations was not. The criteria for determining whether the literature values available qualified for inclusion were as follows. First, the mean height and weight of the group had to be reported in the original study. Second, metabolic means from a sufficient number of speeds to provide a minimum value for the energy expended per unit distance, or metabolic cost of transport, needed to be available. Third, to avoid speeds in the walk-run transition range that were too fast to be true walking speeds, we implemented a standardized maximum-speed cut-off using an analog of the Froude number (51) adapted from Alexander (2):

$$\text{Fr} = \text{walking speed}/\sqrt{\text{g} \cdot (\text{ht} \cdot 0.52)}, \quad (1)$$

where walking speed is in units of m/s, height is in meters, and g is the gravitational constant in m/s^2. The Froude number is widely used to quantify speeds that are equivalent for walkers and runners who differ in body size. The standard Froude index does so using leg length. Here, as previously, we used a Froude number analog that substitutes height for leg length because studies on walking metabolism generally report the height means of the groups tested, but often do not report leg length. To avoid including values that were at or above the walk-run transition we removed data points with a Froude analog value of ≥ 0.65. We limited our analysis to subjects of normal weight, excluding groups of people who were classified as obese in their respective original publications. We excluded data from subject groups ≥ 65 years of age because the metabolic cost of walking is generally elevated in elderly subjects (35) for reasons that have not yet been fully identified. We included populations of a minimum age of 3–5 years because they exhibit adult-like patterns for gait and metabolism when leg length is taken into account (18, 49).

Digitizing Process

Values for group means were acquired from the tables or figures in prior publications. Those data points acquired from figures were digitized in accordance with the highly accurate techniques now available (21, 43). Original illustrations were enlarged and oriented on a grid to allow precise vertical and horizontal line fits to the data point of interest. Line fits were extended to the *x*- and *y*-axes to determine the *x* and *y* values for each data point. Data point values were also determined using an automated digitizer available online [WebPlotDigitizer (40)].

Data Set Characteristics

Using the inclusion criteria specified, our literature search from the early 1900s to the present yielded 25 subject groups from 10 publications (Table 1) spanning a 50-year period from 1960 to 2010. The number of subjects per population group ranged from 5 to 42. Mean age ranged from 5.2 to 40.7 years, mean height ranged from 1.03 to 1.82 m, and mean body mass ranged from 18.9 to 78.0 kg. Body mass index ranged from 15.5 to 25.4 kg/m^2. A minimum of four and a maximum of six metabolic rate values from different walking speeds were acquired from the different population groups (mean = 5.1 ± 0.7 values per population group), resulting in a total of 127 values in the final data set. Of the 127 group means included, 95 were acquired from subjects walking on treadmills, whereas 32 were acquired from overground walking at constant speeds. The grand mean for the rate of O_2 uptake from the 127 values aggregated was 14.0 ml $O_2 \cdot kg^{-1} \cdot min^{-1}$.

Predictive Accuracy—Original HWS Model vs. ACSM and Pandolf et al.

According to the forms of the three respective literature equations provided in Table 2, literature values were predicted using the ACSM and Pandolf et al. equations on the basis of walking speed. For the original HWS model, literature values were predicted using walking speed, estimated $\dot{V}O_{2rest}$, and the mean height of each population group. The agreement between actual and predicted values across the three equations was evaluated using both the R^2 statistic and SEE.

Table 1. *Literature sources meeting inclusion criteria for use in modeling analysis*

Subjects*	Number	Age, years	Height, m	Mass, kg	RMR†	Reference
Adults	10	23.7	1.76	66.6	3.55	Bastien et al. (5)
Nonobese adults, M	10	20.6	1.82	74.7	3.51	Browning et al. (7)
Nonobese adults, F	10	26.6	1.68	58.7	3.38	
Adults, M	11	19.4	1.73	61.5	3.79	Cotes and Meade (16)
Children aged 3–4	6	4.1	1.03	18.0	6.93	DeJaeger et al.‡ (18)
Children aged 5–6	6	6.2	1.17	21.3	6.26	
Children aged 7–8	6	7.6	1.27	25.2	5.90	
Children aged 9–10	6	9.9	1.40	34.0	5.18	
Children aged 11–12	6	11.6	1.52	39.6	4.76	
Adults	6	24.3	1.77	64.9	3.51	
Nonobese children	17	9.2	1.37	30.3	5.44	Maffeis et al.‡ (29)
Young active adults	30	21.3	1.69	63.2	3.44	Martin et al.‡ (30)
Young sedentary adults	30	20.6	1.65	62.4	3.41	
Adolescents	40	15.5	1.67	62.0	3.81	McCann and Adams‡ (31)
Adults	42	40.7	1.68	71.6	3.17	
Adults, M	12	26.6	1.76	78.0	3.45	Mian et al.‡ (32)
Children age 6	23	6.2	1.19	22.5	6.33	Morgan et al.‡ (33)
Children age 7	23	7.2	1.26	25.9	5.50	
Children age 8	23	8.2	1.32	29.7	4.80	
Children age 9	23	9.3	1.39	34.1	4.17	
Children age 10	23	10.3	1.45	39.4	4.64	
Children	5	5.4	1.14	21.3	6.60	Weyand et al.‡ (49)
Children	9	10.6	1.42	43.4	4.64	
Adults	28	17.3	1.62	56.7	3.90	
Adults	14	22.2	1.77	75.9	3.36	

*Groups without a designation for sex (M, male; F, female) are mixed. †RMR, resting metabolic rate (oxygen units of ml $O_2 \cdot kg^{-1} \cdot min^{-1}$). ‡Means from one or more subject groups were excluded because they did not meet the inclusion criteria.

Table 2. *Prediction equations from previous literature sources*

Equation	Reference
$\dot{V}O_2$ (ml $O_2 \cdot kg^{-1} \cdot min^{-1}$) = (0.1·V) + (1.8·V·G) + 3.5 ml·kg^{-1}·min^{-1}	ACSM (3)
$\dot{V}O_2$ equiv (watts) = 1.5·M +2.0·(M + L)(L/M)^2 + n(M + L)[1.5·V^2 + 0.35·V·G]	Pandolf et al. (36)
$\dot{V}O_2$ (ml $O_2 \cdot kg^{-1} \cdot min^{-1}$) = RMR +0.97·RMR + 4.87·V$^{2.34}$/Ht	Weyand et al. (51)

V, velocity*; M, body mass (kg); Ht, height (m); L, load (body weight units); G, grade (%); η, terrain factor (arbitrary units); RMR, resting metabolic rate (ml $O_2 \cdot kg^{-1} \cdot min^{-1}$). *Units for velocity are reference-specific as follows: V, velocity; ACSM, meters per minute (m/min); Pandolf et al., meters per second (m/s); HWS model, meters per second (m/s).

Walking Metabolism Models

The specific forms of the one-and two-metabolic components used to model the walking, or nonresting portion, of gross walking metabolism were guided by both the primary literature traditions and our recent modeling efforts. Our recently introduced HWS model of walking metabolism appears schematically in Fig. 1 (51). Partitioning gross or total metabolic rates into a baseline component that corresponds to resting metabolic rate and an exercise component is a common practice (31, 41, 49–51). However, the HWS model is atypical in dividing the walking component of the body's total metabolic rate into two components: a constant, predominantly postural component, termed the minimum walking metabolic rate; and a second speed-dependent component. The novel component of the HWS model, the minimum-walk component, is attributed to the support and postural costs of the walking movement and is independent of walking speed (51). The speed-dependent component quantifies the simultaneous influences of walking speed, height, and gait mechanics as previously described (51). The HWS model incorporates body mass into the denominator of each metabolic component and takes the following form:

$$\dot{V}O_{2total} = \underbrace{\dot{V}O_{2rest}}_{\text{Resting Metabolism}} + \underbrace{\underbrace{C_1 \cdot \dot{V}O_{2rest}}_{\text{Minimum Walking}} + \underbrace{\left(C_2 \cdot V^{exp}\right) \cdot Ht^{-1}}_{\text{Speed-Dependent}}}_{\text{Walking Metabolism}} \quad (2)$$

where $\dot{V}O_{2total}$ is the body's total rate of oxygen uptake; $\dot{V}O_{2rest}$ is the body's supine resting rate of oxygen uptake; C_1 is a coefficient that describes the minimum walking rate of oxygen uptake as a multiple of the resting rate; and C_2 is a coefficient describing the speed-dependent increases in the rate of oxygen uptake as a function of walking velocity, V, raised to the exponent, exp, divided by the height (Ht) of the individual. Hence the sum of the model's second and third components represents the metabolic rate attributable to walking ($\dot{V}O_{2walk}$). All the terms in Eq. 2 are expressed in mass-specific units of oxygen uptake of ml $O_2 \cdot kg^{-1} \cdot min^{-1}$ in accordance with literature convention and for consistency with the original publication for the HWS model. The theoretical basis for the model, including its mass-specific form, has been previously provided (51). Per our scientific objectives, Fig. 1, Eq. 2, and our previous work, the term "metabolic rate" is used to refer to mass-specific rates of oxygen uptake throughout the manuscript.

Resting Metabolic Rates

The resting portion of the gross or total walking metabolic rates in our literature data set was determined on the basis of height, weight, sex, and age for each of the 25 population means using the prediction equations of Schofield et al. (42). These equations have been extensively validated and are known to predict resting metabolic rates with a high degree of accuracy, typically in the range of 0.5 ml $O_2 \cdot kg^{-1} \cdot min^{-1}$ (19, 26, 38, 39, 47, 50). Because all of the predictive models tested incorporated the same Schofield-derived resting metabolic rate quantity, this portion of the total or gross metabolic rate attributed to $\dot{V}O_{2rest}$ did not differ across all the model types tested. We did not use measured $\dot{V}O_{2rest}$ data because these values were not reported in most of our literature sources. We converted the units of kJ/day from the Schofield equation to oxygen units of ml $O_2 \cdot kg^{-1} \cdot min^{-1}$ using the conversion factor of 20.1 J per milliliter of oxygen. Schofield equations modified to oxygen units appear in Table 4 of the original HWS manuscript (51).

Modeling Iterations, Analyses, and Equations

Models of three basic forms for describing the metabolic rate vs. walking speed (V) relationship were evaluated: linear ($\propto V^{1.0}$), exponential ($\propto V^{2.0}$), and exponential with an inverse relationship to height ($\propto V^{2.0}$/Ht). For each of the three model types, both one- and two-component versions were derived. The equations corresponding to these six different model derivations are provided in Table 3. The procedures used to determine the best fits of these model forms to the literature data set are described below.

Model Best-Fit Procedures

For each of the three basic model forms, separate model versions were derived, a first that treated net walking metabolism as a single entity; and a second that partitioned walking metabolism into two components: a constant, largely postural component, and a separate speed-dependent component in accordance with the schematic in Fig. 1. For consistency and ease of interpretation, the postural component of walking metabolism was modeled the same way across the three model types, specifically as a multiple of $\dot{V}O_{2rest}$, therefore equal to the quantity $C_1 \cdot \dot{V}O_{2rest}$ according to Eq. 2.

To maximize the fits provided by each equation, the coefficients derived were those that provided the best fit to the data points acquired from the literature sources (i.e., highest R^2 value) across the range of height, weight, and walking speeds present. The coefficient describing the minimum walking metabolic rate (C_1) in the two-component models, and the coefficient describing the speed-dependent walking metabolic rate (C_2) in all models were specifically optimized to minimize the sum-squared error of prediction. The optimizer function in Microsoft Excel was used because of its ability to optimize a coefficient while holding other values such as estimated resting metabolic rate, walking velocity, and height fixed at their known values [Microsoft Excel Solver, Excel 2010 version (24)]. Once best-fit equations were derived they were used to estimate walking $\dot{V}O_2$ values for all 127 literature data points and subsequently plotted against walking speed.

We also tested a seventh model, the modified HWS model, which has only a two-component form and differed from the first six in that the minimum-walk component was modeled as a constant absolute value (in ml $O_2 \cdot kg^{-1} \cdot min^{-1}$) across all group means rather than as a multiple of the group-specific $\dot{V}O_{2rest}$ values. We did so because our prior results (51) raised the possibility of limited predictive bias being

Table 3. *Predictive equations used in modeling analysis*

Model Form	Equation
One-component linear	$\dot{V}O_{2total} = \dot{V}O_{2rest} + C_1 \cdot V$
Two-component linear	$\dot{V}O_{2total} = \dot{V}O_{2rest} + C_1 \cdot \dot{V}O_{2rest} + C_2 \cdot V$
One-component exponential	$\dot{V}O_{2total} = \dot{V}O_{2rest} + C_1 \cdot V^2$
Two-component exponential	$\dot{V}O_{2total} = \dot{V}O_{2rest} + C_1 \cdot \dot{V}O_{2rest} + C_2 \cdot V^2$
One-component exponential/height	$\dot{V}O_{2total} = \dot{V}O_{2rest} + C_1 \cdot V^2/Ht$
Two-component exponential/height	$\dot{V}O_{2total} = \dot{V}O_{2rest} + C_1 \cdot \dot{V}O_{2rest} + C_2 \cdot V^2/Ht$
Two-component, absolute minimum-walk	$\dot{V}O_{2total} = \dot{V}O_{2rest} + C_1 + C_2 \cdot V^2/Ht$

Ht, height in meters; $\dot{V}O_{2total}$ and $\dot{V}O_{2rest}$ are in oxygen units of ml $O_2 \cdot kg^{-1} \cdot min^{-1}$; C_1 and C_2 are coefficients that were optimized for each equation; V, velocity (m/s).

introduced by quantifying $\dot{V}O_{2Walk\ Minimum}$ as a multiple of $\dot{V}O_{2rest}$. In this case, the equation consisted of $\dot{V}O_{2rest}$, a constant in ml $O_2 \cdot kg^{-1} \cdot min^{-1}$ that replaced the $C_1 \cdot \dot{V}O_{2rest}$ term, and a coefficient (C_2) times walking velocity squared divided by height. Additionally, to further investigate the importance of height as a predictor we also analyzed the modified-HWS model without height in the equation.

Validation of Modified-HWS Model on Data from Individual Subjects

Upon completing our model evaluation we tested how well the derived equation predicted values previously acquired from individual subjects. We did so using previously published level walking metabolic data collected from 57 individuals (30 men, 27 women) whose heights ranged from 1.07 to 1.89 m, and weights ranged from 15.9 to 88.95 kg (51).

Derivation of a Final Generalized Equation

Once the essential elements for broad accurate prediction were formulaically established using the full data set, our final analytic step was to identify the best-fit coefficients for the equation form identified. We did so using only those values in the data set acquired using the gold standard technique for measurements of exercise metabolism, the Douglas bag method (13). For this purpose, we used all the Douglas bag values in the data set excepting those from Maffeis et al. (29), whose walking metabolic rate ($\dot{V}O_{2walk}$) values for subjects of 1.37 m in height were, for unknown reasons, substantially higher than those from other sources in the data set for subjects of similar height. The final equation was derived on 42 group mean values. For these 42 group means, subject height ranged from 1.19 to 1.73 m, weight ranged from 22.5 to 71.6 kg, and walking speed ranged from 0.44 to 1.80 m/s.

Data Set Categorization by Stature

The 127 values for population group-mean metabolic rates in our aggregated data set appear in Fig. 2*A* as a function of walking speed. The influence of height on gross walking metabolic rates led us to classify these values by stature using a three-category scheme of short, intermediate, and tall. These stature classifications were not necessary for, and indeed were not part of, our formal hypothesis tests. Rather, we implemented these classifications to allow for visual evaluation of whether the different model versions evaluated fit the walking metabolic rate values equivalently across the different stature means present in the data set, or were biased toward shorter or taller individuals. The stature, weight, and age means of the populations in the short, intermediate, and tall groups appear in Table 4.

Also, for graphical purposes, within each height classification group, we determined representative metabolic rate vs. speed relationships as follows. For each of the three groups, we averaged the literature metabolic rate data points acquired to determine values at or near six speeds: 0.5, 0.8, 1.0, 1.3, 1.6, and 1.8 m/s. The precise speeds for the respective height groups varied slightly in accordance with the different protocol speeds administered in the different literature sources. This process allowed us to formulate trend lines for the metabolic rate vs. speed relationships that corresponded to the literature values for each of the three respective height classification groups (Fig. 2*B*). These trend lines, which appear in grayscale, were formulated to provide a visual reference for evaluating each model's ability to fit both the stature- and speed-variability present in the data set.

RESULTS

Digitizing Accuracy

The average absolute percent difference between the 20 original numeric values [Fig. 1*A* in (49)] and those acquired via digitization was found to be $<1.00\%$ in 17 of the 20 cases when values were obtained by the grid technique. Across these 20 data points, the error ranged from 0.03 to 2.43% with an overall mean of 0.65%. Using three different published graphs and original data sets [Fig. 1*A* in (49), Fig. 2A in (51), and Fig. 4*A* in (51)] with a combined 47 data points, the absolute percent difference between the measured data and the derived data was $<0.60\%$. When using the automated digitizer, the original values and digitized values across the 47 data points agreed to within an average of 0.51% [WebPlotDigitizer (40)].

Data presentation. The actual vs. predicted values for the equations evaluated for both hypotheses are presented using

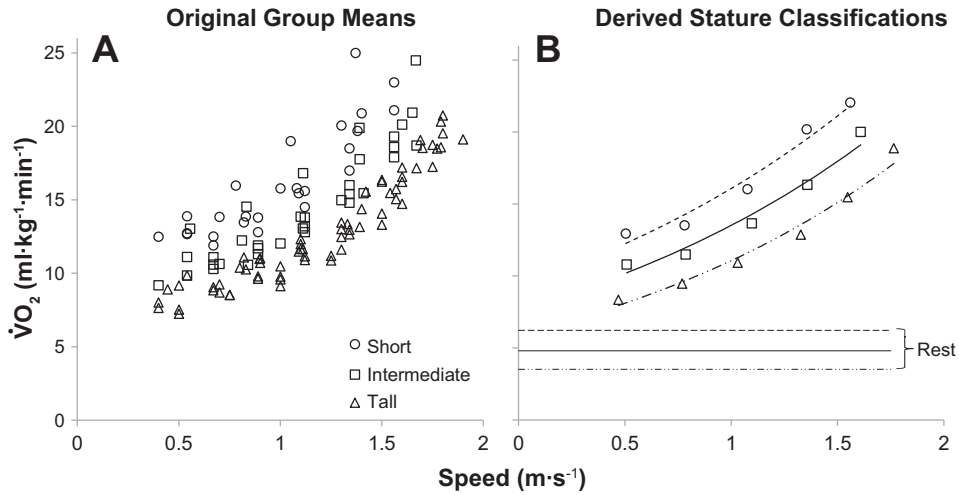

Fig. 2. *A*: gross metabolic rates vs. walking speed for the 127 mean values acquired from the 25 small population groups values in the literature-aggregated data set. The symbols for short (circles), intermediate (squares), and tall (triangles) classifications correspond to the mean height of the subjects in each of the 25 population groups as described in the text. *B*: representative trend lines for the $\dot{V}O_2$ vs. speed relationship for each of the three height classification groups. The horizontal lines in *B* represent the respective contributions of the resting metabolic rate ($\dot{V}O_{2rest}$) to the total measured during walking for each of the height classification groups, short (- - - - -), intermediate (———), and tall (—··—). (For reference purposes, the three stature classification trend lines in *B* appear in grayscale in Figs. 3, *A*, *C*, and *E*, and Figs. 4–7, *A* and *C*. The mean stature for each of the 25 population groups is provided in Table 2.)

Table 4. *Physical characteristics of the three height groups*

Group	Data Points, n	Height, m	Weight, kg	Age, years
1	26	1.18 ± 0.04	22.5 ± 1.2	6.2 ± 0.5
2	35	1.41 ± 0.02	35.8 ± 1.9	9.9 ± 0.4
3	66	1.72 ± 0.02	66.2 ± 2.2	23.2 ± 2.1
Total	127			

Values are means ± SE.

the same graphical format. First, the values predicted for each of the 127 original literature means by the respective equations are plotted as a function of walking speed (Figs. 3–7, *left*). Second, the same respective, predicted values are subsequently plotted vs. their actual values (Figs. 3–7, *right*). The height classification trend lines from Fig. 2*B* appear in grayscale in those figures in which equation-predicted values are plotted in relation to speed (Fig. 3, *A*, *C*, and *E*; and Figs. 4–7, *A* and *C*).

The best-fit coefficients derived for the one- and two-component models of each of the three basic model types (linear, exponential, and exponential with height) appear in Table 5. The goodness-of-fit of each of the six equations derived is provided graphically in two formats that follow the original graphic presentations of the literature values appearing in Fig. 2, *A* and *B*. For each of the six respective best-fit equations derived, one- and two-component version are vertically juxtaposed in the upper and lower portions of Figs. 4, 5, and 6. The one-component model forms and corresponding predictions appear at the *top* of each figure (*A* and *B*), whereas the two-component model forms appear in the *bottom* of each figure (*C* and *D*).

Each illustration of the goodness-of-fit between actual and predicted or estimated values includes an R^2 value for the fit provided and the corresponding SEE. The grand mean for all of the values in the literature data set was 14.0 ml $O_2 \cdot kg^{-1} \cdot min^{-1}$. Accordingly, those fits with SEE values below 1.40 ml $O_2 \cdot kg^{-1} \cdot min^{-1}$ met our criteria of a coefficient of variation of $<10\%$.

Hypothesis Test One: Predictive Accuracy of HWS vs. Standard Equations

The metabolic rates predicted for each of the 127 literature means using the ACSM (3), Pandolf et al. (36), and original HWS equations (51) appear as a function of walking speed in Fig. 3, *C* and *E*, and in relation to the actual values in Fig. 3, *B*, *D*, and *F*. The ACSM and Pandolf et al. equations were largely unable to predict the 127 values in the literature data set. In both cases, the proportion of variance accounted was less than zero, indicating that the error between predicted and actual values was greater than the total variability present in the data set. The HWS equation was considerably more accurate, accounting for just over 90% of the total variability present in these values.

Both the ACSM and Pandolf et al. equations result in significant underprediction of walking metabolic rate for all height groups; however, for the tall group, Pandolf et al. accurately predicts values at the intermediate and faster speeds, whereas the ACSM equation does not (Fig. 3, *A* and *C*). When plotting predicted vs. measured metabolic rates, the tendency toward underprediction by both equations is obvious. Almost all the data points fall on or below the line of identity for the ACSM equation (Fig. 3*B*), and all but a limited number of data points predicted by Pandolf et al. also fall below the line of identity (Fig. 3*D*). In contrast, the values predicted by the original HWS model fall relatively close to their respective height group trend lines (Fig. 3*E*) and to the line of identity (Fig. 3*F*). The predictive error (SEE) of the original HWS model equation was roughly one-fourth that of the ACSM and Pandolf et al. equations. Both ACSM and Pandolf et al. equations had greater predictive error than the benchmark SEE value (1.40 ml $O_2 \cdot kg^{-1} \cdot min^{-1}$), whereas the HWS model equation had appreciably less.

We also tested the predictive accuracy of the ACSM, Pandolf et al., and HWS equations on the subset of literature values from adults only because both ACSM and Pandolf et al. were designed to serve adult-only populations. For adult groups, the R^2 value for measured vs. predicted data points was 0.50 and the SEE was 2.69 ml $O_2 \cdot kg^{-1} \cdot min^{-1}$ using the ACSM equation. For the Pandolf et al. equation, the R^2 value was 0.71 and SEE was 2.06 ml $O_2 \cdot kg^{-1} \cdot min^{-1}$ for the adult values. For both ACSM and Pandolf et al. equations almost all the adult values in the data set were underpredicted. In contrast, the HWS equation resulted in an R^2 of 0.90 and SEE of 1.21 ml $O_2 \cdot kg^{-1} \cdot min^{-1}$ in predicting the same adult values.

Hypothesis Test Two: One- vs. Two-Component Models

Linear model results. The best-fits resulting from the linear forms of one- and two-component metabolic rate vs. speed models appear in Fig. 4. The best-fit from the one-component model slightly underpredicted the values of the shorter groups of subjects and overpredicted the values of taller ones (Fig. 4*A*). The stature-biased predictions were largely absent in the best-fit predicted values from the two-component form of the linear model (Fig. 4*C*). Both the one- and two-component model forms exhibited speed-dependent bias (Fig. 4, *B* and *D*). In both cases, the metabolic rate means at relatively slow and fast walking speeds tended to be underpredicted, whereas those at intermediate walking speeds were generally overpredicted. The goodness-of-fit and SEE of the two- vs. one-component model demonstrated only marginally better agreement ($\Delta R^2 = 0.03$ and ΔSEE $= 0.14$ ml $O_2 \cdot kg^{-1} \cdot min^{-1}$), primarily because the addition of the second component allowed the stature-related stratification of the literature means to be fit somewhat more closely.

Exponential model results. The best-fit equation predictions from the one- and two-component exponential models appear in Fig. 5. The one-component exponential model fit the literature values relatively poorly and was the only one of the six best-fit equations that did not account for at least half of the total variance present in the literature data set ($R^2 < 0.50$; Fig. 5, *A* and *B*). The literature means at the slowest walking speeds were predicted least accurately and were consistently lower than the actual values. The predictions at faster speeds were also in error, being generally higher than the actual values (Fig. 5*B*). In contrast, the best-fit relationship from the two-component exponential model accounted for $>90\%$ of the total variance present in the literature values (Fig. 5*D*) because the addition of the minimum walking component substantially improved the agreement with the actual values at all speeds, particularly the slower ones (Fig. 5*C*). The agreement between the two-component, best-fit estimated and actual values indicated slight speed-dependent bias

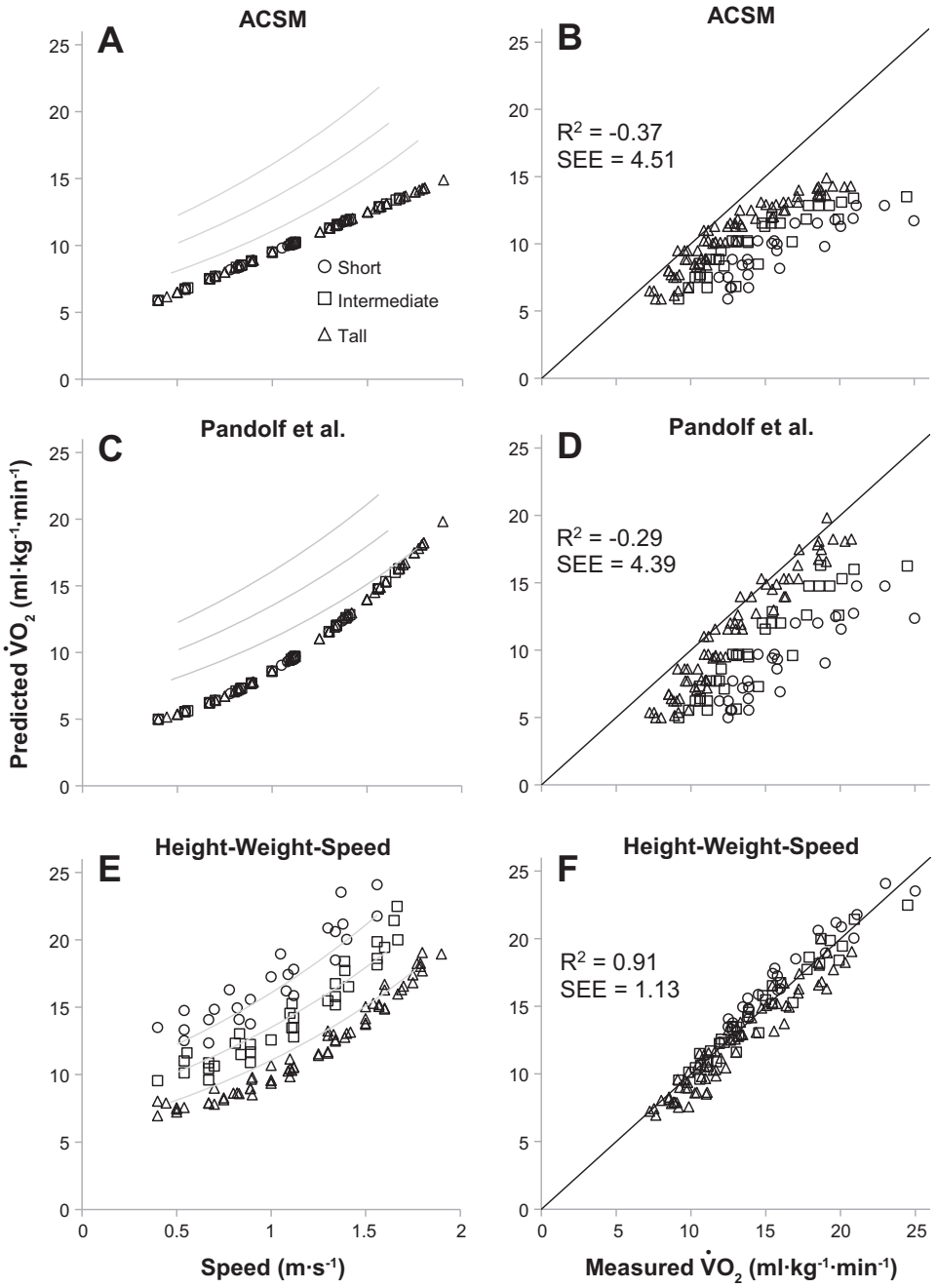

Fig. 3. The gross walking metabolic rates predicted by three standardized equations for the 127 literature means in the data set: the Pandolf et al. (36) equation (*A*), the American College of Sports Medicine (ACSM; 3) equation (*C*), and the original HWS model equations (51) (*D*). In *B*, *D*, and *E*, the model-predicted values appearing in *A*, *C*, and *E*, respectively, are plotted against the actual data set values. The R^2 values calculated against the line of identity, as well as the error of individual predictions (SEE), are included to provide an indication of the predictive accuracy of each model. The error of individual prediction (SEE) was four times greater for the Pandolf et al. and ACSM equations than than for the HWS equation model.

with most of the values at the slower and faster speeds falling just below the line of identity indicating slight underprediction (Fig. 5*D*).

Exponential model with height results. The best-fit equation estimations derived for the two-component exponential model with height included appear in Fig. 6. The addition of height to the exponential model improved the one-component fit to the literature values slightly but did not improve the two-component fit at all. The one-component exponential model with height substantially underestimated the literature values at the slower walking speeds across all three height classification groups (Fig. 6, *A* and *B*). Best-fit estimations at the faster speeds were more accurate but tended toward overestimation, particularly for the values at the fastest walking speeds. The two-component exponential model with height provided a substantially better fit than the one-component model, primarily by improving the accuracy of the estimations for the values at the slowest walking speeds (Fig. 6, *C* and *D*), although a slight tendency toward underestimation among the tallest groups remained. The estimations of the intermediate and faster speed values were generally accurate and without obvious speed-dependent bias or trends. The two-component model with height was the second of the six best-fit equations derived that was able to capture greater than 90% of the total variance present among the literature data set means.

Modified HWS model. The best-fit equation resulting from modeling the minimum-walk component as a constant absolute metabolic rate value was:

$$\dot{V}_{O_{2total}} = \dot{V}_{O_{2rest}} + 3.90 + 6.05\frac{V^2}{Ht}. \quad (3)$$

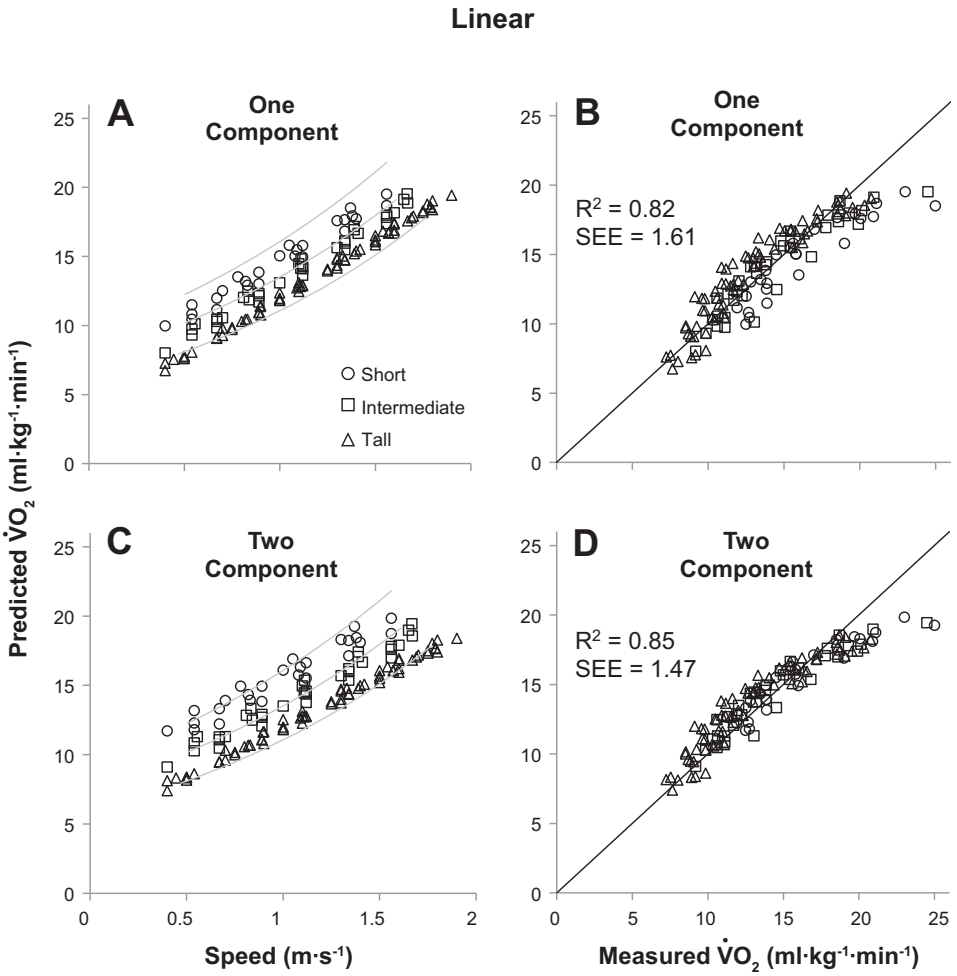

Fig. 4. Model-predicted gross metabolic rate values vs. walking speed for each of the 127 literature means in the data set (*A* and *C*). Predicted values were determined from the best-fit equations derived from the entire data set for the appropriate model type [one-component linear (*A*); two-component linear (*C*)]. In *B* and *D*, the respective model-predicted values that appear in *A* and *C* are plotted against the actual data set values. The height classification trend line means (*gray lines*, *A* and *C*) provide a visual reference for evaluating how closely the respective models predicted the data set values across speed for each of the three height classification groups. The diagonal lines appearing in the measured-predicted plots (*B* and *D*) represent the line of identity. Also provided is the proportion of variance accounted for (R^2) and SEE for the best-fits of the respective model types, here and in subsequent figures.

By comparison, the two-component model with minimum-walk-component treated as a constant absolute value resulted in an SEE of 1.00 ml $O_2 \cdot kg^{-1} \cdot min^{-1}$ (Fig. 7*D*), indicating that this refinement of our HWS model improved the goodness-of-fit to our literature data set. Modifying the first of the two walking, or nonresting, components of the HWS model removed the slight bias toward underprediction at the slowest walking speeds that were present in both of the exponential two-component models. For each of the three height-classification groups, the literature means at the slow, moderate, and faster walking speeds all conformed closely to the corresponding height classification trend lines (Fig. 7*C*). The error present in the values predicted from the modified HWS model vs. the actual literature values was small and equally distributed above and below the line of identity across the full range of walking speeds and metabolic rate values.

The modified-HWS model equation was able to fit the literature values more closely when speed-dependent increases in walking metabolic rates were described as an exponential function with an inverse relationship to height vs. without. When height was not included as a predictor, the SEE was 1.5 times greater and the proportion of variance accounted for was nearly 10% lower (Fig. 7, *B* and D). When height was absent from this form of the model, values were overestimated for the tallest groups and underestimated for the shortest groups (Fig. 7*A*), with the greatest disagreement occurring at the fastest speeds for the shortest subject populations.

Final generalized equation for level walking metabolism. The best-fit equation derived in the form identified as having the least predictive bias, and on the subset of literature values acquired from Douglas bags, and therefore considered to be most valid, was

$$\dot{V}_{O_{2total}} = \dot{V}_{O_{2rest}} + 3.85 + 5.97 \cdot \frac{V^2}{Ht}. \quad (4)$$

DISCUSSION

Our two-step strategy for identifying the elements that are essential for accurate generalized prediction of level human walking metabolism was indeed effective. Our first test revealed that the two leading standardized equations that predict walking metabolism are inadequate for humans of different body sizes walking across a broad range of speeds on level surfaces. Our second test identified the quantitative elements that are required for accurate generalized predictions, but lacking in the leading standardized equations. In both cases, the primary conclusion supported is that accurate generalized predictions are possible when the body's walking, or nonresting, metabolism is quantified with two components, but not possible when quantified with only one.

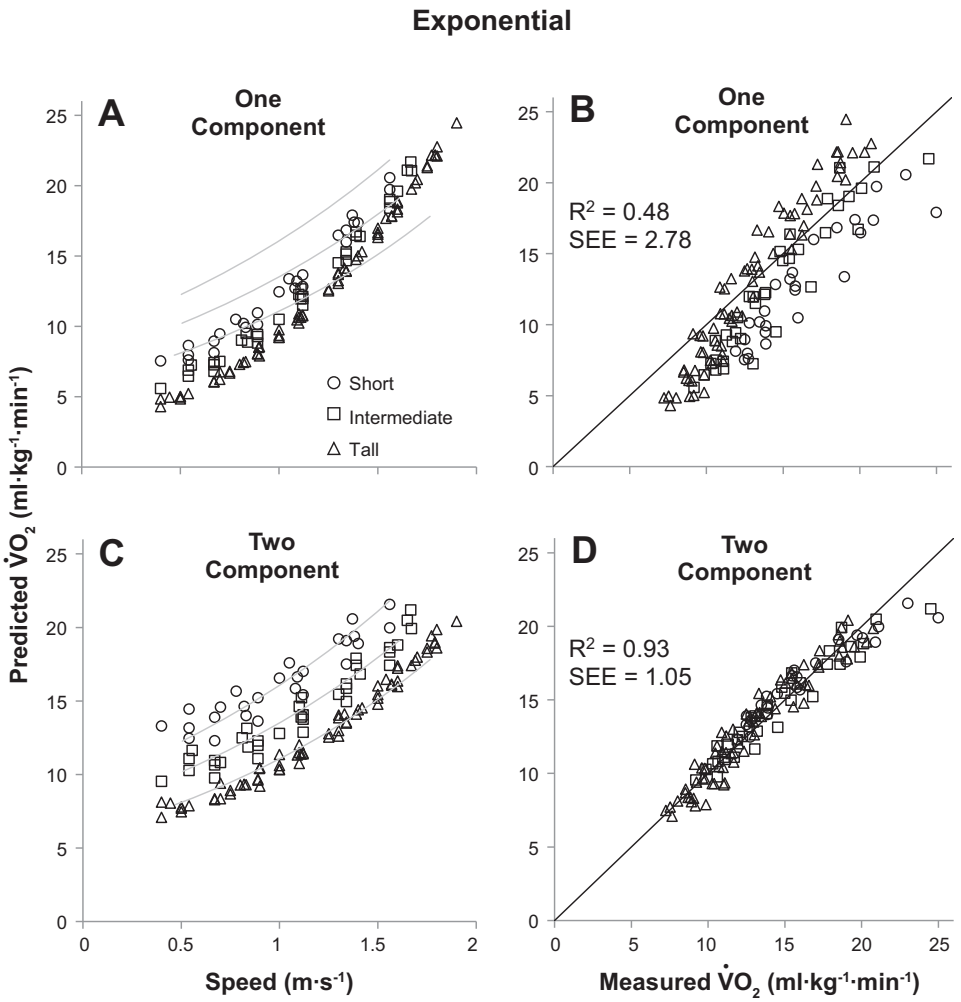

Fig. 5. Model-predicted gross metabolic rate values vs. walking speed for each of the 127 literature means in the data set (*A* and *C*). Predicted values were determined from the best-fit equations derived on the entire data set for the appropriate model type [one-component exponential (*A*); two-component exponential (*C*)]. The respective model-predicted values that appear in *A* and *C* are plotted against the actual data set values in *B* and *D*. The height classification trend line means (*gray lines*, *A* and *C*) provide a visual reference for evaluating how closely the respective exponential models predicted the data set values across speed for each of the three height classification groups.

Quantitatively, our first hypothesis test indicated that the group-mean metabolic rate values in our data set were predicted four times more accurately (SEE) by the HWS model equation, which includes two components for walking metabolism, vs. the leading literature equations (3, 36) that include only one (Fig. 3). The relative differences in predictive error of the leading standard equations vs. that of the HWS equation identified here actually exceed those we previously reported (51) on individual data. This quantification of larger differences in the independent data set compiled here indicates that our original study did not in fact overrepresent across-equation differences in predictive accuracy as it might have. Our second hypothesis test outcome indicated that in each of the three model forms, the best fits possible to the literature data were unable to account for either the speed- or stature-related variance present when they included only one component to describe the walking, or the nonresting, portion of the body's total metabolism (Figs. 4–6, *A* and *B*). In two out of three model types evaluated, the SEE was more than twice as large when walking metabolism was modeled with one component vs. two. Collectively, across the three model types on average, the one- vs. two-metabolic component versions provided poorer overall fits ($\Delta R^2 = -0.27$) with substantially larger predictive errors (ΔSEE $= +1.21$ ml $O_2 \cdot kg^{-1} \cdot min^{-1}$).

Hypothesis Test One: Predictive Accuracy of Existing One- vs. Two-Component Equations

Our first hypothesis test revealed that predictions of level human walking metabolism were roughly four times more accurate when based on our two-component HWS model equation vs. the leading one-component equations from the literature (Fig. 3). Certainly, some of the difference in predictive accuracy observed across these equations would be expected given *1*) the presence of an additional metabolic component in the HWS model, *2*) the formulation and validation of the HWS model on a data set similarly heterogeneous to that aggregated here, and *3*) the broader conditional objectives the ACSM and Pandolf et al. equations were meant to serve for adult-only populations (3, 36). The first two factors we have addressed throughout the manuscript, the last we were able to partially address here. For the 66 adult-population values in our literature data set, the respective predictive errors of the ACSM and Pandolf et al. equations were 2.2 and 1.7 times greater than that of the HWS model equation. Thus much of the difference in predictive error we identified for the entire data set was also present even when comparisons were limited to values from the adult-only populations that the ACSM and Pandolf et al. equations were meant to serve.

A primary contributor to the relative predictive errors we report is the substantial skew with which the leading literature

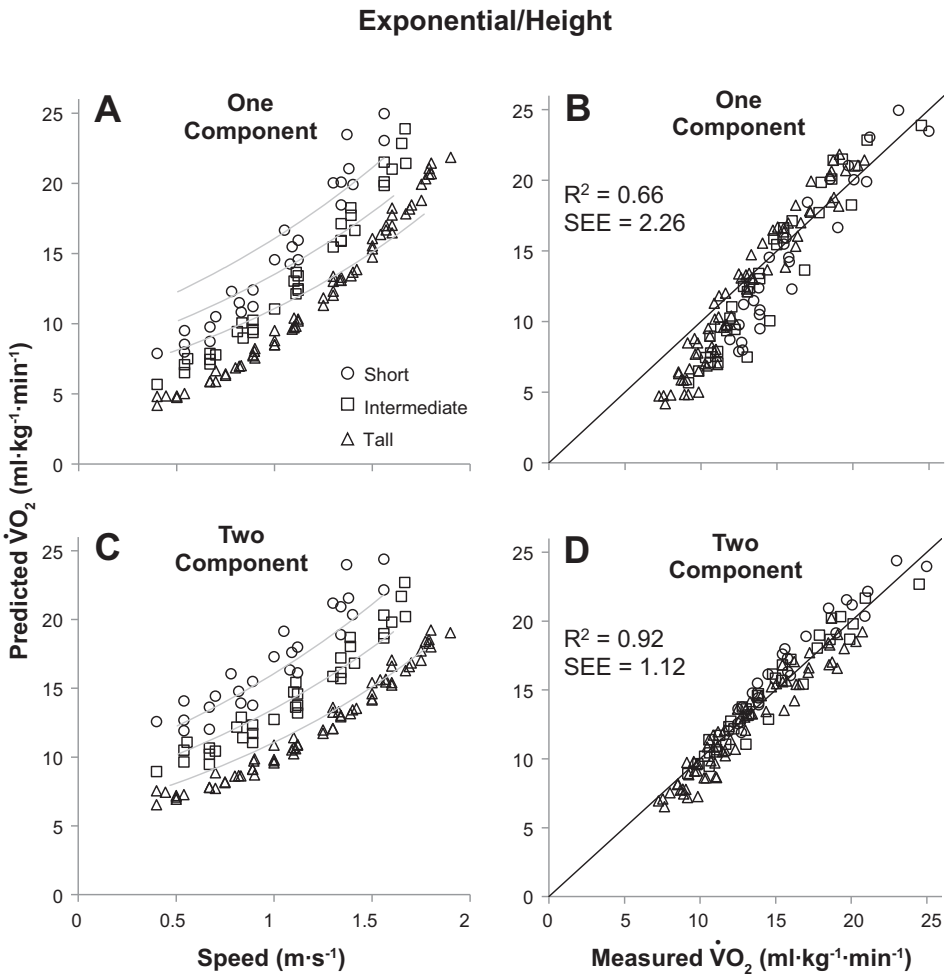

Fig. 6. Model-predicted gross metabolic rate values vs. walking speed for each of the 127 literature means in the data set (*A* and *C*). Predicted values were determined from the best-fit equations derived from the entire data set for the appropriate model type [one-component exponential with an inverse relationship to height (*A*); two-component exponential with an inverse relationship to height (*C*)]. The respective model-predicted values that appear in *A* and *C* are plotted against the actual data set values in *B* and *D*,

equations predict the existing literature data. Of the 254 total values predicted by the ACSM and Pandolf et al. equations combined only seven were overpredicted, whereas the remaining 247 values were underpredicted by these two equations (Fig. 3, *B* and *C*). Although the tendency toward underprediction has been noted previously for the ACSM equation (1, 8, 10, 25, 51), the substantial intrinsic bias of both equations has not been previously documented. Almost certainly, a portion of the bias identified is attributable to the narrow original derivations of the respective equations. The Pandolf et al. equation was derived from data from six male soldiers of similar body size (36). The level portion of the ACSM equation was derived from only three adult men (22). The skew and systematic error now evident for both of these widely used equations under level conditions highlights a significant weakness in this heavily researched area. Leading generalized equations were derived from populations that were too small and homogeneous to provide broadly accurate predictions.

Hypothesis Test Two: One vs. Two Metabolic Components for Walking Metabolism?

The distribution of values in our literature data set (Fig. 2, *A* and *B*) requires accurate formulaic descriptions to account for two visually evident features: *1*) the near-baseline differences in total metabolic rates at slow walking speeds that are related to stature and mass, and *2*) the curvilinear increases in walking metabolic rates across speed that have modest slope differences across stature groups (Fig. 2, *A* and *B*). The first feature is unsurprising given that the greater mass-specific rates of resting metabolism in shorter, less-massive individuals are well established (42). The constant $\dot{V}O_{2rest}$ values that we used across all our model iterations (Table 1, Fig. 2*B*, *horizontal lines*) addressed this reasonably because this single factor accounted for an appreciable portion of the across-group differences in total metabolic rates at slower walking speeds. The second feature posed the perhaps greater quantitative challenge of simultaneously describing a metabolic rate vs. speed relationship that is curvilinear for all of the population groups in the data set, but with greater stratification than can be accounted for by differences in resting metabolism alone. One consequence of these distribution features was that best-fit differences between one- and two-component model versions differed substantially by model type.

The form of our linear model resulted in almost no difference in the relative goodness of the fits provided between the one- and two-component versions. In both cases, group-specific differences in $\dot{V}O_{2rest}$ values allowed group differences at slower speeds to be reasonably approximated. Metabolic rate increases across speed were described by slope values that differed little between one- and two-component best-fit ver-

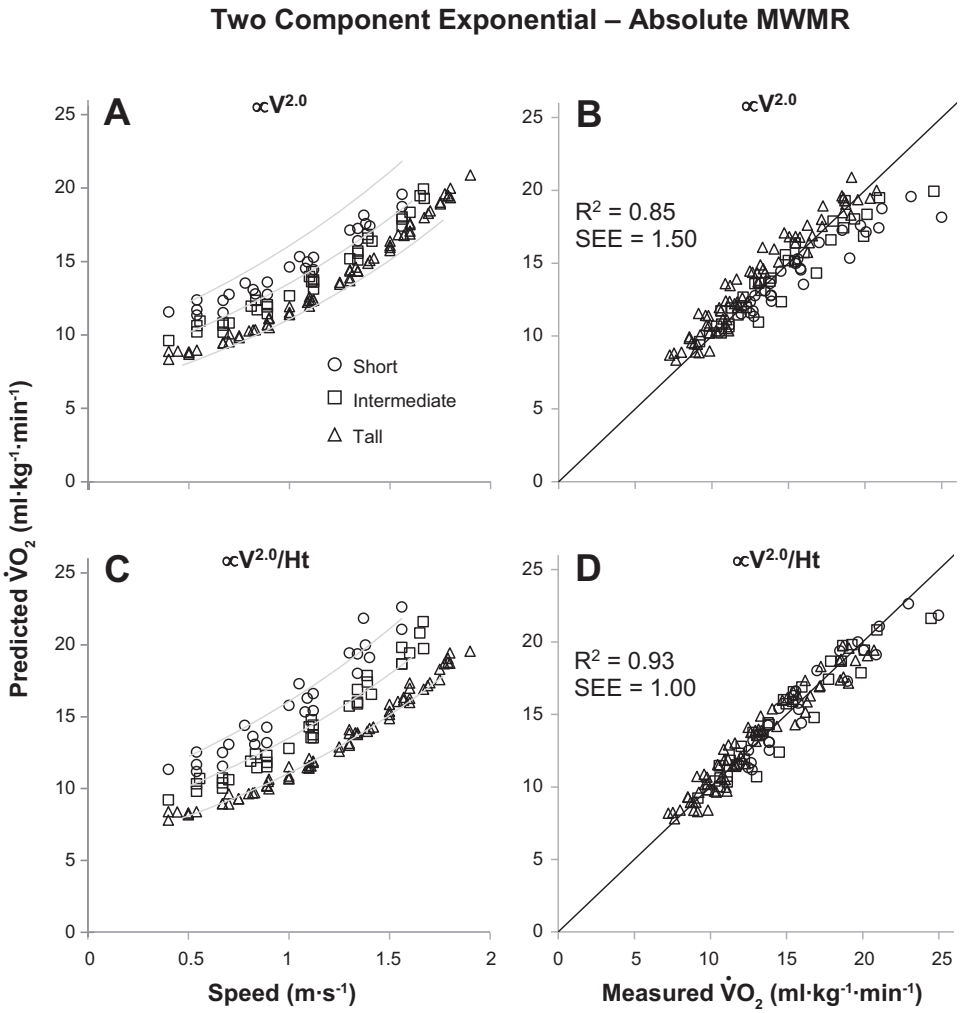

Fig. 7. Model-predicted gross metabolic rate values vs. walking speed for each of the 127 literature means in the data set (*A* and *C*). Predicted values were determined from the best-fit equations deived from the entire data set for the appropriate model type [two-component exponential model with a numeric constant for the first component (*A*); two-component exponential model with a numeric constant for the first component and an inverse relationship to height for the second (*C*)]. The model-predicted values that appear in *A* and *C* are plotted against the actual data set values in *B* and *D*.

sions (Table 5). Consequently, both the goodness-of-fit increase ($\Delta R^2 = +0.03$) and predictive error decrease (ΔSEE = -0.14 ml $O_2 \cdot kg^{-1} \cdot min^{-1}$) that resulted from the addition of a second component were negligible. The inability of a linear model to describe the curvilinear metabolic rate vs. speed relationship resulted in substantial speed-dependent error in the best-fits achieved by both versions.

In contrast to the similar best-fits observed across one- and two-component versions of the linear model type, respective best-fit differences across both exponential model types were large. For both the exponential models with and without height included, describing the entire walking, or nonresting, portion of the total metabolic rate as single component substantially overpredicted the slope of the metabolic rate vs. speed relationship. The exaggerated slopes forced by single-component exponential fits resulted in large underestimations of metabolic rate values at slower speeds and overestimations at faster ones (Figs. 5*A* and 6*A*, respectively). The addition of the second component to both model types reduced the slopes (Table 5) to align more closely with those actually present (Figs. 5*C* and 6*C*). Improved slope alignment also allowed model best-fit estimations at slower walking speeds to align more closely with the actual values of the different height groups. Consequently, both two-component exponential model versions were able to account for >90% of the total data set variance with predictive errors ≤10% of the grand mean.

Although the best-fits provided by our two-component exponential models exceeded our general criteria for good overall fits, both exhibited modest speed-dependent estimation bias vs. the line of identity. Slower-speed values were underestimated by both versions, whereas faster speed values were underestimated by the exponential model version that did not include height (Figs. 5*D* and 6*D*). The nature of the speed-dependent estimation bias present was consistent with our postulation that

Table 5. *Empirical derivations of model coefficients*

Model	C_1	C_2	Exponent
One-component linear		8.46	
Two-component linear	0.33	7.33	
One-component exponential		5.85	2
Two-component exponential	0.92	3.86	2
One-component exponential/height		9.08	2
Two-component exponential/height	0.77	6.43	2
Two-component absolute minimum walking metabolic rate	3.90*	6.05	2

*This value has units of ml $O_2 \cdot kg^{-1} \cdot min^{-1}$ whereas the other C_1 column values lack units per Eq. 2.

modeling the minimum-walk component as a multiple of group-specific $\dot{V}O_{2rest}$ values might overestimate across-group differences at slower walking speeds. Accordingly, we modified our two-component exponential model with height (Eq. 3) to describe the minimum-walk component using the same constant (ml $O_2 \cdot kg^{-1} \cdot min^{-1}$) across all 25 population groups. The resulting best-fit exhibited little to no discernible speed-dependent bias vs. the line of identity, accounted for a slightly greater proportion of the total variance, and had the lowest predictive error of all seven of our best-fit modeling iterations (Fig. 7*D*).

Body-Size Dependency of Walking Economy: Is Height Needed for Predictive Accuracy?

On the asis of our previous findings, we anticipated that the model forms with the speed-dependent component expressed inversely to height would better describe walking metabolic rates than models that did not include this feature. However, across the two-component exponential models, this was not the case. The best-fit provided by the two-component model that did incorporate height to describe speed-dependent increases in walking metabolic rates was no better than the best-fit provided by the two-component exponential model that did not (Fig. 5*D* vs. Fig. 6*D*). This result may at first seem inconsistent with two previous findings: *1*) of a near-inverse relationship between stature and the energy walkers expend per unit distance (49); and *2*) the predictive accuracy previously achieved when incorporating height in the same formulaic manner (51). However, the cursory interpretation that height is unimportant is incorrect.

The consistency with which gross, mass-specific walking metabolic rates have been reported to be inversely related to height has been essentially absolute (15, 18, 29, 31, 33, 49, 51). Indeed, this consistency is responsible for the distribution of walking metabolic rate values by stature classification groups evident in our literature data set (Fig. 2). Although a portion of the stature-related differences in the gross metabolic rates consistently observed results from the greater resting metabolic rates of smaller, less massive individuals, the majority of the difference is attributable to the walking or nonresting portion [Fig. 2 here, Fig. 1 in (49)]. Indeed, when we analyzed the current walking metabolic rate data (i.e., $\dot{V}O_{2total} - \dot{V}O_{2rest}$ per Eq. 1) to quantify the height-transport cost relationship (COT, O_2/kg·m) at the mechanically equivalent walking speeds that different-sized individuals typically self-select per our earlier analysis (49), we again found a large, negative, and nearly inverse relationship ($COT \propto Ht^{-0.77}$). Thus on a strictly biological level, our results here and those from previous literature are consistent in indicating that height is a fundamental determinant of level human walking economy.

The relative unimportance of height as a predictor across our exponential models resulted from the majority of the height-related variance being accounted for in the first of our two-model components of walking metabolism. Because this first component, the minimum-walk component, was modeled as a multiple of resting metabolic rates that vary by stature and mass (Table 3), the minimum-walk component values across different stature groups were greater for shorter populations and smaller for large ones, thereby accounting for much of the stature-related variance in the walking metabolic rates. Thus the incorporation of height into the second and speed-dependent metabolic component (as V^2/Ht) did not improve the best-fit provided because the stature-related variance had already been largely accounted for. This aforementioned effect becomes visually apparent in the modified HWS iterations that treated the minimum-walk component as a constant and therefore did not indirectly incorporate the influence of height into this portion of walking metabolism (Fig. 7). The version of this iteration which did not include a heightvariety of technologies-related treatment in either walking component, was unable to account for stature-related variation in metabolic rates across all speeds, particularly faster ones (Fig. 7, *A* and *B*). However, when height was added to the speed-dependent component of this model version, the best-fits for populations of different statures across all speeds were the closest of all of our model iterations (Fig. 7, *C* and *D*).

Why Are Two Nonresting Components Needed to Describe Human Walking Metabolism?

The most immediate scientific question raised by our conclusion that two metabolic components are required to adequately describe human walking metabolism is: To what extent does the two-component conclusion from our whole-body modeling approach correspond to internal physiological reality? Clearly, the ability to selectively activate tissues and tissue compartments within the muscular system across speed makes our simplified two-component description theoretically possible. The first component purportedly represents a constant minimum walking metabolic "baseline" set by the volume of muscle recruited largely to satisfy postural requirements. The second component purportedly represents speed-dependent increases in metabolic rates resulting from disproportionate increases in muscular activation across faster walking speeds. However, direct evaluation of these ideas is limited by the inability to measure metabolic rates within the body on a tissue-by-tissue basis.

Given this basic measurement limitation, investigators have used a number of indirect approaches to infer differential tissue contributions to the body's total walking metabolic rates. Of these, two partially overlapping approaches have been the most informative. The more direct of the two has been the use of surface electromyography (EMG) to measure the electrical activity of individual muscles (11, 12, 23, 34). The EMG studies available provide reasonable support for disproportionate increases in neuromuscular activity at faster walking speeds. Several of these indicate that hip flexor and extensor muscles that are largely inactive at slower walking speeds become activated at faster ones. These studies also demonstrate disproportionately large increases in knee extensor muscle activity across faster speeds that coincide with the greater knee extensor moments also observed (6, 23, 34). A less direct but more comprehensive approach is the detailed musculoskeletal modeling (20, 34, 37) that has advanced rapidly in the last decade. This approach uses forward dynamic simulations based on extensive kinematic, anatomical, neural, and physiological inputs. When applied across walking speeds, these detailed models also identify de novo recruitment of hip flexor and extensor muscles, and disproportionate increases in knee extensor muscle activation across the faster walking speeds.

Finally, we note that earlier investigators who adopted a combined theoretical-empirical approach to modeling whole-body walking metabolic rates reached a two-component conclusion similar to ours. Workman and Armstrong (53) used an energy-per-step framework in conjunction with direct measurements to develop their original equation for predicting level walking metabolic rates. Their lengthy equation, which also incorporates height, has been shown to be relatively accurate across a range of walking speeds and for different individuals (51). A retrospective scientific consideration of their work by the original authors led them to conclusions that have been largely overlooked, but are highly relevant here. Both the conceptual model [Fig. 5 in (52)] and quantitative conclusions they ultimately reached agree closely with ours even though the data and theoretical framework used were fully independent.

Summary and Future Recommendations:

On a practical level, empirical evidence now exists to conclude that the HWS model offers a more accurate alternative to the ACSM or Pandolf et al. equations for nonobese children and adults (<65 years) walking on firm, level surfaces. In addition to the accuracy already noted, our modified HWS equation offers several other noteworthy features. First, the HWS equation (Eq. 3) appears to be similarly accurate for both treadmill and overground conditions because we found virtually no difference in the goodness-of-fit (Eq. 3 and Fig. 7*C*) between the values from these conditions ($\Delta R^2 = 0.03$ and ΔSEE = 0.15 ml $O_2 \cdot kg^{-1} \cdot min^{-1}$). Second, two of the three metabolic terms in the HWS equations presented can be combined by adding a minimum-walk component constant to a population-specific $\dot{V}O_{2rest}$ value to provide a concise two-term equation. Finally, for adult-only populations, the need for population-specific $\dot{V}O_{2rest}$ values can be eliminated without any appreciable loss of accuracy. Simply using a global $\dot{V}O_{2rest}$ constant of 3.3 ml $O_2 \cdot kg^{-1} \cdot min^{-1}$, added to the 3.85 ml $O_2 \cdot kg^{-1} \cdot min^{-1}$ constant for the minimum-walk component from Eq. 4 yields the following equation:

$$\dot{V}_{O_{2total}} = 7.15 + 5.97 \cdot \frac{V^2}{Ht}, \quad (5)$$

which fits our adult literature data set values with an $R^2 > 0.93$ and an SEE of <1.0 ml $O_2 \cdot kg^{-1} \cdot min^{-1}$.

Our expectation is that our final modified-HWS equations (Eqs. 4 and 5) will prove to be accurate in subsequent validations, but a degree of caution is warranted. We opted to derive the final form using only the Douglas bag values in our literature data set because measurements from both laboratory and portable metabolic systems are typically slightly but systematically higher than Douglas bag values. Accordingly, Eq. 4 represents our best present generalized equation to describe what the actual O_2 uptake values during level walking will be. To assess this expectation on values acquired from individuals per the expected use of the equation, we evaluated Eq. 4 using data previously acquired from individual subjects (51). The resulting predictions conformed to the level of accuracy expected, with a resultant R^2 of 0.88 and SEE of 1.35 ml $O_2 \cdot kg^{-1} \cdot min^{-1}$ for a height, weight, and age-stratified group of 57 subjects. However, we note that the laboratory metabolic system we use provides excellent agreement with Douglas bag values, whereas many others do not (4, 17). Accordingly, users of those metabolic systems that tend to provide slightly but systematically higher values may experience better agreement with the best-fit equation derived on the full literature data set (Eq. 3), which includes values acquired from these systems. However, given the general acceptance of the Douglas bag method as the most valid technique, we believe Eq. 4 represents the concise, broadly accurate generalized equation we sought to identify.

Concluding Remarks

The emergence of an accurate, robust generalized relationship to predict the energy expended during level human walking is arguably scientifically overdue in addition to being practically opportune. From a basic standpoint, human walking has been studied far more extensively than any other animal gait. Nonetheless, a concise, relationship with predictive capabilities that could generalize across walking speeds and regardless of body size had not emerged (51) due to a tradition of focusing heavily on across-population differences rather than identifying the truly generalized relationships. This record contrasts with the robust, generalized relationships that exist for mammalian metabolism at rest (28) and during locomotion (44–46). In each of these cases, generalized relationships formulated on the basis of large data sets were established decades ago. Indeed, our experimental strategy here drew directly upon the comparative tradition of maximizing both speed and body-size related influences on locomotor metabolism.

From a practical standpoint, the relationship we report could be used to predict walking energy expenditure either with or without contemporary technology because the inputs required are minimal. Although present use is limited to level surfaces, under such conditions only velocity data are required if height and body weight are known. Thus low-tech field uses can be implemented with only time and distance inputs to compute an average velocity. In fitness settings, the equations we present here (Eqs. 3 and 4) could be used during level treadmill walking at known speeds. Across settings, technology-enabled implementations abound because many wearable sensors now provide velocity data (14). These include global positioning systems, geo-locating smart phones, and precision pedometers that determine speed from a variety of technologies and which are available from numerous manufacturers.

As health, medicine, military, and personal monitoring merge with mobile technologies, the accuracy of the generalized relationships available will be a primary determinant of the validity of the data streams that will inevitably become both widely available and heavily used.

ACKNOWLEDGMENTS

We thank Dr. Kyle Roberts for statistical input and consultation, and Drs. Laurence Ryan and Kenneth Clark for scientific input and suggestions.

GRANTS

This work was made possible in part by U.S. Department of Defense Medical and Materiel Command Grant DAMD17-03-2-005 and Award W81XWH-12-2-0013, and by internal funds from Southern Methodist University to P.G. Weyand.

DISCLOSURES

No conflicts of interest, financial or otherwise, are declared by the authors.

AUTHOR CONTRIBUTIONS

L.W.L. and P.G.W. conception and design of research; L.W.L. and P.G.W. performed experiments; L.W.L. and P.G.W. analyzed data; L.W.L. and P.G.W. interpreted results of experiments; L.W.L. and P.G.W. prepared figures;

L.W.L. and P.G.W. drafted manuscript; L.W.L. and P.G.W. edited and revised manuscript; L.W.L. and P.G.W. approved final version of manuscript.

REFERENCES

1. **Agiovlasitis S, Motl RW, Fernhall B.** Prediction of oxygen uptake during level treadmill walking in people with multiple sclerosis. *J Rehabil Med* 42: 650–655, 2010.
2. **Alexander R.** Estimates of speeds of dinosaurs. *Nature* 261: 129–130, 1976.
3. **American College of Sports Medicine.** *Guidelines for Graded Exercise Testing and Prescription* (7th ed). Philadelphia: Lippincott, Williams and Wilkins, 2013.
4. **Bassett DR, Howley ET, Thompson DL, King GA, Strath SJ, McLaughlin JE, Parr BB.** Validity of inspiratory and expiratory methods of measuring gas exchange with a computerized system. *J Appl Physiol* 91: 218–224, 2001.
5. **Bastien GJ, Willems PA, Schepens B, Heglund NC.** Effect of load and speed on the energetic cost of human walking. *Eur J Appl Physiol* 94: 76–83, 2005.
6. **Biewener AA, Farley CT, Roberts TJ, Temaner M.** Muscle mechanical advantage of human walking and running: implications for energy cost. *J Appl Physiol* 97: 2266–2274, 2004.
7. **Browning RC, Baker EA, Herron JA, Kram R.** Effects of obesity and sex on the energetic cost and preferred speed of walking. *J Appl Physiol* 100: 390–398, 2006.
8. **Browning RC, Reynolds MM, Board WJ, Walters KA, Reiser RF 2nd.** Obesity does not impair walking economy across a range of speeds and grades. *J Appl Physiol* 114: 1125–1131, 2013.
9. **Bubb W, Martin A, Howley E.** Predicting oxygen uptake during level walking at speeds of 80–130 m/min. *J Cardiopulm Rehabil* 5: 462–465, 1985.
10. **Butts NK, Knox KM, Foley TS.** Energy costs of walking on a dual-action treadmill in men and women. *Med Sci Sports Exerc* 27: 121–125, 1995.
11. **Cappellini G, Ivanenko YP, Poppele RE, Lacquaniti F.** Motor patterns in human walking and running. *J Neurophysiol* 95: 3426–3437, 2006.
12. **Carrier DR, Anders C, Schilling N.** The musculoskeletal system of humans is not tuned to maximize the economy of locomotion. *Proc Natl Acad Sci USA* 108: 18631–18636, 2011.
13. **Carter J, Jeukendrup AE.** Validity and reliability of three commercially available breath-by-breath respiratory systems. *Eur J Appl Physiol* 86: 435–441, 2002.
14. **Case MA, Burwick HA, Volpp KG, Patel MS.** Accuracy of smartphone applications and wearable devices for tracking physical activity data. *JAMA* 313: 625–626, 2015.
15. **Censi L, Toti E, Pastore G, Ferro-Luzzi A.** The basal metabolic rate and energy cost of standardised walking of short and tall men. *Eur J Clin Nutr* 52: 441–446, 1998.
16. **Cotes JE, Meade F.** The energy expenditure and mechanical energy demand in walking. *Ergonomics* 3: 97–120, 1960.
17. **Crouter SE, Antczak A, Hudak JR, DellaValle DM, Haas JD.** Accuracy and reliability of the ParvoMedics TrueOne 2400 and MedGraphics VO2000 metabolic systems. *Eur J Appl Physiol* 98: 139–151, 2006.
18. **DeJaeger D, Willems PA, Heglund NC.** The energy cost of walking in children. *Pflugers Arch* 441: 538–543, 2001.
19. **De Lorenzo A, Tagliabue A, Andreoli A, Testolin G, Comelli M, Deurenberg P.** Measured and predicted resting metabolic rate in Italian males and females, aged 18–59 y. *Eur J Clin Nutr* 55: 208–214, 2001.
20. **Delp SL, Arnold AS, Piazza SJ.** Graphics-based modeling and analysis of gait abnormalities. *Biomed Mater Eng* 8: 227–240, 1998.
21. **de Oliveira IR, Santos-Jesus R, Po AL, Poolsup N.** Extracting numerical data from published reports of pharmacokinetics investigations: method description and validation. *Fundam Clin Pharmacol* 17: 471–472, 2003.
22. **Dill DB.** Oxygen used in horizontal and grade walking and running on the treadmill. *J Appl Physiol* 20: 19–22, 1965.
23. **Franz JR, Kram R.** The effects of grade and speed on leg muscle activations during walking. *Gait Posture* 35: 143–147, 2012.
24. **Fylstra D, Lasdon L, Watson J, Waren A.** Design and use of the Microsoft Excel Solver. *Interfaces* 28: 29–55, 1998.
25. **Hasegawa H, Inui F.** Influence of higher-grade walking on metabolic demands in young untrained Japanese women. *J Strength Cond Res* 21: 405–408, 2007.
26. **Johnstone AM, Rance KA, Murison SD, Duncan JS, Speakman JR.** Additional anthropometric measures may improve the predictability of basal metabolic rate in adult subjects. *Eur J Clin Nutr* 60: 1437–1444, 2006.
28. **Kleiber M.** Body size and metabolism. *Hilgardia* 6: 315–351, 1932.
29. **Maffeis C, Schutz Y, Schena F, Zaffanello M, Pinelli L.** Energy expenditure during walking and running in obese and nonobese prepubertal children. *J Pediatr* 123: 193–199, 1993.
30. **Martin PE, Rothstein DE, Larish DD.** Effects of age and physical activity status on the speed-aerobic demand relationship of walking. *J Appl Physiol* 73: 200–206, 1992.
31. **McCann DJ, Adams WC.** A dimensional paradigm for identifying the size-independent cost of walking. *Med Sci Sports Exerc* 34: 1009–1017, 2002.
32. **Mian OS, Thom JM, Ardigo LP, Narici MV, Minetti AE.** Metabolic cost, mechanical work, and efficiency during walking in young and older men. *Acta Physiol (Oxf)* 186: 127–139, 2006.
33. **Morgan DW, Tseh W, Caputo JL, Keefer DJ, Craig IS, Griffith KB, Akins MB, Griffith GE, Krahenbuhl GS, Martin PE.** Prediction of the aerobic demand of walking in children. *Med Sci Sports Exerc* 34: 2097–2102, 2002.
34. **Neptune RR, Sasaki K, Kautz SA.** The effect of walking speed on muscle function and mechanical energetics. *Gait Posture* 28: 135–143, 2008.
35. **Ortega JD, Farley CT.** Individual limb work does not explain the greater metabolic cost of walking in elderly adults. *J Appl Physiol* 102: 2266–2273, 2007.
36. **Pandolf KB, Givoni B, Goldman RF.** Predicting energy expenditure with loads while standing or walking very slowly. *J Appl Physiol Respir Environ Exercise Physiol* 43: 577–581, 1977.
37. **Pandy MG.** Simple and complex models for studying muscle function in walking. *Philos Trans R Soc Lond B Biol Sci* 358: 1501–1509, 2003.
38. **Piers LS, Diffey B, Soares MJ, Frandsen SL, McCormack LM, Lutschini MJ, O'Dea K.** The validity of predicting the basal metabolic rate of young Australian men and women. *Eur J Clin Nutr* 51: 333–337, 1997.
39. **Rodriguez G, Moreno LA, Sarria A, Fleta J, Bueno M.** Resting energy expenditure in children and adolescents: agreement between calorimetry and prediction equations. *Clin Nutr* 21: 255–260, 2002.
40. **Rohatgi A.** *WebPlotDigitizer* (edition 3.6), January, 2015.
41. **Schmidt-Nielsen K.** Locomotion: energy cost of swimming, flying, and running. *Science* 177: 222–228, 1972.
42. **Schofield WN, Schofield C, James WPT.** Basal metabolic rate-Review and prediction together with an annotated bibliography of source material. *Hum Nutr Clin Nutr* 1: 5–96, 1985.
43. **Sistrom CL, Mergo PJ.** A simple method for obtaining original data from published graphs and plots. *AJR Am J Roentgenol* 174: 1241–1244, 2000.
44. **Taylor CR.** Relating mechanics and energetics during exercise. *Adv Vet Sci Comp Med* 38A: 181–215, 1994.
45. **Taylor CR, Heglund NC, Maloiy GM.** Energetics and mechanics of terrestrial locomotion. I. Metabolic energy consumption as a function of speed and body size in birds and mammals. *J Exp Biol* 97: 1–21, 1982.
46. **Taylor CR, Schmidt-Nielsen K, Raab JL.** Scaling of energetic cost of running to body size in mammals. *Am J Physiol* 219: 1104–1107, 1970.
47. **van der Ploeg GE, Gunn SM, Withers RT, Modra AC, Keeves JP, Chatterton BE.** Predicting the resting metabolic rate of young Australian males. *Eur J Clin Nutr* 55: 145–152, 2001.
48. **van der Walt WH, Wyndham CH.** An equation for prediction of energy expenditure of walking and running. *J Appl Physiol* 34: 559–563, 1973.
49. **Weyand PG, Smith BR, Puyau MR, Butte NF.** The mass-specific energy cost of human walking is set by stature. *J Exp Biol* 213: 3972–3979, 2010.
50. **Weyand PG, Smith BR, Sandell RF.** Assessing the metabolic cost of walking: the influence of baseline subtractions. *Conf Proc IEEE Eng Med Biol Soc* 2009: 6878–6881, 2009.
51. **Weyand PG, Smith BR, Schultz NS, Ludlow LW, Puyau MR, Butte NF.** Predicting metabolic rate across walking speed: one fit for all body sizes? *J Appl Physiol* 115: 1332–1342, 2013.
52. **Workman JM, Armstrong BW.** Metabolic cost of walking: equation and model. *J Appl Physiol* 61: 1369–1374, 1986.
53. **Workman JM, Armstrong BW.** Oxygen cost of treadmill walking. *J Appl Physiol* 18: 798–803, 1963.

J Appl Physiol 123: 1288–1302, 2017.
First published July 20, 2017; doi:10.1152/japplphysiol.00504.2017.

RESEARCH ARTICLE

Walking economy is predictably determined by speed, grade, and gravitational load

Lindsay W. Ludlow and Peter G. Weyand

Locomotor Performance Laboratory, Department of Applied Physiology and Wellness, Southern Methodist University, Dallas, Texas

Submitted 7 June 2017; accepted in final form 18 July 2017

Ludlow LW, Weyand PG. Walking economy is predictably determined by speed, grade, and gravitational load. *J Appl Physiol* 123: 1288–1302, 2017. First published July 20, 2017; doi:10.1152/japplphysiol.00504.2017.—The metabolic energy that human walking requires can vary by more than 10-fold, depending on the speed, surface gradient, and load carried. Although the mechanical factors determining economy are generally considered to be numerous and complex, we tested a minimum mechanics hypothesis that only three variables are needed for broad, accurate prediction: speed, surface grade, and total gravitational load. We first measured steady-state rates of oxygen uptake in 20 healthy adult subjects during unloaded treadmill trials from 0.4 to 1.6 m/s on six gradients: −6, −3, 0, 3, 6, and 9°. Next, we tested a second set of 20 subjects under three torso-loading conditions (no-load, +18, and +31% body weight) at speeds from 0.6 to 1.4 m/s on the same six gradients. Metabolic rates spanned a 14-fold range from supine rest to the greatest single-trial walking mean (3.1 ± 0.1 to 43.3 ± 0.5 ml $O_2 \cdot kg_{\text{-body}}^{-1} \cdot min^{-1}$, respectively). As theorized, the walking portion ($\dot{V}O_{2\text{-walk}} = \dot{V}O_{2\text{-gross}} - \dot{V}O_{2\text{-supine-rest}}$) of the body's gross metabolic rate increased in direct proportion to load and largely in accordance with support force requirements across both speed and grade. Consequently, a single minimum-mechanics equation was derived from the data of 10 unloaded-condition subjects to predict the pooled mass-specific economy ($\dot{V}O_{2\text{-gross}}$, ml $O_2 \cdot kg_{\text{-body + load}}^{-1} \cdot min^{-1}$) of all the remaining loaded and unloaded trials combined (n = 1,412 trials from 90 speed/grade/load conditions). The accuracy of prediction achieved (r^2 = 0.99, SEE = 1.06 ml $O_2 \cdot kg^{-1} \cdot min^{-1}$) leads us to conclude that human walking economy is predictably determined by the minimum mechanical requirements present across a broad range of conditions.

NEW & NOTEWORTHY Introduced is a "minimum mechanics" model that predicts human walking economy across a broad range of conditions from only three variables: speed, surface grade, and body-plus-load mass. The derivation/validation data set includes steady-state loaded and unloaded walking trials (n = 3,414) that span a fourfold range of walking speeds on each of six different surface gradients (−6 to +9°). The accuracy of our minimum mechanics model (r^2 = 0.99; SEE = 1.06 ml $O_2 \cdot kg^{-1} \cdot min^{-1}$) appreciably exceeds that of currently used standards.

metabolism; locomotion; generalized equation; load carriage; algorithm; wearable sensors

THE METABOLIC ENERGY that human walking requires can vary considerably, depending on mechanical and muscular demands. Slow walking on level and declined surfaces elevates metabolism only marginally above the body's basal or resting rates. Fast walking on inclines can elevate the body's resting metabolic rate by an order of magnitude or more. Inclined walking with loads can require metabolic rates that exceed the aerobic maximums of even the fittest human endurance athletes. Because metabolism is a fundamental determinant of the body's physiological state and walking is the most common form of human physical activity, hundreds of studies have examined the metabolic requirements of walking since formal investigation began more than a century ago (78).

Despite extensive and ongoing scientific attention, a generalized understanding of walking metabolism across the full range of conditions humans typically walk remains unavailable. Scores of predictive equations have been developed, but the vast majority have been limited to level surface conditions (10, 46, 59, 71, 73, 77). The two predictive equations with greatest conditional breadth, those of Pandolf et al. (56) and the American College of Sports Medicine (ACSM) (3), are the most widely used. However, both were formulated using very small sample sizes, have somewhat unclear scientific foundations, do not include declined conditions, and generally underpredict walking metabolic rates under the predominantly level conditions under which they have been thus far evaluated (46).

A primary difficulty in identifying the determinants of the metabolic cost, or economy of human walking is isolating the limited metabolic signal present under typical experimental conditions. The large majority of investigations have understandably been limited to level surface conditions. However, long periods of ground force application to support the body's weight (12, 36) and conservative, pendulum-like gait mechanics that minimize muscular work (11, 12) constrain gait-induced elevations in whole body metabolism two to four times the body's supine resting rate across the level walking speeds typically used. Additionally, quantitative approaches to isolating and predicting the walking, or nonresting, portion of the body's total metabolic rate have been inconsistent and are potentially confounding (1, 75). Some studies analyze the body's gross metabolic rates without implementing a baseline subtraction (15, 33, 38, 44), some subtract supine resting metabolic rate (46, 47, 76), and some subtract a measured rate of sitting metabolism (32), whereas many subtract a preexercise standing metabolic rate (13, 14, 16, 19, 20, 27–29, 65, 72). The rationale for standing metabolic rate subtractions is unclear because standing, like walking, includes a nonresting metabolic cost of supporting the body's weight against gravity (75).

Address for reprint requests and other correspondence: P. G. Weyand, Locomotor Performance Laboratory, Dept. of Applied Physiology and Wellness. Southern Methodist University. 5538 Dyer St., Dallas, TX 75206 (e-mail: pweyand@smu.edu).

Signal size and isolation issues have undoubtedly contributed to the lack of consensus regarding the determinants of human walking economy. At present, a substantial portion of the metabolic cost has been attributed to each of the following mechanical factors: gravitational support force requirements (29, 45, 46, 74), the mechanical work of lifting and accelerating the body's mass (29), the pushing and braking that the trailing and leading limbs perform, respectively, against one another during double contact (19, 43), swinging of the limbs (18, 27, 51), lateral stabilization of the body's center of mass (20), and others. Similarly unresolved is whether the per kilogram metabolic costs of body mass vs. external mass affixed to the torso are equal (6, 26, 30, 37, 45, 51, 58, 67). Finally, the validity of existing explanations for the substantial differences in walking economy observed across different surface gradients (3, 8, 49, 54, 56) is largely unknown.

Here, we used speed, grade, and torso loading as experimental tools to vary mechanical demands and maximize the range of gait-induced metabolic signals obtained. We reasoned that conservative gait mechanics should effectively reduce metabolic demands to those required to satisfy the gross mechanical requirements across these broad test conditions. This approach has previously been applied successfully to gaits such as running and bipedal hopping that provide large, easily isolated metabolic signals (41, 62). Analytically, we approached this question by building upon our prior work that successfully predicted both speed and body size-related variability under level conditions by using a two-component description of walking metabolism (46, 76): a first component that is constant across speed and a second that increases as a function of the velocity of walking squared (2, 76).

We hypothesize that the walking economy of adult humans can be predicted across a broad range of conditions from three basic mechanical variables: speed, surface grade, and the total weight (i.e., body plus load) supported against gravity. Successful test outcomes would provide a predictive and analytical tool with broad application. Potential uses include exercise prescription, physiological monitoring, performance prediction, and modeling of rates of heat production and fatigue. The rapid advancement of wearable sensing technologies capable of incorporating the three basic inputs in our model could avail broad, nearly immediate use to the general public during daily living.

METHODS

Experimental Design and Overview

We adopted a two-step approach to testing the hypothesis that the economy of human walking across a broad range of conditions can be predicted from three basic mechanical requirements: speed, grade, and total gravitational load. The two-step sequence was implemented to facilitate the acquisition of the large volume of data needed to develop a robust, multiconditional model. The data set ultimately compiled includes 3,414 steady-state walking trials acquired from 32 subjects over a period spanning 2 yr.

In *part I*, we measured walking economy across a broad range of walking speeds on six different grades in 20 subjects. In *part II*, we measured walking economy across a slightly narrower range of speeds on the same six grades under three different load conditions: unloaded (1.0 W_b), +18% added torso weight (1.18 W_b), and +31% added torso weight (1.31 W_b).

In contrast to our prior investigations of walking on level surfaces only (46, 76), height was not included in the present model for both scientific and pragmatic reasons. Scientifically, our objective of developing a generalized equation for predicting human walking metabolism in an adult population across a broad range of conditions did not require an age- or height-stratified sample. Pragmatically, the volume and intensity of the testing protocol was too rigorous to reasonably include children.

Minimum Mechanics Model of Walking Metabolism

For predictive purposes, our minimum mechanics model partitions the body's total metabolic rate into one resting and two walking components. In the original, level-only formulations (45, 76), the model was expressed as

$$\dot{V}O_{2\text{-gross}} = \dot{V}O_{2\text{-rest}} + \underbrace{C_1 \times \dot{V}O_{2\text{-rest}}}_{\text{MWMR}} + \underbrace{C_2 \times V^2/Ht}_{\text{SDWMR}} \quad (1)$$

where $\dot{V}O_{2\text{-gross}}$ is the body's gross, or total, metabolic rate; $\dot{V}O_{2\text{-rest}}$ is supine, resting metabolic rate; C_1 is the coefficient describing the model's first walking metabolic component, the minimum walking metabolic rate (MWMR) as a multiple of the resting metabolic rate; C_2 is the coefficient describing the model's second metabolic component, speed-dependent walking metabolic rate (SDWMR), V is the velocity of walking in meters/seconds, and Ht is height in meters. Above and throughout this article, all the metabolic terms are expressed in mass-specific units of oxygen uptake (ml $O_2 \cdot kg^{-1} \cdot min^{-1}$), in keeping with physiological convention for weight-bearing exercise and the scientific rationale for the model.

Multiconditional Formulation of the Minimum Mechanics Model

We expanded the prior level-only version of the model to the multiconditional purposes examined here by incorporating grade as follows:

$$VO_{2\text{-gross}} = \underbrace{VO_{2\text{-rest}}}_{\text{Rest}} + \underbrace{\underbrace{(C_1 \times G) + VO_{2\text{-walk min}}}_{\text{Minimum Walking}} + \underbrace{(1 + (C_2 \times G)) \times (C_3 \times V^2)}_{\text{Speed-dependent}}}_{\text{Walking Metabolism}} \quad (2)$$

where $\dot{V}O_{2\text{-gross}}$, $\dot{V}O_{2\text{-rest}}$, and V are as defined above, $\dot{V}O_{2\text{-walk min}}$ is a constant, G is the positive surface inclination expressed in percent grade, C_1 is a coefficient describing the minimum walking metabolic rate in conjunction with grade, C_2 is a coefficient describing the influence of grade on speed-dependent walking metabolism, and C_3 is a coefficient that describes the influence of velocity on speed-dependent walking metabolism regardless of grade. The number 1 is included in the speed-dependent walking metabolism term to prevent this portion of walking metabolic rate from equaling zero at 0% grade. A $C_{decline}$ coefficient was also derived to quantify walking, or nonresting, metabolic rates on negative grades as a fraction of the level values provided by the final equation.

The specific values of four coefficients, C_1, C_2, C_3, and $C_{decline}$, and one constant, $\dot{V}O_{2walk\text{-}min}$, were determined empirically. All $\dot{V}O_2$ terms are expressed in ml $O_2 \cdot kg^{-1} \cdot min^{-1}$, whereas V has the units of meters per second. The physiological basis of the model is provided below.

Model Formulaic and Scientific Rationale

The model assumes that elevations in the body's metabolic rate above supine resting rates due to walking *1*) result entirely from the activity of skeletal muscle, *2*) are attributable primarily to the activity of the limb muscles to support the weight of the body, or body plus load, against gravity (69, 70), and *3*) vary across grade in accordance with muscular contractions that elevate, maintain, or lower the body's center of mass during each step (34, 35, 49, 50).

Our third assumption deviates from the long-standing practice of modeling walking and running metabolic rates on positive grades as a separate, supplemental metabolic component to level metabolic rates. Although a distinguished tradition for this practice exists from the pioneering work of Zuntz (78) and Dill (17) forward (3, 8, 25, 56), a physiological justification for doing so is lacking. Contemporary observations document progressive alterations in the contractile activity (24, 61) and neuromuscular activation (65) across different grades in accordance with our assumption.

Added Load: Modeling Validation and Signal Isolation Analysis

The walking portion of the body's metabolic rate was isolated by subtracting each subject's measured supine resting metabolic rate from the total or gross metabolic rate measured during exercise ($\dot{V}O_{2\text{-walk}} = \dot{V}O_{2\text{-gross}} - \dot{V}O_{2\text{-rest}}$). In the event that each kilogram of added torso weight incurred an equal metabolic cost to each kilogram of body weight as postulated, load-induced increases in the walking portion of the body's total metabolic rate should be directly proportional to the additional load carried; thus

$$\dot{V}O_{2walk\text{-}L}/\dot{V}O_{2walk\text{-}UL} = W_{body+load}/W_{body} \quad (3)$$

where $\dot{V}O_{2walk\text{-}L}$ and $\dot{V}O_{2walk\text{-}UL}$ are walking metabolic rates under loaded and unloaded conditions, respectively, $W_{body\ +\ load}$ is the total weight of the body plus load and W_{body} is body weight only. Accordingly, our model predicts that the ratio of loaded to unloaded walking metabolic rate ($\dot{V}O_{2walk\text{-}L}/\dot{V}O_{2walk\text{-}UL}$) will equal the ratio of loaded to unloaded walking weight, which here equaled 1.18 and 1.31, respectively, across all of the speed and grade trials administered for the respective load conditions.

Signal Isolation Analysis

We also used the loaded walking data acquired to evaluate the effectiveness of signal isolation via resting metabolic rate subtractions. We did so by repeating the above analysis with two methods for quantifying walking metabolic rates that were expected to be inaccurate. The first was to examine load-induced increases in metabolic rates without implementing a baseline subtraction, thereby making the untenable assumption that the body's resting or basal metabolic requirement becomes zero during exercise (i.e., $\dot{V}O_{2\text{-walk}} = \dot{V}O_{2\text{-gross}}$). The second was to subtract a preexercise standing metabolic rate ($\dot{V}O_{2\text{-walk}} = \dot{V}O_{2\text{-total}} - \dot{V}O_{2\text{-stand}}$) that likely overestimates the body's baseline metabolic rate requirements that are present during walking. This second approach ignores the elevations above supine resting metabolic rates that result from standing (68, 75). The error introduced from these two alternative approaches is expected to skew the ratios of $\dot{V}O_{2walk\text{-}L}/\dot{V}O_{2walk\text{-}UL}$ on the left side of *Eq. 3*: negatively for the zero under-subtraction treatment and positively for the standing over-subtraction treatment. In both cases, ratio skewing is expected to be signal size dependent, affecting trials with the lowest gross metabolic rates most and trials with the greatest gross metabolic rates least.

Because of the considerable variability present in the literature for standing metabolic rate values, we compiled values reported from those laboratories and investigators who have frequently subtracted measured standing rates from gross exercise rates to isolate walking metabolism. A representative literature average was used to assess the error potentially introduced.

Experimental Protocol and Measurements

Subjects. Twenty subjects each participated in *parts I* (males, $n = 13$; females, $n = 7$) and *II* (males, $n = 12$; females, $n = 8$) of the study (Table 1). Because eight subjects participated in both *parts I* and *II*, the total number of participating subjects was 32. All subjects were physically active and without contraindications for exercise according to the cardiovascular guidelines set forth by the American College of Sports Medicine. Each provided written, informed consent before testing in accordance with the protocol approved by the Institutional Review Board of Southern Methodist University.

Table 1. *Subject characteristics by group*

Group	*n* (Males)	Age, yr	Mass, kg	Height, cm
Experimental	10 (6)	28.1 ± 2.3	73.6 ± 4.7	170.9 ± 3.5
Validation	10 (7)	26.4 ± 1.6	75.2 ± 6.0	170.5 ± 2.7
Load	20 (12)	30.2 ± 1.1	73.9 ± 2.7	171.8 ± 1.8

Values are means ± SE.

Treadmill testing protocol: part I. The 20 subjects in *part I* completed 5-min walking trials at five treadmill speeds (0.4, 0.7, 1.0, 1.3, and 1.6 m/s) on each of six different grades (−6, −3, 0, 3, 6, and 9°). Subjects reported to the laboratory for one session for measurement of resting, sitting, and standing metabolic rates, one session for measuring maximal aerobic rates, and a minimum of five sessions for measurement of walking economy at different speeds and grades without added weight. For the resting, sitting, and standing test session, subjects were asked to arrive at the laboratory as close to waking as possible, to refrain from exercise on the morning of the test, and to avoid caffeine and food consumption for a minimum of 8 h before testing. For the five walking sessions, each combination of grade and speed was tested on separate days to acquire two steady-state metabolic rates for each trial condition. Each subject was equipped with Brooks (Cascade Trail model) shoes.

Treadmill testing protocol: part II. The 20 subjects in *part II* completed 5-min treadmill walking trials at three speeds (0.6, 1.0, and 1.4 m/s) at six different grades (−6, −3, 0, 3, 6, and 9°) under three load conditions: unloaded (1.0 W_b), +18% added body mass (1.18 W_b), and +31% of added body mass (1.31 W_b). Nine of the 20 subjects completed an additional speed of 1.8 m/s for the two declined conditions. Each of the 20 *part II* subjects reported to the laboratory on a minimum of 8 different days for test sessions. As for the *part I* subjects, one early morning session was devoted to measuring post-absorptive resting, sitting, and standing metabolic rates. Maximal aerobic rates were measured in a single separate test session. The other six sessions were devoted to steady-state walking at the speeds, grades, and loads required. For each of the walking sessions, data from two grades, and all three load and speed conditions were acquired. Six sessions were required to acquire duplicate, separate-day walking metabolic measurements at each combination of grade, speed, and load. Within sessions, breaks occurred when it was necessary to change the treadmill grade and load or upon subject request. A subset of the data from 10 subjects has been reported previously (45).

Loads were added based on each subject's body weight rounded to the nearest 10-lb. increment. The exact percentage of body mass carried by each subject varied, with the group average values being 18 and 31%, respectively, for the two loaded conditions. Loads were added using vacuum-sealed steel shot packaged in 0.5, 1.0, and 2.0-lb. pouches. The weight added was distributed symmetrically about the torso by placing the blocks with shot into a military style backpack (5.11 Rush72; 5.11, Irvine, CA) posteriorly and vest (5.11 TacTec plate carrier) anteriorly. Seven blocks were fit into a tightly fitting backpack configuration to minimize or eliminate bouncing and load shifting. Vest blocks of equal weight were inserted into 14 tightly attached MOLLE pouches (5.11 C5 case).

The duplicate-trial walking metabolic rates acquired in *part I* and *part II* ($n = 3{,}414$) were averaged to obtain single trial-specific means for the modeling analysis. Trials were not administered above 85% of the subject's measured maximum rate of aerobic metabolism to avoid fatigue and nonsteady-state conditions.

Metabolic Measurements. Metabolic rates were determined by indirect calorimetry using a computerized metabolic system (TrueOne 2400; Parvo Medics, Sandy, UT). Samples of expired gases were collected during walking, supine resting, sitting, and standing. Col-

lection occurred through a one-way breathing valve and tubing that directed flow first through a pneumotach for measurement of volume flow rates and then into a mixing chamber. Expired air was sampled from the mixing chamber with O_2 and CO_2 fractions analyzed using paramagnetic and infrared gas analyzers, respectively. Rates of oxygen uptake ($\dot{V}O_2$) were determined from the average value during the last 2 min of each 5-minute trial.

Resting, sitting, and standing rates of oxygen uptake were acquired in the early morning with the subjects in a postabsorptive state. In each of these nonwalking measurement conditions, subjects were instructed to remain awake and refrain from fidgeting or any unnecessary motion. Resting rates were determined from the lowest, consecutive-segment, 10-min average over a 30-min test period. Sitting and standing metabolic rates were determined from the lowest, consecutive-segment, 5-min average during the 15-min test period. Maximum aerobic rates were determined using a continuous, grade-incremented, treadmill-running protocol to failure. Resting metabolic rates were also estimated using the population equation of Schofield (64).

Throughout this article, metabolic rates are reported in units of oxygen uptake. In all cases, mass-specific units denoting either body mass only (kg_{-body}), or body-plus-load mass (kg_{-total}) are reported per the widespread conventions for expressing weight-bearing exercise rates and per the scientific foundation of our model.

Minimum Mechanics Model Formula Derivation and Validation

Hypothesis evaluation relied upon a cross-validation design that match-paired and split the 20 *part I* subjects into experimental and validation groups of 10 subjects each. Subjects were randomly assigned to experimental and validation groups after being match-paired by stature and body mass. Empirical values for our three-input, minimum mechanics model of walking metabolism were determined using the data from the 10 experimental group subjects only. In accordance with prior procedures (45, 76), the optimizer function in Excel was used for the empirical derivation of the values, providing the best overall fits to the experimental group data while holding all other values constant (23). Here, the values of four coefficients, C_1, C_2, C_3, and $C_{decline}$, and one constant, $\dot{V}O_{2walk\text{-}min}$, were optimized empirically using the data of the experimental group subjects. The predictive accuracy of the model across speed and grade without loads was then evaluated on 10 validation group subjects, whose data were not used in the model's empirical formulation.

Subsequently, the walking economy values of all 20 *part II* subjects were predicted using the model formulated from the data of the experimental group subjects in *part I*. Model predictions across load conditions assumed equal per kilogram metabolic requirements for body vs. added weight. This assumption allowed the model formulated in *part I* to be used without modification to predict walking economy across the load conditions examined in *part II*. The body weight term in the model equation was modified to include the total weight supported against gravity (i.e., body plus load) under loaded conditions. A one-way ANOVA ($\propto = 0.05$) was used to test the effect of load condition on walking economy per total body-plus-load mass ($ml\ O_2 \cdot kg_{-total}^{-1} \cdot min^{-1}$).

Model Accuracy Comparisons

The predictive accuracy of our optimized minimum mechanics model of walking metabolism was directly compared with the two most commonly used predictive standards, those of the American College of Sports Medicine (ACSM) and Pandolf et al. (56), using the equations provided in Table 2. Because the ACSM equation was not formulated to include declined or added load conditions, negative grade predictions for this model were generated here by using the level condition equation, whereas load carriage predictions were generated by incorporating added load weight into body weight. The one quantitative addition needed to generate predictions using Pandolf et al. (56) for all conditions here was the utilization of the declined extension for Pandolf et al.'s (56) equation developed by Santee et al. (63). The predictions derived from the ACSM and Pandolf et al. (56) model equations were compared with those obtained from our minimum mechanics model for both the validation group subjects from *part I* and the load group subjects in *part II*. The agreement between measured and predicted values was evaluated primarily via the standard error of the estimate (SEE) and secondarily using the r^2 statistic. A first modified Bland-Altman (42) analysis of the performance of our two-component model, ACSM, and Pandolf et al. (56) across speed and grade was conducted on the data acquired from validation group subjects in *part I*. A second modified Bland-Altman analysis was conducted using the data acquired across all the speeds, grades, and load conditions completed by the 20 subjects who participated in *part II* of the study.

Data are reported as means ± SE throughout unless otherwise specified.

Table 2. *ACSM and Pandolf et al. (56) prediction equations*

Equation	Reference
$\dot{V}O_2\ (ml\ O_2 \cdot kg^{-1} \cdot min^{-1}) = (0.1 \cdot V) + (1.8 \cdot V \times G) + 3.5\ ml \cdot kg^{-1} \cdot min^{-1}$	ACSM (3)
$\dot{V}O_2\text{-equiv (watts)} = 1.5 \cdot M + 2.0 \cdot (M + L)\ (L/M)^2 + \eta\ (M + L)\ [1.5 \cdot V^2 + 0.35 \cdot V \times G]$	Pandolf et al. (56)
$\text{Decline CF} = \eta[G \cdot (W + L) \cdot V]/3.5 - \{[(W + L) \cdot (G + 6)^2]/W\} + (25 - v^2)$	Santee et al. (63)

ACSM, American College of Sports Medicine; V, velocity; M, body mass (kg); L, load (body weight units); G, grade (%); η, terrain factor, (arbitrary units). For V, units are reference specific: ACSM, m/min; Pandolf et al. (56) and decline CF [Santee et al. (63)], m/s.

RESULTS

Metabolic Rates: Resting, Sitting, Standing, and Aerobic Maximums

The mean measured supine resting metabolic rate for all 32 subjects was 3.13 ± 0.07 ml $O_2 \cdot kg^{-1} \cdot min^{-1}$ (range: 2.34–3.82 ml $O_2 \cdot kg^{-1} \cdot min^{-1}$). The corresponding mean for sitting metabolic rates was 3.16 ± 0.08 ml $O_2 \cdot kg^{-1} \cdot min^{-1}$ (range: 2.22–4.24 ml $O_2 \cdot kg^{-1} \cdot min^{-1}$), whereas the mean measured standing rate was 3.51 ± 0.08 ml $O_2 \cdot kg^{-1} \cdot min^{-1}$ (range: 2.62–4.55 ml $O_2 \cdot kg^{-1} \cdot min^{-1}$).

The mean overall supine resting value measured for the 20 *part I* subjects of 3.05 ml $O_2 \cdot kg^{-1} \cdot min^{-1}$ was used to generate our minimum mechanics model predictions for both *part I* and *part II*. The supine resting values predicted for all 32 subjects using the population equations of Schofield et al. (64) based on height, weight, and sex of 3.21 ± 0.05 ml $O_2 \cdot kg^{-1} \cdot min^{-1}$ agreed to within <0.1 ml $O_2 \cdot kg^{-1} \cdot min^{-1}$ of the mean measured value provided above.

The mean maximum rates of aerobic metabolism for the male and female participants were 53.2 ± 1.6 and 45.7 ± 3.0 ml $O_2 \cdot kg^{-1} \cdot min^{-1}$, respectively.

Standing Metabolic Rates: Literature Values

The mean standing metabolic rate compiled from the subject test population means in 12 literature sources (Table 3) of 4.5 ± 0.19 ml $O_2 \cdot kg^{-1} \cdot min^{-1}$ was 1.4 times greater than the mean supine resting metabolic rate measured of the 32 subjects tested here.

Table 3. *Standing metabolic rates from the walking metabolism literature*

	Reported Stand Value, ml $O_2 \cdot kg^{-1} \cdot min^{-1}$	Author(s)	Year
	5.6	Bastien et al. (6)	2005
	3.9	Browning et al. (9)	2006
	4.5	Collins and Kuo (13)	2010
	4.4	Collins et al. (14)	2015
	5.8	DeJaeger et al. (16)	2001
	4.4	Farley and McMahon (21)	1992
	4.9	Gottschall and Kram (27)	2005
	4.6	Grabowski et al. (29)	2005
	4.5	Martin et al. (48)	1992
	3.9	Silder et al. (65)	2012
	4.1	Silder et al. (66)	2013
	3.4	Vanderpool et al. (72)	2008
Average	4.5		
Minimum	3.4		
Maximum	5.8		

Walking Economy: Individual Variability

Individual variability in walking economy was limited, with the mean standard deviation from each of the 90 different trial conditions averaging <0.8 ml $O_2 \cdot kg_{\text{-body}}^{-1} \cdot min^{-1}$. When individual variability was quantified in relation to each trial mean as a coefficient of variation (= standard deviation/trial mean), values ranged from a minimum of 0.034 to a maximum of 0.122. In general, coefficient of variation values tended to be greater for trials eliciting lower metabolic rates.

Walking Economy Across Speed, Grade, and Load

The grand mean for all walking metabolic rates measured across the 90 different speed, grade, and load trial conditions administered was 14.4 ± 0.21 ml $O_2 \cdot kg_{\text{-body}}^{-1} \cdot min^{-1}$, representing a 4.7-fold elevation on average of the body's supine, resting metabolic rate. Across these 90 different trial conditions, individual walking metabolic rates spanned a nearly 10-fold range from a minimum of 4.8 ml $O_2 \cdot kg_{\text{-body}}^{-1} \cdot min^{-1}$ to a maximum of 45.4 ml $O_2 \cdot kg_{\text{-body}}^{-1} \cdot min^{-1}$.

The gross metabolic rates measured, expressed in relation to body mass (i.e., per $kg_{\text{-body}}$) across all the speed, grade, and load conditions administered appear in Fig. 1. The same gross, or total, metabolic rates measured, expressed per kilogram total, or load plus body mass (i.e., per $kg_{\text{-total}}$), appear in Fig. 2*A*. The corresponding rates due to walking (i.e., net rates = $\dot{V}O_{2\text{-gross}} - \dot{V}O_{2\text{-rest}}$), expressed per $kg_{\text{-total}}$ appear in Fig. 2*B*. Across each of the six different grades examined, walking metabolic rates increased from roughly two to four times across the fourfold range of test speeds administered from 0.4 to 1.6 m/s, with greater increases being observed on

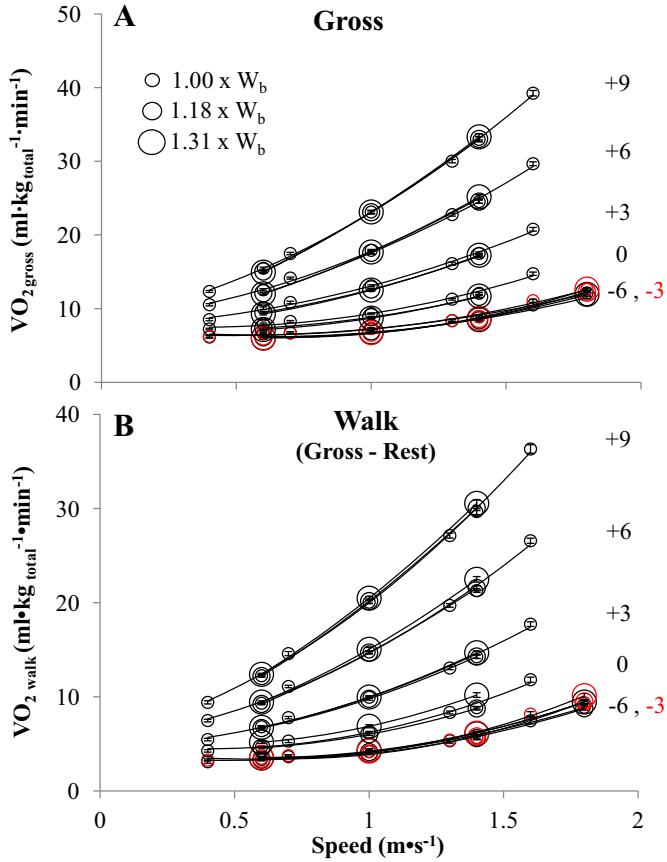

Fig. 2. Gross metabolic rates per total mass (body + load) vs. walking speed for all 3 load and 6 grade conditions tested. Data are presented as gross metabolic rates (*A*) and walking metabolic rates determined from gross − supine resting metabolic rate (*B*). Means for the −3° condition are illustrated in red.

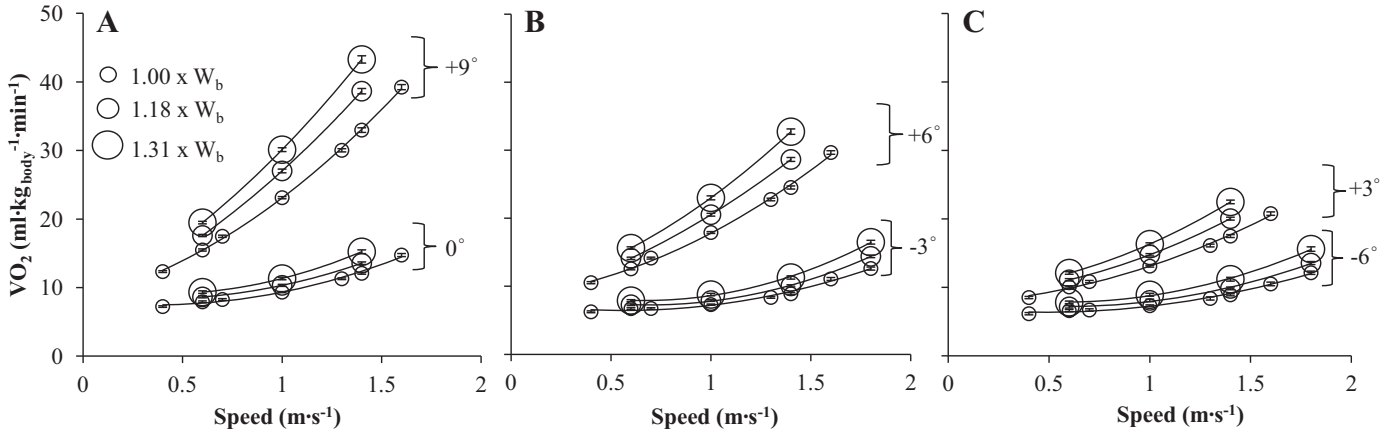

Fig. 1. Mass specific gross metabolic rates calculated/kg body mass and expressed as a function of walking speed for all 3 load and 6 grade conditions tested [0 and 9 (*A*), −3 and 6 (*B*), and −6 and 3° (*C*), separated for clarity]. Error bars represent the standard error of the mean in all figures. W_b, body weight.

the steeper positive grades. At all grades, speed-induced increases in walking metabolic rates were slightly curvilinear.

The influence of grade on walking economy was larger than that of speed (Figs. 1 and 2). At any given speed in the protocol, walking metabolic rates spanned a minimum range of fourfold and as much as sevenfold range from the −6 to +9° grade conditions examined. The grade-induced differences present at any speed were an approximately linear function of grade across positive grades from 0 to 9°. In contrast, grade-induced differences in walking metabolic rates from 0 to −6° were not linear. The differences observed between the 0 and −3° conditions were relatively small, and there were essentially no differences between the −3 and −6° conditions.

The addition of either 18 or 31% of the body's weight resulted in proportional increases in walking metabolic rates regardless of the speed or grade of the walking trial (Fig. 1). Consequently, when the load-induced increases in the body's mass-specific (i.e., per kg_{-body}) walking metabolic rates were expressed in relation to the total load carried, or per kg_{-total}, there were no discernable differences across any of the 20 speed and grade conditions for which each of the three load conditions were administered (Fig. 2). There was no effect of load condition on walking economy per kilogram total load (ml $O_2 \cdot kg_{-total}^{-1} \cdot min^{-1}$; ANOVA, $\propto = 0.05$).

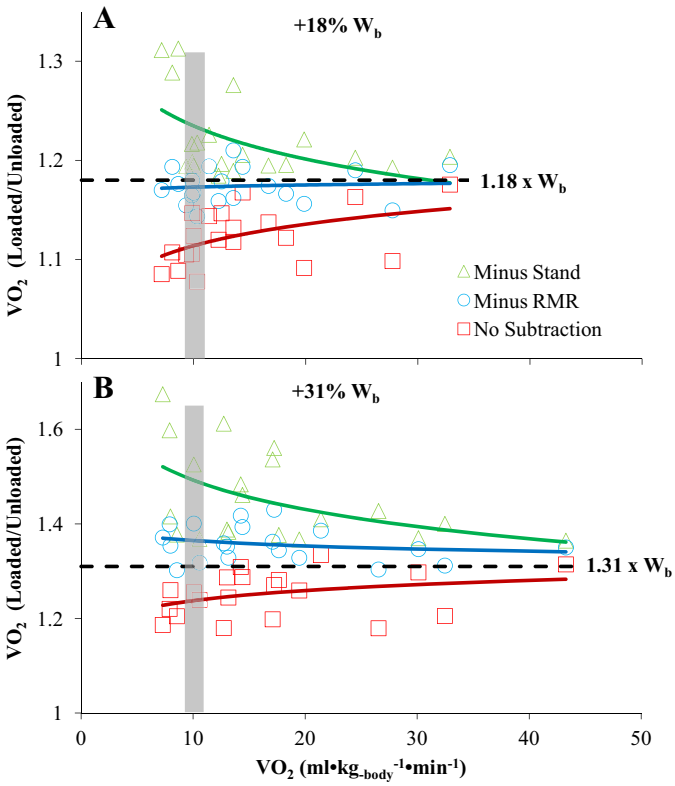

Fig. 3. The ratio of loaded to unloaded metabolic rates for the +18 (*A*) and +31% load conditions (*B*) vs. the body's gross metabolic rate during loaded walking. Ratios were determined using 3 different baseline subtraction methods: no subtraction (red squares and curve fits), gross metabolic rate − supine resting metabolic rate (blue circles and curve fits), and gross metabolic rate − average standing metabolic rate reported in the literature (green triangles and curve fits). Dashed horizontal lines represent the relative VO_2 increases predicted for respective conditions: 1.18 (*A*) and 1.31 (*B*). Logarithmic trend lines are included for each baseline subtraction method. Shaded gray vertical bars highlight the metabolic rates for level walking at the speeds typically self-selected (1.0–1.3 m/s).

Table 4. *Empirically derived minimum mechanics model equation values*

Experimental group	*n*	C_1	$\dot{V}O_{2\text{-walk-min}}$	C_2	C_3	$C_{decline}$	r^2	SEE
Value	10	0.32	3.28	0.19	2.66	0.73	0.98	1.12

SEE, standard error of estimate.

Added Load: Modeling Validation and Signal Isolation Analysis

The ratios of loaded to unloaded walking economy ($\dot{V}O_{2\text{-L}}/\dot{V}O_{2\text{-UL}}$) observed across all speeds and grades for the two respective load conditions appear in Fig. 3, A and *B*, (+18 and +31%, respectively), where they are plotted in relation to the gross metabolic rates ($\dot{V}O_{2\text{-gross}}$) measured. When walking metabolic rates were determined by subtracting supine resting rates from the gross rates measured (i.e., $\dot{V}O_{2\text{-walk}} = \dot{V}O_{2\text{-gross}} - \dot{V}O_{2\text{-rest}}$), load-induced increases in walking metabolism were a close function of the load added regardless of the speed, grade, and gross metabolic rate elicited by the trial (Fig. 3, blue open circles and curve fits, and Table 3). The mean value for the ratio of $\dot{V}O_{2\text{-L}}$ to $\dot{V}O_{2\text{-UL}}$ across the 20 common speeds and grades administered with the lighter load was 1.17 ± 0.004. The mean overall ratio for the heavier load from these 20 speeds and grades was 1.35 ± 0.006. There was no discernable trend across the gross metabolic rates measured under either load condition.

Both alternative data treatments of the gross metabolic rates measured during walking were signal size dependent. When no baseline quantity was subtracted (Fig. 3, red open squares and curve fits), the ratio of loaded to unloaded walking metabolic rates ($\dot{V}O_{2\text{-L}}/\dot{V}O_{2\text{-UL}}$) was appreciably less than the relative increase in load. For both the +18 and +31% added load conditions, ratios were lowest at low metabolic rates and greatest at the highest ones. For both load conditions, the ratios progressively approached a value directly proportional to the relative load added as the measured gross metabolic rates increased.

The opposite pattern was observed when the literature standing value of 4.5 ml $O_2 \cdot kg^{-1} \cdot min^{-1}$ was subtracted from the $\dot{V}O_{2\text{-gross}}$ values measured (where $\dot{V}O_{2\text{-walk}} = \dot{V}O_{2\text{-gross}} - \dot{V}O_{2\text{-stand}}$; Fig. 3, green open triangles and curve fits). Subtraction of the literature standing values from measured rates resulted in ratios of loaded to unloaded walking metabolic rates ($\dot{V}O_{2\text{-L}}/\dot{V}O_{2\text{-UL}}$) that were appreciably greater than the respective relative increase in load for both conditions. For both the +18 and +31% added load conditions, the ratios observed were greatest at low metabolic rates and least at the highest ones. In both cases, the ratios progressively decreased toward a value proportional to the relative load added as the measured gross metabolic rates increased.

Predictive Accuracy of the Minimum Mechanics Model

Part I. The optimized coefficients for our minimum mechanics model of walking metabolism derived from the experimental group subjects appear in Table 4. The accuracy of the model equation predictions on the validation group subject's data is provided in Fig. 4, *A* and *B*. Equation-predicted curves and the

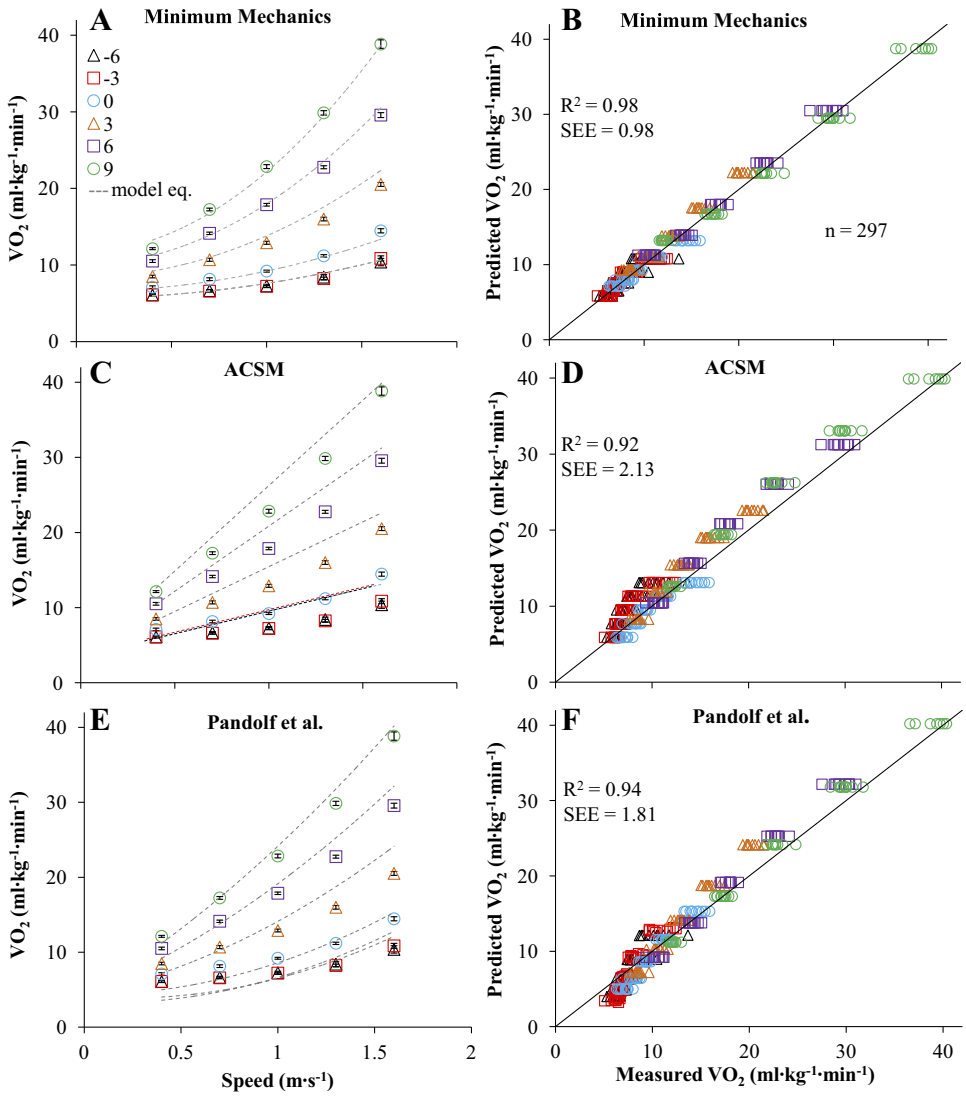

Fig. 4. Measured metabolic rate means during unloaded walking for the experimental group subjects vs. walking speed (all symbols in *A*, *C*, and *E*) in relation to the metabolic rates predicted (dashed lines) by our minimum-mechanics model (*A*), the American College of Sports Medicine (ACSM) equation (*C*), and the Pandolf et al. (56) equation (*E*) on each of the 6 surface grades investigated. Measured metabolic rates for each of the walking trials completed by validation group subjects vs. those predicted by our minimum mechanics model (*B*), the ACSM equation (*D*), and the Pandolf et al. (56) equation (*F*). Diagonal lines in *B*, *D*, and *F* represent the lines of identity. Declined gradient predictions were calculated using the level equation for ACSM and the declined extension of the Pandolf et al. (56) equation by Santee et al. (63).

experimental group mean values measured for each unloaded speed and grade appear in Fig. 4*A*, whereas the measured vs. equation-predicted values for each of the individual subjects in the validation group are plotted in Fig. 4*B*. The overall error of individual prediction, or SEE value, for the individual measured metabolic rates for the validation group subjects of <1.0 ml $O_2 \cdot kg^{-1} \cdot min^{-1}$ corresponded to 7.4% of overall mean measured. The proportion of the total variance in the 297 measured metabolic rates for the validation group subjects accounted for by the minimum-mechanics model was $>98\%$.

The overall error of individual prediction of our minimum mechanics model was roughly one-half that of the ACSM and Pandolf et al. equations on average when evaluated with the SEE statistic. The equivalent evaluations of the ACSM and Pandolf et al. equations are presented in relation to speed and grade means for the validation group subjects (Fig. 4, *C* and *E*) and measured vs. equation-predicted values (Fig. 4, *D* and *F*). The ACSM equation generally overpredicted declined and inclined values while slightly underpredicting level values. The Pandolf et al. (56) equations tended to underpredict level and declined values while also overpredicting the values obtained on positive grades. Consequently, the respective SEE values for the ACSM and Pandolf et al. (56) equations corresponded to 15.8 and 13.4%, respectively, of the overall mean measured for the validation group subjects across all of the trials completed (2.13/13.5 = 15.8 and 1.81/13.5 = 13.4%).

Part II. Both economy vs. speed and actual vs. predicted model accuracies for the minimum mechanics model, ACSM and Pandolf et al. (56) across the three load conditions administered for *part II* appear in Fig. 5. Because of the close relationship between increases in mass-specific metabolic rates and added gravitational loads relative to body weight, the accuracy of the minimum mechanics model under loaded conditions was almost the same as under unloaded conditions (Fig. 5, *A* and *B*). The absolute accuracy of the ACSM equation also declined marginally vs. the prediction of the unloaded values in *part I*, whereas that of the Pandolf et al. (56) equation improved marginally by 0.1 ml $O_2 \cdot kg^{-1} \cdot min^{-1}$.

Modified Bland-Altman Analysis

The difference between measured and model-predicted values in ml $O_2 \cdot kg_{\text{-total}}{}^{-1} \cdot min^{-1}$ for the three predictive models evaluated, minimum mechanics, ACSM, and Pandolf et al.

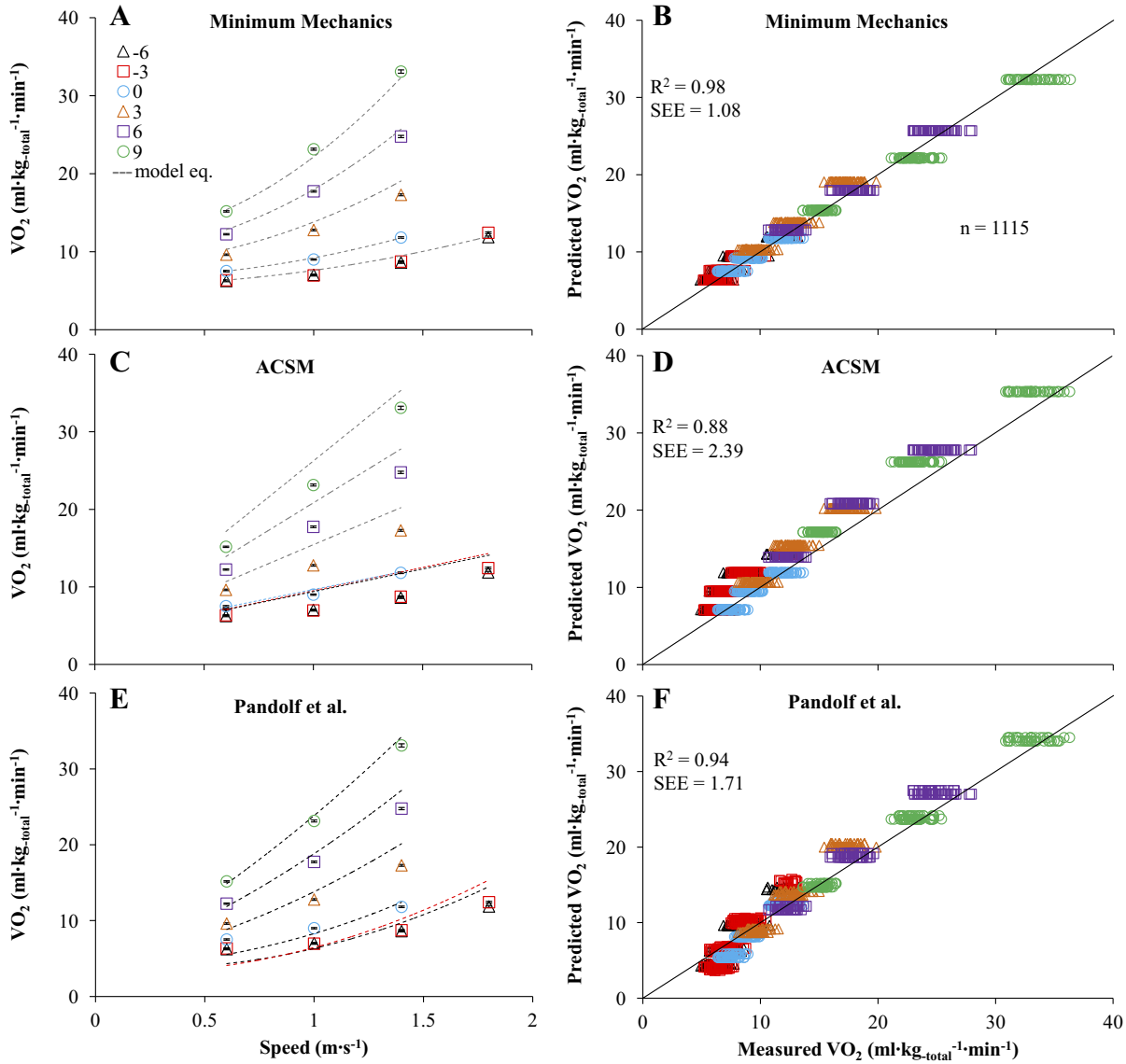

Fig. 5. Measured metabolic rate means during loaded walking for load group subjects vs. walking speed (all symbols in *A*, *C*, and *E*) in relation to the metabolic rates predicted (dashed lines) by our minimum-mechanics model (*A*), the ACSM equation (*C*), and the Pandolf et al. (56) equation (*E*) on each of the 6 surface grades investigated. Measured metabolic rates for each of the walking trials completed by load group subjects vs. those predicted by our minimum-mechanics model (*B*), the ACSM equation (*D*), and the Pandolf et al. (56) equation (*F*). Diagonal lines in *B*, *D*, and *F* represent the lines of identity. Declined gradient predictions were determined using the level equation for the ACSM and the declined extension of the Pandolf et al. (56) equation by Santee et al. (63).

(56), appear for the unloaded trials completed by validation group subjects in *part I* in Fig. 6, *A*, *C*, and *E*, respectively. For the minimum mechanics model, the mean overall difference was nearly equal to zero per the ideal (−0.36 ml O_2·kg^{-1}·min^{-1}), the standard deviation of the prediction was relatively small, and little speed- or grade-dependent bias in the accuracy of the predictions was evident. For both the ACSM and Pandolf et al. (56) equations, the standard errors of estimate were nearly twice as large and exhibited bias predominantly across grade. In both cases, the established standardized equations tended to underpredict metabolic rates at lower grades and lower metabolic rates and overpredict at higher ones. The overall predictive error for ACSM was larger, as was the zero error baseline vs. the equation of Pandolf et al. (56). The same error analysis for the three loaded conditions using the three predictive equations appears in Fig. 6, *B*, *D*, and *F*. The grade- and signal size-dependent predictive bias patterns of the loaded conditions were similar to those in the unloaded trials in *part I*.

DISCUSSION

Per our minimum mechanics hypothesis, we were able to predict walking economy accurately across a broad range of conditions from only three mechanical variables: speed, grade, and the total weight supported against gravity. Across more than 1,400 individual values from 90 different speed, grade, and load trial conditions and gross metabolic rates that ranged from two to 14 times the body's resting rate, our model predicted the rates we measured with a standard error of estimate of just >1.0 ml O_2·kg^{-1}·min^{-1} out of an overall mean nearly 14 times larger (14.6 ± 0.2 ml O_2·$kg_{-body}{}^{-1}$·min^{-1}; n =

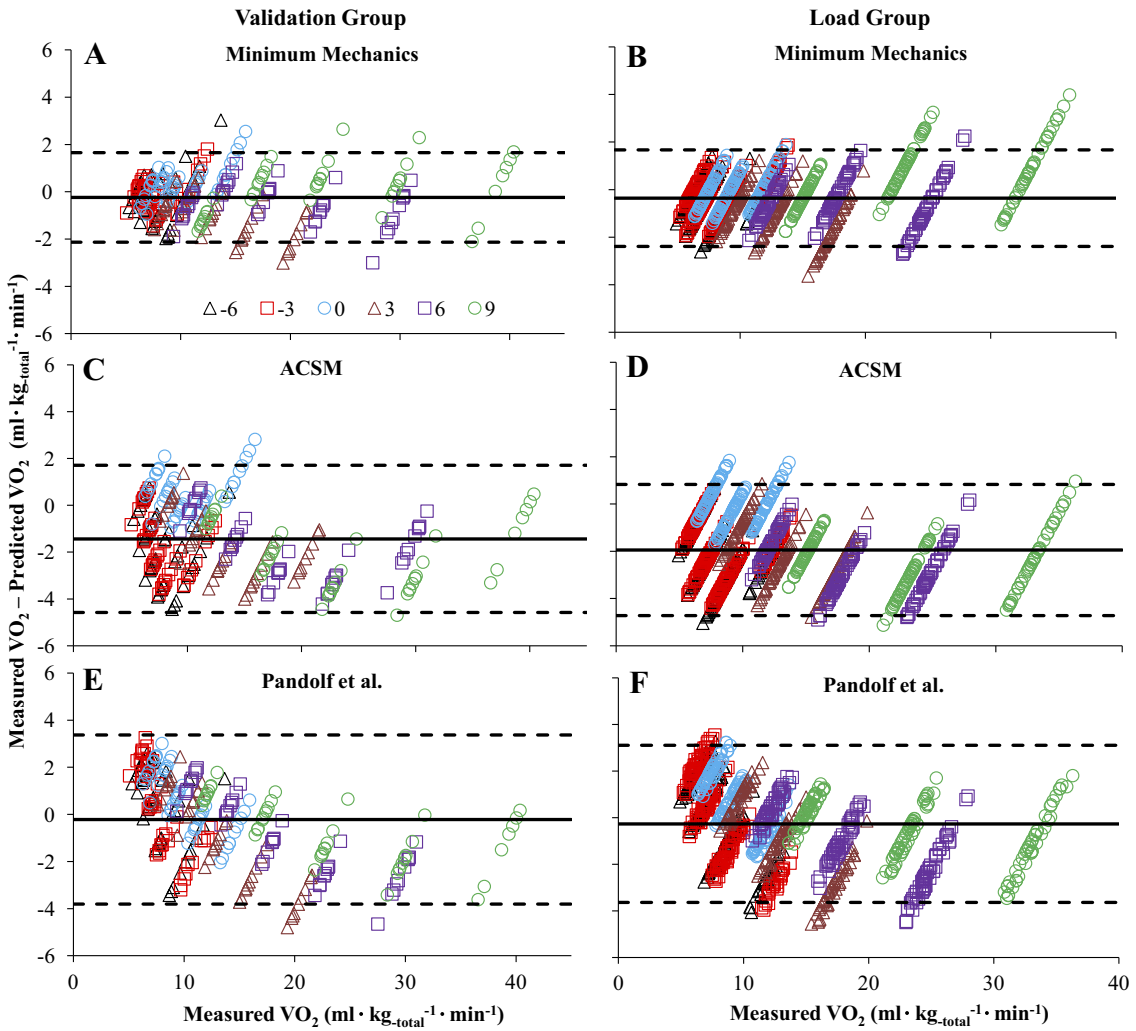

Fig. 6. Validation and load group modified Bland-Altman plots for our minimum mechanics model (*A* and *B*), the ACSM model equation (*C* and *D*), and the Pandolf et al. (56) model equation (*E* and *F*), illustrating the difference between measured and equation-predicted gross metabolic rates during walking. Horizontal black lines represent the average predictive error of the respective equations. Dashed horizontal lines correspond to the average error ± 2 SD.

1,412). The relative agreement between the model-predicted and measured values across nearly 300 speed and grade values in *part I* and across >1,100 speed, grade, and load values in *part II* was >98% in each case (Figs. 4*B* and 5*B*). Before specifically considering the economy influences of each of the three mechanical variables we altered, we note that our outcomes offer capabilities and scientific insights not previously available. Practically, the extension of generalized predictive capabilities to declined gradients that are equally present in the natural world, but not included in earlier predictive equations, offers a more comprehensive field tool than previously available. Scientifically, if support forces were not the fundamental determinant of walking economy as modeled, accurate metabolic predictions across the 90 different speed, grade, and load conditions investigated here would have been unlikely, if not impossible.

Loaded Walking Economy Is Determined by the Total Mass Supported Against Gravity

Many investigations under level-only conditions have reported that, on a per kilogram basis, each unit of additional torso mass incurs a relatively greater metabolic cost than each kilogram of body mass (6, 29–31, 37). However, our 738 individual loaded walking trials spanning a 2.5-fold range of speeds on six different grades consistently supported the alternative conclusion that each kilogram of body and load mass incurs the same metabolic cost (Figs. 2 and 3 and Table 5). This is evident from the agreement between the ratios of loaded to unloaded walking economy ($\dot{V}O_{2\text{-walk-L}}/\dot{V}O_{2\text{-walk-UL}}$; *Eq. 3*) and loaded to unloaded walking weight ($W_{body\ +\ load}/W_{body}$) to within <1% for the lighter load (+17.4% with +17.6% added weight), 5% for the heavier load (+35.8% with +31.0% added weight), and <3% (+2.5 ± 0.4%; $n = 40$) overall for the speed and grade means acquired from both added-load conditions.

Although load-induced increases in walking metabolism might have been greater than our model predictions for the trials inducing greater elevations in the body's metabolic rate (51), no discernable pattern was present. Deviations from the relative increases expected based upon the weight added ($W_{body\ +\ load}/W_{body}$; *Eq. 3*) were negligible across speed and either absent or inconsistent across the −6 to +9° slopes tested

Table 5. *Ratios of loaded to unloaded walking economy for all load trials*

Grade (°)	Load (× W_b)	Speed, m/s				Average
		0.6	1.0	1.4	1.8	
−6	1.176	1.170	1.193	1.165	1.16	1.173
−3	1.176	1.176	1.143	1.210	1.19	1.181
0	1.176	1.156	1.150	1.166	NA	1.157
3	1.176	1.155	1.159	1.179	NA	1.164
6	1.176	1.167	1.179	1.193	NA	1.180
9	1.176	1.174	1.190	1.195	NA	1.186
−6	1.310	1.371	1.399	1.401	1.393	1.391
−3	1.310	1.359	1.362	1.430	1.417	1.392
0	1.310	1.303	1.312	1.354	NA	1.323
3	1.310	1.302	1.318	1.352	NA	1.324
6	1.310	1.328	1.344	1.386	NA	1.353
9	1.310	1.328	1.346	1.350	NA	1.342
				Average		
1.18 × W_b		1.166	1.169	1.185	1.178	
1.31 × W_b		1.332	1.347	1.379	1.405	

NA, not available.

(Table 5). The possibility of load-related deviation being responsible for marginally greater relative increases for the heavier vs. lighter load condition as suggested by several investigators (25, 26, 38, 51, 58) to occur for loads >0.3 body weights cannot be completely ruled out. However, evaluation is difficult in our data because our heaviest load corresponded to the load threshold suggested (51). Evaluation of this possibility more broadly in the existing literature is difficult for several other reasons. First, the data available from loads >0.3 times body weight are limited and include unbalanced loading schemes that compromise economy regardless of load mass (40, 44). Second, the most informative heavy-load study available (67), which involved balanced torso loads of ≤1.0 times body mass, concluded that there is little and perhaps no difference in per kilogram costs between body and load mass. Third, the apparently poor mass-specific economy reported for both lighter (29–31, 37) and heavier load masses (6) from level-only investigations appears to be an analytic artifact introduced by resting metabolism oversubtractions (see APPENDIX).

Mechanistically, our load results are consistent with the manner in which our model incorporates the mechanical consequences of added mass, with each kilogram of body or load mass supported requiring the application of the same ground support force (= 1.0 kg × gravitational acceleration) over the course of each stride. Assuming the limb's leverage is not altered by balanced loading, the volume of limb extensor muscle activated, and, therefore, the rate at which chemical energy is used, to provide the requisite support forces should be a direct function of the total body-plus-load mass supported. This interpretation is fully consistent with the neuromuscular activation data available from the tissue level under different load conditions (52, 66).

Isolating Walking Metabolism Requires a Valid Resting Baseline Subtraction

The close agreement between the ratio of loaded to unloaded economy and the ratio of loaded to unloaded walking weight across the four- to fivefold range of gross metabolic rates measured under two load conditions (Fig. 3) indicates that two factors almost certainly remained essentially constant as assumed: *1*) the metabolic requirements per kilogram added load ($\dot{V}O_{2\text{-kg-total}}$, Figs. 2*B* and 3), as noted above, and *2*) the basal metabolic requirements of the body's nonlocomotor tissues as implied by earlier studies examining O_2 delivery to these tissues across rest and exercise conditions (4). Accordingly, the constant ratios for each load condition allow us to infer that the measured supine resting rates we subtracted (3.1 ± 0.1 ml $O_2 \cdot kg_{\text{-body}}^{-1} \cdot min^{-1}$) from the gross bodily rates measured during walking (i.e., $\dot{V}O_{2\text{-gross}} - \dot{V}O_{2\text{-rest}}$) accurately isolated the non-resting fraction of bodily metabolism for which walking was responsible.

Alternatively, if a resting rate that was either too low or too high had been subtracted, positive or negative trends, respectively, would have been observed as the body's gross metabolic rate increased and the fractional contributions of resting to gross metabolic rate decreased. Analysis of the positive and negative trends illustrated in Fig. 3 for the "no-subtraction" and "minus-stand" ratios vs. the body's gross metabolic rate appears in the APPENDIX.

Grade Walking Economy Varies with Muscular Support Force Dynamics

The walking economy data we acquired with and without loads on six different grades support our model's theoretical foundation while extending the grade-walking insights offered by Margaria (49) eight decades ago. This pioneering investigator recognized that the rate at which metabolic energy was expended to support and displace the body on steep positive and steep negative grades matched the metabolic cost of generating force during concentric and eccentric muscular contractions in isolated skeletal muscle. The quantitative agreement between tissue and whole body levels allowed Margaria (49) to deduce that essentially all of the metabolic energy being expended to walk on steep gradients was attributable to supporting and displacing the body's mass either positively via concentric contractions on steep inclines or negatively via eccentric contractions on steep declines. The constant metabolic rates per total kilogram supported across three load conditions on all six inclines (Fig. 2*B*) investigated here reveal that Margaria's support and displacement conclusions from unloaded walking on very steep positive and negative grades also apply to the moderate and intermediate grades we examined here.

The alternative suggestions that significant metabolic requirements exist for factors other than supporting and displacing the body's mass, such as repositioning the limbs between steps (18, 27) and the trailing and leading limbs pushing against one another during double support (19, 43), do not explain our results. The torso loads added here increased ground support force requirements in a direct 1:1 ratio, with no direct effect on limb-repositioning requirements. Thus, if limb repositioning accounted for an appreciable portion of the total walking metabolic rate at any given speed and grade, then load-induced increases in economy should have been substantially less than the 1:1 relationship that consistently resulted across different speeds and grades (Figs. 2*B* and 3). Similarly, the double-stance limb antagonism suggested by some to be a major metabolic requirement during level walking does not occur on inclines and declines of 3° and greater (22). Rather, single-limb data importantly demonstrate (22) that leading and

trailing limbs operate synergistically to simultaneously support and displace the body on positive and negative gradients, respectively, largely in accordance with Margaria and colleagues' (49, 50) insights from very steep grades.

The nearly universal approach to considering graded walking economy by investigators other than Margaria (49) and Minetti et al. (54) has been to do so *1*) only for positive gradients and *2*) to model inclined-only walking metabolic rates as a supplement to a level baseline rate that remains constant across all grades. However, neither the muscular activity present during level walking nor the metabolic requirement of this activity remain as constants across different grades. If this were the case, the extension of this theoretical framework to declined conditions would then logically require subtracting a bodily energy savings accrued during downhill walking from the level baseline requirements rate held constant by these model equations (8, 17, 25, 56). The inability of skeletal muscle to convert lost gravitational potential energy into accumulated chemical energy reveals the physiologically unsound foundation of this prevailing approach (3, 8, 17, 25, 56, 78).

Our formulaic avoidance of modeling inclined and declined walking economy by supplementing or subtracting from a constant level metabolism baseline simplified the quantitative treatment of both (*Eq. 2*) while reducing the number of model terms required. This is most evident from our negative gradient modeling solution, which fractionally reduced all of the body's walking or nonresting metabolism (*Eq. 2*) to describe economy differences vs. nonnegative gradients. The empirically derived decline coefficient of 0.73 (Table 4) is consistent with the metabolic reductions suggested by the slope of the force-velocity curve for eccentric muscular contractions in vivo (60).

Our results, the foundational context provided by Margaria and colleagues (49, 50), and the muscle activation and length-change data now available from the tissue level (24, 61) all support the same mechanistic explanation for differences in walking economy across grade. A small portion of the fivefold range in walking economy values observed across grade at each protocol speed tested here (Fig. 2*B*) can be attributed to within-fiber rates of ATP utilization being greater during concentric uphill vs. eccentric downhill contractions (34, 35, 39, 70). However, the majority is explained by the different per-fiber muscular forces generated under the different grade conditions. Relatively greater volumes of muscle must be activated during the relatively low-force concentric contractions that simultaneously support and elevate the body's weight on positive grades. Relatively smaller muscle volumes are activated during the relatively high-force eccentric contractions that simultaneously support and lower the body on negative grades (24, 61).

Speed-Dependent Walking Economy Is Predicted Accurately by a Two-Component Model

The modeling of our third independent variable partially followed the widely accepted literature convention of describing speed-induced increases in walking metabolic rates as a square function of walking velocity. However, here, as previously (46, 76), we deviated from widespread convention in doing so for only a portion of the body's walking metabolism; a separate portion was modeled as a constant across speed. This approach, although more mathematically descriptive than physiologically mechanistic, ultimately provided highly accurate descriptions of the two- to fourfold increases in walking metabolic rates observed across the fourfold range of speeds investigated on the six different grades (Figs. 2, 3, 4, and 5). The somewhat larger relative increases on the more positive grades and smaller ones on the level and declined gradients were described equally well by our two-component approach.

The relatively small departure of walking metabolic rates from linearity across speed on each of the six grades tested (Figs. 1 and 2), in conjunction with our velocity-squared description of only a portion of walking metabolism, made the high degree of predictive accuracy possible (Figs. 4 and 5, *A* and *B*). The nearly linear relationship may perhaps be explained by a mechanistic relationship between the duration of the foot-contact time when ground force is applied and the rate of ATP utilization in the muscle fibers recruited to apply support forces, as suggested by Taylor (70). The approach was successfully applied to level human walking by Hoyt et al. (36), who expressed rate of ground force application in terms of body weight and time of foot-ground contact (W_b/t_c), but has been explored only limitedly since (31). Our earlier efforts employing body size stratification and stride frequency variation as experimental tools (74) support the possibility that the W_b/t_c approach may provide a general mechanistic explanation for human walking economy across speed that we report for the different grades investigated here.

Predictive Accuracy of Existing Standard Models

A primary factor enabling us to develop a model with greater conditional breadth and roughly one-half the predictive error of the two leading standards was the singly-focused nature of our effort. In contrast, both the ACSM (3); and Pandolf et al. (56) model equations are amalgams of a series of smaller studies and data sets (for ACSM, see Refs 17 and 55; for Pandolf et al, see Refs. 25 and 26). The piecemeal formulation of these older standards, although impressive in terms of the accuracy achieved, also has intrinsic limitations. The intrinsic strengths and weaknesses that resulted explain the patterns of agreement between actual and predicted values that appear in Figs. 4 and 5 for the loaded and unloaded data sets and in Fig. 6 from the modified Bland-Altman mean difference plots. These patterns also reflect the formulaic differences resulting from the distinct intellectual legacies of the three models.

For the ACSM model equation, a minor weakness (Figs. 4, *C* and *D*, 5, *C* and *D*, and 6, *C* and *D*), given the broad purpose served, is the inability to fully describe the walking metabolic rate speed using a linear relationship. This understandable simplification is responsible for a small portion of the scatter above and below the lines of identity in Figs. 4*D* and 5*D*. However, the more significant limitation of the ACSM model equation is the overprediction of walking metabolic rates on all nonzero grades. For the declined gradients, overprediction resulted from the need to use the level condition predictions because the model equation does not extend to negative gradients. This conditional limitation and the consistent overprediction of inclined walking metabolic rates resulted in most of the predicted values falling above the line of identity (Figs. 4*D* and 5*D*) and a mean predictive error that was roughly 2 ml $O_2 \cdot kg_{body}^{-1} \cdot min^{-1}$ too low for both the loaded and

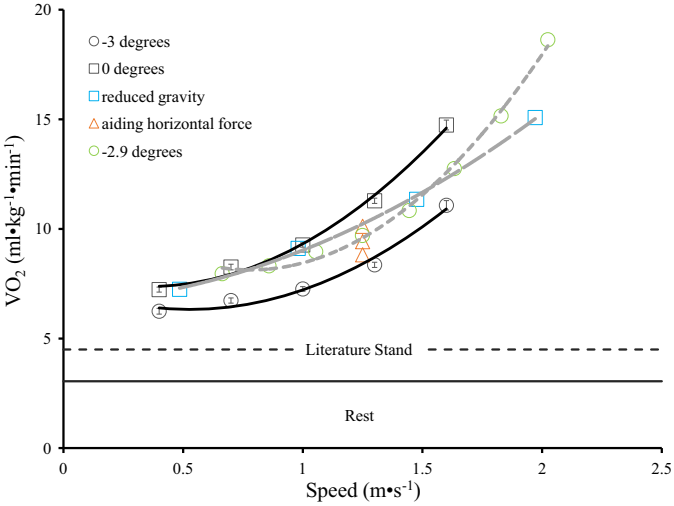

Fig. 7. Mean measured gross metabolic rates vs. walking speed for our unloaded subjects walking on 0 (squares) and −3° (circles) surface gradients. Horizontal lines correspond to the resting metabolic rate mean measured for our subjects (solid line) and the average standing metabolic rates (dashed line) reported from the 12 literature studies appearing in Table 3. Literature data from walking downhill (1), with assisted pulling (27) and under reduced gravity (21), are also illustrated.

unloaded conditions (black horizontal lines in Figs. 6*C* and 6*D*).

The greater conditional breadth of the Pandolf et al. (56) model equation resulted in slightly better overall performance (Figs. 4, *E* and *F*, 5, *E* and *F*, and 6, *E* and *F*) vs. the ACSM model equation. The considerable length of the Pandolf et al. (56) equation resulted in part from the more complex incorporation of load compared with our model as well as the arduous work required of Santee et al. (63) to extend the original model to negative grades. The elaborate final equation that incorporates at least four identifiable components of walking metabolism was able to predict the multiconditional variation present in both of our data sets reasonably well, resulting in a mean overall error near zero (black horizontal lines in Fig. 6, *E* and *F*). Predictive error was most pronounced across slower speeds and at lower metabolic rates for two reasons. The first is a conflation of resting metabolism with unloaded and loaded standing metabolic terms. These modeling choices do not seem scientifically well justified in terms of either the tight economy-load linkage we report (Figs. 2*B* and 3, Table 5, and APPENDIX) or differences in standing vs. walking posture (7) that likely decouple the metabolic requirements of supporting body weight across these different conditions. These factors in combination with a description that slightly overestimates the slope of the walking metabolic rate vs. speed relationship resulted in consistent underpredictions at slower walking speeds and a tendency toward overprediction at faster ones. These limitations are responsible for the pattern of predictive error in the modified Bland-Altman plots (Fig. 6, *E* and *F*) that are most evident at lower metabolic rates.

Concluding Remarks

Given the ubiquity of human walking and general availability of the basic inputs our model requires to predict walking metabolic rates, broad potential for application exists. Traditional uses such as exercise prescription, energy balance and weight management, and metabolic rate assessments from walking speeds and grades are directly computational. However, new applications may also be enabled by the accuracy of our minimum mechanics model. A half century ago, Astrand and Rhyming (5) were able to develop a submaximal test for estimating maximal aerobic power in part because of the accuracy with which they were able to predict cycling metabolic rates from mechanical work rates. In their original work, these authors reported being able to do so with an accuracy of ±6.0% for 67% of their cycling trials. The accuracy of our walking predictions here approached that of Astrand and Rhyming's (5) cycling predictions. Here, 63% of our unloaded level and inclined walking trials fell within the ±6.0% standard.

Finally, we note that new technological tools, like wearable sensors and digital topographical maps, expand potential usage well beyond traditional realms. These and other contemporary tools may allow our minimum mechanics model to be used to determine hiking route transport costs, sustainable walking speeds with and without loads, and instantaneous rates of metabolism and bodily heat production in the field. If the total supported load is known, these capabilities are potentially available from any technology that can provide speed and grade data in the field.

APPENDIX

The agreement between the ratios of loaded to unloaded walking economy and loaded to unloaded walking weight (*Eq. 3*) across two load conditions with 20 specific trial speed and grade conditions each (Fig. 3, *A* and *B*, blue circles and line fits) enables an informative analysis. Specifically, deviation from economy ratios specified a priori on the basis of load weight can be used to detect resting baseline under- and oversubtractions. At lower metabolic rates particularly, the relatively greater influence of incorrect subtractions on the smaller unloaded values in the denominator vs. the loaded values of the numerator ($\dot{V}O_{2\text{-walk-L}}/\dot{V}O_{2\text{-walk-UL}}$) introduces inequality with the respective walking weight ratios ($W_{body\ +\ load}/W_{body}$).

First, we consider an undersubtraction that incorrectly assumes that the body's basal metabolic requirement during walking is zero (i.e., $\dot{V}O_{2\text{-gross}} = \dot{V}O_{2\text{-walk}}$). Not removing any contribution of resting to the gross metabolic rate signal measured during walking disproportionately inflates the metabolic requirements of walking in the unloaded condition. Accordingly, ratios of loaded to unloaded walking economy that are smaller than the ratios of loaded to unloaded walking weight should result from doing so. Indeed, this is precisely what we observed, as nearly all the zero-subtraction economy ratios from 40 different load condition trials administered were lower than the ratio of loaded to unloaded walking weight (Fig. 3, *A* and *B*, red squares and line fits).

Next, we consider an oversubtraction that results from using a measured preexercise standing metabolic rate, or equivalent, as a surrogate for the body's resting metabolic rate. The average literature value of 4.5 ml $O_2 \cdot kg^{-1} \cdot min^{-1}$ in Table 3 exceeds the supine resting values measured for our subjects here (mean = 3.1 ml $O_2 \cdot kg_{body}^{-1} \cdot min^{-1}$; $n = 32$) by 1.4 ml $O_2 \cdot kg^{-1} \cdot min^{-1}$. Removing a quantity larger than the actual contributions of resting to the gross metabolic rates measured disproportionately deflates the metabolic requirements of walking in the unloaded condition. Therefore, this data treatment should result in economy ratios that are greater than the respective condition/weight ratios. As illustrated (Fig. 3, *A* and *B*, green triangles and curve fits), this is precisely what we observed.

For both the under- and oversubtraction data treatments, economy ratio deviation from respective condition weight ratios was signal size

dependent. In each case, economy ratios progressively approached the condition weight ratios as the body's gross metabolic rates increased. At the greatest metabolic rates for which the resting subtraction quantities have the least influence, the economy ratios from all three subtraction methods converged at or very near the values of the weight ratios from the respective conditions: 1.18 for the lighter load and 1.31 for the heavier one (Figs. 3*A* and 3*B*, respectively). Convergence at the greatest metabolic rates where economy ratio values are minimally affected by the subtracted quantity results from the direct influence of balanced torso loads on walking economy. These observations allow the error potentially introduced by incorrect baseline oversubtractions to be reasonably quantified.

The error potentially introduced by an oversubtraction of 1.4 ml $O_2 \cdot kg^{-1} \cdot min^{-1}$ is substantial because the metabolic rates measured under typical walking conditions are quite small (Fig. 7). For example, on a level surface at an intermediate walking speed of 1.0 m/s in the unloaded condition, 1.4 ml $O_2 \cdot kg^{-1} \cdot min^{-1}$ constitutes 15.1% of the body's gross metabolic rate and 22.7% of the walking rates based on our data. For our level walking economy data illustrated in Fig. 7, the resulting underestimations of walking metabolic rates range from a maximum of 33.9% at 0.4 m/s to a minimum of 12.0% at 1.6 m/s. Accordingly, across-speed analyses and other scientific assessments are directly affected and potentially confounded by the baseline quantity subtracted. The recent analysis of the most economical walking speed (ml $O_2 \cdot kg^{-1} \cdot min^{-1}$) by Abe et al. (1) illustrates this phenomenon. These authors reported that the speed identified as most economical differed over a 20% range, depending upon the baseline quantity subtracted from their gross metabolic rates. Potential effects for those conditions and interventions that elicit relatively low walking metabolic rates, such as walking downhill, in simulated reduced gravity, and with assistive pulling, will be most heavily influenced by the specific value of the baseline quantity subtracted. As Fig. 7 illustrates, in many of these cases, the literature standing subtraction eliminates most of the originally measured metabolic signal.

The factors responsible for the common usage of preexercise, or in some cases postexercise, standing metabolic rates as a resting baseline subtraction quantity are less clear than the difficulties potentially introduced. Scientifically, the justification for subtracting a baseline rate that includes a metabolic cost of supporting the body's weight against gravity is questionable since gravitational support is the primary determinant of walking metabolism. Conceivably, a standing subtraction would be justified if one wanted to assess a difference between the metabolic requirements of supporting the body while stationary vs. doing so while walking. However, the scientific objective that would be served by doing so is unclear. More generally, a rationale for subtracting any quantity greater than the body's supine resting rate is difficult to identify, particularly since doing so eliminates a portion of the body's walking metabolism that the subtraction is meant to isolate.

A basic quantitative issue with preexercise standing metabolic rates in Table 3 also exists. These measures are substantially greater on average than the values reported in the literature from those studies for which measuring standing metabolic rate was a primary rather than a secondary objective. The mean standing metabolic rate we measured under postabsorptive conditions here of 3.53 ± 0.08 ml $O_2 \cdot kg^{-1} \cdot min^{-1}$ is representative of this difference. Our mean is nearly 1.0 ml$\cdot kg^{-1} \cdot min^{-1}$ lower than the literature mean in Table 3 but in good agreement with the dedicated standing values appearing in the classic (68) and more recent literature (53). The factors responsible for the greater mean and considerable between-study variability in the standing values in Table 3 are difficult to identify from the limited measurement information available in many of these studies. Possible elevating factors include the preexercise condition, brief measurement period durations, and perhaps other factors.

Because advances in exoskeletons (14, 57), prosthetics (33), and other assistive devices continue to bring about reductions in walking metabolism, valid baseline subtractions are necessary if the effect sizes resulting from these and other interventions are to be accurately quantified. More generally, these results identify resting supine metabolic rates as a sound standard for quantifying exercise metabolic rates more broadly.

Practical Baseline Subtraction Suggestions for Isolating Walking Metabolism

For circumstances in which resting supine metabolic rate measurements are impractical or impossible, the literature identifies one, and perhaps two, viable alternatives. First, the extensively validated population equations of Schofield et al. (64) provide accurate resting metabolic rate estimates from only sex, height, and weight. For our subjects here, these equations predicted a mean resting metabolic rate (3.21 ± 0.05 ml $O_2 \cdot kg^{-1} \cdot min^{-1}$) that was within 0.08 ml $O_2 \cdot kg^{-1} \cdot min^{-1}$ of the measured mean, with an average individual error of 0.26 ± 0.04 ml $O_2 \cdot kg^{-1} \cdot min^{-1}$. Second, our measurements suggest that sitting metabolism may be able to serve as a reasonable supine resting rate surrogate. The postabsorptive sitting metabolic rates of our subjects were essentially identical to their supine resting rates (3.13 ± 0.07 vs. 3.16 ± 0.08 ml $O_2 \cdot kg^{-1} \cdot min^{-1}$, respectively; $n = 32$).

ACKNOWLEDGMENTS

Jen Nollkamper is acknowledged for extensive efforts that made successful completion of this work possible. We thank Bill Santee for scientific project guidance throughout and Laurence Ryan, Kenneth Clark, and Andrew Udofa for general support, consultation, and input. We also thank our subjects for the quality, and extent of their efforts.

GRANTS

This work was supported by US Army Medical and Materiel Command Award W81XWH-12-2-0013 to P. G. Weyand.

DISCLOSURES

The authors declare competing financial interests. L. W. Ludlow and P. G. Weyand are the inventors of a method for determining walking energy expenditure, which is owned by Southern Methodist University, includes information directly related to the contents of the manuscript, and is in preparation for submission to the US Patent Office.

AUTHOR CONTRIBUTIONS

L.W.L. and P.G.W. conceived and designed research; L.W.L. performed experiments; L.W.L. and P.G.W. analyzed data; L.W.L. and P.G.W. interpreted results of experiments; L.W.L. and P.G.W. prepared figures; L.W.L. and P.G.W. drafted manuscript; L.W.L. and P.G.W. edited and revised manuscript; L.W.L. and P.G.W. approved final version of manuscript.

REFERENCES

1. **Abe D, Fukuoka Y, Horiuchi M.** Economical speed and energetically optimal transition speed evaluated by gross and net oxygen cost of transport at different gradients. *PLoS One* 10: e0138154, 2015. doi:10.1371/journal.pone.0138154.
2. **Alexander RM.** *Principles of Animal Locomotion*. Princeton, NJ: Princeton University, 2006.
3. **American College of Sports Medicine.** *Guidelines for Graded Exercise Testing and Prescription* (7th ed.). Philadelphia, PA: Lippincott, Williams and Wilkins, 2013.
4. **Armstrong RB, Delp MD, Goljan EF, Laughlin MH.** Distribution of blood flow in muscles of miniature swine during exercise. *J Appl Physiol (1985)* 62: 1285–1298, 1987.
5. **Astrand PO, Ryhming I.** A nomogram for calculation of aerobic capacity (physical fitness) from pulse rate during sub-maximal work. *J Appl Physiol* 7: 218–221, 1954.
6. **Bastien GJ, Willems PA, Schepens B, Heglund NC.** Effect of load and speed on the energetic cost of human walking. *Eur J Appl Physiol* 94: 76–83, 2005. doi:10.1007/s00421-004-1286-z.
7. **Biewener AA, Farley CT, Roberts TJ, Temaner M.** Muscle mechanical advantage of human walking and running: implications for energy

cost. *J Appl Physiol (1985)* 97: 2266–2274, 2004. doi:10.1152/japplphysiol.00003.2004.
8. **Bobbert AC.** Energy expenditure in level and grade walking. *J Appl Physiol* 15: 1015–1021, 1960.
9. **Browning RC, Baker EA, Herron JA, Kram R.** Effects of obesity and sex on the energetic cost and preferred speed of walking. *J Appl Physiol (1985)* 100: 390–398, 2006. doi:10.1152/japplphysiol.00767.2005.
10. **Bubb W, Martin A, Howley E.** Predicting oxygen uptake during level walking at speeds of 80–130 m/min. *J Cardiopulm Rehabil* 5: 462–465, 1985.
11. **Cavagna GA, Saibene FP, Margaria R.** External work in walking. *J Appl Physiol* 18: 1–9, 1963.
12. **Cavagna GA, Heglund NC, Taylor CR.** Mechanical work in terrestrial locomotion: two basic mechanisms for minimizing energy expenditure. *Am J Physiol Regul Integr Comp Physiol* 233: R243–R261, 1977.
13. **Collins SH, Kuo AD.** Recycling energy to restore impaired ankle function during human walking. *PLoS One* 5: e9307, 2010. doi:10.1371/journal.pone.0009307.
14. **Collins SH, Wiggin MB, Sawicki GS.** Reducing the energy cost of human walking using an unpowered exoskeleton. *Nature* 522: 212–215, 2015. doi:10.1038/nature14288.
15. **Cotes JE, Meade F.** The energy expenditure and mechanical energy demand in walking. *Ergonomics* 3: 97–119, 1960. doi:10.1080/00140136008930473.
16. **DeJaeger D, Willems PA, Heglund NC.** The energy cost of walking in children. *Pflugers Arch* 441: 538–543, 2001. doi:10.1007/s004240000443.
17. **Dill DB.** Oxygen used in horizontal and grade walking and running on the treadmill. *J Appl Physiol* 20: 19–22, 1965.
18. **Doke J, Donelan JM, Kuo AD.** Mechanics and energetics of swinging the human leg. *J Exp Biol* 208: 439–445, 2005. doi:10.1242/jeb.01408.
19. **Donelan JM, Kram R, Kuo AD.** Mechanical work for step-to-step transitions is a major determinant of the metabolic cost of human walking. *J Exp Biol* 205: 3717–3727, 2002.
20. **Donelan JM, Shipman DW, Kram R, Kuo ADF.** Mechanical and metabolic requirements for active lateral stabilization in human walking. *J Biomech* 37: 827–835, 2004. doi:10.1016/j.jbiomech.2003.06.002.
21. **Farley CT, McMahon TA.** Energetics of walking and running: insights from simulated reduced-gravity experiments. *J Appl Physiol (1985)* 73: 2709–2712, 1992.
22. **Franz JR, Kram R.** The effects of grade and speed on leg muscle activations during walking. *Gait Posture* 35: 143–147, 2012. doi:10.1016/j.gaitpost.2011.08.025.
23. **Fylstra D, Lasdon L, Watson J, Waren A.** Design and use of the Microsoft Excel Solver. *Interfaces* 28: 29–55, 1998. doi:10.1287/inte.28.5.29.
24. **Gabaldón AM, Nelson FE, Roberts TJ.** Mechanical function of two ankle extensors in wild turkeys: shifts from energy production to energy absorption during incline versus decline running. *J Exp Biol* 207: 2277–2288, 2004. doi:10.1242/jeb.01006.
25. **Givoni B, Goldman RF.** Predicting metabolic energy cost. *J Appl Physiol* 30: 429–433, 1971.
26. **Goldman RF, Iampietro PF.** Energy cost of load carriage. *J Appl Physiol* 17: 675–676, 1962.
27. **Gottschall JS, Kram R.** Energy cost and muscular activity required for leg swing during walking. *J Appl Physiol (1985)* 99: 23–30, 2005. doi:10.1152/japplphysiol.01190.2004.
28. **Gottschall JS, Kram R.** Energy cost and muscular activity required for propulsion during walking. *J Appl Physiol (1985)* 94: 1766–1772, 2003. doi:10.1152/japplphysiol.00670.2002.
29. **Grabowski A, Farley CT, Kram R.** Independent metabolic costs of supporting body weight and accelerating body mass during walking. *J Appl Physiol (1985)* 98: 579–583, 2005. doi:10.1152/japplphysiol.00734.2004.
30. **Grenier JG, Peyrot N, Castells J, Oullion R, Messonnier L, Morin JB.** Energy cost and mechanical work of walking during load carriage in soldiers. *Med Sci Sports Exerc* 44: 1131–1140, 2012. doi:10.1249/MSS.0b013e3182456057.
31. **Griffin TM, Roberts TJ, Kram R.** Metabolic cost of generating muscular force in human walking: insights from load-carrying and speed experiments. *J Appl Physiol (1985)* 95: 172–183, 2003. doi:10.1152/japplphysiol.00944.2002.
32. **Handford ML, Srinivasan M.** Sideways walking: preferred is slow, slow is optimal, and optimal is expensive. *Biol Lett* 10: 20131006, 2014. doi:10.1098/rsbl.2013.1006.
33. **Herr HM, Grabowski AM.** Bionic ankle-foot prosthesis normalizes walking gait for persons with leg amputation. *Proc Biol Sci* 279: 457–464, 2012. doi:10.1098/rspb.2011.1194.
34. **Hill AV.** The heat of shortening and dynamic constants of muscle. *Proc Royal Soc Ser B* 126: 136–195, 1938. doi:10.1098/rspb.1938.0050.
35. **Hill AV.** The dimensions of animals and their muscular dynamics. *Sci Prog* 38: 209–230, 1950.
36. **Hoyt RW, Knapik JJ, Lanza JF, Jones BH, Staab JS.** Ambulatory foot contact monitor to estimate metabolic cost of human locomotion. *J Appl Physiol (1985)* 76: 1818–1822, 1994.
37. **Huang TW, Kuo AD.** Mechanics and energetics of load carriage during human walking. *J Exp Biol* 217: 605–613, 2014. doi:10.1242/jeb.091587.
38. **Hughes AL, Goldman RF.** Energy cost of "hard work". *J Appl Physiol* 29: 570–572, 1970.
39. **Huxley AF.** Muscle structure and theories of contraction. *Prog Biophys Biophys Chem* 7: 255–318, 1957.
40. **Knapik JJ, Reynolds KL, Harman E.** Soldier load carriage: historical, physiological, biomechanical, and medical aspects. *Mil Med* 169: 1–45, 2004. doi:10.7205/MILMED.169.1.45.
41. **Kram R, Taylor CR.** Energetics of running: a new perspective. *Nature* 346: 265–267, 1990. doi:10.1038/346265a0.
42. **Krouwer JS.** Why Bland-Altman plots should use X, not (Y+X)/2 when X is a reference method. *Stat Med* 27: 778–780, 2008. doi:10.1002/sim.3086.
43. **Kuo AD, Donelan JM, Ruina A.** Energetic consequences of walking like an inverted pendulum: step-to-step transitions. *Exerc Sport Sci Rev* 33: 88–97, 2005. doi:10.1097/00003677-200504000-00006.
44. **Lloyd R, Cooke CB.** The oxygen consumption with unloaded walking and load carriage using two different backpack designs. *Eur J Appl Physiol* 81: 486–492, 2000. doi:10.1007/s004210050072.
45. **Ludlow LW, Weyand PG.** Estimating loaded, inclined walking energetics: no functional difference between added and body mass. IEEE 13th International Conference on Wearable and Implantable Body Sensor Networks (BSN), 306–311, 2016.
46. **Ludlow LW, Weyand PG.** Energy expenditure during level human walking: seeking a simple and accurate predictive solution. *J Appl Physiol (1985)* 120: 481–494, 2016. doi:10.1152/japplphysiol.00864.2015.
47. **Maffels C, Schutz Y, Schena F, Zaffanello M, Pinelli L.** Energy expenditure during walking and running in obese and nonobese prepubertal children. *J Pediatr* 123: 193–199, 1993. doi:10.1016/S0022-3476(05)81688-9.
48. **Martin PE, Rothstein DE, Larish DD.** Effects of age and physical activity status on the speed-aerobic demand relationship of walking. *J Appl Physiol (1985)* 73: 200–206, 1992.
49. **Margaria R.** Sulla fisiologica e specialmente sul consumo energetico della corsa a varie velocita ed inclinazioni. *Atti Accad Naz Lincei* 7: 299–368, 1938.
50. **Margaria R, Cerretelli P, Aghemo P, Sassi G.** Energy cost of running. *J Appl Physiol* 18: 367–370, 1963.
51. **Marsh RL, Ellerby DJ, Henry HT, Rubenson J.** The energetic costs of trunk and distal-limb loading during walking and running in guinea fowl *Numida meleagris*. *J Exp Biol* 209: 2050–2063, 2006. doi:10.1242/jeb.02226.
52. **McGowan CP, Duarte HA, Main JB, Biewener AA.** Effects of load carrying on metabolic cost and hindlimb muscle dynamics in guinea fowl (Numida meleagris). *J Appl Physiol (1985)* 101: 1060–1069, 2006. doi:10.1152/japplphysiol.01538.2005.
53. **Miles-Chan JL, Sarafian D, Montani JP, Schutz Y, Dulloo A.** Heterogeneity in the energy cost of posture maintenance during standing relative to sitting: phenotyping according to magnitude and time-course. *PLoS One* 8: e65827, 2013. doi:10.1371/journal.pone.0065827.
54. **Minetti AE, Ardigò LP, Saibene F.** Mechanical determinants of gradient walking energetics in man. *J Physiol* 472: 725–735, 1993. doi:10.1113/jphysiol.1993.sp019969.
55. **Nagle FJ, Balke B, Naughton JP.** Gradational step tests for assessing work capacity. *J Appl Physiol* 20: 745–748, 1965.
56. **Pandolf KB, Givoni B, Goldman RF.** Predicting energy expenditure with loads while standing or walking very slowly. *J Appl Physiol Respir Environ Exerc Physiol* 43: 577–581, 1977.
57. **Panizzolo FA, Galiana I, Asbeck AT, Siviy C, Schmidt K, Holt KG, Walsh CJ.** A biologically-inspired multi-joint soft exosuit that can reduce the energy cost of loaded walking. *J Neuroeng Rehabil* 13: 43, 2016. doi:10.1186/s12984-016-0150-9.

58. **Pierrynowski MR, Winter DA, Norman RW.** Metabolic measures to ascertain the optimal load to be carried by man. *Ergonomics* 24: 393–399, 1981. doi:10.1080/00140138108924861.
59. **Ralston HJ.** Energy-speed relation and optimal speed during level walking. *Int Z Angew Physiol* 17: 277–283, 1958.
60. **Reeves ND, Narici MV.** Behavior of human muscle fascicles during shortening and lengthening contractions in vivo. *J Appl Physiol (1985)* 95: 1090–1096, 2003. doi:10.1152/japplphysiol.01046.2002.
61. **Roberts TJ, Marsh RL, Weyand PG, Taylor CR.** Muscular force in running turkeys: the economy of minimizing work. *Science* 275: 1113–1115, 1997. doi:10.1126/science.275.5303.1113.
62. **Roberts TJ, Kram R, Weyand PG, Taylor CR.** Energetics of bipedal running. I. Metabolic cost of generating force. *J Exp Biol* 201: 2745–2751, 1998.
63. **Santee WR, Blanchard LA, Speckman KL, Gonzalez JA, Wallace RF.** *Load carriage Model Development and Testing with Field Data. Technical Note TN03-3*. Natick, MA: US Army Research Institute of Environmental Medicine, 2003.
64. **Schofield WN.** Predicting basal metabolic rate, new standards and review of previous work. *Hum Nutr Clin Nutr* 39, *Suppl* 1: 5–41, 1985.
65. **Silder A, Besier T, Delp SL.** Predicting the metabolic cost of incline walking from muscle activity and walking mechanics. *J Biomech* 45: 1842–1849, 2012. doi:10.1016/j.jbiomech.2012.03.032.
66. **Silder A, Delp SL, Besier T.** Men and women adopt similar walking mechanics and muscle activation patterns during load carriage. *J Biomech* 46: 2522–2528, 2013. doi:10.1016/j.jbiomech.2013.06.020.
67. **Soule RG, Pandolf KB, Goldman RF.** Energy expenditure of heavy load carriage. *Ergonomics* 21: 373–381, 1978. doi:10.1080/00140137808931734.
68. **Smith HM,** *Gaseous Exchange and Physiological Requirements for Level and Grade Walking*. Washington, DC: Carnegie Institute, 1922.
69. **Taylor CR.** Force development during sustained locomotion: a determinant of gait, speed and metabolic power. *J Exp Biol* 115: 253–262, 1985.
70. **Taylor CR.** Relating mechanics and energetics during exercise. *Adv Vet Sci Comp Med* 38A: 181–215, 1994.
71. **van der Walt WH, Wyndham CH.** An equation for prediction of energy expenditure of walking and running. *J Appl Physiol* 34: 559–563, 1973.
72. **Vanderpool MT, Collins SH, Kuo AD.** Ankle fixation need not increase the energetic cost of human walking. *Gait Posture* 28: 427–433, 2008. doi:10.1016/j.gaitpost.2008.01.016.
73. **Waters RL, Hislop HJ, Thomas L, Campbell J.** Energy cost of walking in normal children and teenagers. *Dev Med Child Neurol* 25: 184–188, 1983. doi:10.1111/j.1469-8749.1983.tb13742.x.
74. **Weyand PG, Smith BR, Puyau MR, Butte NF.** The mass-specific energy cost of human walking is set by stature. *J Exp Biol* 213: 3972–3979, 2010. doi:10.1242/jeb.048199.
75. **Weyand PG, Smith BR, Sandell RF.** Assessing the metabolic cost of walking: the influence of baseline subtractions. *Conf Proc IEEE Eng Med Biol Soc* 2009: 6878–6881, 2009. doi:10.1109/IEMBS.2009.5333126.
76. **Weyand PG, Smith BR, Schultz NS, Ludlow LW, Puyau MR, Butte NF.** Predicting metabolic rate across walking speed: one fit for all body sizes? *J Appl Physiol (1985)* 115: 1332–1342, 2013. doi:10.1152/japplphysiol.01333.2012.
77. **Workman JM, Armstrong BW.** Oxygen cost of treadmill walking. *J Appl Physiol* 18: 798–803, 1963.
78. **Zuntz N.** Ueber den stoffvenbrauch des hundes bei muskelarbeit. *Arch Ges Physiol* 68: 191–211, 1897. doi:10.1007/BF01661859.

Walking energy expenditure: a loaded approach to algorithm development

Lindsay W. Ludlow and Peter G. Weyand
Department of Applied Physiology and Wellness
Southern Methodist University
Dallas, TX, USA
pweyand@smu.edu

Sensor-based predictions for walking energy expenditure require sufficiently versatile algorithms to generalize to a variety of conditions. Here we test whether our height-weight-speed (HWS) model validated across speed under level conditions is similarly accurate for loaded walking. We hypothesized that increases in walking energy expenditure would be proportional to added load when resting metabolism was subtracted from gross walking metabolism. After subtracting resting metabolic rate, walking energy expenditure was found to increase in direct proportion to load at walking speeds of 0.6, 1.0, and 1.4 $m \cdot s^{-1}$. With load carriage treated as body weight, the predictive algorithms derived using the HWS model were similar for loaded and unloaded conditions. Determination of the direct relationship between load and energy expenditure for level walking provides insight which may be used to refine algorithms, such as the HWS model, for use in body sensors to monitor physiological status in the field.

Keywords—load carriage, sensors, generalized equation, algorithm, metabolism

I. INTRODUCTION

Prediction and monitoring of whole-body energy expenditure depends heavily on the accuracy of the algorithms utilized. For individuals at rest, algorithms that accurately predict metabolic rates from body size, sex, and age have been established for decades [1]. For individuals during locomotion, however, the algorithms currently available are not equivalently accurate [2,3]. Prediction of the latter is considerably more difficult because of the many factors that influence the extent to which whole-body metabolism is elevated during locomotion. These include but are not limited to: height, weight, speed, grade, terrain, and load carriage.

Recent work indicates that whole-body locomotor metabolism can be predicted accurately under certain controlled conditions. Specifically, we found that walking metabolic rates on firm, level surfaces could be predicted to within 8% if the height, weight, and speed of the walker are known. Thus, under these controlled conditions, sensors capable of [4,5] providing walking speed could be used in conjunction with height and weight to accurately estimate whole-body metabolic rates. Here, under the same conditions, we test whether our existing HWS algorithm can similarly describe walking metabolic rates when torso loads are carried.

Theoretically, the existing HWS model might accurately account for loaded metabolic rates if the added load is treated as additional body weight in the existing equation. A critical issue for considering this possibility is the method used to partition the body's total metabolic rate into resting vs. walking portions. A common approach has been to subtract a standing metabolic rate to represent the resting component [7,8]. However, during quiet standing, metabolic rates have been reported to be 1.15 – 1.5 times greater than those obtained during a traditional supine resting measurement (RMR) [8,9,10,11,12,13]. The variability in standing metabolic rates may explain some of the inconsistency thus far reported in the metabolic responses to walking with loads when the former is the baseline quantity subtracted. While the general consensus has been that metabolic rates increase in proportion to the load carried, results have been somewhat variable [12,14,15].

Here, we used the elevations in locomotor metabolic rates introduced by load carriage as an experimental tool for two purposes. Our first objective was to investigate whether the elevations in locomotor metabolic rates (gross – supine rest) would be directly proportional to loads added to the torso. A direct relationship would allow the influence of added loads on locomotor metabolism to be more easily predicted and modeled. After quantifying the relationship between walking energy expenditure and load, our second objective was to determine if the HWS model would accurately predict unloaded and loaded metabolic rates. If so, the HWS model would provide a robust algorithm for sensor development with potential to determine walking metabolic rate under multiple conditions. We specifically tested the following corresponding hypotheses. First, we hypothesized that the net energy expended while walking (gross – supine rest) would increase in direct proportion to the load carried. Second, we hypothesized that the independent equations derived in the form of the HWS model would be similar for loaded and unloaded conditions.

II. METHODS

A. Experimental Design

To test whether locomotor energy expenditure increases in proportion to added torso load we measured metabolic rate under three conditions: unloaded (i.e. body weight only, W_b), and two added load conditions equaling 1.17 W_b, and 1.31 W_b. We utilized metabolic data acquired from all three load conditions, as well as metabolic rates during supine rest and quiet standing, to assess the influence of the baseline quantity subtracted. Using supine rest as our baseline subtraction

This work was made possible by grant DAMD17-03-2-005 and award W81XWH-12-2-0013 from the Medical and Materiel command of the United States DOD.

quantity, we assessed whether walking metabolic rates increased in direct proportion to the loads carried.

B. Subjects

Ten volunteer subjects, 5 male and 5 female (means ± SEM, age = 29.6 ± 1.4 years, height = 171.6 ± 2.2 cm, mass = 67.0 ± 2.9 kg) participated in the study after providing written informed consent in accordance with the Institutional Review Board of Southern Methodist University. All subjects were healthy and did not have cardiovascular risk factors as a contraindication for exercise according to the guidelines set forth by the American College of Sports Medicine. Subjects reported to the laboratory on eight different days for testing sessions consisting of a VO_{2max} test, 6 sessions of loaded and unloaded walking, and a final session for measurement of metabolic rate during supine rest, and quiet standing. For the final session, subjects were instructed to arrive at the laboratory immediately after waking, to avoid exercise prior to testing and refrain from eating and caffeine use for eight hours prior.

C. Gross Metabolic Rates

Metabolic rates were determined from indirect calorimetry through the measurement of expired gases during supine resting, quiet standing, and walking at three different treadmill speeds and under three different load conditions (no load, ~15% of body weight, ~30% of body weight) using a computerized metabolic system (Parvo Medics TrueOne 2400, Sandy, UT, USA). A one-way breathing valve and tubing were used to collect expired gases and direct flow through a pneumotach, which measured volume flow rates, and into a mixing chamber. Aliquots of expired air were sampled from the mixing chamber and analyzed for O_2 and CO_2 fractions using paramagnetic and infrared gas analyzers, respectively. Data were collected continuously, with rates of oxygen uptake averaged over a two minute period under steady-state conditions. Resting metabolic rates were determined from the lowest 10-minute average during a 30-minute, supine resting trial. The lowest five minute average during the final 10 minutes of a 15-minute trial was used to determine standing metabolic rate.

D. Treadmill Testing Protocol

Walking bouts were conducted on a level treadmill at speeds of 0.6, 1.0, and 1.4 $m \cdot s^{-1}$. All speeds were completed under the following loaded conditions: unloaded, carrying ~15% body weight, and carrying ~30% bodyweight. Subjects were weighed on their first visit to the laboratory and assigned a loading scheme based on their weight rounded to the nearest ten pound increment. Therefore the exact percentage of body weight carried varied slightly from 15% and 30% for some subjects, with the average actual percent body weight across the 10 subjects coming out to 17% and 31% for the two different load carriage conditions. For the loaded trials, weight was carried both on the front in a vest and on the back in a backpack and was symmetrically distributed about the torso. For each condition, walking trials lasted for five minutes to ensure that the final two minutes were under steady-state conditions. All loaded conditions and walking speeds were repeated on two separate days, and the average of the steady-state values from the two trials was taken to determine gross energy expenditure.

E. Relationship Between Load and Metabolic Rate

Net metabolic rate was calculated by subtracting supine resting energy expenditure from gross energy expenditure while walking. In order to determine whether metabolic rate increases in direct proportion to the mass of the load carried we calculated the ratio of energy expenditure while loaded ($E_{metab\ L}$) to energy expenditure unloaded ($E_{metab\ U}$) at all walking speeds for both gross and net metabolic rates. We then plotted these values against the ratio of total mass (M_{Total}) to body mass (M_{Body}) for each walking speed.

F. Height-Weight-Speed Model Equation Derivations

Walking metabolic rates were estimated using the previously published HWS model [6]. The HWS model is comprised of three components: a resting metabolic rate (RMR), a minimum walking metabolic rate which is modeled as a multiple of RMR, and a speed-dependent metabolic rate, as shown by equation 1 below.

$$VO_2 = RMR + C_1 \cdot RMR + C_2 \cdot V^2 \cdot height^{-1} \quad \text{(eq. 1)}$$

All of the terms for the HWS model were derived and are reported in mass-specific units of oxygen uptake in $ml \cdot kg^{-1} \cdot min^{-1}$. However, illustrated metabolic rates are presented in SI units ($W \cdot kg^{-1}$).

For the present study, the coefficients C_1 and C_2 were derived to obtain a best fit to the data set. Optimized coefficients were obtained for the unloaded and loaded conditions alone, as well as with the unloaded and loaded conditions combined. The optimizer function in Excel was used to determine the values of C_1 and C_2 such that the sum squared error was minimized. The Excel optimizer (Microsoft Excel Solver, Excel 2010 version) was chosen due to its ability to optimize a coefficient while holding other values (resting metabolic rate, walking speed, and subject height) constant [16]. Once the forms of the equations were derived they were used to describe walking metabolic rates for each subject across all walking speeds and load conditions. The R^2 values for measured versus predicted values, as well as the standard error of estimate (SEE) were calculated for each equation. An accurate model fit was evaluated using the criteria of a value for SEE of less than 10% of the grand mean.

III. Results

A. Gross Metabolic Rates

The mean standing metabolic rate was 1.1 times greater than the mean for supine rest (1.16 ± 0.03 vs. 1.27 ± 0.04 $W \cdot kg^{-1}$; Fig. 1). Between-subject variability was appreciable, with standing values ranging from 1.03 to 1.19 times greater than respective supine resting values. The difference between metabolic rate during supine rest and during quiet standing varied for most, but not all subjects, as several subjects had essentially the same values under the two conditions (Fig. 2).

Walking metabolic rates increased across walking speeds under all three load conditions (Fig. 1). Further, load carriage resulted in an increase in walking energy expenditure at all walking speeds that was in direct proportion to the load carried (Fig. 1).

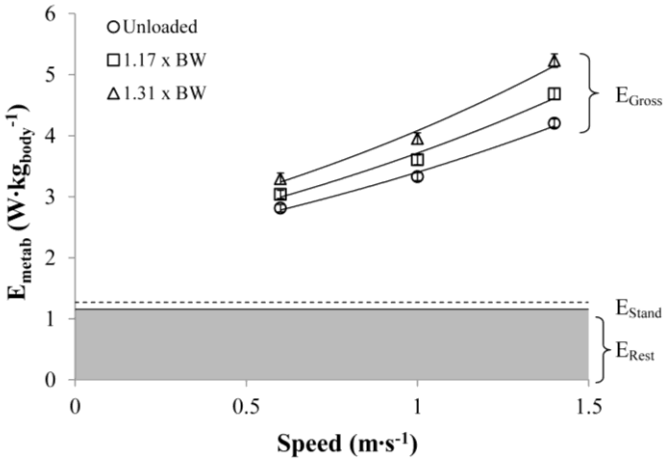

Fig. 1. Mass-specific gross metabolic rate (E_{metab}) increases with walking speed under all three load conditions. E_{metab} is plotted for walking without load, walking with a load equal to ~17% of body weight, and with a load of ~31% of body weight. On the y-axis, the value for kilograms includes the weight of the subject plus the weight of the load carried (kg_{total}^{-1}). Metabolic rate during quiet standing and during supine rest are depicted as constants.

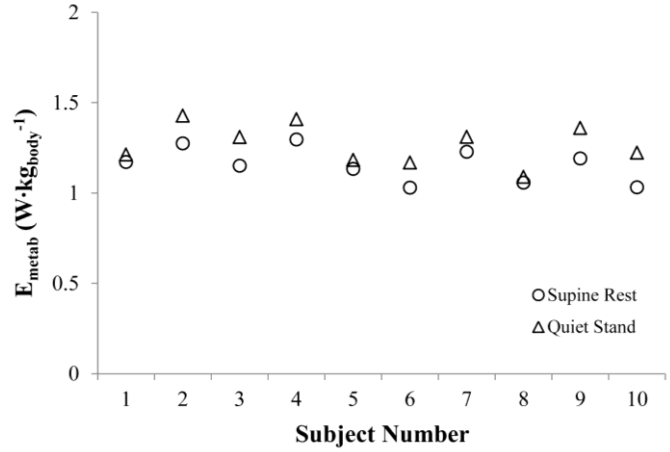

Fig. 2. Individual mass-specific gross metabolic rates (E_{metab}) during supine rest and quiet standing. Subjects are represented on the graph in ascending order of body mass from 52.2 to 82.8 kg.

B. Relationship Between Load and Metabolic Rate

Across all walking speeds, increases in gross metabolic rates in the loaded conditions were not proportional to the loads carried (Fig. 3). However, increases in net walking metabolic rates under loaded conditions were almost exactly proportional to the load carried as hypothesized. When subtracting energy expenditure for supine rest to calculate net metabolic rate, we found that walking energy expenditure increased in proportion to load carried across all three walking speeds (Fig. 3). For example, at 1 $m \cdot s^{-1}$, when subjects carried a load that was 31% greater than their body weight, gross metabolic rate only increased by 19%, whereas net metabolic rate increased by 29%.

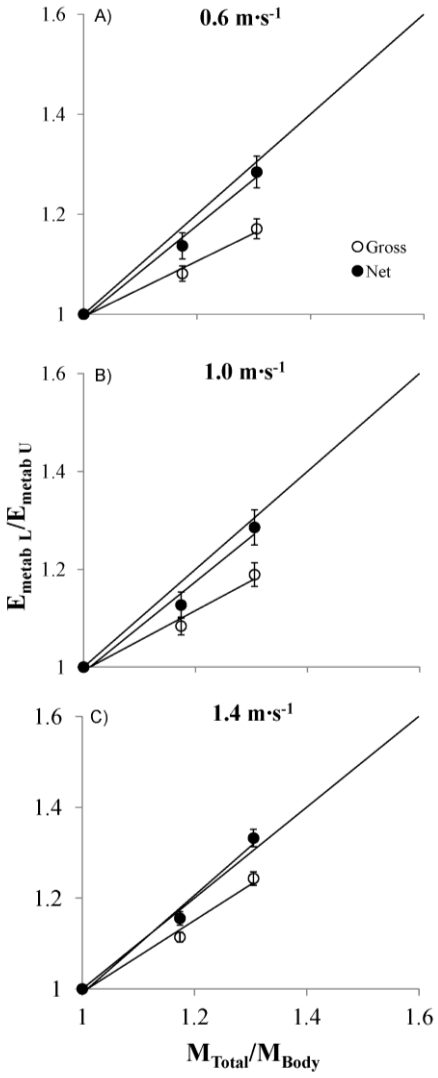

Fig 3. Net metabolic rate increases in direct proportion to load carried. Panels A-C depict the ratio of metabolic rate while carrying load ($E_{metab\ L}$) to metabolic rate while unloaded ($E_{metab\ U}$) plotted against the ratio of total mass (body mass + load; M_{Total}) to body mass (M_{body}). Gross metabolic rate and net metabolic rate are plotted for walking speeds of 0.6 (Panel A), 1.0 (Panel B), and 1.4 $m \cdot s^{-1}$ (Panel C). The diagonal line indicates direct proportionality between the X and Y values such that metabolic rate is proportional to the mass of the load carried.

C. HWS Model Predictions of Walking Energy Expenditure

The optimized HWS model coefficients for the unloaded, loaded, and all three load conditions combined appear in Table 1. The unloaded, loaded, and combined loaded and unloaded model derivations produced similar values for both coefficients in the HWS model equation. Further, using the three optimized equations to provide best fits of the data produced similar values for R^2 and standard error of estimate (SEE). For the optimized HWS model on the unloaded data, an R^2 of 0.91 and SEE of 0.52 mls $O_2 \cdot kg^{-1} \cdot min^{-1}$ were attained (Table 1). For the loaded data, the optimized equation resulted in a best fit with an R^2 of 0.85 and SEE of 0.72 mls $O_2 \cdot kg^{-1} \cdot min^{-1}$ (Table 1). When loaded and unloaded conditions were combined, the optimized HWS model fits produced an R^2 of 0.84 and SEE of 0.74 mls $O_2 \cdot kg^{-1} \cdot min^{-1}$ (Table 1). For all three equations, the

SEE was less than 10% of the grand mean, thus meeting our criteria for model accuracy,

Model	C_1	C_2	exponent	R^2	SEE
Unloaded	1.00	4.37	2	0.91	0.52
Loaded	0.76	4.56	2	0.85	0.72
Unloaded + Loaded	0.84	4.49	2	0.84	0.74

Table 1. Empirical Derivations of the Height-Weight-Speed Model Equation with all metabolic units, including SEE, expressed in mls $O_2 \cdot kg^{-1} \cdot min^{-1}$.

IV. Discussion

Our first finding was that the energy expended for level walking, when determined as the quantity: (gross – supine rest), increases in direct proportion to the load carried. We found direct proportionality across all three speeds and the two load conditions we tested. This finding is of particular importance as it allows for added torso load to be directly incorporated into predictive algorithms for walking metabolism. Second, as hypothesized, we found that the HWS model provided accurate descriptions of walking metabolic rate both with and without load. The independent equations derived in the form of the HWS model for loaded and unloaded conditions (Table 1) were nearly identical.

A. Baseline Subtractions

Metabolic rates measured during quiet standing are commonly utilized as a baseline subtraction quantity in order to determine net walking metabolic rates. However, the typical elevations observed in the energy expended in the standing vs. supine resting condition (Fig. 1) seem likely to result from the muscular activation required for postural support [17,18,19]. Accordingly, standing metabolism seems unlikely to generally represent the body's true resting metabolic rate. Moreover, subtracting standing rates from the gross metabolic rates measured during walking risks subtracting out a portion of the metabolic energy expended to support the body's weight against gravity while walking. In light of the substantial evidence of a relationship between weight supported and walking energy expenditure across studies of load carriage [12,14,15], obesity [11], and weight loss [20] the use of standing metabolic rate as a standard baseline subtraction measure should be carefully considered in accordance with experimental objectives. If the objective is the most valid partitioning of the resting vs. walking portions of the body's gross locomotor metabolic rates, our results suggest supine resting values are likely to provide a more valid baseline quantity than quiet standing for doing so.

The above conclusion is based in part upon the individual variability observed in standing metabolic rate values. When our measured standing values were expressed in relation to supine resting values, the elevations observed for different individuals ranged from 1.03 to 1.19 times the latter value. The variability observed raises the possibility that quiet standing may include a skill component that influences the extent of the elevations observed above supine rest. At present, the correct interpretations of measured standing metabolic rates, both in general and as a baseline subtraction quantity, are not fully clear.

B. Load Carriage and Energy Expenditure

As hypothesized, we found that walking metabolic rates (gross - supine rest) increased in close proportion to the loads carried and regardless of speed. Across the three speeds and two loading conditions included here, the mean deviation from the direct proportionality expected was 1.6 ± 0.85%. Others have reported previously that when net metabolic rates are determined by subtracting standing metabolism from gross walking metabolism, metabolic rate to increase in a fashion that is greater than proportional to load carriage [12]. We found the standing metabolic rate values to be larger than resting metabolic rate, thus load-induced increases in metabolic rate would also be greater than the added load using the standing metabolic rate subtraction. Our data are consistent with a multitude of prior experimental results indicating that the primary determinant of locomotor metabolic rates is the weight that must be supported against gravity, whether the body's weight only or the body's weight plus an external load [21,22].

C. Estimating Walking Energy Expenditure

While numerous equations have been derived to predict walking energy expenditure, the accuracy many of these equations under conditions such as load carriage is not known [6]. Predictive accuracy is of critical importance in order for algorithms for walking energy expenditure to be incorporated into sensor technologies. In the set of ten subjects presented here, the optimized HWS model provides accurate (SEE < 10% of grand mean) descriptions of walking metabolism across a range of walking speeds both with and without load carriage. Our data indicate that the HWS model is an attractive candidate for use in body sensor devices to estimate walking energy expenditure.

D. Conclusions and Recommendations

Our results indicate that level walking metabolic rates increase in close proportion to added torso loads across a range of speeds and loads up to nearly one-third of the body's weight. This finding should simplify the incorporation of torso loads into predictive equations for sensor-based and other field applications. Accurate determination of the relationship between load carriage and energy expenditure is of particular military importance to predicting and monitoring the performance of soldiers in the field, and also for the general population seeking accurate methods for quantifying energy expenditure during exercise that involves load carriage (e.g. weighted vest, backpacking). Additional efforts will be needed to expand predictive capabilities to include additional load, grade and terrain conditions.

Acknowledgments

We thank Jennifer Nollkamper and Emily Field for their help in subject recruitment and data collection.

References

[1] W.N. Schofield. "Predicting basal metabolic rate, new standards and review of previous work," Hum. Nutr. Clin. Nutr., vol. 39, Supp. 1, pp. 5-41, 1985.

[2] American College of Sports Medicine Guide to Exercise Testing and Prescription, 6th edition, Lippincott, Williams & Wilkins, 2000.

[3] K. Pandolf, B. Givoni, and R.K. Goldman, "Predicting energy expenditure with loads while standing or walking very slowly," J. Appl. Physiol., vol. 43, pp. 577-581, 1977.

[4] R.W. Hoyt, J.J. Knapik, J.F. Lanza, B.H. Jones, and J.S. Staab. "Ambulatory foot contact monitor to estimate metabolic cost of human locomotion," J. Appl. Physiol., vol. 76, pp. 1818-1822, 1994.

[5] P.G. Weyand et al. "Ambulatory estimates of maximal aerobic power from foot-ground contact times and heart rates in running humans," J. Appl. Physiol., vol. 91, pp. 451-458, 2001.

[6] P.G. Weyand, B.R. Smith, N.S Schultz, L.W. Ludlow, M.R. Puyau, and N.F. Butte. "Predicting metabolic rate across walking speed: one fit for all body sizes?," J. Appl. Physiol., vol. 115, pp. 1332-1342, 2013.

[7] J.M. Donelan, R. Kram, and A.D. Kuo. "Mechanical work for step to step transitions is a major determinant of the metabolic cost of human walking," J. Exp. Biol., vol. 205, pp. 3717-3727, 2002.

[8] D.J. McCann and W.C. Adams. "A dimensional paradigm for identifying the size-independent cost of walking," Med Sci. Sports Exerc., vol. 34, pp 1009-1017, 2002.

[9] V.T. Inman, H.J. Ralston, and F. Todd, Human Walking. Baltimore, MD, Williams & Wilkins, 1981.

[10] D. DeJaeger, P.A. Willems, and N.C. Heglund, "The energy cost of walking in children," Pflügers Arch. Eur. J. Physiol., vol. 441, pp. 538-543, 2001.

[11] R. C. Browning, E. A. Baker, J. A. Herron, and R. Kram, "Effects of obesity and sex on the energetic cost and preferred speed of walking," J. Appl. Physiol., vol. 100, pp. 390-398, 2006.

[12] T.M. Griffin, T.J. Roberts, and R. Kram, "Metabolic cost of generating muscular force in human walking: insights from load-carrying and speed experiments," J. Appl. Physiol., vol. 95, pp. 172-183, 2003.

[13] P.G. Weyand, B.R. Smith, and R.F. Sandell. "Assessing the metabolic cost of walking: the influence of baseline subtractions," Conf. Proc. IEEE Eng. Med. Biol. Soc., pp. 6878-6881, 2009.

[14] R.F. Goldman, and P.F. Iampietro. "Energy cost of load carriage," J. Appl. Physiol., vol. 17, pp. 675-676

[15] G. J. Bastien, P.A. Willems, B. Schepens, and N.C. Heglund, "Effect of load and speed on the energetic cost of human walking," Eur J. Appl. Physiol. vol. 94, pp. 76-83, 2005.

[16] D. Fylstra, L. Lasdon, J. Watson, and A. Waren. "Design and Use of the Microsoft Excel Solver," Interfaces. vol. 28, pp. 29-55, 1998.

[17] J.V. Basmajian and C. De Luca, "Muscles Alive: Their Functions Revealed by Electromyography," Williams & Wilkins, Baltimore, 1985.

[18] J. Joseph and A. Nightingale, "Electromyography of posture: leg muscles in males," J. Physiol. vol. 117, pp. 484-491, 1952.

[19] I .D. Loram, C.N. Maganaris and M. Lakie, "The passive, human calf muscles in relation to standing: the non-linear decrease from short range to long range stiffness," J. Physiol., vol. 584, pp. 661-675, 2007.

[20] G. R. Hunter, J. P. McCarthy, D.R. Bryan, P.A. Zuckerman, M.M. Bamman, and N.M. Byrne, "Increased strength and decreased flexibility are related to reduced oxygen cost of walking," Eur. J. Appl. Physiol., vol. 104, pp. 895-901, 2008.

[21] R. Kram, and C.R. Taylor. "Energetics of running: a new perspective," Nature, vol. 346, pp. 265-267, 1990.

[22] C.R. Taylor. "Relating mechanics and energetics during exercise," Adv. Vet. Sci. Comp. Med., vol. 38A, pp. 181-215, 1994.

© 2017. Published by The Company of Biologists Ltd | Journal of Experimental Biology (2017) 220, 247-258 doi:10.1242/jeb.138057

RESEARCH ARTICLE

A general relationship links gait mechanics and running ground reaction forces

Kenneth P. Clark[1,2], Laurence J. Ryan[1] and Peter G. Weyand[1,*]

ABSTRACT

The relationship between gait mechanics and running ground reaction forces is widely regarded as complex. This viewpoint has evolved primarily via efforts to explain the rising edge of vertical force–time waveforms observed during slow human running. Existing theoretical models do provide good rising-edge fits, but require more than a dozen input variables to sum the force contributions of four or more vague components of the body's total mass (m_b). Here, we hypothesized that the force contributions of two discrete body mass components are sufficient to account for vertical ground reaction force–time waveform patterns in full (stance foot and shank, m_1=0.08m_b; remaining mass, m_2=0.92m_b). We tested this hypothesis directly by acquiring simultaneous limb motion and ground reaction force data across a broad range of running speeds (3.0–11.1 m s^{-1}) from 42 subjects who differed in body mass (range: 43–105 kg) and foot-strike mechanics. Predicted waveforms were generated from our two-mass model using body mass and three stride-specific measures: contact time, aerial time and lower limb vertical acceleration during impact. Measured waveforms (N=500) differed in shape and varied by more than twofold in amplitude and duration. Nonetheless, the overall agreement between the 500 measured waveforms and those generated independently by the model approached unity (R^2=0.95 ±0.04, mean±s.d.), with minimal variation across the slow, medium and fast running speeds tested ($\Delta R^2 \leq 0.04$), and between rear-foot (R^2=0.94±0.04, N=177) versus fore-foot (R^2=0.95±0.04, N=323) strike mechanics. We conclude that the motion of two anatomically discrete components of the body's mass is sufficient to explain the vertical ground reaction force–time waveform patterns observed during human running.

KEY WORDS: Impact forces, Two-mass model, Spring–mass model, Running performance, Motion sensing, Wearable sensors

INTRODUCTION

Running ground reaction forces are of fundamental physical and biological importance. Acutely, they determine the body's state of motion, limb-loading rates and tissue stresses. Over time, they influence the health and functional status of the tissues, limb and runner. However, the mechanical basis of the vertical force–time waveform patterns described most extensively for human runners (Cavanagh, 1987; Munro et al., 1987) continues to be a matter of significant disagreement (Chi and Schmitt, 2005; Clark et al., 2014; Denoth, 1986; Derrick, 2004; Lieberman et al., 2010; Nigg, 2010; Shorten and Mientjes, 2011). The current discordance is at least partially attributable to the mechanical complexities of the limbs and bodies responsible for the forces present at the limb–ground interface. Human and other vertebrate runners are mechanically complex in their body and limb-segment morphology, tissue properties, neural control of muscle forces, and joint and limb stiffnesses. These features allow body mass components to accelerate differently with respect to one another and the ground. Because the total waveform corresponds to the acceleration of the body's entire mass, the summed accelerations of different mass components must somehow determine the instantaneous forces and waveform patterns observed.

At present, the most common approach to explaining the force–time waveform patterns of human runners are lumped element, spring–mass systems that include four or more hypothetical mass components with multiple springs and dashpots (Fig. 1A). Most current versions include 14 or more input variables derived via forward dynamics simulations (Chi and Schmitt, 2005; Liu and Nigg, 2000; Ly et al., 2010; Nigg and Liu, 1999; Nikooyan and Zadpoor, 2011; Zadpoor and Nikooyan, 2010). Per their intended purpose, these models are able to provide close, *post facto* fits to the rising edge of the force–time waveforms that result from rear-foot strike mechanics at jogging speeds under a variety of surface, footwear and other conditions (Ly et al., 2010; Zadpoor and Nikooyan, 2010). However, these models do not attempt to predict the falling edge of the waveform, they do not explain the differently shaped waveforms that typically result from fore-foot strike mechanics, and their ability to fit waveforms from intermediate and fast running speeds is completely unknown.

A scientific justification for including numerous mass components to account for vertical ground reaction force–time waveforms was importantly provided by a direct motion-to-force experiment conducted by Bobbert et al. (1991) a quarter century ago. These investigators demonstrated that the total waveform can indeed be reasonably predicted from the summed accelerations of seven body mass components at modest running speeds. Recently, we have theorized that an alternative approach may allow the number of masses needed for full waveform prediction to be reduced from seven to only two.

Our approach (Clark et al., 2014) divides the body's mass into two, anatomically based, invariant, mass components: the first corresponding to the mass of the lower limb (m_1, 8% total body mass) and the second corresponding to the remainder of the body's mass (m_2, 92% total body mass; Fig. 1B). The model theoretically allows the full vertical force–time waveform to be predicted from the force contributions corresponding to the two body mass components. Impulse 1 results from the vertical collision of m_1 with the running surface and impulse 2 results from the vertical accelerations of m_2 throughout the ground contact period (Clark et al., 2014). Our introductory effort (Clark et al., 2014) was able to

[1]Southern Methodist University, Locomotor Performance Laboratory, Department of Applied Physiology & Wellness, Dallas, TX 75206, USA. [2]West Chester University, Human Performance Laboratory, Department of Kinesiology, West Chester, PA 19383, USA.

*Author for correspondence (pweyand@smu.edu)

P.G.W., 0000-0002-0588-0321

Received 25 January 2016; Accepted 24 October 2016

Journal of Experimental Biology

Journal of Experimental Biology (2017) 220, 247-258 doi:10.1242/jeb.138057

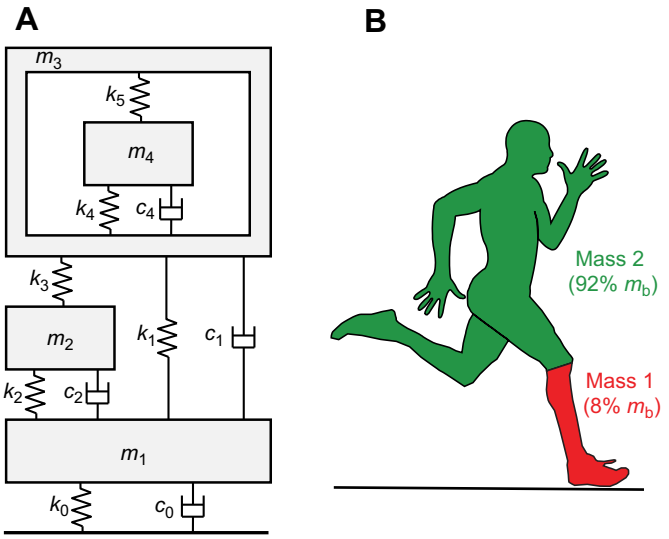

Fig. 1. Multi-mass model and two-mass model. (A) Representative multi-element spring–mass-damper model (diagram adapted from Nigg, 2010). This type of model relates variations in ground reaction forces to mechanical characteristics of specific elements in the model. (B) The two-mass model is a computational model incorporating the known mass distributions of the human body as illustrated. Mass 1 (m_1) represents the lower limb (8% total body mass, m_b) and mass 2 (m_2) represents the remainder of the body's mass (92% total body mass). Prior to touchdown, m_1 typically has a greater vertical velocity than m_2 as a result of the extension of the leg prior to impact.

account for essentially all of the variation present in four vertical force–time waveforms (R^2 range: 0.95–0.98, mean=0.97±0.01) selected for their amplitude, duration and shape heterogeneity. However, the close fits achieved resulted from *post facto* selection of the input parameters to maximize the goodness of each fit.

Here, we undertook a direct, experimental test of the hypothesis that the motion of two discrete body mass components is sufficient to predict running vertical ground reaction force–time waveforms in full. The two-mass model requires only body mass and three stride-specific measures as inputs: contact time, aerial time and lower limb acceleration. Because these three inputs can be readily acquired from a variety of video or other inexpensive motion-sensing technologies, our model potentially offers economical options for generating running ground reaction force waveforms without a force platform. Additionally, the concise running force–motion linkage provided could be applied to footwear, prosthetic and orthotic design, or used to inform gait interventions designed to reduce injuries or enhance running performance.

MATERIALS AND METHODS

Model formulation

Although the physical motion of running occurs in three spatial dimensions, the total vertical ground reaction force waveform is determined by the forces due to the instantaneous vertical accelerations of the body mass components. Our computational model utilizes experimental measurements to determine the parameters linking running motion to impulse forces, thus avoiding the limitations of modeling ground reaction forces with single-axis or single-body mass–spring-damper systems (Nikooyan and Zadpoor, 2011). The fundamental premise of the two-mass model (see Appendix for detailed derivation) is that the total vertical ground reaction force waveform is composed of two overlapping bell-shaped impulses due to the vertical collision of the lower limb (J_1) with the running surface and the concurrent vertical accelerations of the rest of the body (J_2) during ground contact. The total ground reaction impulse J_T is the sum of J_1 and J_2 and can be determined by the total stance-averaged vertical ground reaction force $F_{T,avg}$ during the ground contact time t_c:

$$J_T = J_1 + J_2 = F_{T,avg} t_c. \quad (1)$$

The model assumes steady-speed level running where the speed is constant and the net vertical displacement of the center of mass of the body is zero over each step. Thus, the time-averaged vertical ground reaction force must equal the body's weight and $F_{T,avg}$ can be determined if contact time t_c and aerial time t_a are known:

$$F_{T,avg} = m_b \boldsymbol{g} \frac{t_c + t_a}{t_c}, \quad (2)$$

where m_b is body mass and $\boldsymbol{g}$ is gravitational acceleration ($\boldsymbol{g}$=9.8 m s^{-2}), and the quantity t_c+t_a equals the step time, t_{step}.

Impulse J_1 corresponds to the vertical deceleration of m_1 during surface impact:

$$J_1 = F_{1,avg}(2\Delta t_1) = \left(m_1 \frac{\Delta v_1}{\Delta t_1} + m_1 \boldsymbol{g}\right)(2\Delta t_1), \quad (3)$$

where m_1 is 8.0% of the body's mass (Plagenhoef et al., 1983; Winter, 1990), Δt_1 is the time interval between touchdown and the vertical velocity of m_1 slowing to zero, Δv_1 is the change in vertical velocity of m_1 during Δt_1, and $F_{1,avg}$ is the average force during the total time interval ($2\Delta t_1$) of impulse J_1, here defined as the impact interval. A single ankle marker is used to measure Δv_1 and Δt_1, which determine the vertical acceleration of the lower limb mass m_1 (Fig. 2). The lower limb attains a relatively constant positive velocity after the impact interval (Fig. 2C), resulting in a near-zero acceleration of m_1 (Fig. 2D) and negligible force (Fig. 2E). Thus, J_1 can be represented by a finite impulse during the impact interval. Kinematic data for the ankle marker position during the impact interval for representative rear-foot strike (RFS) and fore-foot strike (FFS) subjects appear in Fig. 3. For highest accuracy of the Δt_1 measurement, a velocity threshold and projection method is used to eliminate minor fluctuations in the ankle marker velocity profile near zero (see Appendix). To assess the accuracy of this projection method, the measured ankle marker velocity at the projected time to zero was quantified for all footfalls.

Impulse J_2 corresponds to the remainder of the body's mass and is determined from total ground reaction impulse J_T in Eqn 1 and impulse J_1 in Eqn 3:

$$J_2 = F_{2,avg} t_c = J_T - J_1, \quad (4)$$

where $F_{2,avg}$ is the average force of impulse J_2 during the contact time t_c.

The raised cosine bell (RCB) curve function was used to generate the $F(t)$ waveforms of J_1 and J_2 for both foundational and empirical reasons. The RCB function is unique among all bell curve functions in that it can be derived from the first two terms of the Fourier series (see Appendix). Analyses of vertical ground reaction force–time waveforms from jumping in place indicate that using a function consisting of two bell curves provides a superior representation and requires a lower number of Fourier terms than a half-sine curve (Racic and Pavic, 2009). Direct waveform comparisons indicate that the RCB function provides superior descriptions versus both the half-cosine and Gaussian functions (see cos^2 data in table 2 of Sim et al., 2008) when vertical ground reaction force impulses are generated at frequencies ≥2 Hz.

Journal of Experimental Biology

Journal of Experimental Biology (2017) 220, 247-258 doi:10.1242/jeb.138057

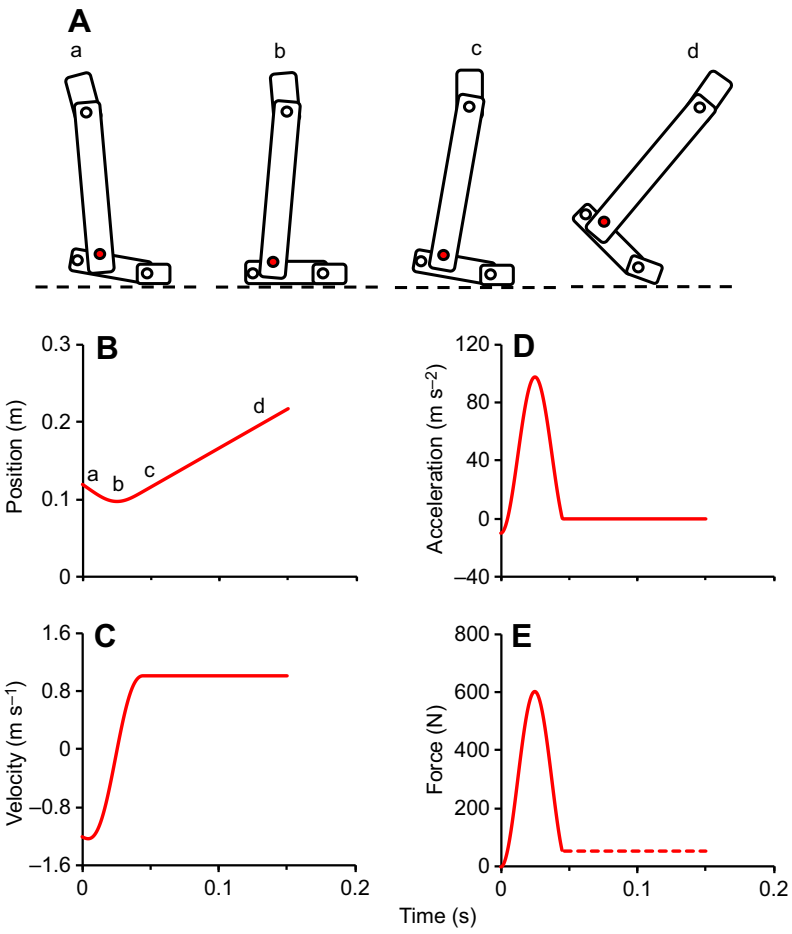

Fig. 2. Lower limb motion and force during ground contact. (A) A stick figure illustration of mass segment m_1 motion (a–d) during the foot–ground portion of a running step. The red circle represents the axis of rotation of the ankle joint. (B–E) Corresponding schematic graphs for vertical position (B), velocity (C), acceleration (D) and force (E) of lower limb mass m_1 versus time during the ground contact phase. After the impact interval, m_1 reaches a relatively constant positive velocity, resulting in near-zero acceleration of m_1 and a negligible force contribution from the lower limb mass for the remainder of the ground contact phase. A simplifying assumption of the two-mass model is that the force resulting from the acceleration of m_1 can be accurately modeled by a finite impulse during the impact interval.

Thus, each impulse uses the RCB function for the force waveform $F(t)$ during the interval $B-C \leq t \leq B+C$:

$$F(t) = \frac{A}{2}\left[1 + \cos\left(\frac{t-B}{C}\pi\right)\right], \quad (5)$$

where $A=2F_{avg}$ is the peak amplitude, B is the center time of the peak and C is the half-width time interval. For higher accuracy, the waveform function for impulse J_2 includes an offset to account for the force plate threshold and an asymmetry adjustment to account for the center of mass height difference at takeoff and touchdown. A J_2 force peak corresponding to the minimum height of the center of mass was set at $0.47t_c$ based on the observations of Cavagna et al. (1977, see their table 4) for human running (see Appendix for additional details).

The total force curve $F_T(t)$ is the sum of the two individual force waveforms representing impulse J_1 and impulse J_2 :

$$F_T(t) = F_1(t) + F_2(t). \quad (6)$$

Model force–time waveforms

Model-predicted versus measured vertical force waveforms were tested for both individual footfalls and trial-averaged force data. For the individual footfall predictions, the input parameters of body mass, ground contact time, subsequent aerial time, m_1 vertical velocity at touchdown and impact interval time Δt_1 were used to generate the model-predicted waveform, which was then compared with the measured waveform from that footfall. For the trial-averaged waveform comparisons, the input parameters from each right footfall were averaged for that trial. A minimum of three and a maximum of six right footfalls were included in the trial average, depending on the number of steps completed during the trial. The measured input parameters from each trial average were used to generate a model-predicted waveform, which was then compared

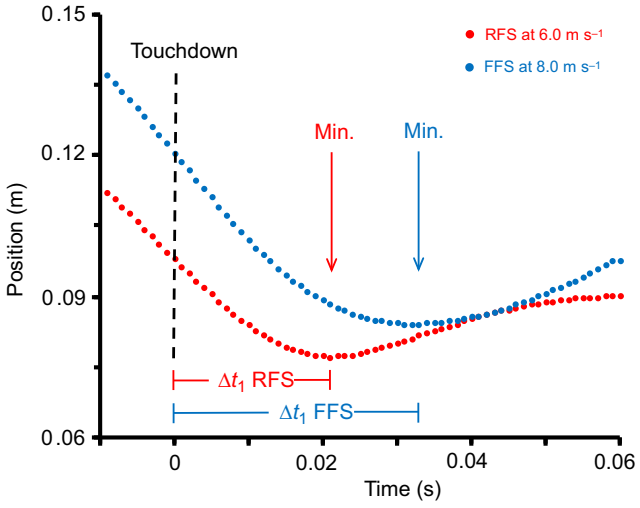

Fig. 3. Ankle marker vertical position versus time data just prior to touchdown and during the initial ground contact phase for a representative rear-foot strike (RFS) and fore-foot strike (FFS) runner. After touchdown, the ankle marker decreases in vertical position until it reaches its lowest position above the running surface (Min.); the time interval for this deceleration is bracketed by Δt_1 for the RFS and FFS, respectively.

Journal of Experimental Biology (2017) 220, 247-258 doi:10.1242/jeb.138057

with the measured trial-averaged waveform. An example of this data treatment appears in Fig. 4, including a series of original measured waveforms (Fig. 4A), the trial-average model-predicted waveform (Fig. 4B), and the model-predicted versus trial-average measured waveform (Fig. 4C). Both single-footfall and trial-averaged predictions were assessed to evaluate whether the number of footfalls included influences the predictive accuracy of the model.

To validate the anatomical mass fractions in our model, waveforms were alternatively generated with literature-suggested impact-mass minimum and maximum values (Derrick, 2004). A smaller m_1 quantity of 1.5% was used (representing the approximate mass of the foot; Plagenhoef et al., 1983; Winter, 1990; Hamill and Knutzen, 2009) with a corresponding m_2 quantity of 98.5%. A larger m_1 quantity of 16% was used (representing the approximate mass of the entire stance limb; Plagenhoef et al., 1983; Winter, 1990; Hamill and Knutzen, 2009) with a corresponding m_2 quantity of 84.0%. We predicted that across both speed and foot-strike mechanics, values along the rising edge of the waveform would be under-predicted with an m_1 quantity of 1.5% and over-predicted with an m_1 quantity of 16%.

Statistical analysis

The predictive accuracy of the model was assessed on the 500 individual footfalls acquired using both the R^2 statistic and the root mean square error (RMSE) statistic, global values that quantify goodness of fit in relative and absolute terms, respectively. These statistical assessments are broadly used for a variety of purposes, including quantifying the degree of overlap present in time-series data per prior practice (Cohen, 2013; Clark et al., 2014; Clark and Weyand, 2014; Morin et al., 2005). The footfall sample size was sufficiently large to detect very small differences in model performance across foot-strike type and speed using the R^2 and RMSE statistics.

A two-way ANOVA was used to evaluate whether goodness-of-fit and RMSE values varied as a function of speed (slow, medium, fast) and foot-strike (rear- versus fore-foot categories) classifications ($P \leq 0.05$, Table 1) on all 500 footfall waveforms acquired.

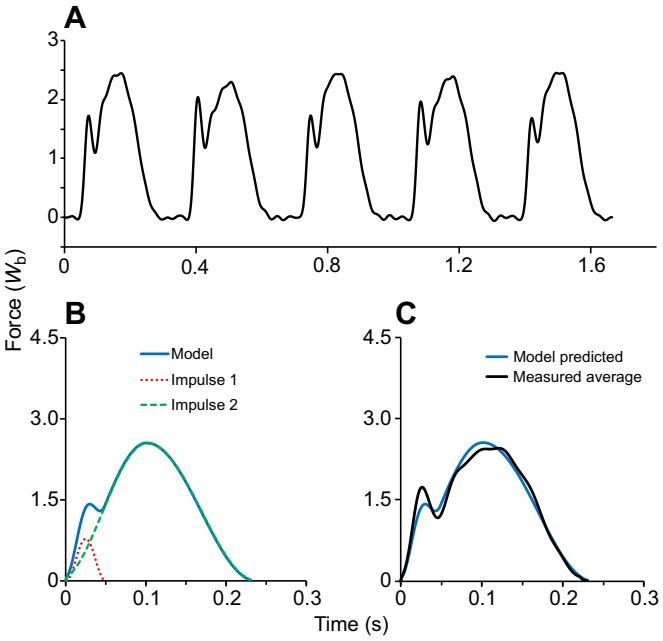

Fig. 4. Measured and predicted force–time waveforms. (A) Five consecutive vertical ground reaction force–time waveforms from a RFS subject jogging at 4 m s^{-1}. Force units were standardized to body weight (W_b). The first, third and fifth step illustrated were footfalls from the right leg. (B) The average values from the three right footfalls were used as input parameters to create a trial-averaged impulse 1 and trial-averaged impulse 2, which combined to form the trial-averaged model force waveform. (C) The model-predicted force waveform and measured average force waveform for the three right footfalls.

Subjects and participation

A total of 42 subjects, 23 men and 19 women, volunteered and provided written informed consent. The consent process and all experimental procedures were approved by, and conformed to, the approval terms granted by the Institutional Review Board of Southern Methodist University. All subjects were between 18 and 37 years of age and engaged in regular physical activity at the time of testing. The mean age and size characteristics of the men and women were as follows: men: age=23.3±5.0 years, range=18–37 years; height=1.79±0.07 m, range=1.69–1.95 m; mass=81.1±8.5 kg, range=71.0–101.5 kg; and women: age=22.5±1.7 years, range=18–36 years; height=1.68±0.06 m, range=1.55–1.78 m; mass=63.3±9.4 kg, range=43.4–82.0 kg. Subjects included recreationally trained individuals, intercollegiate team-sport athletes, and professional track and field athletes, four of whom were Olympic medalists in sprint or hurdle events.

Data acquisition

Data were collected across a range of speeds (3.0 m s^{-1} to top speed) on a three-axis, custom-built high-speed force treadmill (AMTI, Watertown, MA, USA) capable of speeds of over 20 m s^{-1}. To ensure that the model was being evaluated at speeds that required a normal running gait, only trials above a Froude speed of 1.0 [$v/\sqrt{(gL_0)}>1.0$] were included in the statistical analysis. For both submaximal and maximal tests, subjects followed testing procedures similar to those described in Weyand et al. (2000, 2010). Thirty-nine of the 42 subjects completed trials up to top speed, and these subjects were habituated to high-speed treadmill running during one or more familiarization sessions before undergoing top speed testing. All subjects wore standardized black compression shirts and shorts, and the same model of running shoes (Nike Waffle Racer version 7.0, Beaverton, OR, USA).

Kinetic and kinematic data collection and analysis

Ground reaction force data were acquired at 1000 Hz and were post-filtered using a low-pass, fourth-order, zero-phase-shift Butterworth filter with a cutoff frequency of 25 Hz (Winter, 1990). For each footfall, the vertical ground reaction force applied during the contact period was determined from the time during which the vertical force signal exceeded a threshold of 40 N. Additionally, trial-averaged vertical ground reaction force waveforms were generated for individual subjects at different trial speeds by averaging the force from each millisecond of the contact period for the right-foot waveforms that had corresponding kinematic data.

For each trial, 3.46 s of video data were collected using a high-speed video system consisting of three Fastec Imaging HiSpec 2G cameras (Mikrotron GmbH, Unterschleissheim, Germany) operating at 1000 frames s^{-1}. Subjects wore reflective markers on the heel and ball of the foot on the lateral aspect of the right running shoe, as well as on the lateral aspect of the joint axes of rotation of the right ankle, knee and hip to capture these respective positions during the trials. A single-frame video file of each subject was

Journal of Experimental Biology (2017) 220, 247-258 doi:10.1242/jeb.138057

Table 1. R^2 and RMSE (W_b) statistics for individual modeled-predicted waveforms

	Speed			
Foot-strike type	Slow (3–4 m s^{-1})	Medium (5–6 m s^{-1})	Fast (≥7 m s^{-1})	Total
R^2 RFS	0.94±0.05 (*N*=70)	0.97±0.02 (*N*=50)	0.93±0.05 (*N*=57)	0.94±0.04 (*N*=177)
R^2 FFS	0.97±0.02 (*N*=73)	0.96±0.03 (*N*=82)	0.93±0.05 (*N*=168)	0.95±0.04‡ (*N*=323)
R^2 total	0.96±0.04* (*N*=143)	0.96±0.03* (*N*=132)	0.93±0.05 (*N*=225)	**0.95±0.04** (*N*=500)
RMSE RFS	0.18±0.08 (*N*=70)	0.15±0.05 (*N*=50)	0.23±0.07 (*N*=57)	0.19±0.08 (*N*=177)
RMSE FFS	0.16±0.07 (*N*=73)	0.18±0.08 (*N*=82)	0.28±0.09 (*N*=168)	0.23±0.10 (*N*=323)
RMSE total	0.17±0.07* (*N*=143)	0.17±0.07* (*N*=132)	0.27±0.09 (*N*=225)	**0.21±0.09** (*N*=500)

Values are means±s.d. RMSE, root mean square error; W_b, force units standardized to body weight; FFS, fore-foot strike; RFS, rear-foot strike.
*Significantly different versus fast speed (P≤0.001). ‡Significantly different versus RFS (P≤0.01).

recorded prior to testing to serve as a reference for the kinematic analyses. To assess the predictive accuracy of the model across different foot-strike types, footfalls were classified as RFS if the first surface contact occurred on the posterior half of the foot, and FFS if the first surface contact occurred on the anterior half.

The procedures used in extracting three-dimensional marker coordinates from the high-quality multiple camera videos consisted of correcting image distortions, calibrating the three-dimensional space and digitizing the markers. The calibration and digitization routines extensively used functions from the MATLAB Image Processing Toolbox (MathWorks, Natick, MA, USA). The calibration and digitization MATLAB routines were developed by the Hedrick Lab at the University of North Carolina (Hedrick, 2008). A resolution of 0.7 mm was measured under dynamic conditions using the high-speed video system with the custom MATLAB image correction, calibration and digitization routines. Data acquisition timing for the AMTI DigiAmp amplifier and Fastec Imaging cameras was synchronized through hardware interfaces. The digitized marker data were filtered at 25 Hz using the same filter as for the force data.

RESULTS

Overall agreement between model-predicted and measured waveforms

The goodness-of-fit agreement (R^2) between the 500 ground reaction force waveforms we measured and those predicted by our two-mass model approached unity as hypothesized (Table 1). The corresponding error of prediction expressed in force units standardized to the body's weight was slightly greater than $0.2W_b$ and was equal to 11.5% of the mean stance-averaged vertical force from all 500 trials ($1.82\pm0.23W_b$). The R^2 and RMSE statistics for the 108 trial-averaged waveform values were nearly identical to those for the 500 individual waveforms. Specifically, the goodness of fit between model-predicted and measured trial-averaged ensemble waveforms was only 0.01 greater (R^2=0.96±0.03) than the individual footfall value, while the RMSE of prediction was only $0.02W_b$ less ($0.19\pm0.07W_b$) than the corresponding individual footfall values.

Predictive accuracy across foot-strike types and running speeds

The goodness-of-fit between the model-predicted and measured waveforms (R^2) was nearly identical (ΔR^2=0.01) for the 177 RFS versus 323 FFS waveforms (Table 1). Because of the large number of footfalls tested and minimal variability in model predictive accuracy, the 0.01 greater R^2 value for the FFS versus RFS waveforms was significantly different statistically. Corresponding RMSE differences for the RFS versus FFS waveform predictions were small (ΔRMSE=+$0.04W_b$) and not statistically different.

The goodness-of-fit between the model-generated and actual waveforms was slightly, but significantly, better for waveforms acquired from slow and medium speeds versus those from fast speeds. The R^2 values, when averaged for the waveforms from the three speed ranges (R^2 total, Table 1) regardless of foot-strike type, were slightly, but significantly lower (ΔR^2=−0.03) for the faster versus medium and slower speed trials. Similarly, the RMSE of the model fits to the slow and medium speed waveforms were not different from one another; however, both were significantly smaller than the error of prediction for the waveforms from the fastest speeds. Similar across-speed patterns were present for both the R^2 and RMSE statistics when the waveforms were analyzed within either the RFS or FFS mechanics categories (Table 1).

The waveforms generated with the two-mass model accurately predicted the more rapid rising edges of the RFS versus FFS waveforms, including transient rising-edge peaks when present, regardless of the running speed, and total waveform amplitude and duration (Figs 5A,C,E and 6A,C,E). Waveform shape variability across foot-strike types was accurately predicted from the shorter deceleration periods of the m_1 mass segment for RFS versus FFS (Δt_1, Table 2) with little difference in the overall J_1 impulse values (Fig. 5B,D,F versus Fig. 6B,D,F; Δv_1, Table 2) at similar speeds. From slower to faster speeds, J_1 impulses predicted by the model became greater for both RFS and FFS waveforms as a result of the greater pre-impact ankle velocities (Table 2). The close fits to the middle and later portions of all the waveforms resulted largely or exclusively from the J_2 impulse predicted from the model because the m_1 impact deceleration event concluded during the first quarter to half of the total contact period.

The measured ankle marker velocity at the time our projection technique identified a zero value was, on average, −0.05±0.04 m s^{-1} for the 500 individual trials. All but two of the footfalls had a measured velocity within ±0.20 m s^{-1} of a literal zero value (i.e. 0.00 m s^{-1}).

Model predictive accuracy with alternative m_1 segment values

Poorer agreement between model-predicted and measured waveforms resulted from using m_1 segment values that were either smaller or larger than the originally assigned anatomical model value of 8.0% of m_b. As hypothesized, waveforms generated using lesser m_1 values (m_1=1.5% with m_2=98.5% of m_b) consistently under-predicted the force values measured along the rising edge of the waveforms (Figs 7A,D,G and 8A,D,G). Conversely, waveforms generated using greater m_1 values (m_1=16.0% with m_2=84.0% of m_b) consistently over-predicted measured rising-edge force values (Figs 7C,F,I and 8C,F,I). Differences were more pronounced at the faster trial speeds because of the greater m_1 segment decelerations and correspondingly larger J_1 impulses at faster speeds.

Journal of Experimental Biology (2017) 220, 247-258 doi:10.1242/jeb.138057

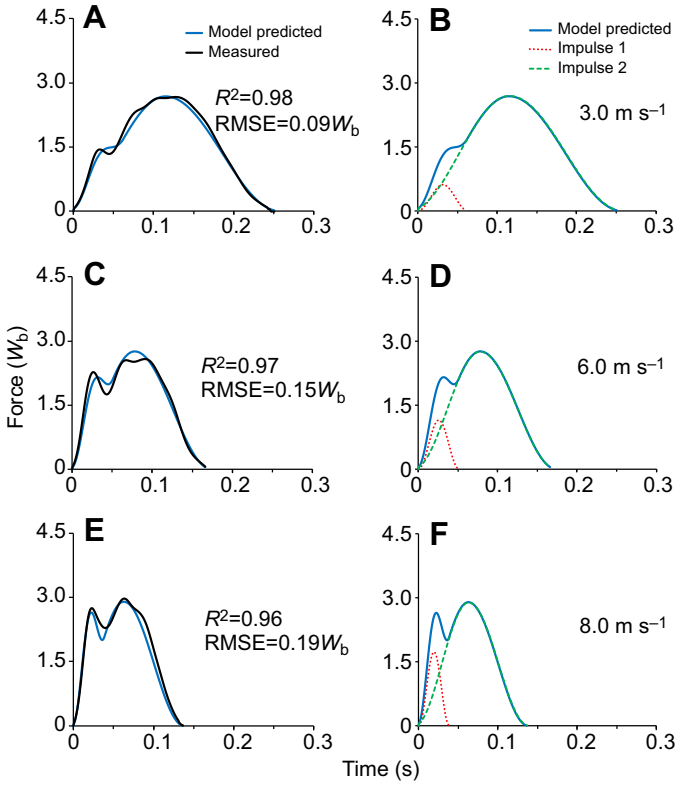

Fig. 5. Vertical ground reaction force–time waveforms for RFS trials. Trials for an individual subject took place at 3.0 m s^{-1} (A,B), 6.0 m s^{-1} (C,D) and 8.0 m s^{-1} (E,F). A, C and E illustrate the model-predicted waveform (solid blue line) from the average kinematics measured during the trial compared with a measured average of the vertical ground reaction force waveforms (solid black line). B, D and F illustrate the sum of the first impulse (dotted red line) and second impulse (dashed green line) to form the total model-predicted waveform (solid blue line).

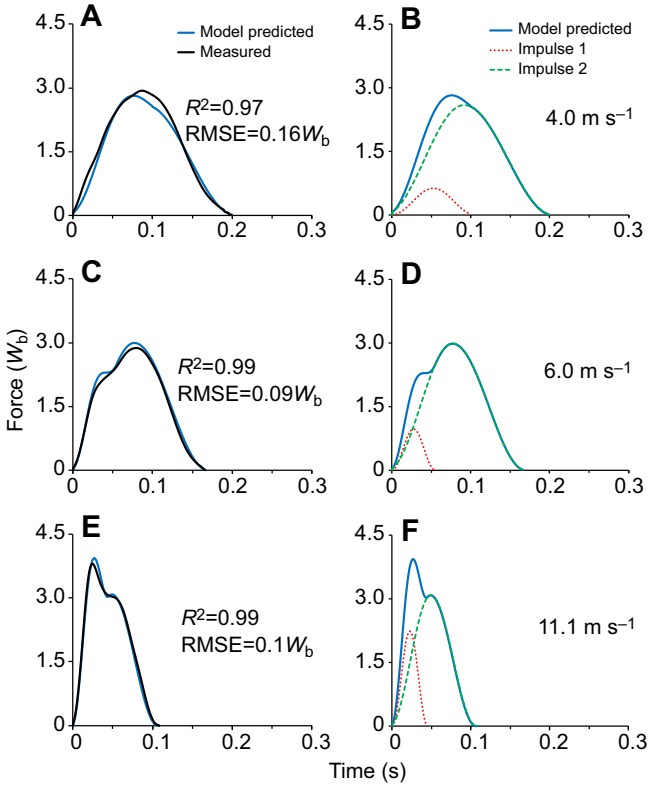

Fig. 6. Vertical ground reaction force–time waveforms for FFS trials. Trials for an individual subject took place at 4.0 m s^{-1} (A,B), 6.0 m s^{-1} (C,D) and 11.1 m s^{-1} (E,F). A, C and E illustrate the model-predicted waveform (solid blue line) from the average kinematics measured during the trial compared with a measured average of the vertical ground reaction force waveforms (solid black line). B, D and F illustrate the sum of the first impulse (dotted red line) and second impulse (dashed green line) to form the total model-predicted waveform (solid blue line).

The R^2 goodness of fit values for the 500 individual footfall waveforms generated using m_1 values equal to 1.5% and 16.0% of m_b accounted for 12% and 21% less variance, respectively, versus the original m_1=8.0% results (m_1−1.5% R^2=0.83±0.16 and m_1−16.0% R^2=0.74±0.21). Predictive error values for the waveforms generated using the two alternative m_1 segment values were approximately twice as large as those obtained using the original 8.0% value (m_1−1.5% RMSE=0.36±0.17W_b; m_1−16.0% RMSE=0.47±0.24W_b).

DISCUSSION

As hypothesized, we found that the force contributions of two discrete body mass components do indeed suffice to predict running vertical ground reaction force–time waveforms in full. Our two-mass, two-impulse model independently predicted nearly all of the variation in measured running ground reaction force waveforms, which differed considerably in their shape, amplitude and duration. Although our prior, best-fit analysis indicated that this outcome might be theoretically possible (Clark et al., 2014), an experimental test incorporating simultaneous motion and force data had not been previously undertaken. Our direct test here indicated that regardless of whether our 42 human subjects jogged, ran at intermediate speeds or sprinted, and whether they first contacted the running surface with the fore or rear portions of their feet, there was near-complete agreement between the model-predicted and measured force–time waveforms across the 500 footfalls we analyzed (Table 1). Thus, we conclude that the vertical ground reaction forces of human runners can be broadly understood from the motion of two discrete portions of the body: (1) the contacting lower limb and (2) the remainder of the body's mass.

Two-mass model: scientific and technical elements

A primary scientific challenge here was not knowing *a priori* how well the waveform contributions from the 92% of the body's mass could be predicted when modeled as a single mass component. Conceivably, the summed force contributions resulting from the motion of the head, arms, trunk, upper portion of the contacting leg and full mass of the non-contacting leg might defy accurate prediction when treated as a single mass (Bobbert et al., 1991). This large, multi-jointed mass component lacks a fixed, readily measurable center because of the non-uniform motion of the different segments that comprise it. Hence, the complexity of the within-segment and total motion of our model's mass component m_2 and its corresponding force contribution would be difficult to measure and predict from positional data. We ultimately implemented an indirect approach that allowed the force contributions of mass m_2 to be quantified without position and time data. We simply subtracted impulse J_1 from the total ground reaction impulse J_T, after quantifying the latter from body mass, gravity and the contact proportion of the total step time (Eqns 1–3). The resulting fits supported the efficacy of the approach as the agreement between model-predicted and measured waveforms was

Journal of Experimental Biology (2017) 220, 247-258 doi:10.1242/jeb.138057

Table 2. Impulse 1 kinematic input parameters for individual modeled-predicted waveforms (*N*=500)

	Speed			
Foot-strike type	Slow (3–4 m s^{-1})	Medium (5–6 m s^{-1})	Fast (≥7 m s^{-1})	Total
RFS				
Δv_1 (m s^{-1})	0.85±0.02	1.28±0.03	2.01±0.04	1.35±0.04
Δt_1 (s)	0.029±0.0005	0.023±0.0003	0.019±0.0002	0.024±0.0004
	(*N*=70)	(*N*=50)	(*N*=57)	(*N*=177)
FFS				
Δv_1 (m s^{-1})	1.30±0.04	1.37±0.02	2.08±0.03	1.72±0.03
Δt_1 (s)	0.046±0.0011	0.034±0.0008	0.027±0.0003	0.033±0.0006
	(*N*=73)	(*N*=82)	(*N*=168)	(*N*=323)
All footfalls				
Δv_1 (m s^{-1})	1.08±0.03	1.34±0.02	2.06±0.02	1.59±0.02
Δt_1 (s)	0.038±0.0010	0.030±0.0007	0.025±0.0004	0.030±0.0004
	(*N*=143)	(*N*=132)	(*N*=225)	(*N*=500)

Values are means±s.d. Δv_1, change in vertical velocity of m_1 during Δt_1; Δt_1, time interval between touchdown and the vertical velocity of m_1 slowing to zero.

consistently excellent over the later portions of the stance period where the total waveform is predominantly determined by impulse J_2 (Figs 5A,C,E and 6A,C,E, waveform trailing edges).

A potential limitation of our impulse subtraction approach was the required assumption that the net vertical displacement of the body's center of mass over the course of one or many strides is zero. However, our analysis indicated that little to no predictive error was introduced by this assumption under our level, treadmill-running test conditions. We found similar levels of predictive accuracy for trial-averaged and individual-footfall waveforms even though non-zero vertical displacements of the center of mass, when considered on a per-step basis, could have been substantially greater over the course of an individual step versus multiple consecutive steps. However, for our across-speed comparisons, it seems likely that our slightly less accurate waveform predictions for the fastest speeds, where step-to-step mechanics are generally less consistent versus medium and slower speeds (Weyand et al., 2010), are probably attributable to marginally greater violations of this assumption for the faster trials (Table 1).

An additional technical challenge involved accurate and consistent quantification of the duration of mass component m_1's impact-period deceleration to a zero velocity (i.e. Δt_1 in Eqn 3; see also Fig. 2) for all footfalls. Following RFS impacts, the ankle marker position–time trajectories consistently provided a discrete vertical position minimum corresponding to the zero velocity needed to quantify half-impact duration Δt_1 in our model (Fig. 3). However, for some FFS footfalls, the rates of the positional change versus time during the last fraction of the deceleration period were less consistent and more prolonged than the FFS data in Fig. 3. This led us to implement an ankle marker projection technique (see Appendix) to avoid basing impulse J_1 predictions on Δt_1 values that, in these cases, are not representative of the overall timing of the

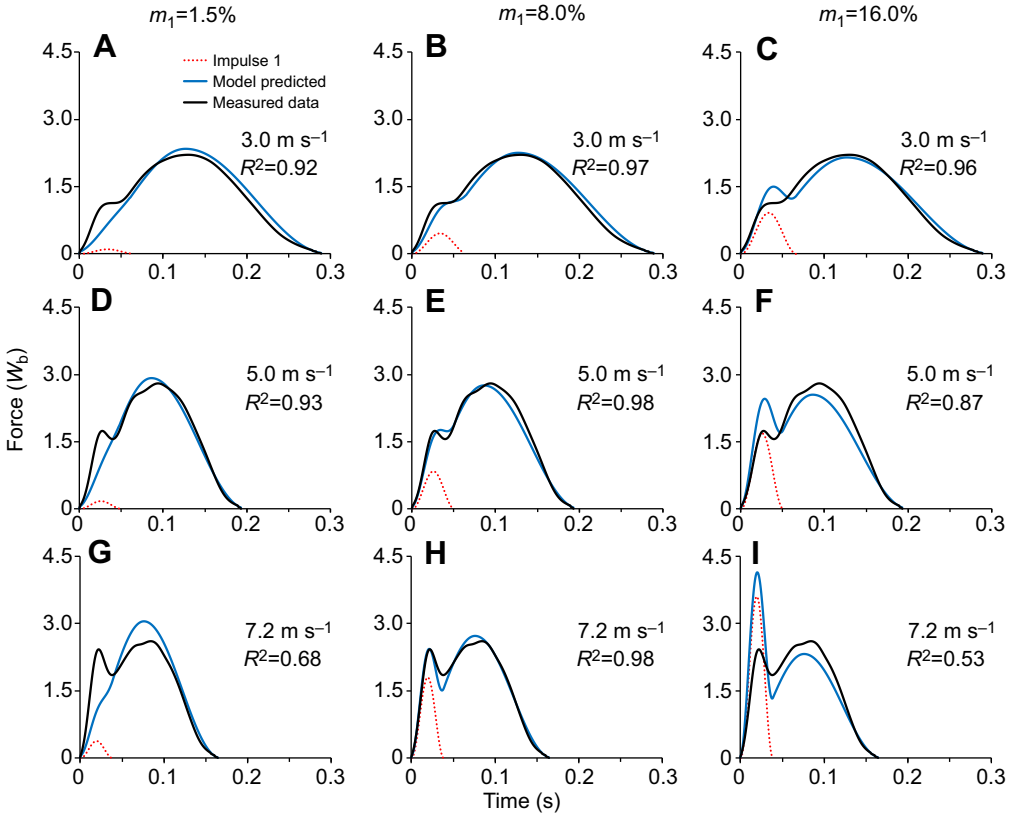

Fig. 7. The vertical ground reaction force–time waveforms generated by the model for RFS trials with varied m_1 values. For all panels, the solid black line represents the average of the vertical ground reaction force data measured during the trial, the solid blue line represents the model-predicted waveform from the average kinematics measured during the trial and the input m_1 and m_2 values, and the dotted red line represents the impulse resulting from the impact of m_1 with the running surface. (A–C) Measured and predicted at 3.0 m s^{-1}; (D–F) measured and predicted at 5.0 m s^{-1}; and (G–I) measured and predicted at 7.2 m s^{-1}. A, D and G illustrate waveforms predicted using m_1 values of 1.5% total body mass and m_2 values of 98.5% total body mass; B, E and H illustrate waveforms predicted using m_1 values of 8.0% total body mass and m_2 values of 92.0% total body mass; and C, F and I illustrate waveforms predicted using m_1 values of 16.0% total body mass and m_2 values of 84.0% total body mass.

Journal of Experimental Biology (2017) 220, 247-258 doi:10.1242/jeb.138057

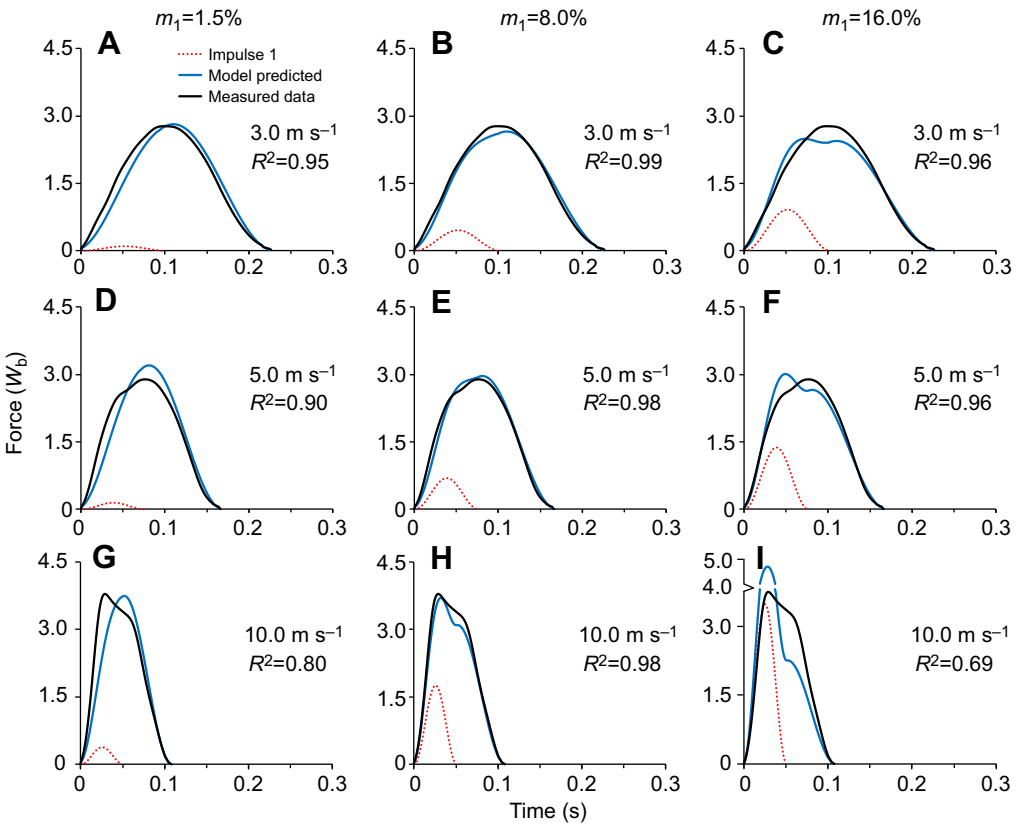

Fig. 8. The vertical ground reaction force–time waveforms generated by the model for FFS trials with varied m_1 values. For all panels, the solid black line represents the average of the vertical ground reaction force data measured during the trial, the solid blue line represents the model-predicted waveform from the average kinematics measured during the trial and the input m_1 and m_2 values, and the dotted red line represents the impulse resulting from the impact of m_1 with the running surface. (A–C) Measured and predicted at 3.0 m s^{-1}; (D–F) measured and predicted at 5.0 m s^{-1}; and (G–I) measured and predicted at 10.0 m s^{-1}. A, D and G illustrate waveforms predicted using m_1 values of 1.5% total body mass and m_2 values of 98.5% total body mass; B, E and H illustrate waveforms predicted using m_1 values of 8.0% total body mass and m_2 values of 92.0% total body mass; and C, F and I illustrate waveforms predicted using m_1 values of 16.0% total body mass and m_2 values of 84.0% total body mass.

impact-deceleration event. Upon implementation across all 500 footfalls, we found that the measured ankle marker velocities at the time that the projection technique identified a zero velocity value were very near the true zero value desired (mean v_{ankle}=−0.05 ±0.04 m s^{-1}). Given the overall mean ankle marker vertical velocity, Δv_1, of −1.59±0.02 m s^{-1} at impact across all 500 footfalls (Δv_1, Table 2), this method, on average, captured 97% of m_1 total post-impact deceleration to zero.

The ability to consistently predict rising-edge waveform peaks that occurred from 15 to 50 ms after initial impact is a noteworthy aspect of our model validation. As the timing of rising-edge peaks on individual waveforms is determined by the overlap of the two impulses in our model, successful prediction required precisely capturing the timing of both the high- (J_1) and low-frequency (J_2) components of the waveforms. The timing of impulse J_1 was determined from motion data, and was therefore fully independent of our force data, filtering and processing routines. Conversely, the timing of impulse J_2 was directly dependent on our force data and processing routines, and was therefore fully independent of our kinematic data and processing routines. Had even a minor degree of temporal inaccuracy been present in either our kinematic or kinetic data, the predictive accuracy with which the two-mass model identified rising-edge force peaks would not have been possible.

Integrating two-mass model and multi-mass model results

Our experimental goal was to identify the most concise mechanical explanation that running ground reaction force waveforms might have. The multi-mass models, in contrast, were formulated to evaluate the potential influence of numerous factors on the waveform rising edge. Many of the features incorporated into the multi-mass models provide reasonable theoretical representations of the numerous, potentially influential musculoskeletal complexities present (Liu and Nigg, 2000; Ly et al., 2010; Nigg and Liu, 1999; Nikooyan and Zadpoor, 2011; Zadpoor and Nikooyan, 2010). These include mass components that vary in stiffness, that are both rigid and wobbling in nature, and that are connected with both serial and parallel elements (Fig. 1A). While the quantitative descriptions derived for these features undoubtedly include uncertainty, their basic influence on the RFS jogging waveforms thus far analyzed are plausible and largely consistent with other experimental and modeling approaches (Gruber et al., 1998; LaFortune et al., 1996; Pain and Challis, 2001; Shorten and Mientjes, 2011). Accordingly, our demonstration that a substantially more concise model can account for running ground reaction force waveforms in full should not be regarded as incompatible with the more theoretical results the multi-mass models have provided. Indeed, the most reasonable conclusion from the different approaches is that the collective influence of the many biological complexities incorporated into the multi-mass models is, in sum, accurately described by the concise impulse–momentum relationships the two-mass model provides.

The force–motion relationship for human running: general or foot-strike specific?

In contrast to the prevailing view that the impact forces resulting from RFSs and FFSs involve different mass quantities (Lieberman et al., 2010; Nigg, 2010), our results indicate that mass quantities and force–motion relationships do not differ across strike types. This becomes fully apparent when J_1 impact impulses are quantified using measured, foot-strike-specific deceleration durations in conjunction with the invariant, anatomically based mass quantities in our model. With both factors in place, we were able to accurately predict the waveforms in full for both foot-strike types at slow, intermediate and fast running speeds alike.

As is evident from both our impulse J_1 illustrations (Figs 5 and 6) and the Δv_1 values in Table 2, rising-edge force peaks that are generally visible for RFS but not FFS waveforms can be fully attributed to the different m_1 deceleration durations we measured. Longer FFS deceleration durations reduce and delay the J_1 peak force values; they also result in greater waveform force contributions from impulse J_2 at the time of the J_1 force peak. In combination, these timing-dependent factors typically do not allow the J_1 impulse peak to introduce a localized force peak along the rising edge of the full waveform (Fig. 6B and Fig. 8B,E). We found this to be the case even though the total ground reaction impulses resulting from FFSs in our data set were just as large as those resulting from RFSs (note: J_1 impulses are $\propto\Delta v_1$ in Table 2). One noteworthy exception to these general foot-strike-specific waveform patterns has recently been documented for specialized sprinters (Clark and Weyand, 2014). These fore-foot striking athletes have waveforms that are characterized by prominent rising-edge force peaks that result from brief, large J_1 impulse peaks. The high pre-impact limb velocities (Δv_1) and brief impact deceleration periods (Δt_1) of specialized sprinters introduce conspicuous rising-edge force peaks, particularly at faster running speeds (Fig. 6E,F and Fig. 8H).

Our waveform predictions using alternative mass fractions for segments m_1 and m_2 also support the validity of describing FFS and RFS waveforms with the same fractional body mass quantities and force–motion relationships. As hypothesized for these alternative mass distributions, substantially reducing the lower limb mass value of m_1 from the anatomical fractional value of 0.08 (Plagenhoef et al., 1983) to the much lower value of 0.015 resulted in predicted rising-edge force values that fell consistently below measured values (Figs 7A,D,G and 8A,D,G). Conversely, substantially increasing the m_1 fractional mass value to 0.16 resulted in predicted rising-edge force values that fell consistently above the measured values (Figs 7C,F,I and 8C,F,I). The magnitudes of the respective predictive errors and trends observed across speed were similar for the two foot-strike types using the aforementioned alternative m_1 fractional mass values. In both cases, the increases in the magnitude of the J_1 impulse across speed introduced greater predictive errors at higher versus lower speeds. More globally, the contrast between the systematic predictive errors present in both sets of alternative-mass generated waveforms versus the near-full agreement achieved with the original values provides strong support for the validity of the anatomical values originally assigned to mass components m_1 and m_2 in our two-mass model.

General considerations, applications and concluding remarks

The accuracy and conciseness of our mechanical explanation for the variable ground reaction force–time patterns of dozens of human runners performing across their full range of speeds raises a noteworthy possibility. Our two-mass, two-impulse approach may offer a mechanical explanation that generalizes to the ground reaction force–time patterns of other running species. However, for non-human runners, the lesser distal-limb mass segments typically present (Hildebrand, 1960; Rubenson et al., 2011) could alter both the form and applicability of the two-mass approach. Minimally, species-specific mass distributions would need to be incorporated to generate waveforms from the basic stride measures included in the model. In this regard, comparative anatomical variation constitutes both a challenge and an experimental opportunity to evaluate the basic tenets of the model. More broadly, the testable hypotheses the model offers should be tractable using a variety of direct and indirect approaches.

Finally, our empirical validation of a concise model that can fully predict running vertical ground reaction forces offers basic insights with immediate potential for application. In contrast to simplified, single-mass models (Blickhan, 1989; Blum et al., 2009; Farley and Gonzalez, 1996; McMahon and Cheng, 1990; Silder et al., 2015), which are incapable of capturing the high-frequency, impact-phase components of the waveform (Bullimore and Burn, 2007; Clark and Weyand, 2014; Shorten and Mientjes, 2011), and multi-mass models that do not account for the whole waveform and are too theoretical and complex for practical application, the two-mass model requires only body mass and very limited motion data in order to predict the waveform in full. These attributes enable indirect assessment of impact forces, limb loading rates, and other informative, force-based outcomes using video or other inexpensive motion-sensing technologies. Potential model applications include: informing the design of running robots, exoskeletons and prostheses, the customization of running shoes and orthotics from individual gait mechanics, the development of wearable ground force sensors, and the improvement of evidenced-based feedback for gait analyses, intervention and modification.

APPENDIX

Impulse determination

The model assumes steady-speed horizontal running where the net vertical displacement of the center of mass of the body is zero over each step and the speed is constant. Each step is defined by a contact time t_c with vertical ground reaction force $F(t)$, and an aerial time t_a where the force is zero. Under these conditions, a runner supports an average of one body weight during the step time ($t_{step}=t_c+t_a$). This can be expressed using the formal mathematical definition of the average value of the force function $F(t)$ over the interval $t=0$ to t_{step}:

$$\frac{1}{t_{step}}\int_0^{t_{step}} F(t)\mathrm{d}t = m_b\boldsymbol{g}, \quad \text{(A1)}$$

where body weight is defined by the product of mass m_b and gravitational acceleration $\boldsymbol{g}$=9.8 m s^{-2}. This equation yields the total average force $F_{T,avg}$ during the contact time interval:

$$F_{T,avg} = m_b\boldsymbol{g}\frac{t_{step}}{t_c}. \quad \text{(A2)}$$

The total ground reaction impulse J_T can simply be determined from body weight and t_{step}:

$$J_T = F_{T,avg}t_c = m_b\boldsymbol{g}\,t_{step}. \quad \text{(A3)}$$

The ground reaction force is a result of the acceleration $a_i(t)$ of body components i with mass m_i contacting the ground:

$$\Sigma F_i(t) = \Sigma m_i a_i(t). \quad \text{(A4)}$$

The average force due to each body component is:

$$\Sigma(F_{i,avg} - m_i\boldsymbol{g}) = \Sigma(m_i a_{i,avg}), \quad \text{(A5)}$$

$$\Sigma F_{i,avg} = \Sigma(m_i a_{i,avg} + m_i\boldsymbol{g}). \quad \text{(A6)}$$

The ground reaction force is the sum of two distinct impulse waveforms. Each impulse waveform has an associated $F_{i,avg}$ and time interval. Impulse J_1 results from the acceleration of the lower limb during the limb impact interval. Impulse J_2 results from the acceleration of the remainder of the body's mass during the entire contact interval. The total ground reaction impulse J_T is the sum of J_1 and J_2:

$$J_T = J_1 + J_2. \quad \text{(A7)}$$

Journal of Experimental Biology (2017) 220, 247-258 doi:10.1242/jeb.138057

Impulse J_1 is quantified from the vertical deceleration of m_1 during surface impact:

$$J_1 = F_{1,\text{avg}}(2\Delta t_1) = \left(m_1\frac{\Delta v_1}{\Delta t_1} + m_1\boldsymbol{g}\right)(2\Delta t_1), \quad \text{(A8)}$$

where m_1 is 8.0% of the body's mass, Δt_1 is the time interval between touchdown and the vertical velocity of m_1 slowing to zero, Δv_1 is the change in vertical velocity of m_1 during Δt_1, and $F_{1,\text{avg}}$ is the average force during the total time interval ($2\Delta t_1$) of impulse J_1.

Impulse J_2 corresponds to the remainder of the body's mass and is determined from J_1 in Eqn A8 and total ground reaction impulse J_T in Eqn A3:

$$J_2 = F_{2,\text{avg}}t_c = J_T - J_1. \quad \text{(A9)}$$

Force curve function

The bell-shaped force curve $F(t)$ for each impulse (J_1, J_2) can be accurately modeled using the RCB curve (Clark et al., 2014). The raised cosine function can be derived from the first two terms of the Fourier series:

$$F(t) = \alpha_0 + \sum_{n=1}^{N}\alpha_n\sin(2\pi f_n t + \theta_n), \quad \text{(A10)}$$

where α_0 is the mean of the signal, and f_n, α_n and θ_n are the frequency, amplitude and phase angle of the nth harmonic (Clark and Weyand, 2014; Winter, 1990). The first two terms are:

$$F(t) = \alpha_0 + \alpha_1\sin(2\pi f_1 t + \theta_1). \quad \text{(A11)}$$

The peak of this function can be referenced to t=0 by defining phase $\theta_1=\pi/2$:

$$F(t) = \alpha_0 + \alpha_1\cos(2\pi f_1 t). \quad \text{(A12)}$$

Term α_0 is the mean of the function, and term α_1 is the amplitude of the function. Each term is defined by the total peak amplitude A, resulting in $\alpha_0=\alpha_1=A/2$. The peak is located at center time B. Frequency f_1 can be expressed in terms of width parameter C, which is defined from the peak at $t=B$ to the time where $F(t)$ decays to zero, resulting in $f_1=1/(2C)$. The constants A, B and C are inserted into Eqn A12 to yield the raised cosine periodic function:

$$F(t) = \frac{A}{2} + \frac{A}{2}\cos\left(\frac{\pi}{C}(t-B)\right). \quad \text{(A13)}$$

The RCB curve is defined over a finite time interval of one period:

$$F(t) = \begin{Bmatrix} 0 & \text{for} \quad t < B - C \\ \frac{A}{2}\left[1 + \cos\left(\frac{t-B}{C}\pi\right)\right] & \text{for} \quad B - C \le t \le B + C \\ 0 & \text{for} \quad t > B + C \end{Bmatrix}, \quad \text{(A14)}$$

where A is the peak amplitude, B is the center time of the peak and C is the half-width time interval. Because of the simple properties of this function, peak amplitude $A=2F_{\text{avg}}$, and the area under the curve is $J=AC$.

Impulse J_1 has force waveform $F_1(t)$ during the interval $B_1-C_1\le t\le B_1+C_1$:

$$F_1(t) = \frac{A_1}{2}\left[1 + \cos\left(\frac{t-B_1}{C_1}\pi\right)\right], \quad \text{(A15)}$$

where $A_1=2F_{1,\text{avg}}$ using $F_{1,\text{avg}}$ in Eqn A8, and B_1 and C_1 equal the time Δt_1 after touchdown for the vertical velocity of m_1 to reach zero.

Impulse J_2 has force waveform $F_2(t)$ during the interval $B_2-C_2\le t\le B_2+C_2$:

$$F_2(t) = \frac{A_2}{2}\left[1 + \cos\left(\frac{t-B_2}{C_2}\pi\right)\right], \quad \text{(A16)}$$

where $A_2=2F_{2,\text{avg}}$ using $F_{2,\text{avg}}$ in Eqn A9, and B_2 and C_2 equal $0.5t_c$ for a symmetrical waveform.

The total force curve $F_T(t)$ is the sum of these two individual force waveforms:

$$F_T(t) = F_1(t) + F_2(t). \quad \text{(A17)}$$

Impulse J_1 ankle marker velocity considerations

Impulse J_1 results from the acceleration of the lower limb during the limb impact interval and is quantified by Eqn A8. Δv_1 and Δt_1 are determined using ankle marker kinematics to represent the motion of the lower limb mass m_1. The lower limb attains a relatively constant positive velocity after the impact interval (Fig. 2C), resulting in a near-zero acceleration of m_1 (Fig. 2D) and negligible force $F_1=m_1\boldsymbol{g}$ (Fig. 2E) as described in Eqn A6. This force is less than 55 N for a subject with body mass m_b=70 kg and lower limb mass m_1=5.6 kg (m_1=0.08×70 kg). Thus, J_1 can be modeled by a finite impulse during the impact interval.

Kinematic data for the ankle marker position during the impact interval for representative RFS and FFS subjects appear in Fig. 3. Δt_1 is the time interval between touchdown and the vertical velocity of m_1 slowing to zero. For some FFS runners at slower speeds, minor fluctuations in the ankle marker velocity–time profile near the end of the m_1 impact interval can create variability in the Δt_1 measurements as a result of slow m_1 impact velocities and skin marker motion artifact during the impact interval (Bobbert et al., 1991). Accordingly, Δt_1 was quantified using a technique that represented the functional end of the m_1 impact time interval. An ankle marker velocity of -0.25 m s^{-1} was used as a threshold point, and the previous 10 ms of data were utilized for a linear projection of the ankle marker velocity to zero. For consistency in analysis, this method was applied to all ankle marker kinematics data, regardless of the speed or foot-strike mechanics of the runner (see Results).

Impulse J_2 asymmetry considerations

The temporal location of the peak of impulse J_2 is dependent on the relative location of the center of mass at touchdown and takeoff. Idealized spring–mass running has symmetrical center of mass displacement, and thus a symmetrical profile where the location of peak B_2 is $0.50t_c$. However, the stance leg is more extended at takeoff than at touchdown (Blickhan, 1989), and this causes the center of mass height to be lower at touchdown than at takeoff (Cavagna, 2006), which results in an asymmetrical impulse J_2 profile. The model waveform $F_2(t)$ for impulse J_2 can be modified to include width parameters to control the symmetry:

$$F_2(t) = \begin{Bmatrix} 0 & \text{for } t < B_2 - C_{2L} \\ \frac{A_2}{2}\left[1+\cos\left(\frac{t-B_2}{C_{2L}}\pi\right)\right] & \text{for } B_2 - C_{2L} \le t \le B_2 \\ \frac{A_2}{2}\left[1+\cos\left(\frac{t-B_2}{C_{2T}}\pi\right)\right] & \text{for } B_2 < t \le B_2 + C_{2T} \\ 0 & \text{for } t > B_2 + C_{2T} \end{Bmatrix}, \quad \text{(A18)}$$

where A_2 is the peak amplitude, B_2 is the center time of the peak, C_{2L} is the leading half-width time interval, and C_{2T} is the trailing half-width time interval. The location of peak B_2 was set at $0.47t_c$ as per

the center of mass asymmetry originally reported by Cavagna et al. (1977) (see their table 4). With the symmetry control, C_{2L}=B_2 and C_{2T}=t_c−B_2.

Impulse J_2 threshold considerations

A baseline noise level is present in all force platforms. To establish accurate and reproducible contact measurements, a threshold value is specified such that any ground reaction force signal below this value is zero. The threshold setting can be incorporated into the impulse J_2 model waveform $F_2(t)$. Eqn A18 can be solved for the width parameters C_2:

$$C_2 = \frac{|t - B_2|\pi}{\cos^{-1}((2F_2/A_2) - 1)}. \quad \text{(A19)}$$

This equation is specifically evaluated for each width parameter at time t where the force F_2 is equal to the threshold. A force threshold of 40 N was used for the AMTI high-speed force treadmill system. The leading width parameter C_2=C_{2L} is determined at the first channel (t=1 ms) and the trailing width parameter C_2=C_{2T} is determined at the last channel (t=t_c). Leading and trailing width parameters C_{2L} and C_{2T} are calculated using the same peak location B_2 and peak amplitude A_2.

The peak amplitude is recalculated after the width parameters are changed in order to preserve the impulse. The impulse after the calculation of width parameters (J_{2A}) should approximately equal the impulse before the calculation of width parameters (J_{2B}):

$$J_{2A} = J_{2B}, \quad \text{(A20)}$$

$$\frac{1}{2}A_{2A}C_{2LA} + \frac{1}{2}A_{2A}C_{2TA} = \frac{1}{2}A_{2B}C_{2LB} + \frac{1}{2}A_{2B}C_{2TB}, \quad \text{(A21)}$$

$$A_{2A} = A_{2B}\frac{C_{2LB} + C_{2TB}}{C_{2LA} + C_{2TA}}. \quad \text{(A22)}$$

As a result of this recalculation, the impulse is approximately equal to the original impulse and the values at the first and last channel are approximately equal to the threshold value.

Acknowledgements

The authors thank Andrew Udofa for his help with data collection and the artwork in Fig. 1B, and the participants for their time and effort.

Competing interests

The authors declare competing financial interests. P.G.W., L.J.R. and K.P.C. are the inventors of US Patent no. 8363891 which is owned by Southern Methodist University and contains scientific content related to that presented in the manuscript. The patent is licensed to SoleForce LLC in which the three aforementioned individuals are equity partners.

Author contributions

Each of the three authors, K.P.C., L.J.R. and P.G.W., contributed substantially to the conception of the study, the implementation and evaluation of the model presented, and writing the manuscript.

Funding

This work was supported in part by a US Army Medical and Materiel Command award [W81XWH-12-2-0013] to P.G.W.

References

Blickhan, R. (1989). The spring-mass model for running and hopping. *J. Biomech.* **22**, 1217-1227.

Blum, Y., Lipfert, S. W. and Seyfarth, A. (2009). Effective leg stiffness in running. *J. Biomech.* **42**, 2400-2405.

Bobbert, M. F., Schamhardt, H. C. and Nigg, B. M. (1991). Calculation of vertical ground reaction force estimates during running from positional data. *J. Biomech.* **24**, 1095-1105.

Bullimore, S. R. and Burn, J. F. (2007). Ability of the planar spring-mass model to predict mechanical parameters in running humans. *J. Theor. Biol.* **248**, 686-695.

Cavagna, G. A. (2006). The landing–take-off asymmetry in human running. *J. Exp. Biol.* **209**, 4051-4060.

Cavagna, G. A., Heglund, N. C. and Taylor, C. R. (1977). Mechanical work in terrestrial locomotion: two basic mechanisms for minimizing energy expenditure. *Am. J. Physiol.* **233**, $R^2$43-$R^2$61.

Cavanagh, P. R. (1987). The biomechanics of lower extremity action in distance running. *Foot Ankle* **7**, 197-217.

Chi, K.-J. and Schmitt, D. (2005). Mechanical energy and effective foot mass during impact loading of walking and running. *J. Biomech.* **38**, 1387-1395.

Clark, K. P. and Weyand, P. G. (2014). Are running speeds maximized with simple-spring stance mechanics? *J. Appl. Physiol.* **117**, 604-615.

Clark, K. P., Ryan, L. J. and Weyand, P. G. (2014). Foot speed, foot-strike and footwear: linking gait mechanics and running ground reaction forces. *J. Exp. Biol.* **217**, 2037-2040.

Cohen, J. (2013). *Statistical Power Analysis for the Behavioral Sciences*. New York, NY: Academic press.

Denoth, J. (1986). Load on the locomotor system and modeling. In *Biomechanics of Running Shoes* (ed. B. M. Nigg), pp. 63-116. Illinois: Human Kinetics Publishers, Inc.

Derrick, T. R. (2004). The effects of knee contact angle on impact forces and accelerations. *Med. Sci. Sports Exerc.* **36**, 832-837.

Farley, C. T. and Gonzalez, O. (1996). Leg stiffness and stride frequency in human running. *J. Biomech.* **29**, 181-186.

Gruber, K., Ruder, H., Denoth, J. and Schneider, K. (1998). A comparative study of impact dynamics: wobbling mass model versus rigid body model. *J. Biomech.* **31**, 439-444.

Hamill, J. and Knutzen, K. M. (2009). *Biomechanical Basis of Human Movement*, 3rd edn. Philadelphia, PA: Lippincott Williams & Wilkins.

Hedrick, T. L. (2008). Software techniques for two- and three-dimensional kinematic measurements of biological and biomimetic systems. *Bioinspir. Biomim.* **3**, 034001.

Hildebrand, M. (1960). How animals run. *Sci. Am.* **202**, 148-157.

Lafortune, M. A., Hennig, E. M. and Lake, M. J. (1996). Dominant role of interface over knee angle for cushioning impact loading and regulating initial leg stiffness. *J. Biomech.* **29**, 1523-1529.

Lieberman, D. E., Venkadesan, M., Werbel, W. A., Daoud, A. I., D'Andrea, S., Davis, I. S., Mang'Eni, R. O. and Pitsiladis, Y. (2010). Foot strike patterns and collision forces in habitually barefoot versus shod runners. *Nature* **463**, 531-535.

Liu, W. and Nigg, B. M. (2000). A mechanical model to determine the influence of masses and mass distribution on the impact force during running. *J. Biomech.* **33**, 219-224.

Ly, Q. H., Alaoui, A., Erlicher, S. and Baly, L. (2010). Towards a footwear design tool: influence of shoe midsole properties and ground stiffness on the impact force during running. *J. Biomech.* **43**, 310-317.

McMahon, T. A. and Cheng, G. C. (1990). The mechanics of running: how does stiffness couple with speed? *J. Biomech.* **23** Suppl. 1, 65-78.

Morin, J.-B., Dalleau, G., Kyröläinen, H., Jeannin, T. and Belli, A. (2005). A simple method for measuring stiffness during running. *J. Appl. Biomech.* **21**, 167-180.

Munro, C. F., Miller, D. I. and Fuglevand, A. J. (1987). Ground reaction forces in running: a reexamination. *J. Biomech.* **20**, 147-155.

Nigg, B. M. (2010). *Biomechanics of Sport Shoes*. Calgary, AB: Topline Printing Inc.

Nigg, B. M. and Liu, W. (1999). The effect of muscle stiffness and damping on simulated impact force peaks during running. *J. Biomech.* **32**, 849-856.

Nikooyan, A. A. and Zadpoor, A. A. (2011). Mass-spring-damper modelling of the human body to study running and hopping – an overview. *Proc. Inst. Mech. Eng. H* **225**, 1121-1135.

Pain, M. T. G. and Challis, J. H. (2001). The role of the heel pad and shank soft tissue during impacts: a further resolution of a paradox. *J. Biomech.* **34**, 327-333.

Plagenhoef, S., Evans, F. G. and Abdelnour, T. (1983). Anatomical data for analyzing human motion. *Res. Quar. Exerc. Sport,* **54**, 169-178.

Racic, V. and Pavic, A. (2009). Mathematical model to generate asymmetric pulses due to human jumping. *J. Eng. Mech.* **135**, 1206-1211.

Rubenson, J., Lloyd, D. G., Heliams, D. B., Besier, T. F. and Fournier, P. A. (2011). Adaptations for economical bipedal running: the effect of limb structure on three-dimensional joint mechanics. *J. R. Soc. Interface* **58**, 740-755.

Shorten, M. and Mientjes, M. I. V. (2011). The 'heel impact' force peak during running is neither 'heel' nor 'impact' and does not quantify shoe cushioning effects. *Footwear Sci.* **3**, 41-58.

Silder, A., Besier, T. and Delp, S. L. (2015). Running with a load increases leg stiffness. *J. Biomech.* **48**, 1003-1008.
Sim, J., Blakeborough, A., Williams, M. S. and Parkhouse, G. (2008). Statistical model of crowd jumping loads. *J, Struct. Eng.* **134**, 1852-1861.
Weyand, P. G., Sternlight, D. B., Bellizzi, M. J. and Wright, S. (2000). Faster top running speeds are achieved with greater ground forces not more rapid leg movements. *J. Appl. Physiol.* **89**, 1991-1999.
Weyand, P. G., Sandell, R. F., Prime, D. N. L. and Bundle, M. W. (2010). The biological limits to running speed are imposed from the ground up. *J. Appl. Physiol.* **108**, 950-961.
Winter, D. A. (1990). *Biomechanics and Motor Control of Human Movement*, 2nd edn. New York: John Wiley and Sons, Inc.
Zadpoor, A. A. and Nikooyan, A. A. (2010). Modeling muscle activity to study the effects of footwear on the impact forces and vibrations of the human body during running. *J. Biomech.* **43**, 186-193.

© 2014. Published by The Company of Biologists Ltd | The Journal of Experimental Biology (2014) 217, 2037-2040 doi:10.1242/jeb.099523

SHORT COMMUNICATION

Foot speed, foot-strike and footwear: linking gait mechanics and running ground reaction forces

Kenneth P. Clark, Laurence J. Ryan and Peter G. Weyand*

ABSTRACT

Running performance, energy requirements and musculoskeletal stresses are directly related to the action–reaction forces between the limb and the ground. For human runners, the force–time patterns from individual footfalls can vary considerably across speed, foot-strike and footwear conditions. Here, we used four human footfalls with distinctly different vertical force–time waveform patterns to evaluate whether a basic mechanical model might explain all of them. Our model partitions the body's total mass ($1.0M_b$) into two invariant mass fractions (lower limb=0.08, remaining body mass=0.92) and allows the instantaneous collisional velocities of the former to vary. The best fits achieved (R^2 range=0.95–0.98, mean=0.97±0.01) indicate that the model is capable of accounting for nearly all of the variability observed in the four waveform types tested: barefoot jog, rear-foot strike run, fore-foot strike run and fore-foot strike sprint. We conclude that different running ground reaction force–time patterns may have the same mechanical basis.

KEY WORDS: Force-motion, Biomechanics, Running performance, Barefoot running

INTRODUCTION

The bodily motion of terrestrial animals that use bouncing gaits is determined by the action–reaction forces between the limbs and the ground. However, the predominant orientation of these forces during straight-path, level running and hopping is not in the horizontal direction of travel (Cavagna et al., 1977). Horizontal force requirements are minimized by an effective step-to-step maintenance of forward momentum once an animal is up to speed. Vertical force requirements, in contrast, can exceed body weight by a factor of two or more during periods of limb–ground contact (Weyand et al., 2000). Large vertical forces result from two factors: the need for stride-averaged vertical forces to equal the body's weight, and limb–ground contact periods that comprise only a fraction of the total stride time. Consequently, the vertically oriented ground reaction forces exceed horizontal forces by a factor of five or more, and lateral forces by greater margins.

The vertical force versus time waveforms of individual running and hopping footfalls can vary considerably in duration, amplitude and shape. This variation has been documented for a variety of species (Cavagna et al., 1977) and most comprehensively for humans (Bobbert et al., 1991; Munro et al., 1987). At present, several factors are known to introduce the shape variation that occurs predominantly in the initial portion of these force–time waveforms. These include: running speed (Bobbert et al., 1991; Kuitunen et al., 2002; Munro et al., 1987; Weyand et al., 2009; Weyand et al., 2010), the portion of the foot that initially contacts the running surface (Cavanagh, 1987; Chi and Schmitt, 2005; Dickinson et al., 1985; Ker et al., 1989; Lieberman et al., 2010; Nigg et al., 1987) and footwear (Liu and Nigg, 2000; Ly et al., 2010; Nigg et al., 1987; Nigg and Liu, 1999; Zadpoor and Nikooyan, 2010). Current understanding rests heavily on the two types of models most frequently used to interpret these waveforms: the spring-mass model and multi-mass models. Models of both types are well-founded and have undergone extensive evaluation. However, neither was formulated to explain these waveforms in full.

The most basic treatment of the vertical force–time waveforms is provided by the classic spring-mass model (Blickhan, 1989; McMahon and Cheng, 1990). The single-mass approach models running and hopping animals as a lumped point-mass mass bouncing on a massless leg spring. This single-mass model explains many aspects of running and hopping gaits with remarkable accuracy given its mechanical simplicity (Bullimore and Burn, 2007; Farley et al., 1993; Ferris and Farley, 1997; McMahon and Cheng, 1990). However, this classic model was formulated largely for broad evaluative purposes, not specific quantitative ones. Accordingly, the perfectly symmetrical force–time waveforms the model predicts (Bullimore and Burn, 2007; Robilliard and Wilson, 2005) cannot account for the non-symmetrical components that the force–time waveforms inevitably contain. These include, but are not limited to, heel-strike impacts at slow speeds and extremely rapid rising edges at faster ones (Kuitunen et al., 2002; Weyand et al., 2009; Weyand et al., 2010).

A second, more complex variety of multi-mass models developed from the two-mass ideas initially put forward by McMahon (McMahon et al., 1987) and Alexander (Alexander, 1988). These models have evolved in their complexity, largely by building upon Alexander's two-mass, stacked-spring model (Alexander, 1988; Alexander, 1990; Derrick et al., 2000; Ker et al., 1989). Contemporary versions include at least four masses and more than a dozen spring, mass and damping elements (Liu and Nigg, 2000; Ly et al., 2010; Nigg and Liu, 1999; Nikooyan and Zadpoor, 2011; Zadpoor and Nikooyan, 2010). In contrast to the single-mass models, a primary objective of the multi-mass models has been to provide detailed explanations of waveform variability, specifically the impact and rising-edge variability observed for human joggers (Nigg, 2010; Zadpoor and Nikooyan, 2010). However, the relatively specific objective of the multi-mass models has limited the breadth of their application. Evaluations typically ignore the descending edge of the waveforms and have been limited to jogging speeds. Accordingly, the ability of the now-elaborate, multi-mass models to explain either the falling edge of jogging waveforms or the entirety of the waveforms from intermediate and fast running speeds is not known.

Here, we seek to explain running ground reaction forces in full with an approach that is slightly more complex than the single-mass

Southern Methodist University, Locomotor Performance Laboratory, 5538 Dyer Street, Department of Applied Physiology and Wellness, Dallas, TX 75206, USA.

*Author for correspondence (pweyand@smu.edu)

Received 5 November 2013; Accepted 20 March 2014

The Journal of Experimental Biology (2014) doi:10.1242/jeb.099523

models, but considerably simpler than current multi-mass models. For this purpose, we formulated a two-mass model that theorizes that running vertical force–time waveforms consist of two components, each corresponding to the motion of a discrete portion of the body's mass. A smaller component (m_1) corresponds to the impact of the lower limb with the running surface while a larger component (m_2) corresponds to the accelerations of the remainder of the body's mass (Fig. 1A). We hypothesize that our two-mass model can explain running ground reaction force–time waveforms in their entirety across different speed, foot-strike and footwear conditions.

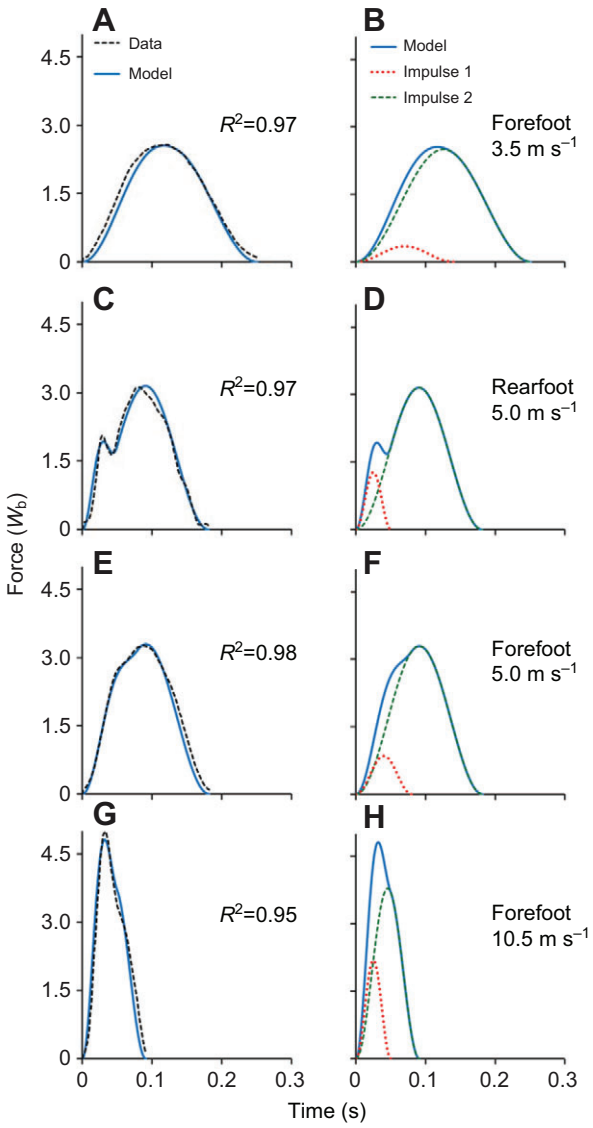

Fig. 1. Modeled versus actual vertical ground reaction force waveforms from four different running footfalls. (A,B) Barefoot, fore-foot strike at 3.5 m s^{-1}; (C,D) shod, rear-foot strike at 5.0 m s^{-1}; (E,F) shod, fore-foot strike at 5.0 m s^{-1}; (G,H) shod, fore-foot strike at 10.5 m s^{-1}. A, C, E and G illustrate the two-mass model (solid blue line) compared with the digitized waveforms (dashed black line). B, D, F and H illustrate the contributions of the first impulse (J_1, dotted red line) and second impulse (J_2, dashed green line) to the total predicted by the model (solid blue line). Modeled versus digitized waveform R^2 values are provided in the figure; root mean square error values were 0.15, 0.16, 0.15 and 0.35W_b for waveforms 1–4, respectively. [Note: the model assumes that the force contributed by m_1 after impulse J_1 has ended is zero; original sources for waveforms 1–4 were: Lieberman et al. (Lieberman et al., 2010), their fig. 1c, step #1; Weyand et al. (Weyand et al., 2000), their fig. 1B, step #2; Weyand et al. (Weyand et al., 2010), their fig. 1A, step #1; Weyand et al. (Weyand et al., 2009), their fig. 1B, step #1 of the intact-limb runner.]

RESULTS AND DISCUSSION

In keeping with our hypothesis, our two-mass model was able to account for virtually all of the duration, amplitude and force–time pattern variability present in the vertical ground reaction force waveforms analyzed. Despite the large differences in waveform characteristics introduced by different speed, foot-strike and footwear conditions, our model accounted for an average of 97% of the individual force–time relationships (mean R^2=0.97±0.01) and a minimum of 95% (Fig. 1). The accuracy of these fits across the heterogeneous waveforms tested suggests that two mechanical phenomena, acting in parallel, are sufficient to explain running ground reaction forces: (1) the collision of the lower limb with the running surface, and (2) the motion of the remainder of the body's mass throughout the stance phase.

The accuracy of the fits achieved using a model with only two mass components and with mass component values held constant across conditions differs from prevailing paradigms in several respects. First, while the sequential additions of third, fourth and fifth mass components to multi-mass models over the last two decades (Liu and Nigg, 2000; Ly et al., 2010; Nigg and Liu, 1999; Nikooyan and Zadpoor, 2011; Zadpoor and Nikooyan, 2010) may describe physical and mechanical reality as theorized (Nigg, 2010; Zadpoor and Nikooyan, 2010), these additional masses may also be unnecessary for waveform prediction. Second, the conclusion that the mass quantity decelerated upon foot–ground impact differs substantially for rear foot versus forefoot impacts (Lieberman et al., 2010; Nigg, 2010) should be reconsidered. The close fits we report here using a constant value of 8.0% of the body's mass across all foot-strike conditions indicates that a variable 'effective mass' may be unnecessary for accurate modeling and could be mechanically incorrect. For example, if we predict the sprint running waveform analyzed here (Fig. 1G,H) using the effective mass proportions suggested for a forefoot impact [m_1=1.7% and m_2=98.3% of total body mass M_b (Lieberman et al., 2010)] with a speed-specific foot collisional velocity (Mann and Herman, 1985) (Table 1), the rising edge of the sprint waveform is substantially under-predicted and the overall goodness of fit is considerably reduced (R^2=0.95 to 0.82; see supplementary material Fig. S1). Third, the model's general features and simplifying assumptions permit impulse J_1 and J_2 durations and forces to be independent. In contrast, the dual 'stacked spring-mass' model-type (Alexander, 1990; Derrick et al., 2000; Ker et al., 1989) that Alexander originally introduced (Alexander, 1988) uses a serial, coupled configuration that may be incapable of predicting the brief simultaneous impulses responsible for the characteristic pattern of sprint running waveforms.

Indeed, the model's design was essential for achieving close fits to waveforms with variable rising edges, smooth falling edges and significantly different durations. Given the fixed-mass value of our lower-limb mass component, the close fits to the variable rising edges were achieved predominantly via the two model inputs (Table 1) responsible for the shape of collisional impulse J_1 (Fig. 1). Values for the first of the two, the vertical velocity of the lower limb at touchdown, are well-supported by the waveform-specific literature values available. Values for the second, the deceleration time of the lower limb upon touchdown, are well-supported by the detailed analysis of Nigg et al. (Nigg et al., 1987) for waveform 2, but are lacking for the other three. Fits along the smoother falling edges depend directly upon impulse J_2 because

Table 1. Waveform information

Waveform	Reference	Fig. 1 panels	Speed ($m\,s^{-1}$)	Foot-strike	Shod condition	Mass (kg)	t_c (s)	t_a (s)	Δt_1 (s)	v_{zlimb} at touchdown ($m\,s^{-1}$)	
										Model	Published
1	Lieberman et al., 2010	A, B	3.5	Fore-foot	Barefoot	70.00	0.251	0.087	0.070	−0.80	−0.80[a]
2	Weyand et al., 2000	C, D	5.0	Rear foot	Shod	72.06	0.181	0.136	0.025	−1.70	−1.60[b]
3	Weyand et al., 2010	E, F	5.0	Fore-foot	Shod	69.21	0.182	0.152	0.040	−1.70	−1.60[b]
4	Weyand et al., 2009	G, H	10.5	Fore-foot	Shod	69.21	0.091	0.136	0.025	−3.10	−3.00[c]

t_c, contact time; t_a, aerial time; Δt_1, time interval between touchdown and vertical velocity of component m_1 slowing to zero; v_{zlimb}, vertical velocity of lower limb.
[a]Data from Nigg et al. (Nigg et al., 1987), table 1 in their appendix; listed value is −0.80 m s^{-1} at running speed of 3.0 m s^{-1}.
[b]Data from Nigg et al. (Nigg et al., 1987), table 1 in their appendix.
[c]Data derived from Mann and Herman (Mann and Herman, 1985); listed value is a horizontal foot velocity of −7.93 m s^{-1} at a running speed of 10.21 m s^{-1}.

of the early conclusion of the J_1 collisional event. Given a known physical basis for determining total impulse J_T from contact and step times (Eqn 1; see Materials and methods), correctly quantifying impulse J_2 depends solely on the quantity subtracted for impulse J_1 (Eqn 2). While empirical validation clearly remains for several elements of our model, the fits achieved using anatomical mass inputs, realistic lower-limb velocities, and one mechanical explanation across conditions raise the possibility that the running force–motion relationship may be more general than previously recognized.

An additional factor in the accuracy of the fits we report was undoubtedly the model evaluation method adopted. The method chosen allowed us to assess a greater variety of waveforms than would have been possible via direct experimentation, but also involved two potential limitations. First, because the model fits were generated by varying the inputs, the goodness-of-fit values obtained should be regarded as the upper performance limits of the model. Second, the digitizing process enabling our approach might have transformed the literature waveforms into more model-conducive shapes. We were able to evaluate this second possibility empirically by applying the inputs used to fit two of the digitized waveforms (3 and 4) to the original waveform data. This process yielded fits that were the same or slightly greater for the original (respective R^2 values of 0.98 and 0.96) versus digitized versions because the original waveforms were so closely reproduced by digitizing (see supplementary material Tables S1–S4).

We close by providing respective, illustrative examples of the basic and applied advances made possible by the concise physical basis of our two-mass model. One basic insight provided by the framework of the model is the identification of a mechanical strategy that runners can adopt to achieve faster speeds. By simply increasing the lower limb's velocity prior to touchdown, and reducing deceleration time during impact, runners can elevate the collisional impulse (J_1) and total ground reaction forces as needed to attain faster speeds (Weyand et al., 2000; Weyand et al., 2009; Weyand et al., 2010). Both the existing literature data (Table 1) and our modeling results (Fig. 1) are consistent with this being a primary mechanism by which faster human runners do, in fact, attain faster sprint running speeds.

In application, the conciseness of the model could translate into practical techniques for determining ground reaction forces indirectly. At present, the lone indirect assessment method available (Bobbert et al., 1991) is scientifically rigorous, but impractical for broad usage. The existing technique involves the instantaneous summation of the accelerations of seven body segments based on high-frequency positional data from 10 bodily locations. In contrast, the scientific basis of our two-mass model (Eqns 1–6) reduces the data needed for indirect force determinations to three basic variables: aerial time, contact time and the vertical velocity of the lower limb. Thus, our model may allow video and other motion capture techniques to become practical tools for determining vertical ground reaction forces without direct measurement.

MATERIALS AND METHODS

Model formulation

Because the net vertical displacement of the body over time during steady-speed, level running is zero, the time-averaged vertical ground reaction force must equal the body's weight. Thus, the total stance-averaged vertical force F_{Tavg} can be determined if foot–ground contact time t_c and aerial time t_a are known:

$$F_{Tavg} = m\boldsymbol{g}\frac{t_{step}}{t_c}, \quad (1)$$

where t_{step} is step time ($t_{step}=t_c+t_a$), m is body mass and $\boldsymbol{g}$ is gravitational acceleration (9.8 m s^{-2}).

The ground reaction force waveform represents the instantaneous acceleration of the body's mass. Accordingly, the waveform can be conceptualized as the sum of the instantaneous accelerations of different segments that make up the body's total mass (Bobbert et al., 1991). In our model (Fig. 1), impulse J_1 results from the acceleration of the lower limb during surface impact, and J_2 corresponds to the acceleration of the remainder of the body's mass. The total impulse J_T, is the sum of J_1 and J_2:

$$J_T = J_1 + J_2 = F_{Tavg}t_c. \quad (2)$$

Impulse mass m_1 is the 8.0% of the body's total mass attributed to the lower limb, while impulse mass m_2 is the remaining 92.0%. Impulse J_1 is quantified from the deceleration of m_1 during surface impact:

$$J_1 = F_{1avg}(2\Delta t_1) = m_1\left(\frac{\Delta v_1}{\Delta t_1} + \boldsymbol{g}\right)(2\Delta t_1), \quad (3)$$

where Δt_1 is the time interval between touchdown and vertical velocity of m_1 slowing to zero, Δv_1 is the change in vertical velocity of m_1 during Δt_1, and F_{1avg} is the average force during the total time interval ($2\Delta t_1$) of impulse J_1. After the J_1 time interval, the model assumes F_{1avg}=0. J_2 is determined from J_1 and total impulse J_T as:

$$J_2 = J_T - J_1 = F_{2avg}t_c, \quad (4)$$

where F_{2avg} is the average force of J_2 during the interval t_c.

Modeled waveforms

The bell-shaped force curves $F(t)$ for J_1 and J_2 are a result of non-linear elastic collisions (Cross, 1999) that can be accurately modeled using the raised cosine function:

$$F(t) = \begin{cases} \frac{A}{2}\left[1+\cos\left(\frac{t-B}{C}\pi\right)\right] & \text{for } B-C \le t \le B+C \\ 0 & \text{for } t < B-C \text{ and } t > B+C \end{cases}, \quad (5)$$

where A is the peak amplitude, B is the center time of the peak and C is the half-width time interval. Because of the symmetrical properties of this

function, peak amplitude $A=2F_{avg}$, and the area under the curve is $J=AC$. The total force waveform $F_T(t)$ is the sum of each impulse waveform:

$$F_T(t)=\frac{A_1}{2}\left[1+\cos\left(\frac{t-B_1}{C_1}\pi\right)\right]+\frac{A_2}{2}\left[1+\cos\left(\frac{t-B_2}{C_2}\pi\right)\right]. \quad (6)$$

A_1 is calculated from F_{1avg} using the Δv_1 and Δt_1 terms in Eqn 3, and B_1 and C_1 equal the time Δt_1 after touchdown for the vertical velocity of m_1 to reach zero. A_2 is calculated from F_{2avg} in Eqn 4, and B_2 and C_2 equal one-half the contact time t_c.

Modeled versus actual waveforms

We digitized (Engauge, version 4.1) four published waveforms that varied in duration, amplitude and shape (Table 1). Model fits of the four digitized waveforms (Fig. 1) were performed via a manual iterative process that constrained the inputs for Δt_1 and Δv_1 to values deemed realistic on the basis of existing literature. Inputs for t_c and subsequent t_a were determined from the waveforms using a threshold of 60 N. In two cases (waveforms 3 and 4), goodness of fit between modeled and original data waveforms were determined to supplement the evaluation of the digitized versions.

Model fits were quantified in two ways: (1) in force units standardized to the body's weight (W_b) using the root mean square statistic (RMSE), and (2) for goodness of fit using the R^2 statistic. Digitized waveforms were interpolated as needed to provide force data on a per millisecond basis for these analyses. We hypothesized that the model would explain 90% or more (i.e. $R^2 \geq 0.90$) of the force–time variation present in each of the four waveforms analyzed. Data for all digitized, modeled and original waveforms used in the analysis are provided in supplementary material Tables S1–S4.

All variables are presented in SI units, but, per convention, force waveforms are illustrated in mass-specific units.

Acknowledgements

The authors thank Lindsay Wohlers, Geoffrey Brown and the two anonymous reviewers for helpful comments on the manuscript.

Competing interests

The authors declare competing financial interests. Peter Weyand, Laurence Ryan and Kenneth Clark are the inventors of US Patent #8363891 which is owned by Southern Methodist University and contains scientific content related to that presented in the paper. The patent is licensed to SoleForce LLC in which the three aforementioned individuals are equity partners.

Author contributions

Each of the three authors, K.P.C., L.J.R. and P.G.W., contributed substantially to the conception of the study, the implementation and evaluation of the model presented, and the writing of the manuscript.

Funding

This work was supported by a US Army Medical Research and Materiel Command award [W81XWH-12-2-0013] to P.G.W.

Supplementary material

Supplementary material available online at
http://jeb.biologists.org/lookup/suppl/doi:10.1242/jeb.099523/-/DC1

References

Alexander, R. M. (1988). *Elastic Mechanisms in Animal Movement*. Cambridge: Cambridge University Press.
Alexander, R. M. (1990). Three uses for springs in legged locomotion. *Int. J. Rob. Res.* **9**, 53-61.
Blickhan, R. (1989). The spring-mass model for running and hopping. *J. Biomech.* **22**, 1217-1227.
Bobbert, M. F., Schamhardt, H. C. and Nigg, B. M. (1991). Calculation of vertical ground reaction force estimates during running from positional data. *J. Biomech.* **24**, 1095-1105.
Bullimore, S. R. and Burn, J. F. (2007). Ability of the planar spring-mass model to predict mechanical parameters in running humans. *J. Theor. Biol.* **248**, 686-695.
Cavagna, G. A., Heglund, N. C. and Taylor, C. R. (1977). Mechanical work in terrestrial locomotion: two basic mechanisms for minimizing energy expenditure. *Am. J. Physiol.* **233**, R243-R261.
Cavanagh, P. R. (1987). The biomechanics of lower extremity action in distance running. *Foot Ankle* **7**, 197-217.
Chi, K. J. and Schmitt, D. (2005). Mechanical energy and effective foot mass during impact loading of walking and running. *J. Biomech.* **38**, 1387-1395.
Cross, R. (1999). Dynamic properties of tennis balls. *Sports Engineering* **2**, 23-33.
Derrick, T. R., Caldwell, G. F. and Hamill, J. (2000). Modeling the stiffness characteristics of the human body while running with various stride lengths. *J. Appl. Biomech.* **16**, 36-51.
Dickinson, J. A., Cook, S. D. and Leinhardt, T. M. (1985). The measurement of shock waves following heel strike while running. *J. Biomech.* **18**, 415-422.
Farley, C. T., Glasheen, J. and McMahon, T. A. (1993). Running springs: speed and animal size. *J. Exp. Biol.* **185**, 71-86.
Ferris, D. P. and Farley, C. T. (1997). Interaction of leg stiffness and surfaces stiffness during human hopping. *J. Appl. Physiol.* **82**, 15-22, discussion 13-14.
Ker, R. F., Bennett, M. B., Alexander, R. M. and Kester, R. C. (1989). Foot strike and the properties of the human heel pad. *Proc. Inst. Mech. Eng. H* **203**, 191-196.
Kuitunen, S., Komi, P. V. and Kyröläinen, H. (2002). Knee and ankle joint stiffness in sprint running. *Med. Sci. Sports Exerc.* **34**, 166-173.
Lieberman, D. E., Venkadesan, M., Werbel, W. A., Daoud, A. I., D'Andrea, S., Davis, I. S., Mang'eni, R. O. and Pitsiladis, Y. (2010). Foot strike patterns and collision forces in habitually barefoot versus shod runners. *Nature* **463**, 531-535.
Liu, W. and Nigg, B. M. (2000). A mechanical model to determine the influence of masses and mass distribution on the impact force during running. *J. Biomech.* **33**, 219-224.
Ly, Q. H., Alaoui, A., Erlicher, S. and Baly, L. (2010). Towards a footwear design tool: influence of shoe midsole properties and ground stiffness on the impact force during running. *J. Biomech.* **43**, 310-317.
Mann, R. and Herman, J. (1985). Kinematic analysis of Olympic sprint performance: men's 200 meters. *Int. J. Sport Biomech.* **1**, 151-162.
McMahon, T. A. and Cheng, G. C. (1990). The mechanics of running: how does stiffness couple with speed? *J. Biomech.* **23 Suppl. 1**, 65-78.
McMahon, T. A., Valiant, G. and Frederick, E. C. (1987). Groucho running. *J. Appl. Physiol.* **62**, 2326-2337.
Munro, C. F., Miller, D. I. and Fuglevand, A. J. (1987). Ground reaction forces in running: a reexamination. *J. Biomech.* **20**, 147-155.
Nigg, B. M. (2010). *Biomechanics of Sport Shoes*. Calgary, AB: Topline Printing Inc.
Nigg, B. M. and Liu, W. (1999). The effect of muscle stiffness and damping on simulated impact force peaks during running. *J. Biomech.* **32**, 849-856.
Nigg, B. M., Bahlsen, H. A., Luethi, S. M. and Stokes, S. (1987). The influence of running velocity and midsole hardness on external impact forces in heel-toe running. *J. Biomech.* **20**, 951-959.
Nikooyan, A. A. and Zadpoor, A. A. (2011). Mass-spring damper modeling of the human body to study running and hopping – an overview. *Proc. Inst. Mech. Eng. H* **225**, 1121-1135.
Robilliard, J. J. and Wilson, A. M. (2005). Prediction of kinetics and kinematics of running animals using an analytical approximation to the planar spring-mass system. *J. Exp. Biol.* **208**, 4377-4389.
Weyand, P. G., Sternlight, D. B., Bellizzi, M. J. and Wright, S. (2000). Faster top running speeds are achieved with greater ground forces not more rapid leg movements. *J. Appl. Physiol.* **89**, 1991-1999.
Weyand, P. G., Bundle, M. W., McGowan, C. P., Grabowski, A., Brown, M. B., Kram, R. and Herr, H. (2009). The fastest runner on artificial legs: different limbs, similar function? *J. Appl. Physiol.* **107**, 903-911.
Weyand, P. G., Sandell, R. F., Prime, D. N. and Bundle, M. W. (2010). The biological limits to running speed are imposed from the ground up. *J. Appl. Physiol.* **108**, 950-961.
Zadpoor, A. A. and Nikooyan, A. A. (2010). Modeling muscle activity to study the effects of footwear on the impact forces and vibrations of the human body during running. *J. Biomech.* **43**, 186-193.

Are running speeds maximized with simple-spring stance mechanics?

Kenneth P. Clark and Peter G. Weyand

J Appl Physiol 117:604-615, 2014. First published 31 July 2014; doi:10.1152/japplphysiol.00174.2014

Journal of Applied Physiology publishes original papers that deal with diverse areas of research in applied physiology, especially those papers emphasizing adaptive and integrative mechanisms. It is published 12 times a year (monthly) by the American Physiological Society, 9650 Rockville Pike, Bethesda MD 20814-3991. ISSN: 0363-6143, ESSN: 1522-1563. Visit our website at http://www.the-aps.org/.

J Appl Physiol 117: 604–615, 2014.
First published July 31, 2014; doi:10.1152/japplphysiol.00174.2014.

Are running speeds maximized with simple-spring stance mechanics?

Kenneth P. Clark and Peter G. Weyand

Southern Methodist University, Locomotor Performance Laboratory, Department of Applied Physiology and Wellness, Dallas, Texas

Submitted 24 February 2014; accepted in final form 24 July 2014

Clark KP, Weyand PG. Are running speeds maximized with simple-spring stance mechanics?. *J Appl Physiol* 117: 604–615, 2014. First published July 31, 2014; doi:10.1152/japplphysiol.00174.2014.—Are the fastest running speeds achieved using the simple-spring stance mechanics predicted by the classic spring-mass model? We hypothesized that a passive, linear-spring model would not account for the running mechanics that maximize ground force application and speed. We tested this hypothesis by comparing patterns of ground force application across athletic specialization (competitive sprinters vs. athlete nonsprinters, $n = 7$ each) and running speed (top speeds vs. slower ones). Vertical ground reaction forces at 5.0 and 7.0 m/s, and individual top speeds ($n = 797$ total footfalls) were acquired while subjects ran on a custom, high-speed force treadmill. The goodness of fit between measured vertical force vs. time waveform patterns and the patterns predicted by the spring-mass model were assessed using the R^2 statistic (where an R^2 of 1.00 = perfect fit). As hypothesized, the force application patterns of the competitive sprinters deviated significantly more from the simple-spring pattern than those of the athlete, nonsprinters across the three test speeds ($R^2 < 0.85$ vs. $R^2 \geq 0.91$, respectively), and deviated most at top speed ($R^2 = 0.78 \pm 0.02$). Sprinters attained faster top speeds than nonsprinters (10.4 ± 0.3 vs. 8.7 ± 0.3 m/s) by applying greater vertical forces during the first half (2.65 ± 0.05 vs. 2.21 ± 0.05 body wt), but not the second half (1.71 ± 0.04 vs. 1.73 ± 0.04 body wt) of the stance phase. We conclude that a passive, simple-spring model has limited application to sprint running performance because the swiftest runners use an asymmetrical pattern of force application to maximize ground reaction forces and attain faster speeds.

sprinting performance; musculoskeletal mechanics; ground reaction forces; gait; spring-mass model

RUNNING SWIFTLY IS AN ATHLETIC attribute that has captivated the human imagination from prehistoric times through the present day. However, interest in running speed as an athletic phenomenon has probably never been greater than at present. A number of factors have heightened contemporary interest and focused it upon the determinants of how swiftly humans can run. These factors include the globalization and professionalization of athletics, the parallel emergence of a performance-training profession, advances in scientific and technical methods for enhancing performance, and record-breaking sprint running performances in recent international competitions. Yet despite interest, incentives, and intervention options that are arguably all without precedent, the scientific understanding of how the fastest human running speeds are achieved remains significantly incomplete.

At the whole-body level, the basic gait mechanics responsible for the swiftest human running speeds are well established. Contrary to intuition, fast and slow runners take essentially the same amount of time to reposition their limbs when sprinting at their different respective top speeds (36, 38). Hence, the time taken to reposition the limbs in the air is not a differentiating factor for human speed. Rather, the predominant mechanism by which faster runners attain swifter speeds is by applying greater forces in relation to body mass during shorter periods of foot-ground force application (36, 38). What factors enable swifter runners to apply greater mass-specific ground forces? At present, this answer is unknown. Moreover, the limited scientific information that is available offers two competing possibilities.

The first possibility is drawn from the classic view of steady-speed running mechanics. In this classic view, runners optimize force production, economy, and overall performance by using their legs in a spring-like manner during each contact period with the ground (13, 16, 31). During the first portion of the stance phase, the limb is compressed as the body is pulled downward by the force of gravity, storing strain energy in the elastic tissues of the leg. In the latter portion of the stance phase, this strain energy is released via elastic recoil that lifts and accelerates the body into the next step (30). The stance phase dynamics observed have been modeled as a lumped point-mass bouncing atop a massless leg spring (2, 4, 18, 19, 26, 32). This simple model makes the basic predictions illustrated in Fig. 1*A*: *1*) the ground reaction force vs. time waveform will take the shape of a half-sine wave, *2*) the displacement of the body's center of mass during the compression and rebound portions of the contact period will be symmetrical about body weight, and *3*) the peak force will occur at midstance when the center of mass reaches its lowest position. Despite its mechanical simplicity, the classic spring-mass model provides relatively accurate predictions of the vertical force vs. time waveforms observed at slow and intermediate running speeds.

The second possibility emerges from the more limited ground reaction force data that are available from humans running at faster speeds. These more limited data (3, 5, 10, 23, 25, 35, 37, 38) generally exhibit vertical ground reaction force vs. time waveforms that are asymmetrical and therefore not fully consistent with the simple, linear-spring pattern predicted by the spring-mass model. Indeed, the tendency toward asymmetry appears to be most pronounced in the ground reaction force waveforms from the fastest speeds (3, 10, 37, 38), which show an appreciably steeper rising vs. trailing edge and a force peak that occurs well before midstance (Fig. 1*B*, *Example 1*). The more asymmetrical pattern at faster speeds may result from greater impact-phase limb decelerations (14) that elevate the ground reaction forces in the early portion of the stance phase. This mechanism would enhance ground force application within the short contact periods available during sprint running (36, 38) and appears to be consistent with gait kinematics used by the fastest human sprinters (24).

Address for reprint requests and other correspondence: P. Weyand, Locomotor Performance Laboratory, Dept. of Applied Physiology and Wellness, Southern Methodist Univ., 5538 Dyer St., Dallas, TX 75206 (e-mail: pweyand@smu.edu).

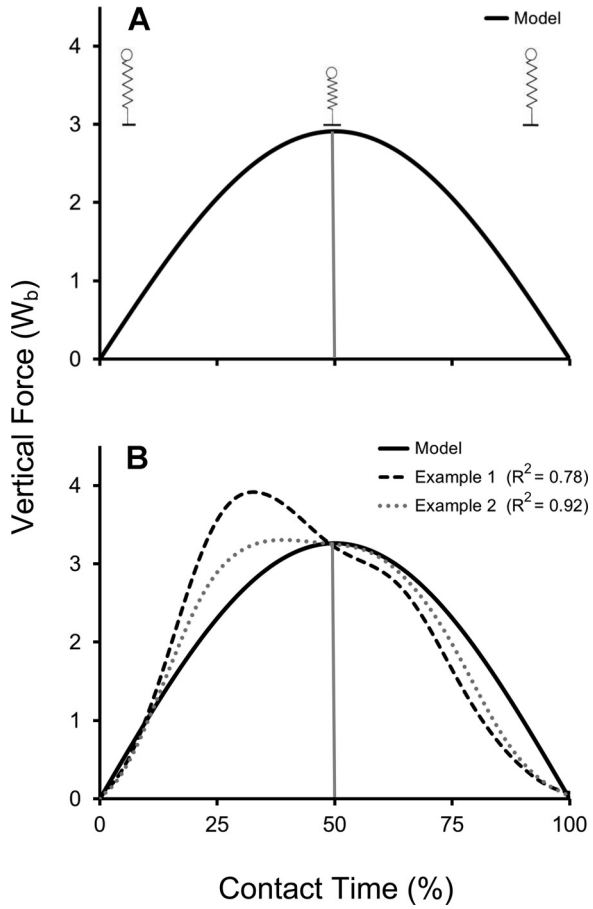

Fig. 1. A schematic illustration of the classic spring-mass model [modified with permission from (12)] during forward running and the half-sine waveform representing the vertical force produced by the mathematical expression of the model (*A*). The half-sine waveform representing the spring-mass model (solid black line) vs. two different example waveforms. *Example 1* (dashed black line) has relatively poor conformation to the model, whereas *Example 2* (dotted gray line) has relatively better conformation to the model (*B*). Ground reaction forces are presented in mass-specific form (i.e., after standardization to body weight) in all illustrations.

We undertook this study to evaluate whether or not the fastest human running speeds are achieved using simple, linear-spring stance mechanics. We did so using the vertical ground reaction force vs. time relationship predicted by the spring-mass model in Fig. 1*A* as a null standard for comparisons. We quantified conformation to, or deviation from, the pattern of ground force application predicted by the spring-mass model from the degree of overlap (i.e., goodness of fit, R^2) between modeled and measured waveforms as illustrated in Fig. 1*B*. Two experimental tools were used to test the idea that the fastest human running speeds are attained using an asymmetrical pattern of ground force application that deviates from the simple, linear spring predictions of the spring-mass model: *1*) athletic specialization and 2) running speed. In the first case, we hypothesized that patterns of ground force application of competitive sprinters would deviate more from spring-mass model predictions than those of athlete nonsprinters. In the second case, for subjects in both groups, we hypothesized that patterns of ground force application would deviate more from spring-mass model predictions at top speed vs. slower running speeds.

METHODS

Experimental Overview and Design

Spring model predictions. Per the methods outlined by Alexander et al. (2) and Robilliard and Wilson (32), half-sine wave formulations of the vertical ground reaction force waveforms predicted by the spring-mass model were determined from the runner's contact time (t_c), aerial time (t_{aer}), and step time ($t_{step} = t_c + t_{aer}$):

$$F(t)/W_b = \begin{cases} \left(\frac{\pi}{2}\right) \cdot \left(\frac{t_{step}}{t_c}\right) \cdot \sin\left(\pi \cdot \left(\frac{t}{t_c}\right)\right), & 0 \le t < t_c \\ 0, t_c \le t < t_{step} \end{cases} \quad (Eq.\ 1)$$

where $F(t)$ is the force at time t and W_b is the force of the body's weight. The peak mass-specific force, F_{peak}/W_b, occurs during ground contact t_c at time $t = t_c/2$:

$$\frac{F_{peak}}{W_b} = \left(\frac{\pi}{2}\right) \cdot \left(\frac{t_{step}}{t_c}\right) \quad (Eq.\ 2)$$

The degree of overlap between the measured vertical ground reaction force-time waveforms vs. those predicted by the spring-mass model was determined using the R^2 goodness of fit statistic and mass-specific force values as follows. First, differences between the force values measured during each millisecond and the overall waveform mean value were squared and summed to obtain an index of the total variation present within the waveform, or the total sum of squares [$SS_{total} = \Sigma(F/W_{b,\ measured} - F/W_{b,\ mean})^2$]. Next, the predictive error of the spring model was determined from the difference between the spring-modeled values (*Equations 1* and *2*) and measured force values also using the same sum of squares method [$SS_{error} = \Sigma(F/W_{b,\ measured} - F/W_{b,\ spring\ model})^2$]. Finally, the proportion of the total force waveform variation accounted for by the spring-mass model was then calculated using the R^2 statistic:

$$R^2 = 1 - \left(\frac{SS_{error}}{SS_{total}}\right) \quad (Eq.\ 3)$$

Accordingly, our spring-model goodness of fit R^2 values have a theoretical maximum 1.00 (where $R^2 = 1.00$ is exact agreement with the spring model). In practice, and on the basis of prior literature (14), we expected patterns that were relatively well predicted by the model to have R^2 agreement values $\geq$0.90 and patterns that were predicted relative poorly to have agreement values $<$0.90. This somewhat subjective threshold was identified simply to facilitate goodness-of-fit interpretations. The example waveforms appearing in Fig. 1*B* provide a frame of reference between the degree of waveform overlap with the spring-model and corresponding numeric R^2 values. In accordance with our respective hypotheses, we predicted that: *1*) the R^2 values for competitive sprinters would be significantly lower than those of athlete nonsprinters, and *2*) the R^2 values at top speed would be significantly lower than those at slower running speeds for the subjects in both groups.

In addition to the relative values provided by our R^2 spring-model goodness of fit index, we also quantified the agreement between measured patterns of ground force application and the spring model-predicted patterns in the units of force most relevant to sprinting performance (F/W_b). We did so using the root mean square error (RMSE) statistic as follows:

$$RMSE = \sqrt{\left(\frac{SS_{error}}{n}\right)} \quad (Eq.\ 4)$$

where n equals the number of observations. Accordingly, larger RMSE values will result from patterns of ground force application that deviate more from the spring-mass model, and vice versa. Hence, the RMSE can be here conceptualized as an index of force disagree-

ment between the measured force waveforms vs. those predicted by the spring-mass model expressed in force units of the body's weight. Thus for this second statistic, we predicted RMSE values would be: *1*) significantly greater for competitive sprinters vs. athlete nonsprinters, and *2*) significantly greater at top speed vs. slower speeds for the subjects in both groups.

We analyzed only the vertical component of the ground force because previous work (10, 36, 38) has directly linked stance-average, mass-specific vertical ground reaction forces to the sprinting speeds attained:

$$\text{Speed} = \left(\frac{F_{\text{avg}}}{W_b}\right) \cdot L_c \cdot Freq_{\text{step}} \qquad (Eq.\ 5)$$

where speed is the body's forward running velocity, F_{avg}/W_b is the stance-averaged vertical force applied to the running surface in units of the body's weight, L_c is the length of contact, or forward distance the body travels during the foot-ground contact period, and $Freq_{\text{step}}$ is $1/(t_{\text{step}})$. The equation has been shown to be accurate within 3.0% or less during steady-speed running (38). Because we used a simple vertical spring-mass model rather than a planar model for hypothesis testing, horizontal ground reaction forces were not included in the analysis.

Design and data acquisition strategies. For the competitive sprinter group, we recruited only track athletes who specialized in the 100- and 200-meter events and who had intercollegiate track and field experience or the equivalent. For the athlete nonsprinter group, we recruited athletes who regularly ran at high speeds for their sport specialization, but who were not competitive sprinters. In both groups, we recruited and enrolled only those athletes with midfoot and forefoot strike patterns because the fast subjects we were seeking to enroll do not heel strike when running at high speeds.

We maximized ground reaction force data quality and quantity by conducting tests on a high-speed force treadmill capable of acquiring data from a large number of consecutive footfalls at precisely controlled speeds. Acquiring equivalently robust data for the purpose of quantifying patterns of foot-ground force application using in-ground force plates would be difficult, or perhaps impossible, given that overground conditions greatly limit the number of footfalls acquired, and substantially increase the variability present in both running speeds and foot-strike patterns. For athletic subjects running on a treadmill vs. overground, prior studies have demonstrated a close correspondence between sprint running performances (9), sprinting kinematics (20), and patterns of ground force application at speeds at which comparative data are available (22, 29).

Although we acquired data from many speeds, we used the ground reaction force data from only three of these for hypothesis testing: 5 m/s, 7 m/s, and individual top speed.

Subjects and Participation

A total of 14 subjects (8 men, 6 women) volunteered and provided written, informed consent in accordance with the requirements of the local institutional review board. All subjects were between 19 and 31 yr of age and regularly active at the time of the testing. The compositions of the competitive sprinter group (age 23.9 ± 1.6 yr, height 1.72 ± 0.03 m, mass 73.8 ± 4.3 kg) and the athlete nonsprinter group (age 21.7 ± 1.5 yr, height 1.77 ± 0.03 m, mass 75.8 ± 4.6 kg) were gender balanced; both included four men and three women. Subjects ranged in athletic experience from intercollegiate team-sport athletes to professional, world-class track athletes. In the athlete, nonsprinter group, all seven subjects had intercollegiate athletic experience. In the competitive sprinter group, six of the seven subjects had intercollegiate track and field experience, five had international experience, and four had participated in both the Olympics and Track and Field World Championships. Physical characteristics and athletic specializations of all participants appear in Table 1. Also provided are the 100- and 200-m personal records of the competitive sprinters.

Measurements

Top speed. Participants were habituated to running on a custom, high-speed force treadmill during one or more familiarization sessions before undergoing top speed testing. For all trials, subjects were fastened into a safety harness attached to an overhead suspension that would support them above the treadmill belt in the event of a fall. The harness and ceiling suspension had sufficient slack to not impede the subjects' natural running mechanics. A progressive, discontinuous treadmill protocol similar to that described by Weyand et al. (36) was administered to determine each subject's top speed. The protocol began at speeds of 2.5 or 3.0 m/s and typically increased in 1.0 m/s increments for each trial at slower speeds and 0.2–0.5 m/s at faster speeds. Trial speeds were progressively increased until a speed was reached at which the subject could not complete eight consecutive steps without backward movement exceeding 0.2 m on the treadmill. Subjects typically made two to three unsuccessful attempts at the failure speed before the test was terminated. The top speed successfully completed was within 0.3 m/s of the failure speed for all subjects. For each trial, subjects straddled the treadmill belt as it was increased to the desired trial speed. Handrails on the sides of the treadmill were set at waist-height and aided subjects in their transition onto the moving belt. Once the treadmill belt had increased to the selected speed, subjects transitioned onto the belt by taking several steps before releasing the handrails. Data acquisition was not initiated until the subject had released the rails. There was no limit on the number of handrail-assisted steps the subjects could complete during their transition onto the belt. Trials at speeds slower than 5 m/s typically lasted 10 to 20 s, whereas trials at speeds faster than 5 m/s

Table 1. *Physical and descriptive characteristics of subjects*

Group	Sex	Age, yr	Height, m	Mass, kg	Sport	100-m PR, s	200-m PR, s
Sprinter	Male	28	1.85	91.6	Track and Field	9.96	20.57
Sprinter	Male	23	1.78	83.4	Track and Field	10.06	20.29
Sprinter	Male	20	1.74	74.4	Track and Field	10.26	21.10
Sprinter	Male	19	1.70	71.8	Track and Field	10.80	22.20
Sprinter	Female	23	1.70	61.8	Track and Field	11.12	22.29
Sprinter	Female	31	1.70	74.1	Track and Field	11.04	22.33
Sprinter	Female	23	1.60	59.4	Track and Field	11.52	24.04
Nonsprinter	Male	23	1.95	101.5	NCAA varsity football		
Nonsprinter	Male	19	1.74	72.7	NCAA club lacrosse		
Nonsprinter	Male	30	1.74	74.6	Former NCAA varsity soccer		
Nonsprinter	Male	20	1.79	78.4	Intercollegiate distance runner		
Nonsprinter	Female	19	1.76	72.6	Intercollegiate varsity soccer		
Nonsprinter	Female	20	1.70	64.4	Intercollegiate varsity soccer		
Nonsprinter	Female	21	1.74	66.3	Intercollegiate varsity soccer		

typically lasted less than 5 s. Subjects were instructed to take full recovery between trials. They typically took 1–2 min between slow and intermediate speed trials, and 1–10 min between faster speeds trials. To reduce the risk of injury or muscle soreness, testing was terminated before top speed was attained if the subjects reported muscle or joint discomfort.

Treadmill force data. Ground reaction force data were acquired at 1,000 Hz from a high-speed, three-axis, force treadmill (AMTI, Watertown, MA). The treadmill uses a Baldor BSM100C-4ATSAA custom high-speed servo motor and a Baldor SD23H2A22-E stock servo controller, and is capable of speeds of >20 m/s. The custom embedded force plate has a length of 198 cm and a width of 68 cm, and interfaces with an AMTI DigiAmp amplifier running NetForce software. The force data were postfiltered using a low-pass, fourth-order, zero-phase-shift Butterworth filter with a cutoff frequency of 25 Hz (39).

Stride timing, length, and center of mass motion variables were determined as follows. For each footfall, contact times were determined from the time the vertical force signal exceeded a threshold of 40 N. Aerial times were determined from the time elapsing between the end of one period of foot-ground contact and the beginning of the next. Step times were determined from the time elapsing during consecutive foot-ground contact and aerial times. Step frequencies were determined from the inverse of step times. Limb repositioning, or swing times, were determined from the time a given foot was not in contact with the running surface between consecutive steps. Contact lengths were determined by multiplying the time of foot-ground contact by the speed of the trial. Trial speeds were determined from the average belt velocity over time. The vertical displacement of the center of mass during ground contact period was determined by double integration of the vertical force waveforms following the procedures described by Cavagna (12).

Force data acquired. Individual subjects completed 12–20 treadmill trials during their top speed tests to failure. The number of consecutive footfalls from which force waveforms were acquired during these tests was generally greater for the slower, less demanding trials. For example, we typically acquired >20 consecutive footfalls for slow and intermediate speeds, 10–20 at moderately fast speeds, and 8–12 during top-speed and near top-speed trials.

The number of footfalls acquired at the subset of three speeds used for formal statistical testing purposes reflect the general pattern of acquiring fewer footfalls at faster speeds. For the competitive sprint and athlete nonsprint subjects, the average number of footfalls acquired at the three hypothesis test speeds were as follows: 31 and 28 at 5.0 m/s, 23 and 13 at 7.0 m/s, and 10 and 9 at top speed, respectively. The number of force waveforms acquired from the three selected speeds used for statistical testing purposes was 797. The total number of footfalls acquired from all subjects at all speeds was >3,000.

For illustrative purposes, ensemble-averaged waveforms were determined for individual subjects and the two subject groups at all of the trial speeds completed including the top sprinting speed. For individual subjects at each speed of interest, ensemble-averaged waveforms were generated by averaging the force from each millisecond of the stance period for all of the waveforms acquired. At those speeds completed by all seven subjects of the respective groups, the seven individual ensemble-averaged waveforms were combined to form ensemble-averages for each of the respective groups. These group force–time waveforms were compiled by standardizing the vertical force values to units of the body's weight and time values to the percentage of the total stance contact time. Neither the individual nor group ensemble averages were used for formal hypothesis testing purposes.

To provide a supplementary assessment of waveform shape characteristics, we also performed a basic Fourier analysis similar to that described by Alexander and Jayes (1), and which appears in the APPENDIX.

Statistics

Both hypothesis tests were evaluated using a two-factor ANOVA (group × speed) that analyzed the mean goodness of fit (R^2 values) between spring-model predicted ground reaction force waveforms and those directly measured from our subjects. Secondary tests of the same hypotheses were conducted using the RMSE statistic. For both force application hypothesis test one (group effect) and test two (speed effect), the a priori thresholds for significance were set at $\alpha = 0.05$. Homogeneity of variance was tested using the Fligner-Killeen test.

Percentage differences between group means for all variables were calculated as: {(larger − smaller)/[(larger + smaller)/2]} × 100. For stance-averaged vertical forces, mean percentage differences were calculated after subtracting a baseline value equal to 1.0 W_b for running at zero speed, or standing.

RESULTS

Top Speeds and Stance-Averaged Vertical Forces

Group means (±SE) for top speeds, stance-averaged vertical forces, contact times, aerial times, swing times, and contact lengths at top speed appear in Table 2. The table includes the overall group means for the competitive sprinters and athlete nonsprinters as well as the within-group means for the men and women. For the overall means, the between-group differences in two variables, top speed ($\Delta = 1.64$ m/s) and stance-averaged vertical forces ($\Delta = 0.21\ W_b$), when expressed on a percentage basis (top speed $\Delta = 17.2\%$; stance-average vertical force $\Delta = 19.2\%$), were nearly identical. The similar percentage differences in top speed and stance-averaged force means variables across the groups resulted from the lack of variation in mean contact lengths and step frequencies (Equation 5).

When considered by sex, between-group differences in top speeds and stance-averaged vertical forces were both slightly larger for women vs. men (top speed $\Delta = 1.76$ vs. 1.56 m/s;

Table 2. *Top-speed gait mechanics*

Group	Top Speed, m/s	F_{avg}, W_b	L_c, m	t_c, s	t_{aer}, s	T_{sw}, s	$Freq_{step}$, s^{-1}
Sprinter							
Males	10.84 ± 0.12	2.18 ± 0.02	1.10 ± 0.04	0.102 ± 0.004	0.114 ± 0.004	0.330 ± 0.010	4.65 ± 0.14
Females	9.73 ± 0.35	2.22 ± 0.06	0.96 ± 0.05	0.099 ± 0.002	0.118 ± 0.004	0.335 ± 0.006	4.61 ± 0.06
Average	10.36 ± 0.27	2.20 ± 0.03	1.04 ± 0.04	0.100 ± 0.002	0.116 ± 0.003	0.332 ± 0.006	4.63 ± 0.08
Nonsprinter							
Males	9.28 ± 0.17	2.01 ± 0.07	1.04 ± 0.06	0.112 ± 0.006	0.111 ± 0.006	0.334 ± 0.012	4.49 ± 0.14
Females	7.97 ± 0.19	1.95 ± 0.01	0.96 ± 0.02	0.121 ± 0.001	0.113 ± 0.005	0.346 ± 0.010	4.29 ± 0.10
Average	8.72 ± 0.29	1.99 ± 0.04	1.01 ± 0.03	0.116 ± 0.004	0.112 ± 0.004	0.340 ± 0.008	4.40 ± 0.09

Values are means ± SE. L_c, length of contact; t_c, runner's contact time; t_{aer}, runner's aerial time; t_{SW}, swing time; $Freq_{step}$, $1/(t_{step})$.

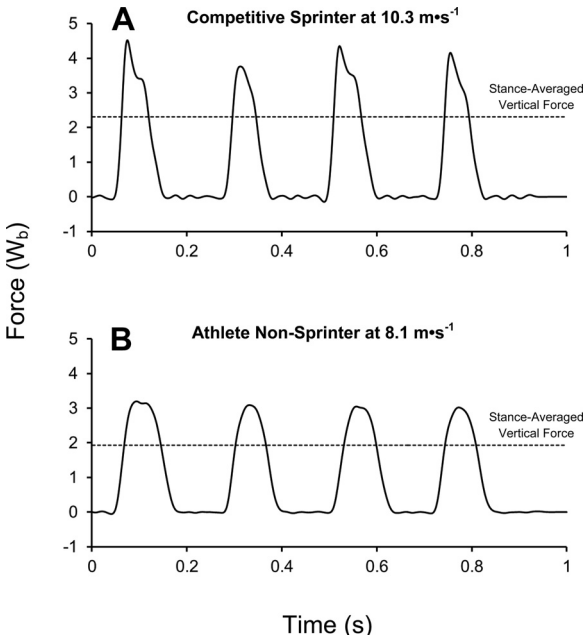

Fig. 2. Vertical ground reaction forces from four consecutive steps for a female competitive sprinter (*A*) and a female athlete nonsprinter (*B*) at their individual top speeds (10.3 and 8.1 m/s, respectively). The stance-averaged vertical forces applied during the respective trials are represented by the dashed horizontal lines. The competitive sprinter applies greater stance-averaged and peak vertical forces during briefer contact phases than the athlete nonsprinter.

stance-averaged vertical force $\Delta = 0.27$ vs. 0.17 W_b). Because neither step frequencies nor stance-averaged vertical forces varied appreciably by gender, the top speed differences between male and female subjects resulted largely from differences in contact lengths. The latter were 10.8% shorter for the overall female vs. male mean (female vs. male ΔL_c sprinters = 13.6%, athlete nonsprinters = 8.0%).

Patterns of Ground Force Application as a Function of Running Speed

Ground force application data from the same two female subjects, one sprinter and one athlete nonsprinter, appear in Figs. 2 through 4 to allow the relationships between original force waveforms (Fig. 2), stance-averaged vertical forces (Fig. 3), and patterns of ground force application (Fig. 4) to be fully illustrated. The step-by-step, ground reaction force waveforms from the respective top-speed trials of these athletes (Fig. 2, *A* and *B*, respectively) were greater in magnitude and briefer in duration for the competitive sprinter vs. the athlete nonsprinter.

The mass-specific, stance-averaged vertical forces for both athletes (Fig. 3, *A* and *B*) increased in a largely linear fashion with speed, from a jog of 3.0 m/s through top speed, with values for the sprinter being 0.2 W_b greater across common speeds. Ensemble-averaged patterns of ground force application for the respective athletes at the same trial speeds (Fig. 4, *A* and *B*) illustrate that both athletes had relatively symmetrical waveforms at the slowest speed of 3.0 m/s. With increases in speed above 3.0 m/s, patterns of ground force application by the sprinter became progressively less symmetrical. The corresponding waveforms for the athlete nonsprinter were relatively symmetrical across all speeds, including her top sprinting speed.

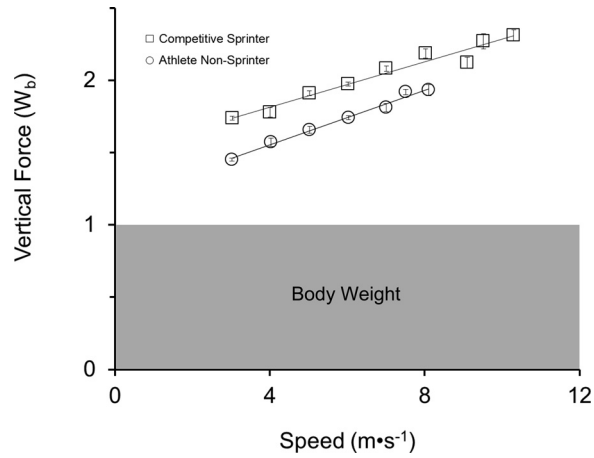

Fig. 3. Stance-averaged, vertical force (mean ± SE) vs. running speed for the same female competitive sprinter (squares) and female athlete nonsprinter (circles) whose data appear in Fig. 2. For both subjects, stance-averaged vertical forces increased across the range of speeds (linear best fits illustrated). The competitive sprinter applied greater forces at equal speeds and top speed.

Patterns of Ground Force Application vs. the Spring-Mass Model Predictions

Ensemble-averaged patterns of ground force application at 5.0 m/s, 7.0 m/s, and top speed, as well as their quantitative

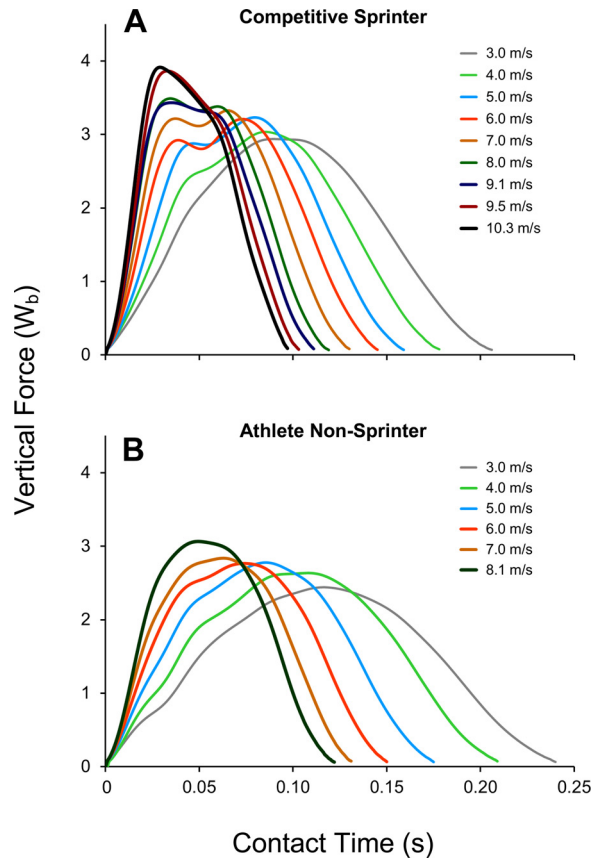

Fig. 4. Trial-averaged composite vertical ground reaction force-time waveforms across running speeds for the same female competitive sprinter (*A*) and female athlete nonsprinter (*B*) whose data appear in Figs. 2 and 3. For both subjects, stance-averaged vertical forces increased and ground contact times decreased across the range of speeds. (Confidence intervals are omitted for clarity, here and in subsequent figures).

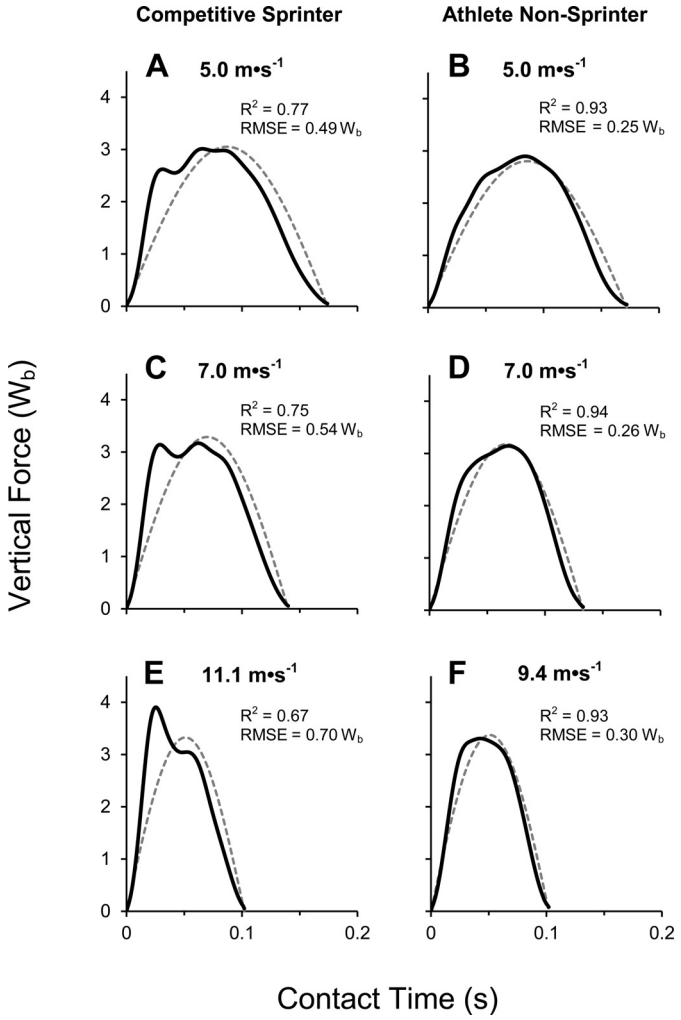

Fig. 5. The trial-averaged composite vertical ground reaction force-time waveforms for a representative male competitive sprinter and representative male athlete nonsprinter are plotted against the half-sine waveform predicted by the spring-mass model for 5.0 m/s, 7.0 m/s, and each individual's top speed (11.1 and 9.4 m/s for the competitive sprinter and athlete nonsprinter, respectively). The waveforms of the competitive sprinter progressively deviated from the spring-mass model as the speeds increased from 5.0 m/s to 7.0 m/s to top speed (*A*, *C*, and *E*), whereas the waveforms of the athlete nonsprinter generally conformed to the spring-mass model at all speeds (*B*, *D*, and *F*).

relationship to the spring-mass model predicted waveforms, appear in Fig. 5 for one male sprinter (Fig. 5, *A*, *C*, and *E*) and one male athlete nonsprinter (Fig. 5, *B*, *D*, and *F*). The male sprinter's waveforms have a qualitatively biphasic appearance due the rapid rising edge and early force peaks present on the waveforms at all three speeds. Thus patterns of ground force application for the sprinter were generally in relatively poor agreement with the spring-mass model at all three speeds (all R^2 values < 0.80). Because the rising edges of the waveforms were steeper and the early force peaks were greater in magnitude at faster speeds, the degree of conformation of the sprinters waveforms to the spring-mass model predicted waveforms decreased as speed increased, reaching an R^2 minimum of 0.67 at top speed. The ground reaction force waveforms of the male athlete nonsprinter lacked a rapid rising edge and conformed relatively closely to the spring-mass model at all three speeds (R^2 range: 0.93–0.94).

The ensemble-averaged waveform patterns of ground force application for the competitive sprint group and athlete nonsprint groups at the three test speeds (Fig. 6) exhibited the patterns similar to those of the individual athletes in Fig. 5, albeit to a slightly smaller degree. The rising edge of the group ensemble-averaged waveform for the competitive sprinters was steeper in general than that of the athlete nonsprinters, and became progressively more steep at the faster speeds. The group ensemble-averaged patterns of ground force application of the athlete nonsprinters conformed closely to the spring-model predicted waveforms at all three speeds (all R^2 values $\geq$ 0.93), exhibiting little discernible speed-related deviation.

The relative stance times at which the peak force occurred during top speed running, as assessed from the group composite waveforms in Fig. 6, *E* and *F*, were $t = 30.2\%$ of t_c for competitive sprinters and $t = 45.7\%$ of t_c for the athlete nonsprinters. The corresponding values for the percentage of

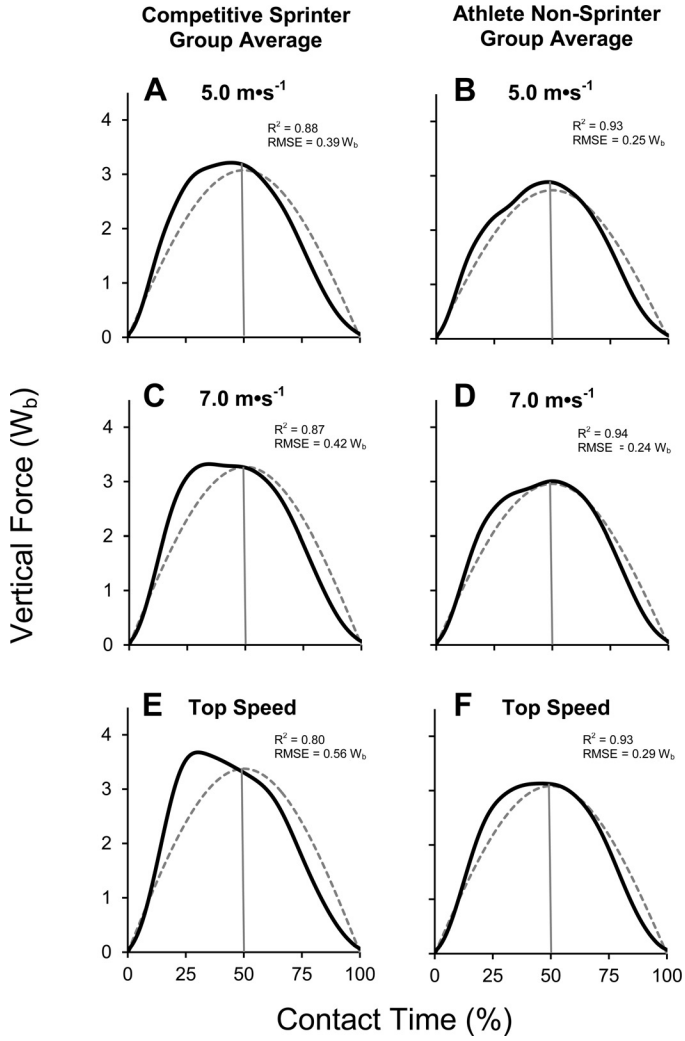

Fig. 6. The trial-averaged composite vertical ground reaction force-time waveform for the competitive sprinter group and the athlete nonsprinter group plotted against the half-sine waveform predicted by the spring-mass model for 5.0 m/s, 7.0 m/s, and top speed. The waveforms of the competitive sprinters progressively deviated from the spring-mass model predictions as the speed increased from 5.0 m/s to 7.0 m/s to top speed (*A*, *C*, and *E*), whereas the waveforms of the athlete nonsprinters generally conformed to the spring-mass model predictions at all speeds (*B*, *D*, and *F*).

the total contact time at which the center of mass reached its minimum height, as determined from the double-integration of the composite, top speed waveforms in Fig. 6, were $t = 40.5\%$ of t_c and $t = 48.7\%$ of t_c for the competitive sprinters and athlete nonsprinters, respectively.

Hypotheses One and Two: Statistical Test Results

The R^2 goodness of fit and RMSE force disagreement values (means ± SE) from the footfall waveforms ($n = 797$) analyzed at 5.0 m/s, 7.0 m/s, and top speed appear in Table 3. In keeping with our first hypothesis, the patterns of ground force application of the competitive sprinters conformed significantly less to the spring-mass model predictions than those of athlete nonsprinters when evaluated with the R^2 goodness of fit statistic (two-factor ANOVA, $F = 243.8$, $P < 0.001$). This was the case even when the much greater variability in the waveforms of the sprinters vs. athlete nonsprinters was taken into account by the Fligner-Killeen test. In partial support of our second hypothesis test using R^2 goodness of fit values, the patterns of ground force application conformed less to the simple spring-predicted pattern for sprinters at top speed than at 5.0 and 7.0 m/s. However, there were no significant differences across speed for athlete nonsprinters whose goodness of fit values were nearly identical at 5.0 m/s, 7.0 m/s, and top speed. Hence, interaction between athletic group and running speed was significant ($F = 51.5$, $P < 0.01$).

The hypothesis test results obtained when RMSE values were used to evaluate patterns of ground force application vs. those predicted by the spring-mass model were fully consistent with the results of the R^2 tests. The main effect of athletic group was significant, and there was an interaction between group and running speed. After again accounting for the lack of homogeneity of variance as tested by the Fligner-Killeen test, the RMSE force disagreement values vs. the simple-spring patterns predicted by the spring-mass model at all three test speeds were significantly greater for the competitive sprinters than the athlete nonsprinters ($F = 442.8$; df = 1, 795; $P < 0.001$). RMSE values were also statistically different across the three running speeds ($F = 104.0$; df = 5, 791; $P < 0.001$) with post hoc testing indicating that this difference was present for the competitive sprinters, but not the athlete, nonsprinters (Table 3).

Table 3. *Mean R^2 agreement and RMSE force disagreement values vs. the spring-mass model predicted waveforms*

Group	Steps, *n*	R^2	RMSE, W_b
Sprinter			
5.0 m/s	218	0.829 ± 0.007	0.440 ± 0.009
7.0 m/s	163	0.843 ± 0.008	0.437 ± 0.012
Top speed	67	0.782 ± 0.016*†	0.571 ± 0.025*†
Nonsprinter			
5.0 m/s	194	0.910 ± 0.003	0.276 ± 0.004
7.0 m/s	89	0.923 ± 0.004	0.276 ± 0.007
Top speed	66	0.915 ± 0.006	0.307 ± 0.012

RMSE, root mean square error. Competitive sprinters differed significantly from athlete nonsprinters across all speeds for both R^2 pattern agreement and RMSE force disagreement values (ANOVA, main effects, $P < 0.001$). Values are means ± SE. *Significantly different from 5.0 m/s; †significantly different from 7.0 m/s.

Individual Variability in Patterns of Ground Force Application

At each of the three analysis speeds, the standard errors about the R^2 and RMSE means were approximately two times greater for the sprinters than the athlete nonsprinters (Table 3). The greatest within-group stratification for both variables existed among the four men in the competitive sprinter group. For the ensemble-averaged waveforms, *subjects 1* and *2* had respective R^2 goodness of fit values to the spring-mass model predicted waveforms of 0.78 and 0.73 across the three test speeds, whereas *subjects* 3 and *4* had respective values of 0.89 and 0.91. The corresponding RMSE values for *subjects 1* and *2* were 0.62 and 0.58 W_b, respectively, vs. 0.35 and 0.37 W_b for *subjects 3* and *4*. Top speed patterns of ground force application for these respective pairs of competitive male sprinters (*subjects 1* and *2*, elite vs. *subjects 3* and *4*, sub-elite) and the corresponding ensemble average of all of the male subjects in the athlete nonsprinter group ($n = 4$) appear in Fig. 7*A*. The trend most evident for male sprinters was present throughout the entire sample. Differences in the stance-average vertical forces applied at top speed were determined entirely during the first half of the stance period (Fig. 7*B*) because all 14 subjects in our sample applied nearly the same vertical force over the second half of the stance phase (1.72 ± 0.04 W_b).

DISCUSSION

Our first objective was to answer the basic question posed in our title: are running speeds maximized with simple-spring stance mechanics? Although selected results did not precisely conform to our predictions, our data in total provided a definitively negative answer. With nearly complete consistency, we found that the runners who applied the greatest mass-specific vertical forces, and thereby attained the fastest speeds, deviated most from the simple-spring pattern of ground force application predicted by the spring-mass model (Figs. 2, 4, 5, 6, and 7; Table 3). Given the need for all runners to reduce periods of ground force application as they run faster, these data provide two closely linked conclusions. First, the simple-spring patterns of ground force application generally regarded as advantageous at slower speeds (15, 16, 31) likely constrain force application and performance at faster ones. Second, deviating from simple-spring, stance mechanics appears to be a strategy that sprinters use (14) to apply the greater mass-specific ground forces needed to attain faster speeds.

Hypothesis Test Outcomes: Simple-Spring Stance Mechanics at the Fastest Speeds?

From a strictly experimental perspective, our first simple-spring hypothesis test outcome conformed to our expectations in full, whereas our second outcome conformed only in part. As predicted, *test 1*, which used athletic specialization as an experimental tool, revealed that the patterns of ground force application of the competitive sprinters deviated more from simple-spring predicted behavior than those of athlete nonsprinters regardless of speed (Table 3). Between-group quantitative differences were sufficiently large to be qualitatively obvious from the shapes of the waveforms, whether for individual athletes (Figs. 4 and 5), or the entire athletic specialty groups (Figs. 6 and 7). However, *test 2*, which used across-

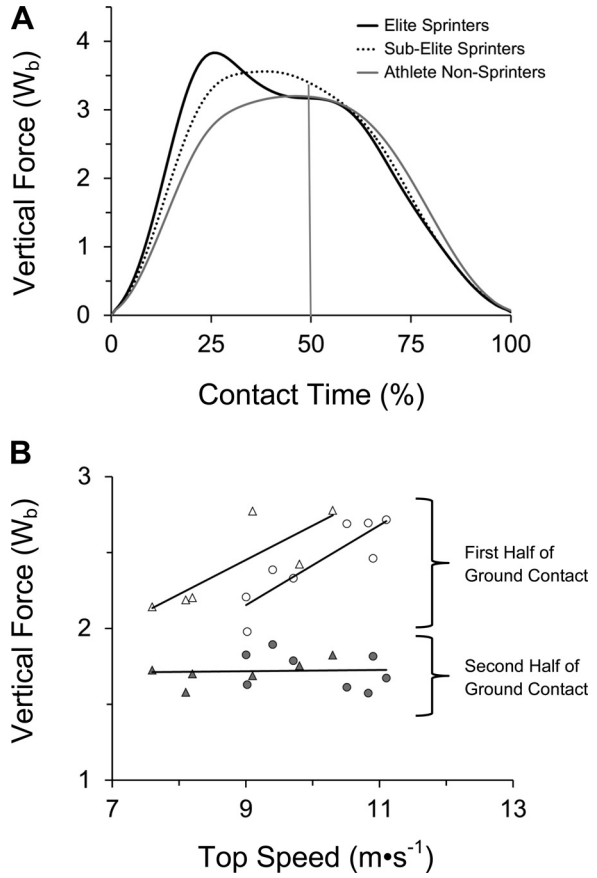

Fig. 7. Trial-averaged composite vertical ground reaction force-time waveforms vs. top speed for the two male elite sprinters (solid black line), the two male sub-elite sprinters (dotted black line), and four male athlete nonsprinters (solid gray line) (*A*). Average vertical forces for the first and second half of the ground contact period for subjects in both groups at top speed (*B*). Circles represent male subjects; triangles represent females subjects; open symbols represent average vertical forces for the first half of the ground contact; shaded symbols represent average vertical forces for the second half of ground contact period. Line fits for the data from the first half of the ground contact period are provided by sex to appropriately account for the leg and contact length differences (Eq. 5, Table 2) that influence top speeds. A single line fit for the data from the second half of the ground contact period is plotted for all 14 subjects because the values are similar in magnitude across group and sex. [Linear best-fit regression equations appearing in *B* that relate ground force to top running speeds are as follows: men first half-stance, force (W_b) = 0.26·Spd − 0.22; women first half contact, force (W_b) = 0.23·Spd + 0.41; all subjects second half contact force (W_b) = 0.004·Spd + 1.68].

speed comparisons as an experimental tool, yielded results that were mixed by athletic specialization; differences across speed were present for the competitive sprinters, but absent for the athlete nonsprinters. For the competitive sprinters, R^2 pattern-agreement and RMSE force-disagreement values at 5.0 and 7.0 m/s were similar to one another (R^2 range 0.83 to 0.85; RMSE range 0.43 to 0.44 W_b; Table 3), whereas their top-speed patterns deviated significantly more from model predictions (R^2 <0.80; RMSE >0.55 W_b). Using our R^2 threshold of 0.90 for simple-spring vs. nonsimple-spring patterns, the sprinters did not conform to simple-spring predictions at any of the three speeds, and deviated most at top speed. In contrast, the athlete nonsprinters used patterns of ground force application that conformed relatively closely (R^2 >0.90) regardless of whether they were running at top speed or the two fixed test speeds of 5.0 and 7.0 m/s (Table 3). Unlike the competitive sprinters, the athlete nonsprinters exhibited virtually no differences in their patterns of ground force application across speed. Both their R^2 pattern-agreement and RMSE force-disagreement values vs. the model predicted patterns model were essentially identical across 5.0 m/s, 7.0 m/s, and top speed (ΔR^2 <0.02; ΔRMSE = 0.03 W_b).

Although our results across running speed were mixed with respect to our hypothesis, the conclusions regarding the force application patterns that maximize running speed were fully consistent. The across-speed results obtained from the competitive sprinters suggest that deviating from a simple-spring pattern of ground force application may be a mechanism these athletes used to attain faster speeds. Athlete nonsprinters, in contrast, did not alter their patterns across speed, nor deviate appreciably from simple-spring pattern at any speed. Notably, we found essentially the same pattern contrasts across individual subjects of differing performance capabilities. Of the four men in the competitive sprinter group, the two nonelite athletes (*subjects 3* and *4*) used top-speed, stance-limb mechanics reflective of their intermediate performance status. Specifically, these two sub-elite men had stance-limb mechanics that deviated more from the simple-spring predicted pattern than the athlete nonsprinters whom they could outperform. However, their mechanics deviated less from the pattern (R^2 means of 0.83 vs. 0.71, respectively) than those of the two world-class men (Fig. 7*A*, Table 3). Collectively, these observations suggest that the deviation from the simple-spring pattern observed for the world-class sprinters may be a force-augmentation mechanism that sub-elite sprinters cannot utilize to the same degree, and that athlete nonsprinters may be generally unable to use at all.

Applicability of the Spring-Mass Model to High-Speed Running

The broad acceptance of the spring-mass model over the course of the last two decades has been heavily based on running and hopping data from relatively slow speeds (4, 18, 19, 26, 33). The more recent application of the model to faster running speeds (25, 27, 34) is understandable given positive results from slower speeds and the limited data available at faster ones (6). The data set we have compiled here includes hundreds of high-speed running footfalls from athletes spanning a broad range of sprinting abilities. The emergent finding from these data that the fastest speeds are achieved via consistent, specific deviation from the model's predictions warrants critical evaluation of the spring-mass model's assumed applicability to sprint running.

One means of assessing relative conformation to the spring-mass model is to examine the model-predicted force-motion dynamics vs. those actually observed. The model predicts that the peak force will occur at the temporal midpoint of the foot-ground contact period (i.e., at t = 50% of t_c), and that the center of mass will reach its lowest position at the same time. We found that our athlete nonsprinters conformed to these model-predicted behaviors somewhat (Fig. 6*F*), whereas our competitive sprint subjects conformed little or not at all. For the competitive sprinters at top speed, the group-averaged, ensemble waveform exhibited a force peak at t = 30% of t_c (Fig. 6*E*), and a corresponding height minimum of the center of

mass at $t = 40\%$ of t_c rather than the model-predicted values of $t = 50\%$ for both. Many of the individual sprinter's waveforms at faster speeds had force peaks that occurred at $t \leq 25\%$ of t_c (Figs. 2*A*, 4*A*, 5*E*), and some exhibited two force peaks, with the first occurring at $t \approx 20\%$ and the second at $t \approx 50\%$ of t_c (Fig. 5*C*). By even generous assessment, these results indicate that the spring-mass model is a poor descriptor of the stance-limb mechanics of high-caliber sprint athletes. These findings also raise basic questions about using the vertical and limb stiffness variables derived from the spring-mass model to describe the mechanics of running at higher speeds (25, 27, 34). The value of these stiffness variables as descriptors of sprint running mechanics is at best unclear if sprinting performance is optimized by not conforming to the assumptions required to calculate them.

The prior success of the spring-mass model as a descriptor of running mechanics raises an immediate question regarding our negative test outcomes for sprinters: why do these athletes not conform to the model when so many other runners and hoppers do? Our results suggest that the performance demands of sprinting are probably not compatible with the stance-limb mechanics predicted by the simple, linear spring in the spring-mass model. The model was formulated as a mechanical approximation for describing the apparently spring-like center of mass dynamics observed in the early, classic studies on gait mechanics (4, 11, 26). The presence of spring-like mechanics that the original investigators inferred at the level of the whole limb have subsequently been measured in selected muscles, tendons, and ligaments that contribute to the limb's overall behavior (21, 30). Indeed, during slower-speed running and hopping, the tissue-level stretch-shortening cycles (21, 31) that conserve mechanical energy could contribute as theorized to waveform patterns that generally conform to the predictions of the spring-mass model at these speeds (8). However, as considered in detail elsewhere (10), the success of sprinters does not depend upon either the conservation of mechanical energy or locomotor economy, but rather upon the ability to apply large mass-specific forces to the ground quickly.

An important caution is warranted in the interpretation of our finding that the mechanics of the fastest human runners generally do not conform to the predictions of the spring-mass model. Specifically, the deviations we report from the simple, linear-spring predicted behavior of the model should not be interpreted more broadly as an absence of either spring-like dynamics or energy storage. Indeed, the greater ground reaction forces observed in faster runners and at faster speeds may coincide with relatively greater tissue strains and energy storage (21, 31). Rather, our findings are best understood within the context of our test objectives and the limitations of the classic spring-mass model. Our objectives required a null standard of comparison for the purpose of quantifying different patterns of ground force application. We used the simple, linear-spring predictions of the spring-mass model for this purpose because these waveforms have served as the literature standard for well over a decade. However, our objectives could have been just as easily met by using some other pattern as a standard of comparison. Accordingly, we caution against interpreting the patterns reported using an energy storage framework.

Ground Force Application Strategies for Speed

Swifter runners are known to attain their faster top speeds primarily by applying greater mass-specific forces to the ground, but the mechanism by which they do so has not been previously identified. Here, two design strategies helped us to elucidate the force application strategy they use. First, we chose to analyze force application on a millisecond-by-millisecond basis rather than by averaging over the full stance period (per Fig. 3) as previously (36–38). Second, we recruited a pool of athletic subjects with a fairly broad range of individual top speeds. The latter strategy included enrolling four sprinters who were world-class track athletes (Table 1, *subjects 1*, *2*, *5*, and *6*) and a fifth who was a national-class athlete with Olympic and world championship experience (*subject 7*). The scores of sprint-running force waveforms acquired from this heterogeneous group of fast-running athletes provided force and speed data not previously available from this population. The consistent manner in which faster runners deviated from the pattern predicted by the simple spring-mass model to apply greater mass-specific forces provided crucial mechanistic insight.

Our finding that speed is maximized via a common force application strategy was certainly not a foregone conclusion at the outset of the study. From a purely theoretical perspective, the data acquired might have resulted in several outcomes other than the one we obtained. For example, faster athletes might have applied greater forces while utilizing a simple, linear-spring pattern. Alternatively, they might have employed an asymmetrical strategy that resulted in the greatest forces occurring later rather than earlier in the stance period. Finally, different athletes might have used different patterns to maximize force application and speed. Our finding that the degree of conformation to a particular pattern was consistently related to magnitude of the mass-specific force applied and top speeds attained provides two basic conclusions. First, our data indicate that the fastest human runners have converged on a common mechanical solution for maximizing ground force and speed. Second, the convergence on a common solution implies the existence of a single most effective mechanism by which human runners can maximize speed.

Indeed, the mechanical strategy identified was so consistent that even simple approaches to examining stance-phase patterns of force application were sufficient to reveal it. When the top speed forces of our 14 subjects were assessed by dividing the stance period into halves (Fig. 7*B*), this simple analysis revealed that individual differences in the total stance-averaged forces were all but completely determined during only one of the two periods. Specifically, we found a strong positive relationship between top speed and the average force applied during the first half of the stance period, and essentially no relationship to the average force applied during the second half. These respective results are illustrated in Fig. 7*B*, with the first-half, best-fit relationships being provided by sex to appropriately account for the leg and contact length differences (Equation 5, Table 2) that directly influence top speeds.

An immediate question raised by our findings is why essentially all of the differences in stance-averaged forces at top speed are attributable to a relatively small portion of the total stance period. We cannot fully answer this question on the basis of force application data alone. However, the

results illustrated in Fig. 7 and those from our Fourier analysis (see APPENDIX) are consistent with the impact-phase, limb-deceleration mechanism we have recently described (14). This mechanism appears to explain how several of the gait features classically associated with competitive sprinters (24) translate into the greater mass-specific ground forces they apply. First, the knee elevation sprinters achieve late in the swing phase appears to contribute to early stance ground force application by allowing greater limb velocities to be achieved prior to foot-ground impact (24). Second, the erect stance-phase posture sprinters adopt likely contributes to the stiffness required to decelerate the limb and body relatively quickly after the instant of foot-ground impact. The progressive, rising-edge deviation observed vs. the simple spring pattern, in relation to both top sprinting speeds (Figs. 5, 6, and 7) and across different speeds in individual sprinters (Figs. 2*A*, 5*A*, 5*C*, 5*E*, 6*A*, 6*C*, 6*E*, and 7) is consistent with the impact-phase, limb deceleration differences that may present across these trials (14).

Concluding Remarks: A Ground Force Signature for Speed

We conclude that a relatively specific, asymmetrical pattern of force application maximizes the ground forces runners can apply during the brief contact periods that sprinting requires. The factors responsible for the pattern are not yet fully known, but result in the fastest sprinters applying substantially greater forces than nonsprinters during the early portion of the stance period. Consistent pattern asymmetry among the swiftest sprinters, and less pronounced pattern asymmetry among less-swift athletes lead us to conclude that *1*) the fastest athletes have converged on a common mechanical solution for speed, and *2*) that less-swift athletes generally do not execute the pattern. On this basis, we suggest that the force-time pattern documented here for the most competitive sprinters in our sample (Fig. 7*A*; supplementary video) constitutes a ground force application signature for maximizing human running speeds.

APPENDIX

Vertical ground reaction force waveforms during running are composed of high-frequency components due to the acceleration of the lower limb during the impact phase, and low-frequency components due to the acceleration of the rest of the body during the entire contact phase (14). Fourier analysis can be used to analyze these components.

Any time-varying signal *s(t)* can be represented as a sum of sine waves [(39), Equation 2.3, p. 28] and can be expressed as:

Table A1. *Fourier terms of competitive sprinter at 11.1 m/s measured force data*

Harmonic	f_n, Hz	a_n, W_b	θ_n, Radians
0		2.1739	
1	9.8039	1.5513	−0.9871
2	19.6078	0.6461	−1.2683
3	29.4118	−0.3049	0.6676
4	39.2157	−0.0678	0.0262

f_n, Frequency of the harmonic; a_n, amplitude of the harmonic; θ_n, phase of the harmonic.

Table A2. *Fourier terms of competitive sprinter at 11.1 m/s modeled half-sine waveform*

Harmonic	f_n, Hz	a_n, W_b	θ_n, Radians
0		2.1739	–
1	9.8039	1.4664	−1.5721
2	19.6078	0.2968	−1.5733
3	29.4118	−0.1297	1.5672
4	39.2157	0.0740	−1.5755

Table A3. *Fourier terms of athlete nonsprinter at 9.4 m/s measured force data*

Harmonic	f_n Hz	a_n, W_b	θ_n, Radians
0		2.1199	
1	9.8039	1.5324	−1.3331
2	19.6078	0.4448	−1.4240
3	29.4118	−0.1038	0.8629
4	39.2157	−0.0382	0.4151

Table A4. *Fourier terms of athlete nonsprinter at 9.4 m/s modeled half-sine waveform*

Harmonic	f_n, Hz	a_n, W_b	θ_n, Radians
0		2.1199	
1	9.8039	1.4299	−1.5721
2	19.6078	0.2895	−1.5733
3	29.4118	−0.1265	1.5672
4	39.2157	0.0722	−1.5755

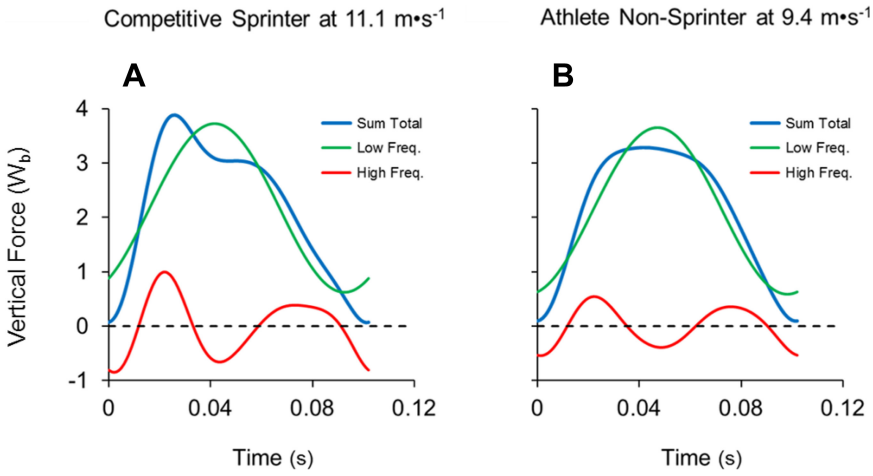

Fig. A1. These graphs are generated from the Fourier terms listed in Table A1 (competitive sprinter at 11.1 m/s) (*A*) and Table A3 (athlete nonsprinter at 9.4 m/s) (*B*). Low-frequency components (green line) include terms $n = 0$ and $n = 1$; high-frequency components (red line) include terms $n = 2$, $n = 3$, and $n = 4$. The summation of all components (blue line) accurately reproduces the original measured data.

$$s(t) = a_0 + \sum_{n=1}^{N} a_n \sin\left(2\pi f_n t + \theta_n\right) \qquad (Eq.\ 6)$$

where a_o is the mean of the signal, and f_n, a_n, and θ_n are the frequency, amplitude, and phase angle of the nth harmonic, respectively. The signal or waveform can be reproduced from these variables using N harmonics, with reproductive accuracy increasing as N increases.

To serve as an example of performing the Fourier analysis, the measured force data and modeled half-sine waveforms from Fig. 5, *E* and *F*, were analyzed using Equation 6. For both the competitive sprinter and the athlete nonsprinter, the trial average contact time was 0.102 s. The force data were measured on an instrumented force treadmill and filtered at 25 Hz. Four harmonics ($n = 4$) were sufficient to accurately reproduce the original measured data and the modeled half-sine waveforms.

Tables A1–A4 provide the terms for the variables described in Equation 6. The waveforms appearing in Fig. A1, *A* and *B*, were generated from the terms listed in Table A1 and Table A3, respectively. Low-frequency components (green line) include terms $n = 0$ and $n = 1$ and high-frequency components (red line) include terms $n = 2$, $n = 3$, and $n = 4$. The summation of all components (blue line) accurately reproduces the measured data.

The appearance of waveform differences above, but not below, the 10 Hz domain, is consistent with the time course of the impact-phase, force-enhancement mechanism proposed recently (14) and included here to explain the differences observed between the patterns of ground force of competitive sprinters vs. athlete, nonsprinters.

ACKNOWLEDGMENTS

We thank Dr. L. Ryan for assistance with data collection, instrumentation, technical support, manuscript critique, and substantial contributions to the scientific analysis; Dr. K. Roberts for contributions to the statistical analysis; Coach A. Behm and Dr. Robert Chapman for strategic guidance and support; and the 14 athletes who made the study possible by volunteering their time and effort.

GRANTS

Support for this study was provided in part by U.S. Army Medical and Materiel Command Award 17-02-2–0053 to P.G.W., and by funding from Southern Methodist University's Simmons School of Education and Human Development to K.P.C.

DISCLOSURES

No conflicts of interest, financial or otherwise, are declared by the author(s).

AUTHOR CONTRIBUTIONS

Author contributions: K.P.C. and P.G.W. conception and design of research; K.P.C. and P.G.W. performed experiments; K.P.C. and P.G.W. analyzed data; K.P.C. and P.G.W. interpreted results of experiments; K.P.C. and P.G.W. prepared figures; K.P.C. and P.G.W. drafted manuscript; K.P.C. and P.G.W. edited and revised manuscript; K.P.C. and P.G.W. approved final version of manuscript.

REFERENCES

1. **Alexander RM, Jayes AS.** Fourier analysis of the forces exerted in walking and running. *J Biomech* 13: 383–390, 1980.
2. **Alexander RM, Maloiy GM, Hunter B, Jayes AS, Nturibi J.** Mechanical stresses during fast locomotion of buffalo *(Syncerus caffer)* and elephant *(Loxodonta africana)*. *J Zool Lond* 189: 135–144, 1979.
3. **Bezodis IN, Kerwin DG, Salo AI.** Lower-limb mechanics during the support phase of maximum-velocity sprint running. *Med Sci Sports Exerc* 40: 707–715, 2008.
4. **Blickhan R.** The spring-mass model for running and hopping. *J Biomech* 22: 1217–1227, 1989.
5. **Bruggeman GP, Arampatzis A, Emrich F, Potthast W.** Biomechanics of double transtibial amputee sprinting using dedicated sprint prostheses. *Sports Technol* 1: 220–227, 2009.
6. **Brughelli M, Cronin J.** A review of the literature on the mechanical stiffness in running and jumping: methodology and implications. *Scand J Sport Med* 18: 417–426, 2008.
7. **Bullimore SR, Burn JF.** Consequences of forward translation of the point of force application for the mechanics of running. *J Theor Biol* 238: 211–219, 2006.
8. **Bullimore SR, Burn JF.** Ability of the planar spring-mass model to predict mechanical parameters in running humans. *J Theor Biol* 248: 686–695, 2007.
9. **Bundle MW, Hoyt RW, Weyand PG.** High speed running performance: a new approach to assessment and prediction. *J Appl Physiol* 95: 1955–1962, 2003.
10. **Bundle MW, Weyand PG.** Sprint exercise performance: does metabolic power matter? *Exerc Sport Sci Rev* 40: 174–182, 2012.
11. **Cavagna GA, Sabiene FP, Margaria R.** Mechanical work in running. *J Appl Physiol* 19: 249–256, 1964.
12. **Cavagna GA.** Force platforms as ergometers. *J Appl Physiol* 39: 174–179, 1975.
13. **Cavagna GA, Heglund NC, Taylor CR.** Two basic mechanisms for minimizing energy expenditure. *Am J Physiol Regul Integr Comp Physiol* 233: R243–R261, 1977.
14. **Clark KP, Ryan LJ, Weyand PG.** Foot speed, foot-strike and footwear: linking gait mechanics and running ground reaction forces. *J Exp Biol* 217: 2037–2040, 2014.
15. **Dalleau G, Belli A, Bourdin M, Lacour JR.** The spring-mass model and the energy cost of treadmill running. *Eur J Appl Physiol* 77: 257–263, 1998.
16. **Dickinson MH, Farley CT, Full RJ, Koehl MA, Kram R, Lehman S.** How animals move: an integrated view. *Science* 288: 100–106, 2000.
17. **Farley CT, Blickhan R, Saiot J, Taylor CR.** Hopping frequency in humans: a test of how springs set stride frequency in bouncing gaits. *J Appl Physiol* 71: 2127–2132, 1991.
18. **Farley CT, Gonzalez O.** Leg stiffness and stride frequency in human running. *J Biomech* 29: 181–186, 1996.
19. **Farley CT, Houdijk HH, Van Strien C, Louie M.** Mechanism of leg stiffness adjustment for hopping on surfaces of different stiffnesses. *J Appl Physiol* 85: 1044–1055, 1998.
20. **Frishberg BA.** An analysis of overground and treadmill sprinting. *Med Sci Sports Exerc* 15: 478–485, 1983.
21. **Ker RF, Bennett MB, Bibby SR, Kester RC, Alexander RM.** The spring in the arch of the human foot. *Nature* 325: 147–149, 1987.
22. **Kram R, Griffin TM, Donelan JM, Chang YH.** Force treadmill for measuring vertical and horizontal ground reaction forces. *J Appl Physiol* 85: 764–769, 1998.
23. **Kuitunen S, Komi PV, Kyröläinen H.** Knee and ankle joint stiffness in sprint running. *Med Sci Sports Exerc* 34: 166–173, 2002.
24. **Mann RV.** The mechanics of sprinting and hurdling. *CreateSpace* 2011.
25. **McGowan CP, Grabowski AM, McDermott WJ, Herr HM, Kram R.** Leg stiffness of sprinters using running-specific prostheses. *J R Soc Interface* 9: 1975–82, 2012.
26. **McMahon TA, Cheng GC.** The mechanics of running: how does stiffness couple with speed? *J Biomech* 23, *Suppl* 1: 65–78, 1990.
27. **Morin JB, Dalleau G, Kyröläinen H, Jeannin T, Belli A.** A simple method for measuring stiffness during running. *J Appl Biomech* 21: 167–180, 2005.
28. **Munro CF, Miller DI, Fuglevand AJ.** Ground reaction forces in running: a reexamination. *J Biomech* 20: 147–155, 1987.
29. **Riley PO, Dicharry J, Franz J, Della Croce U, Wilder RP, Kerrigan DC.** A kinematics and kinetic comparison of overground and treadmill running. *Med Sci Sports Exerc* 40: 1093–1100, 2008.
30. **Roberts TJ, Marsh RL, Weyand PG, Taylor CR.** Muscular force in running turkeys: the economy of minimizing work. *Science* 275: 1113–1115, 1997.
31. **Roberts TJ, Azizi E.** Flexible mechanisms: the diverse roles of biological springs in vertebrate movement. *J Exp Biol* 214: 353–361, 2011.
32. **Robilliard JJ, Wilson AM.** Prediction of kinetics and kinematics of running animals using an analytical approximation to the planar spring-mass system. *J Exp Biol* 208: 4377–4389, 2005.
33. **Srinivasan M, Holmes P.** How well can spring-mass-like telescoping leg models fit multi-pedal sagittal-plane locomotion data? *J Theor Biol* 255: 1–7, 2008.

34. **Taylor MJ, Beneke R.** Spring-mass characteristics of the fastest men on earth. *Int J Sports Med* 33: 667–670, 2012.
35. **Usherwood JR, Hubel TY.** Energetically optimal running requires torques about the centre of mass. *J R Soc Interface* 9: 2011–5, 2012.
36. **Weyand PG, Sternlight DB, Bellizzi MJ, Wright S.** Faster top running speeds are achieved with greater ground forces not more rapid leg movements. *J Appl Physiol* 81: 1991–1999, 2000.
37. **Weyand PG, Bundle MW, McGowan CP, Grabowski A, Brown MB, Kram R, Herr H.** The fastest runner on artificial limbs: different limbs, similar function? *J Appl Physiol* 107: 903–911, 2009.
38. **Weyand PG, Sandell RF, Prime DN, Bundle MW.** The biological limits to running speed are imposed from the ground up. *J Appl Physiol* 108: 950–961, 2010.
39. **Winter DA.** Biomechanics and motor control of human movement (2nd ed.). New York, NY: John Wiley and Sons, 1990.

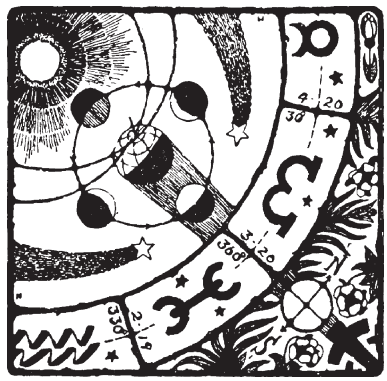

Running impact forces: from half a leg to holistic understanding – comment on Nigg et al.

Kenneth P. Clark[1], Andrew B. Udofa[2], Laurence J. Ryan[2] & Peter G. Weyand[2,*]

1 Department of Kinesiology, West Chester University, West Chester PA, USA

2 Locomotor Performance Laboratory, Department of Applied Physiology and Wellness, Southern Methodist University, Dallas, Texas, USA

* Corresponding author: Department of Applied Physiology and Wellness, Southern Methodist University, Dallas, Texas 75206, USA
Email: pweyand@smu.edu

COMMENTARY

Article History:
Submitted 7th February 2018
Accepted 1st March 2018
Published 18th April 2018

Handling Editor:
Markus Tilp
Karl-Franzens-University Graz, Austria

Editor-in-Chief:
Martin Kopp
University of Innsbruck, Austria

ABSTRACT

Running impact forces have immediate relevance for the muscle tuning paradigm proposed here and broader relevance for overuse injuries, shoe design and running performance. Here, we consider their mechanical basis. Several studies demonstrate that the vertical ground reaction force-time (vGRFT) impulse, from touchdown to toe-off, corresponds to the instantaneous accelerations of the body's entire mass (Mb) divided into two or more portions. The simplest, a two-mass partitioning of the body (lower-limb, M_1=0.08•M_b; remaining mass, M_2=0.92•M_b) can account for the full vGRFT waveform under virtually all constant-speed, level-running conditions. Model validation data indicate that: 1) the non-contacting mass, M_2, often accounts for one-third or more of the early "impact" portion of the vGRFT, and 2) extracting a valid impact impulse from measured force waveforms requires only lower-limb motion data and the fixed body mass fraction of 0.08 for M_1.

Keywords:
Two-mass model – effective mass – ground reaction forces – running performance – spring-mass model

Citation:
Clark , K. P. , Udofa A. B. , Ryan, L. J. & Weyand , P. G. (2018): Running impact forces: from half a leg to holistic understanding – comment on Nigg et al. *Current Issues in Sport Science, 3:107*. doi: 10.15203/CISS_2018.107
This is a commentary on a CISS report article authored by Nigg, B. M., Mohr, M. & Nigg, S. R. (2017). Muscle tuning and preferred movement path – a paradigm shift. *Current Issues in Sport Science, 2:007*. doi: 10.15203/CISS_2017.007

Impact Forces Revisited

Dr. Nigg and colleagues deserve commendation for efforts that have endowed the area of running biomechanics with a sizeable body of empirical observations. These observations have, and undoubtedly will, continue to inform work on a broad range of topics that include running injuries, running shoes and the relationship between the two. Their willingness to confront the experimental challenges involved in studying a largely unpredictable phenomenon like running injuries deserves particular praise.

Here, we focus on the impact force conclusions offered by Nigg, Mohr and Nigg (2017) in their target article. While their contribution purports a lack of importance in overuse injury etiology, there are compelling scientific reasons to consider their basis and importance from an independent, contemporary perspective. These are: 1) the existence of credible evidence supporting a running impact force-overuse injury link (Daoud, Geissler, Wang, Saretsky, Daoud, & Liebermann, 2012; Milner, Ferber, Pollard, Hamill, & Davis, 2006), 2) the direct effect of impact forces on bodily motion and performance (Clark & Weyand, 2014), and 3) the need for valid quantification to advance general understanding and inform specific applications. One noteworthy application is the input signal required by the muscle-tuning paradigm Nigg *et al.* advance in their target article here. More broadly, the inability to quantify running impact forces recently noted by Nigg and colleagues elsewhere (Baltich, Maurer & Nigg, 2015) is obviously a direct impediment to reaching firm conclusions regarding their importance.

From our perspective, the development of a quantitative understanding has been at least partially impeded by two assumptions that have framed the study of running impact forces for decades. These are: 1) assuming that the early portion of the vertical ground reaction force-time waveform can be attributed to a small fraction (i.e. an "effective mass") of the body's total mass (M_b) while ignoring the rest (Chi & Schmitt, 2005; Denoth, 1986; Derrick, 2004; Lieberman, Venkadesan, Werbel, Daoud, D'Andrea, Davis, Mang'eni & Pitsilades, 2010 ; Nigg, 2010; Nigg, Mohr, Nigg, 2017), and 2) assuming that the impact impulse can be quantified using the localized force peak often visible on the rising edge of the measured waveform (Figure 1). Three studies indicate that these assumptions obscure the mechanics of the impact event.

The first study was provided by Bobbert, Schamhardt and Nigg (1991) more than 25 years ago. These investigators demonstrated that the instantaneous accelerations of seven body mass components (comprising 100% of M_b: right and left foot, shank, and upper leg components plus a combined head-arms-torso mass) acquired from motion data, can be summed to provide a close match to the measured total vertical ground reaction force-time (vGRFT) waveform during slow and moderate speed running (i.e. $F_{z1}+F_{z2}+F_{z3}+F_{z4}+F_{z5}+F_{z6}+F_{z7}=F_{z\text{-total}}$; where z designates the vertical component of the ground reaction force). This noteworthy experimental accomplishment was based on Newton's 2nd Law including the first-principle recognition that the measured vGRFT waveform must somehow correspond to the instantaneous accelerations of 100% of the body's mass.

The second insightful study was the detailed temporal and spatial analysis of the rising edge of the vGRFT undertaken by Shorten and Mientjes (2011). From pressure mapping data on the sole of the foot and frequency analyses of measured waveforms, these investigators also concluded that the body's entire mass contributed to the rising edge of the waveform. Per their title, they concluded that the localized, rising-edge waveform force peak widely attributed to heel impact, is in fact, "neither heel, nor impact" during heel-toe running.

The most recent of the three studies involved an experimental effort from our laboratory (Clark, Ryan & Weyand, 2017) that, like Bobbert *et al.* adopted a Newtonian approach. We did so with the goal of identifying the simplest partitioning of the body that might account for the vGRFT waveform in full. Our efforts led to the two body-mass component, two-impulse waveform explanation illustrated in Figure 1. Ultimately, this approach was able to predict 500 measured vGRFT waveforms acquired at speeds from 3.0 to 11.0 m/s regardless of the runner's foot-strike mechanics. Due to the model's conciseness, only three inputs are required to generate the waveforms from a runner's gait mechanics: contact time, aerial time, and the vertical acceleration of the lower limb. The close agreement between model-generated and measured vGRFT waveforms (R^2=0.95) supports the general validity of the two-mass, two-impulse explanation for their mechanical basis.

The Rising Edge of the vGRFT Waveform: Impact Is Not Enough

Clearly, additional experimental work remains to test and refine the existing Newtonian explanations for running vGRFT waveforms. However, the two studies that have successfully linked bodily motion to running ground reaction forces share the foundational recognition that the waveform represents the summed acceleration of 100% of body mass.

The holistic Newtonian view that emerges for the rising-edge of the total vGRFT waveform, broadly conceived elsewhere as an "impact-only" event, is illustrated in Figure 1. The data appearing in the figure have been adapted from original vGRFT data acquired at a speed of 5.0 meters per second from a runner with heel-strike mechanics. As illustrated, the body's full mass contributes to the rising edge of the waveform. Accurately predicting the magnitude and timing of the localized peak, for example, requires summing the impulse contributions of the model's body mass components. Per the illustration, correct prediction of the overall impact mechanics using the two masses in our model relies heavily on the kinematic data used to determine Δt_1 from the period elapsing between the instant of initial foot-ground contact and subsequent time at which mass M_1 slows to a vertical velocity of zero. Correct identification of the localized rising-edge peaks for heel-strikers at all speeds and competitive sprinters at faster ones as previously reported would have been virtually impossible (Clark, Ryan & Weyand, 2017, Figures 5, 6 and 7) without both: 1) accurate

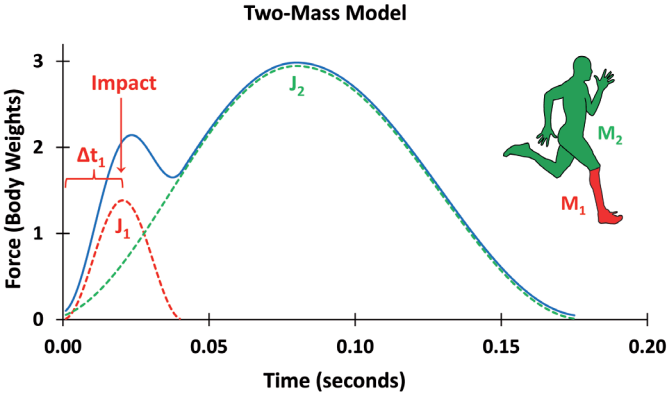

Figure 1: Running vertical ground reaction forces can be quantified as the sum of two impulses: a relatively brief impact impulse (J_1) that corresponds to the deceleration of the foot and shank (M_1=0.08•M_b), and a larger, longer-duration impulse (J_2) that corresponds to the acceleration of the remainder of the body's mass (M_2=0.92•M_b) throughout the stance period. Both impulses begin at the instant of touchdown and contribute substantially to the rising-edge of the force-time waveform. Note that impact impulse, J_1, is quantified from 8% of M_b and the time Δt_1 at which the ankle reaches its minimum vertical position.

kinematic data, and 2) a model capable of predicting the significant variability in the timing and magnitude of rising-edge force peaks across scores of different footfalls.

Figure 1 also reveals the specific manner in which the assumptions required by the effective mass techniques obscure the mechanical basis of the rising edge of the waveform. In the footfall illustrated, the effective mass approach assumes that mass M_2 would make little or no contribution to the rising-edge impulse up to the localized force peak. However, as illustrated, M_2 is actually responsible for roughly one-third of the total impulse over this early period of this illustrated waveform. During slow and moderate speed fore-foot strikes, the impulse contributions of mass M_2 actually exceed those of M_1, primarily because the impact period Δt_1 is relatively longer (Clark, Ryan & Weyand, 2017, Figures 5 and 6, Table 2). Also evident in the figure is that the localized peak on the total vGRFT waveform is not simultaneous with the peak of impact impulse J_1 as implicitly assumed by effective mass quantification techniques. Rather, the time-dependent contributions of impulse J_2 cause the total waveform peak to occur at a later point in time than the J_1 impulse peak. In the case of most forefoot strike waveforms, the longer Δt_1 period results in the rising edge of the measured waveform lacking a localized force peak altogether (Clark, Ryan & Weyand, 2014; Clark, Ryan & Weyand, 2017, Figure 6, Table 2).

Impact Forces and New Paradigms: Retro- and Prospective Considerations

Intuitive appeal and computational simplicity may be responsible for the common conceptualization and quantification of the rising edge of human running vGRFT waveforms as an impact-only phenomenon. However, the works synthesized here: 1) provide a valid mechanical basis for the vGRFTs waveforms based on the body's entire mass, and 2) offer quantitative methods that apply over essentially all level-speed and foot-strike conditions. A two-mass partitioning of the human body allows the full running vGRFT waveform to be predicted from gait motion. The two-mass approach also allows the impact portion of the impulse to be extracted from measured vGRFT waveforms. Doing so requires only motion data from the ankle and the fixed lower-limb mass fraction identified for M_1.

Finally, we applaud Nigg, Mohr and Nigg for proposing muscle tuning and movement path paradigms in an effort to advance basic and applied understanding of running mechanics. We share their view that evaluating these paradigms will be a major and lengthy experimental undertaking. One useful tool for these efforts, directly in the case of muscle tuning and indirectly for preferred movement paths, is the holistic quantitative understanding of impact forces that is currently available.

Funding

This work was supported in part by a US Army Medical and Materiel Command award [W81XWH-12-2-0013] to PGW.

Competing Interests

The authors declare competing financial interests. Peter Weyand, Laurence Ryan and Kenneth Clark are the inventors of US Patent #8363891 which is owned by SMU and contains scientific content related to that presented in the manuscript. The patent is licensed to SoleForce LLC in which the three aforementioned individuals are equity partners.

Data Availability Statement

All relevant data are within the paper.

References

Baltich J., Maurer C., Nigg B.M. (2015). Increased vertical impact forces and altered running mechanics with softer midsole shoes. *PLoS One,* doi:10.1371/journal.pone.012519610.15203/CISS_2016.101

Bobbert, M.F., Schamhardt, H.C., and Nigg, B.M. (1991). Calculation of vertical ground reaction force estimates during running from positional data. *Journal of Biomechanics.* 24, 1095-1105.

Chi, K.J., and Schmitt, D. (2005). Mechanical energy and effective foot mass during impact loading of walking and running. *Journal of Biomechanics.* 38, 1387-1395.

Clark, K.P., Weyand, P.G. (2014). Are running speeds maximized with simple-spring stance mechanics? *Journal of Applied Physiology.* 117, 604-615.

Clark, K.P., Ryan, L.J., Weyand, P.G. (2014). Foot speed, foot-strike and footwear: linking gait mechanics and running ground reaction forces. *Journal of Experimental Biology.* 217, 2037-2040.

Clark, K.P., Ryan, L.J., Weyand, P.G. (2017). A general relationship links gait mechanics and running ground reaction forces. *Journal of Experimental Biology.* 220(2), 247-258.

Daoud A.I., Geissler G.J., Wang F., Saretsky J., Daoud Y.A., Lieberman D.E. (2012) Foot Strike and Injury Rates in Endurance Runners: a retrospective study. *Medicine and Science in Sports and Exercise.* 44(7), 1325-1334.

Denoth, J. (1986). Load on the locomotor system and modeling. In Biomechanics of Running Shoes (ed. B. M. Nigg), pp. 63-116. Illinois: Human Kinetics Publishers, Inc.

Derrick, T. R. (2004). The effects of knee contact angle on impact forces and accelerations. *Medicine and Science in Sports and Exercise.* 36, 832-837.

Lieberman, D.E., Venkadesan, M., Werbel, W.A., Daoud, A.I., D'Andrea, S., Davis, I.S., Mang'eni, R.O., and Pitsiladis, Y. (2010). Foot strike patterns and collision forces in habitually barefoot versus shod runners. *Nature* 463, 531-535.

Milner C.E., Ferber R., Pollard C.D., Hamill J., Davis I.S. (2006). Biomechanical factors associated with tibial stress fractures in female runners. *Medicine and Science in Sports and Exercise,* pp. 38(2), 323-328.

Nigg, B.M. (2010). Biomechanics of Sport Shoes. Calgary, AB: Topline Printing, Calgary. p. 1-41.

Nigg B.M., Mohr M.M., Nigg S. (2017) Muscle tuning and preferred movement path: a paradigm shift. *Current Issues in Sport Science*. DOI 10.15203/CISS_2017.007

Shorten, M., and Mientjes, M.I.V. (2011). The "heel impact" force peak during running is neither "heel" nor "impact" and does not quantify shoe cushioning effects, *Footwear Science*. 3, 41-58.

Scand J Med Sci Sports 2015: 25: 581–582
doi: 10.1111/sms.12520

SCANDINAVIAN JOURNAL OF
MEDICINE & SCIENCE
IN SPORTS

Editorial

Sprint running research speeds up: A first look at the mechanics of elite acceleration

The relationship between force and acceleration has been regarded as seminal since first identified by Isaac Newton. However, more than three centuries after Newton's formulation of the force, mass, acceleration relationship ($F = m{\cdot}a$), we have a limited understanding of the gait mechanics that determine how quickly we can accelerate ourselves. This topic has general relevance for scientific and engineering efforts in legged locomotion, and direct application in athletics. Yet, in contrast to other topics in the rich history of locomotion research (Hill, 1950; Muybridge, 1957; Gray, 1959), maximal, straight-line acceleration has received relatively little attention. Prior work has generally not met either of two basic challenges: first, acquiring ground reaction force data from multiple, sequential steps, and second, enrolling the athletic subjects who excel at this type of performance. In their recent contribution to the *Scandinavian Journal of Medicine and Science in Sports*, Rabita et al. (2015) have met both challenges simultaneously. By contributing the first ground force data on elite sprinters during acceleration, their study complements and extends the understanding of running mechanics established largely under constant-velocity conditions.

Constant-velocity running

One of the fundamentals of running at near-constant velocities on level ground is that runners maintain their horizontal momentum within and across steps. For this reason, the classic work of Cavagna et al. (1964) likened running under constant-velocity conditions to a rubber ball bouncing along the ground. After the initial push or throw, the ball maintains its forward velocity while bouncing through successive ground contact and aerial periods without the application of additional propulsive force. Hence, the primary requirement for runners, once they are up to speed, is to apply sufficient downward forces to counteract gravity and lift the body (back up) into the air for the ensuing step. These mechanics are directly reflected in the respective magnitudes of the vertical and horizontal forces measured under these conditions. At intermediate and faster speeds, the average forces with a vertical orientation (F_z) to the running surface typically exceed those with a horizontal orientation (F_y, i.e., in the fore-aft direction) by a factor of five or more (Kuitunen et al., 2002; Weyand et al., 2009). This magnitude difference exists for two basic reasons. First, like the bouncing ball, runners have very limited propulsive force requirements once they are up to speed. The propulsive forces ($+F_y$) applied during the second half of the stance phase are sufficient to offset the very small velocity reductions that result from the braking forces ($-F_y$) applied during the first half. Second, the gravitational forces acting on the runner's mass are large. Thus, during sprint running, the stance-averaged forces applied in the vertical direction typically exceed twice the body's weight while those applied horizontally (i.e., propulsive and braking phase averages, respectively) are roughly one third. Furthermore, as might be intuited from Newton – the primary attribute of human sprinters is their ability to apply large mass-specific forces (F/m) during the brief contact periods that sprinting requires (Weyand et al., 2000; Clark & Weyand, 2014).

Positive-acceleration running

The speeds runners ultimately attain, and how quickly they do so, depend directly on the fore-aft forces in the acceleration phase of a sprint run. In accordance with the classic Newtonian relationship, the greater the propulsive force in relation to the body's mass, the greater the instantaneous acceleration ($F_y/m = a_y$; Cavagna et al., 1971). However, this requirement exists in addition to the primary requirement present during constant-velocity running of applying sufficiently large, time-averaged vertical forces to support the body's weight against gravity. Previously, the gait mechanics "solution" adopted by the swiftest runners to satisfy these simultaneous requirements has been largely unknown. In their new work, Rabita et al. (2015) were able to obtain ground reaction force data from the sequential steps of both elite and sub-elite sprinters as they ran across 6 m of contiguous, in-ground force platforms. The athletes performed a number of all-out, 40-m trials from starting blocks that were variably positioned on or behind the platforms to capture force data from different steps of the various trials.

The new data nicely demonstrate that the most critical between-athlete differences occur during the initial backward push from the starting position. The initial pushes from the athletes in both the elite and the sub-elite groups were sufficient to achieve more than one third of their respective maximum velocities before touching the ground for their first step after the blocks. However, the elite sprinters applied backward forces that were nearly 20% greater in relation to body mass than their sub-elite counterparts (9.59 N/kg vs 7.74 N/kg, respectively). Doing so enabled the elites to leave the starting blocks with a mean velocity 0.44 m/s greater than that of the sub-elites (3.61 m/s vs 3.17 m/s, respectively), thereby accounting for nearly 80% of the between-group velocity differences for the entire sprint (mean 40-m velocities: 8.16 m/s vs 7.59 m/s, respectively). Propulsive force differences between the two groups were present in the subsequent steps, but to an appreciably smaller degree.

While this new work furthers the understanding of sprinters as athletes adapted for mass-specific ground force application, intriguing issues remain. One of the more salient, and potentially difficult, is identifying the optimal mechanical strategies for rapid accelerations (Mann, 2011). In contrast to the performance requirements of near-constant velocity sprinting (Weyand et al., 2000; Clark & Weyand, 2014), acceleration requirements vary with each and every step. Accordingly, variable incoming velocities and other factors likely dictate step-specific strategies for optimizing ground force application. Consequently, integrated approaches that simultaneously consider balance, body position, and the total ground force applied (Roberts & Scales, 2002; Kugler & Janshen, 2010) have been most enlightening to date. These studies imply that the optimal performance solutions involve limb and body positions that are determined in direct accordance with the magnitude of each push on the ground. In contrast, approaches that emphasize the forces applied in a single axis, or consider horizontal and vertical forces as competing entities, seem unpromising. The limb, after all, simply pushes in accordance with the muscle extensor forces generated across the ankle, knee, and hip joints – and does so without any intrinsic regard to direction.

Future efforts will undoubtedly reveal more regarding the respective roles that motor control, limb motion, and mass-specific strength each play in maximizing acceleration performance. However, at present, Rabita et al. (2015) should be applauded for giving the study of locomotor performance an important figurative push in a new scientific direction.

K. P. Clark, P. G. Weyand
Locomotor Performance Laboratory, Department of Applied Physiology and Wellness, Southern Methodist University, Dallas, TX 75206, USA

References

Cavagna GA, Kofanek L, Mazzoleni S. Mechanics of sprint running. J Physiol 1971: 217 (3): 709–721.

Cavagna GA, Saibene FP, Margaria R. Mechanical work in running. J Appl Physiol 1964: 19 (2): 249–256.

Clark KP, Weyand PG. Are running speeds maximized with simple-spring stance mechanics? J Appl Physiol 2014: 117 (6): 604–615.

Gray J. How animals move. Edinburgh: Pelican Books, 1959.

Hill AV. The dimensions of animals and their muscular dynamics. Sci Prog 1950: 38: 209–230.

Kugler F, Janshen L. Body position determines propulsive forces in accelerated running. J Biomech 2010: 43 (2): 343–348.

Kuitunen S, Komi PV, Kyrolainen H. Knee and ankle joint stiffness in sprint running. Med Sci Sports Exerc 2002: 34 (1): 166–173.

Mann R. The mechanics of sprinting and hurdling. CreateSpace. 2011.

Muybridge E. Animals in motion. Courier Corporation. 1957.

Rabita G, Dorel S, Slawinski J, Sàez-de-Villarreal E, Couturier A, Samozino P, Morin JB. Sprint mechanics in world-class athletes: a new insight into the limits of human locomotion. Scand J Med Sci Sports 2015: 25 (5): 583–594.

Roberts TJ, Scales JA. Mechanical power output during running accelerations in wild turkeys. J Exp Biol 2002: 205 (10): 1485–1494.

Weyand PG, Bundle MW, McGowan CP, Grabowski A, Brown MB, Kram R, Herr H. The fastest runner on artificial legs: different limbs, similar function? J Appl Physiol 2009: 107 (3): 903–911.

Weyand PG, Sternlight DB, Bellizzi MJ, Wright S. Faster top running speeds are achieved with greater ground forces not more rapid leg movements. J Appl Physiol 2000: 89 (5): 1991–1999.

Impact Forces During Running: Loaded Questions, Sensible Outcomes*

Andrew B. Udofa, Laurence J. Ryan, and Peter G. Weyand

Abstract*— Load carriage was used as an experimental tool to evaluate the ability of an anatomically-based, two-mass model of the human body to predict vertical impact and peak forces during running from only four inputs: body weight (W_b), contact time (t_c), aerial time, (t_a), and lower-limb acceleration (a_1). Simultaneous motion and force data were acquired from seven subjects during steady-speed trials (3.0-6.0 m•s^{-1}) on a custom, force-instrumented treadmill under three loading conditions: unloaded (1.0 W_b), 15% added weight (1.15 W_b) and 30% added weight (1.30 W_b). Model-predicted impact and peak forces corresponded with measured values, on average, to within 14.9±1.3% and 13.8±0.6%, respectively (R^2 best-fits=0.82 and 0.88, n=71). Ankle jerk and velocity data derived from optical position-time data suggest wearable sensor acquisition of the model-needed inputs is fully feasible. We conclude that the two-mass model offers a promising approach to quantifying running ground reaction forces using wearable technologies.

Keywords – two-mass model, locomotion, gait, wearable sensors, spring-mass model

I. Introduction

Legged locomotion involves sequential periods of foot-ground force application that repetitively load the limbs. The forces the limbs experience during each loading cycle are substantial. Peak values typically exceed the body's weight during walking and can reach three to five times the body's weight during running. The magnitude of the reaction forces the limbs experience with each step on the ground are of fundamental importance. They determine an individual's functional movement capabilities [1] and directly influence the health of the limb's musculoskeletal tissues. A minimum number of loading cycles is necessary for bone and overall musculoskeletal tissue health while too many loading cycles can lead to overuse injuries. The latter are common among both foot soldiers and weight-bearing endurance athletes due to the thousands of daily loading cycles they often experience. The etiology of overuse injuries appears to be related to both the impact and peak forces the limbs experience during each loading cycle.

The ground reaction forces present during steady-speed running are predominantly vertical in orientation. Vertical force peaks typically exceed horizontal peak values by a factor of five or more and lateral values by a substantially greater margin. Accordingly, there have been many attempts to identify the mechanical determinants of the vertical force-time waveforms present during running. Dedicated mechanical models span a range of complexities from very simple [2] to considerably complex [3,4,5,6]. To date, these models have not provided a full explanation for the waveforms. Consequently, motion-based approaches capable of sensing and predicting the instantaneous force-time values needed to quantify impact forces, peak forces and the associated loading rates are not available.

General developments in wireless interfacing and micro-technology have enabled the production of small devices to monitor health and fitness-related variables using a variety of approaches. Current methods for approximating ground reaction forces range from shoes affixed with pressure insoles [7], shoes instrumented with two 6-axial force and moment sensors [8,9], or five 3-axial sensors [10] all placed on the underside of the shoe. However, these devices can interfere with normal gait mechanics, are typically costly and are often restricted to lab environments. Additionally, pressure inputs from sampling sites on the sole have a complex and variable relationship to impact forces, peak forces and loading rates.

The recently introduced two-mass model [11] is sufficiently concise to provide sensible options for quantifying vertical ground reaction force-time waveforms. The conciseness of the model reduces the input variables required for a wearable sensor to only three in addition to body weight: contact time, aerial time, and vertical acceleration of the ankle of the contact limb. In theory, acquisition of these variables would provide accurate predictions of the entire force-time waveform, and thereby provide the data needed to assess impact forces, peak forces and loading rates. The basic tenants of this model have shown promise in limited theoretical testing thus far. A critical aspect of the model is the division of the body's mass (m_B) into two invariant components (Figure 1A) that are used to decompose the waveform into two impulses (Figure 1B). The first impulse results from the acceleration of the lower limb segment, including the shank and foot ($m_1 = 0.08m_B$). The second impulse results from the accelerations of the remaining 92% of the subject's body mass ($m_2 = 0.92m_B$).

Here, our primary objective was to test the ability of the model to predict impact and peak forces across a range of speeds under three gravitational force conditions: body weight, 1.15 times body weight and 1.30 times body weight. We used torso loading as an experimental tool to alter our model's mass component m_2 while holding mass component m_1 constant.

*This work was made possible by award W81XWH-12-2-0013 from the Medical and Material command of the United States DOD.

P. G. Weyand is with Southern Methodist University, Dallas, TX 75206 USA (e-mail: pweyand@smu.edu).

L.J. Ryan is with Southern Methodist University, Dallas, TX 75206 USA (e-mail: lryan@smu.edu).

A.B. Udofa is with Southern Methodist University, Dallas, TX 75206 USA (e-mail: audofa@smu.edu).

Our *a priori* expectation was that the force-time waveforms acquired across loading conditions and speeds would vary substantially and thereby provide a robust test of how well the motion-based inputs of the two-mass model can predict impact and peak forces of variable magnitudes. Our secondary objective was to examine the motion of the lower-limb segment to evaluate the promise of model implementations involving wearable motion sensors like accelerometers.

II. Methods

A. Subjects

Seven healthy, physically active adults, between 24 and 34 years of age, volunteered and participated in the study: two women (74.3 ± 13.2 kg) and five men (87.8 ± 7.1 kg). All provided written, informed consent in accordance with the requirements of the Southern Methodist University Institutional Review Board.

B. Testing Protocol

Subjects underwent progressive, discontinuous treadmill tests across the same range of speeds under three experimental conditions: unloaded (1.0 W_b), 1.15 times body weight (1.15 W_b), and 1.30 times body weight (1.30 W_b). Per the methods described in Clark and Weyand [12], all trials took place at constant speeds. Here, trials were administered in the same progressive sequence of: 3, 4, 5 and 6 m/s under each loading condition.

Loads were added symmetrically to the torso using military style vests and backpacks. All subjects completed the experimental conditions in the following order: 1.0 W_b, 1.15 W_b, and then 1.30 W_b to allow for progressive habituation to the loaded conditions and minimize the likelihood of musculoskeletal injury. A minimum of two weeks elapsed between testing sessions to ensure full recovery and minimize the likelihood of injury.

C. Data Acquisition

An instrumented force treadmill and motion capture system were used to acquire simultaneous motion and force data. Ground reaction force data were acquired at 1000 Hz with a custom three-axis high-speed force treadmill (AMTI, Watertown, MA). The AMTI-force treadmill is capable of reaching speeds over 20 m/s with negligible belt speed fluctuations with subjects in excess of 140 kg. The embedded force plate (198 cm x 68 cm) interfaces with an AMTI DigiAmp amplifier running NetForce software and has a measurement range of 6000 N. The force data were filtered using a low-pass, fourth order, zero-phase-shift Butterworth filter with a cutoff frequency of 25 Hz [13].

Motion data were obtained from an OptiTrack motion capture system (NaturalPoint, Corvallis, OR) configured with 12 Prime 17W cameras. OptiTrack Motive:Body software was used for camera control, calibration, marker tracking, and positional data export. All data were acquired at 200 frames per second and synchronously triggered to the ground reaction force data through an OptiTrack eSync module. The capture volume was 2.9 m x 1.5 m x 2.2 m and the mean 3D error was less than 1 mm as reported by the Motive:Body calibration algorithm. A 12 marker system was used with placements on the ball of the foot, heel, ankle, knee, hip, and shoulder on each side of the body [13]. The exported marker coordinate data were upsampled to 1000 frames per second and low-pass filtered at 25 Hz using the same filter as the force data. The marker positional data allow for accurate velocity and acceleration calculations for the numerous body segments.

D. Two-Mass Model and Model-Predicted Forces

Force and impulse predictions were determined using the two-mass model [11] where the total vertical force waveform is modeled as the sum of two impulses: a first resulting from the deceleration of the lower limb upon impact and the second corresponding to the accelerations of the remainder of the body's mass during ground contact (Figure 1).

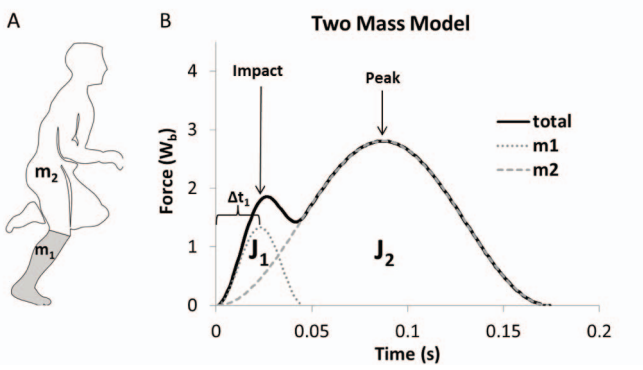

Fig. 1. A. An illustration of the mass components (m_1 and m_2) of our two-mass model of the human body. B. A model-predicted force-time waveform generated from the summation of the impulses, J_1 and J_2, which correspond to the accelerations of mass components m_1 and m_2.

The total impulse J_T during contact is:

$$J_T = J_1 + J_2 \quad (1)$$

where impulse J_1 results from the acceleration of the mass of the lower limb (m_1 = *8.0%* of body mass m_B) during impact, and J_2 corresponds to the acceleration of the remainder of the total mass. The total stance-averaged vertical force is:

$$F_{Tavg} = m_T g \frac{t_c + t_a}{t_c} \quad (2)$$

where t_c and t_a are the contact and aerial times determined from the vertical force signal, m_T is total mass, and g is gravitational acceleration (g = +9.8 m•s^{-2}). The total impulse is:

$$J_T = F_{Tavg}\, t_c \quad (3)$$

The acceleration a_1 due to the impact of the lower limb mass m_1 is determined from the vertical velocity Δv_1 of the ankle marker slowing to zero over the time interval Δt_1:

$$a_1 = \frac{\Delta v_1}{\Delta t_1} \quad (4)$$

The average force F_{1avg} of m_1 during impact is:

$$F_{1avg} = m_1 (a_1 + g) \quad (5)$$

The impulse J_1 of m_1 during the total impact interval $2\Delta t_1$ is:

$$J_1 = F_{1avg} (2\,\Delta t_1) \quad (6)$$

Impulse J_2 is determined from impulse J_1 and total impulse J_T as:

$$J_2 = J_T - J_1 \quad (7)$$

The average force F_{2avg} of m_2 during the contact interval t_c is then:

$$F_{2avg} = \frac{J_2}{t_c} \quad (8)$$

Each impulse (J_1 and J_2) is due to a non-linear elastic collision and has a bell-shaped force vs. time curve. The total force $F_T(t)$ is a summation of the two bell-shaped force curves [11, equation 6]:

$$F_T(t) = F_{1avg}\left[1+\cos\left(\frac{t-\Delta t_1}{\Delta t_1}\pi\right)\right] + F_{2avg}\left[1+\cos\left(\frac{t-(\frac{t_c}{2})}{(\frac{t_c}{2})}\pi\right)\right] \quad (9)$$

E. Data Analysis

Predicted vs. measured impact and peak forces were assessed by quantifying the absolute percentage error between the two values:

$$\%\,Error = \left|\frac{Measured - Predicted}{Measured}\right| \bullet 100 \quad (10)$$

Predicted and measured impact force values were determined at the instant, or millisecond $t = \Delta t_1$ and were therefore simultaneous. Per the model (eq. 4), the time of the impact impulse peak was identified from the instant at which the measured vertical velocity of the lower-limb, or v_1, equaled zero. Predicted and measured peak force values were determined from the maximum values of the waveforms and therefore were generally not simultaneous.

Trials were analyzed at speeds of 3, 4, 5, and 6 m/s which were completed by all subjects under the three loaded conditions. Thirteen of the eighty-four total trials completed were not included in the analysis. Six were excluded due to trial-specific acquisition uncertainties; seven were excluded due to marker occlusions. Therefore, seventy-one trials were analyzed with at least eight footfalls per trial, and 860 footfalls were evaluated in total. Measured impact and peak force values were determined from ensemble-averaged waveforms across footfalls. Corresponding lower-limb acceleration values, Δt_1 and Δv_1, were averaged from the same individual footfalls for each trial and were used to generate model-predicted waveforms. Relationships of best-fit between predicted and measured values were determined using the R^2 goodness of fit statistic with an accompanying standard error of estimate (SEE).

We had two *a priori* expectations with respect to the performance of the two-mass model across load conditions. First, the magnitude of impulse J_1 was not expected to vary with load condition since the mass of the foot and shank are unaffected by torso loading and therefore constant across the three experimental conditions. Second, in contrast, the magnitude of impulse J_2 was expected to vary significantly across the three conditions because total mass, m_T, is a direct function of the body mass and load that must be supported against gravity during each step ($t_a + t_c$).

III. Results

A. Influence of Load on Total Impulse

The total impulses (J_T) predicted by the model and those we measured agreed on average to within 0.4 ± 0.1 % across all the speed and load conditions examined (Table 1).

Table 1. Trial Averaged Impulse Values

Speed	Condition (x W_b)	Model-Predicted J_1 (N•s)	Model-Predicted J_2 (N•s)	Model-Predicted J_T (N•s)	Measured J_T (N•s)
3 m/s	1.00	17.0 ± 2.6	270.3 ± 21.4	287.3 ± 19.8	285.7 ± 18.7
	1.15	19.2 ± 3.4	295.8 ± 22.6	315.0 ± 22.2	313.6 ± 22.5
	1.30	18.6 ± 3.6	307.9 ± 25.0	326.5 ± 23.6	326.8 ± 23.6
4 m/s	1.00	18.2 ± 3.2	251.3 ± 24.0	269.5 ± 22.6	267.8 ± 21.9
	1.15	20.5 ± 3.5	265.5 ± 26.3	285.9 ± 24.8	284.7 ± 25.0
	1.30	20.9 ± 4.2	269.5 ± 31.7	290.4 ± 29.4	288.9 ± 29.4
5 m/s	1.00	20.6 ± 3.3	212.2 ± 22.0	232.7 ± 20.1	232.4 ± 19.6
	1.15	22.9 ± 2.2	247.3 ± 17.3	270.2 ± 16.9	268.7 ± 17.1
	1.30	25.2 ± 2.1	255.2 ± 18.1	280.4 ± 17.5	279.6 ± 17.6
6 m/s	1.00	24.5 ± 2.9	200.3 ± 16.7	224.8 ± 17.0	224.7 ± 16.9
	1.15	26.8 ± 2.1	213.6 ± 13.2	240.3 ± 13.7	240.0 ± 13.7
	1.30	28.2 ± 2.4	220.6 ± 16.5	248.9 ± 17.0	247.9 ± 16.9

Values are means ± SE.

At each running speed, the total impulse increased (Table 1) and the aerial time decreased (Table 2) with increases in load. Within each load condition, total impulse and contact time decreased as running speed increased (Tables 1 and 2).

Table 2. Trial Averaged Contact & Aerial Times

Speed	Condition (x W_b)	t_c (s)	t_a (s)
3 m/s	1.00	0.235 ± 0.017	0.114 ± 0.011
	1.15	0.258 ± 0.014	0.080 ± 0.008
	1.30	0.249 ± 0.012	0.070 ± 0.006
4 m/s	1.00	0.202 ± 0.013	0.125 ± 0.004
	1.15	0.205 ± 0.013	0.096 ± 0.005
	1.30	0.209 ± 0.015	0.078 ± 0.006
5 m/s	1.00	0.168 ± 0.011	0.123 ± 0.008
	1.15	0.181 ± 0.008	0.100 ± 0.005
	1.30	0.179 ± 0.008	0.082 ± 0.005
6 m/s	1.00	0.152 ± 0.007	0.121 ± 0.005
	1.15	0.154 ± 0.005	0.096 ± 0.003
	1.30	0.148 ± 0.005	0.084 ± 0.004

Values are means ± SE.

B. Two-Mass Model-Predicted Impulses: J_1 and J_2

Values for the impact impulse, J_1, when averaged for the trials from the four speeds (J_1 column, Table 1) did not change appreciably across loading conditions, but did increase slightly with speed. However, at each speed, J_1 waveforms typically exhibited load-related variability that altered both the J_1 peaks and Δt_1 durations as illustrated in Figure 2B.

Values for impulse J_2 increased with load at all speeds and accounted for virtually all of the load-related differences in total impulse J_T (Table 1, Figure 2B). Within each load condition, impulse J_2 values decreased as running speed increased.

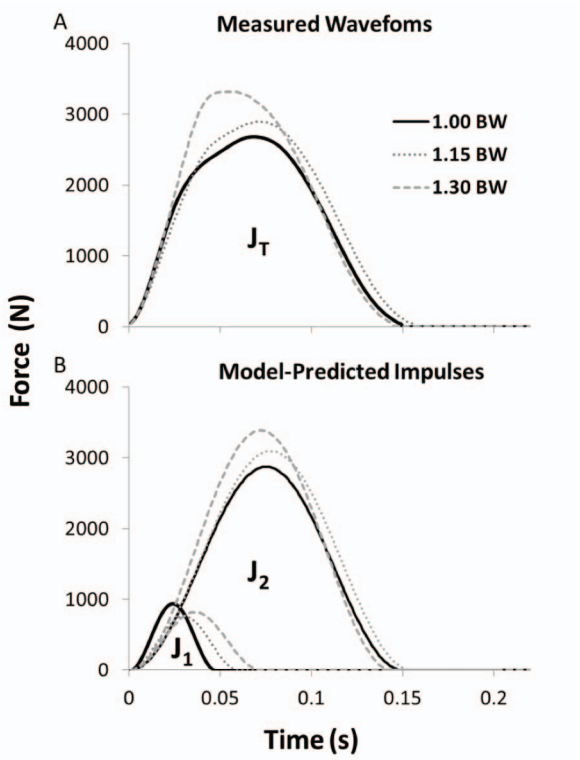

Fig. 2. A. Force, expressed in Newtons, from measured waveforms of a subject running at 6 m/s in the three loading conditions across time in seconds. B. Two-mass model-predicted waveform impulses (J_1 and J_2) from the same loaded and unloaded running trials illustrating the primary effect of the loading on J_2 magnitude.

C. Model Prediction of Impact and Peak Forces

The agreement between the forces predicted at the time of the J_1 peak, Δt_1, from the modeled and measured waveforms was reasonably good, but slightly biased. The best-fit accounted for 82% of the total variability present while the average absolute error vs. the line of identity was 14.9 ± 1.3% (Figure 3A). There was a tendency for the model to slightly under-predict at lower force values and slightly over-predict at higher ones. The best-fit for model-predicted vs. measured peak forces accounted for a larger proportion of the total variation present, with an average absolute error vs. the line of identity that was similar in magnitude, but less variable at 13.8 ± 0.6% (Figure 3B). The model over-predicted peak force values in all instances, but did so relatively consistently. Consequently, differential magnitude bias was not apparent in either the absolute error of prediction or in the best-fit relationship.

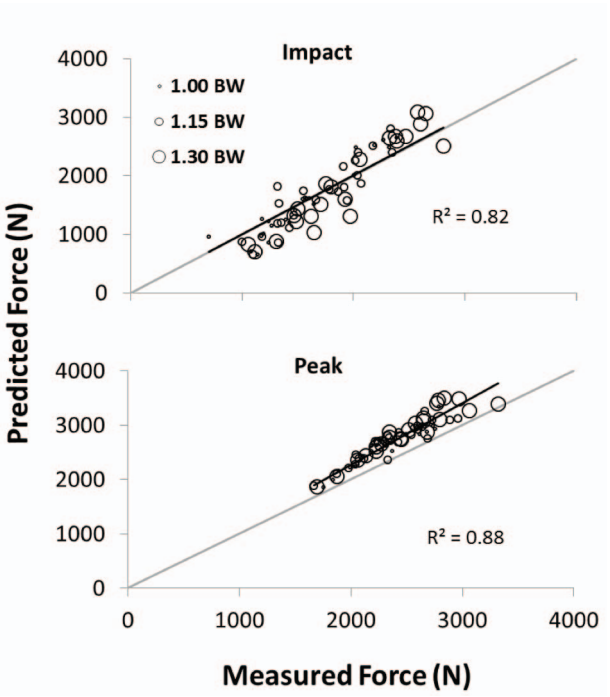

Fig. 3. A. Measured vs. model-predicted impact forces across speeds and loading conditions. B. Measured vs. model-predicted peak forces across speeds and loading conditions. Black lines represents the best-fits with an intercept through the origin. Gray lines represent the line of identity (n=71 trials for both panels).

D. Lower-limb Acceleration, Velocity and Jerk

Two motion variables acquired optically and directly related to lower-limb acceleration are illustrated in Figures 4 and 5. The 1st derivative of the position-time data provides the vertical velocity of the lower-limb during a single footfall, which identifies the parameters Δv_1 and Δt_1 used to model impulse J_1 (Figure 4).

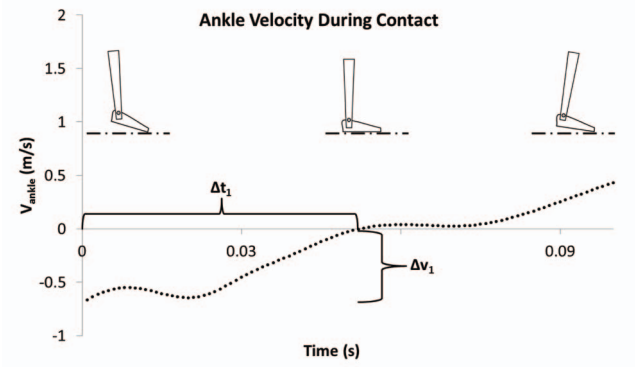

Fig. 4. First derivative of position data (V_{ankle}) taken from an ankle marker of a subject running at 5 m/s illustrating the ankle's vertical velocity slowing to zero over the time interval (Δt_1).

The 3rd derivative of the position-time data provides the vertical jerk of the lower limb which exhibits characteristic patterns at contact and toe-off as illustrated in Figure 5. The respective waveform illustrations are from unloaded running trials, but are generally representative of those present across loading conditions and running speeds.

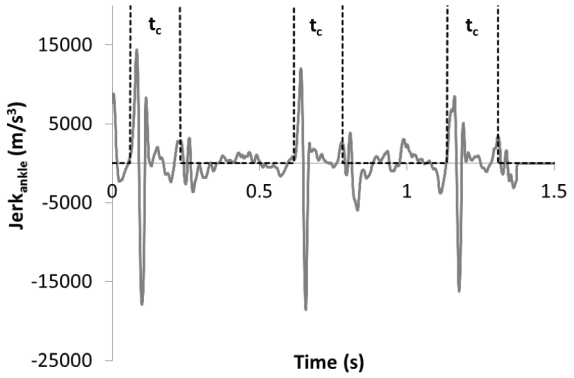

Fig. 5. The third derivative of position data ($Jerk_{ankle}$) taken from the right ankle marker of a subject running at 6 m/s. Note the consistency of the jerk signal at touchdown and toe-off across consecutive contact times.

IV. Discussion

Our test of the ability of the two-mass model to both predict and detect running ground reaction forces and limb loading rates was largely successful. The initial formulation of the model [11] suggested the potential for general accuracy, but did not include any direct experimental evaluations. In our independent test here, the model performed reasonably well across loading and speed conditions that substantially altered the magnitude, timing and shape of vertical ground reaction force waveforms.

The predictive portion of our effort generated values for impact and peak forces (Figure 3) that provided reasonable support for the validity and utility of the model. This result would not have been possible without the near-exact agreement between measured and model-predicted total impulses (J_T, Table 1) that the model requires for waveform decomposition (Figure 1) and instantaneous force predictions. The detection portion of our effort that explored the accelerations of the lower limb within and across footfalls was promising. This effort revealed that the limited gait inputs the two-mass model requires: contact time, aerial time, and lower limb acceleration, should be detectable with wearable motion sensors (Figures 4 and 5). To the best of our knowledge, the results we report are novel in identifying a motion-based approach to quantifying impact and peak forces that may be feasible for implementation using wearable technology.

A. Predicted Impact and Peak Forces

Although the absolute accuracies with which impact and peak forces were predicted was similar, the nature of the error and factors responsible differed (Figure 3). More importantly, the likely etiology of the respective errors observed suggests substantially greater accuracy may be possible with refinements of our model.

Successful prediction of impact forces requires accurate quantification of both the J_1 and J_2 impulses of our model since their sum determines the total force at the time of impact (Δt_1 in Figure 1B). Accordingly, predictive error could be introduced by incorrectly modeling the contributions of either of the model's two impulses. Here, the nature and consistency of the predictive bias observed across all three load conditions (Figure 3A) seems more likely to be attributable to an error in model-predicted impulse timing rather than magnitude. This follows from the magnitude of impulse J_1 being predicted using a constant mass across load and speed, and the magnitude of J_2 being predicted from total loads (eq. 3) with an absence of any discernable load effect on the error observed. Rather, the most consistent change across speed under all three load conditions was the reduction in contact time (Table 2). The predictive error therefore seems most likely to be related to a differential temporal error in predicting the rising edge of impulse J_2 because of the large millisecond-by-millisecond force differences present (Figure 2). Delayed rising-edge predictions would reduce J_2 contributions to the total force at time Δt_1 and result in under-prediction. Conversely, early rising-edge predictions would increase J_2 contributions and result in over-prediction of force at the model-defined impact time. The present analysis does not allow the full quantitative basis for what seems to be a time-related predictive bias to be determined. However, the landing-takeoff asymmetries documented for the height of the center of mass during human running [14] would likely introduce impulse asymmetries in J_2 that would affect rising-edge force values in a manner not currently incorporated into our model.

In contrast to the magnitude bias evident in the prediction of impact forces, peak force predictions were consistently high regardless of force magnitude across the different speeds and load conditions examined (Figure 3B). Consequently, the best-fit between actual and predicted peak forces accounted for a larger portion of the variance present but, the absolute error of prediction equaled that for the impact forces, because predicted values were consistently too large. This over-prediction is due to the model not incorporating the 40 N threshold used to identify the contact period as measured from our force platform. Inclusion of the threshold setting at the beginning and end points of the impulse curve function with preservation of the mathematical area under the curve would lower the peak value. An additional possible factor for the over-prediction observed could be an intrinsic overshoot resulting from the impulse described by the bell curve function itself. In the biomechanics literature, ground reaction force curves are most often modeled using a half sine wave rather than a bell curve function [2]. While this practice is fairly standard, the half-sine function also is known to introduce systematic error bias along the leading and trailing edges of the waveform. The close matching between the bell curve function and collisional impulses measured from small force plates with much lower force thresholds than 40 N [16] suggest to us that a shape or function error is probably not responsible for the over-predictions observed here.

B. Acquiring Model Inputs from Lower-Limb Acceleration

Evaluation of our ankle position-time data to evaluate sensor feasibility also yielded largely positive results which suggest that the two-mass model could be successfully implemented with wearable sensors. The three lower-limb motion inputs the model requires: contact time, aerial time, and lower limb acceleration could be determined from a worn accelerometer rather than the optical technology used here for motion data acquisition. Accelerometer measurement of contact and aerial times using ambulatory monitors on the lower limb is an established technology [17]. Extending these measurements to include lower limb kinematics would simply involve processing a data stream that is already available. The lower limb velocity Δv_1 at touchdown and corresponding time interval Δt_1 for the velocity to reach zero can typically range from Δv_1 = 0.8 m/s, Δt_1 = 0.070 s to Δv_1 = 3.1 m/s, Δt_1 = 0.025 s for running speeds of 3.5 - 10.5 m/s [11]. This is an acceleration range of 1.2 - 12.7 g which can be measured by standard commercial 16 g accelerometers. Additionally, incorporating an inertial measurement unit (accelerometer, gyroscope, and magnetometer) into a wearable sensor would reduce orientation, offset, and integration errors of the lower limb vertical acceleration parameters. The derivative of the acceleration, or jerk, appears to provide consistent characteristics for touchdown and toe-off that would allow for the detection of contact and aerial times via signal processing (Figure 5). Simultaneously, the acceleration data can be integrated to produce a velocity profile which can be used to determine Δt_1, and Δv_1 (Figure 4). Thus, the accelerometer has the ability to provide the parameters needed to predict both J_1 and J_2. The summation of J_1 and J_2 waveforms would then provide impact forces, peak forces, and conceivably also provide reasonable approximations of the entire force-time waveform using this approach.

C. Concluding Remarks

The motion basis of the two-mass model-based approach that we tested here for predicting instantaneous force values deviates from the primary traditions in this area of relying on force and pressure sensors embedded in shoes or insoles. Our motion-based approach may have limited viability under field conditions that deviate from the relatively controlled steady-speed level ground conditions our model assumes. However, a motion-based approach offers at least two possible advantages vs, the direct sensing approaches that are more common. The first is that our motion-based approach can be implemented with non-obtrusive micro-technology like an accelerometer, optical markers, or conceivably even from video data without any wearable requirement at all. The second is that our model's foundation allows, and indeed requires, direct linkage between gait mechanics and ground reaction forces. In this latter regard, the two-mass model implementations are well suited for gait modification purposes ranging from rehabilitation to performance improvement.

ACKNOWLEDGMENTS

The authors thank Ken Clark for his help with data collection and the participants for their time and effort in volunteering for the study.

Peter Weyand, Laurence Ryan and Kenneth Clark are the inventors of US Patent #8363891 which is owned by Southern Methodist University and contains scientific content related to that presented in the paper.

REFERENCES

[1] P. G. Weyand, R. F. Sandell, D. N. Prime, and M. W. Bundle, "The biological limits to running speed are imposed from the ground up," *Journal of Applied Physiology,* vol. 108, pp. 950-961, 2010.

[2] R. Blickhan, "The Spring-Mass Model for Running and Hopping," *Journal of Biomechanics,* vol. 22, pp. 1217-1227, 1989.

[3] T. A. McMahon, **"**Compliance and Gravity in Running," *Biomechanics of Normal and Prosthetic Gait,* vol. 4, pp. 31-37, 1987.

[4] Q. H. Ly, A. Alaoui, S. Erlicher, and L. Baly, "Towards a footwear design tool: Influence of shoe midsole properties and ground stiffness on the impact force during running," *Journal of Biomechanics***,** vol. 43, no. 2, pp. 310-317, 2010.

[5] A. A. Nikooyan and A. A. Zadpoor, **"**Mass-spring damper modeling of the human body to study running and hopping – an overview," *Proceedings of the Institution of Mechanical Engineers, Part H: Journal of Engineering in Medicine,* vol. 225, no.12, pp. 1121-1135, 2011.

[6] B. M. Nigg, A. H. Bahlsen, S. M. Luethi, and S. Stokes, "The influence of running velocity and midsole hardness on external impact forces in heel-toe running," Journal of Biomechanics, vol. 20, pp. 951-959, 1987.

[7] D. T. Fong, Y. Chan, Y. Hong, P. S. Yung, K. Fung, and K. Chan, "Estimating the complete ground reaction forces with pressure insoles in walking," *Journal of Biomechanics,* vol. 41, pp. 2597-2601, 2008.

[8] P. H. Veltink, C. Liedtke, E. Droog, and H. van der Kooij, **"**Ambulatory Measurement of Ground Reaction Forces," *IEEE Transactions on Neural Systems and Rehabilitation Engineering,* vol. 13, no. 3, pp. 423-427, 2005.

[9] H. M. Schepers, H. F. J. M. Koopman, and P. H. Veltink, "Ambulatory Assessment of Ankle and Foot Dynamics," *IEEE Transactions on Biomedical Engineering,* vol. 54, no. 5, pp. 895-902, 2007.

[10] T. Liu, Y. Inoue, and K. Shibata, "New Method for Assessment of Gait Variability Based on Wearable Ground Reaction Force Sensor," *IEEE EMBS Conference,* pp. 2341-2344, 2008.

[11] K. P. Clark, L. J. Ryan, and P. G. Weyand, "Foot speed, foot-strike and footwear: linking gait mechanics and running ground reaction forces," *Journal of Experimental Biology*, vol. 217, pp. 2037-2040, 2014.

[12] K. P. Clark and P. G. Weyand, "Are running speeds maximized with simple-spring stance mechanics?," *Journal of Applied Physiology*, vol. 117, pp. 604-615, 2014.

[13] D. A. Winter, *Biomechanics and Motor Control of Human Movement.* 2. Canada: John Wiley & Sons, Inc., 1990.

[14] G. A. Cavagna, "The landing–take-off asymmetry in human running," *Journal of Experimental Biology,* vol. 209, pp. 4051-4060, 2006.

[15] P. G. Weyand, D. B. Sternlight, M. J. Bellizzi, S. Wright, "Faster top running speeds are achieved with greater ground forces not more rapid leg movements," *Journal of Applied Physiology*, vol. 89, no. 5, pp. 1991-1999, 2000.

[16] R. Cross, "Dynamic properties of tennis balls," *Sports Engineering,* vol. 2, pp. 23-33, 1999.

[17] P. G. Weyand, M. Kelly, T. Blackadar, J. C. Darley, S. R. Oliver, N. E. Ohlenbusch, S. W. Joffe, and R. W. Hoyt, "Ambulatory estimates of maximal aerobic power from foot-ground contact times and heart rates in running humans," *Journal of Applied Physiology*, vol.91, pp. 451-458, 2001.

J Appl Physiol 126: 1315–1325, 2019.
First published February 14, 2019; doi:10.1152/japplphysiol.00925.2018.

RESEARCH ARTICLE

Running ground reaction forces across footwear conditions are predicted from the motion of two body mass components

Andrew B. Udofa,[1] Kenneth P. Clark,[2] Laurence J. Ryan,[1] and Peter G. Weyand[1]

[1]*Locomotor Performance Laboratory, Department of Applied Physiology and Wellness, Southern Methodist University, Dallas, Texas; and* [2]*Human Performance Laboratory, Kinesiology Department, West Chester University of Pennsylvania, West Chester, Pennsylvania*

Submitted 22 October 2018; accepted in final form 6 February 2019

Udofa AB, Clark KP, Ryan LJ, Weyand PG. Running ground reaction forces across footwear conditions are predicted from the motion of two body mass components. *J Appl Physiol* 126: 1315–1325, 2019. First published February 14, 2019; doi:10.1152/japplphysiol.00925.2018.—Although running shoes alter foot-ground reaction forces, particularly during impact, how they do so is incompletely understood. Here, we hypothesized that footwear effects on running ground reaction force-time patterns can be accurately predicted from the motion of two components of the body's mass (m_b): the contacting lower-limb ($m_1 = 0.08m_b$) and the remainder ($m_2 = 0.92m_b$). Simultaneous motion and vertical ground reaction force-time data were acquired at 1,000 Hz from eight uninstructed subjects running on a force-instrumented treadmill at 4.0 and 7.0 m/s under four footwear conditions: barefoot, minimal sole, thin sole, and thick sole. Vertical ground reaction force-time patterns were generated from the two-mass model using body mass and footfall-specific measures of contact time, aerial time, and lower-limb impact deceleration. Model force-time patterns generated using the empirical inputs acquired for each footfall matched the measured patterns closely across the four footwear conditions at both protocol speeds ($r^2 = 0.96 \pm 0.004$; root mean squared error $= 0.17 \pm 0.01$ body-weight units; $n = 275$ total footfalls). Foot landing angles (θ_F) were inversely related to footwear thickness; more positive or plantar-flexed landing angles coincided with longer-impact durations and force-time patterns lacking distinct rising-edge force peaks. Our results support three conclusions: *1*) running ground reaction force-time patterns across footwear conditions can be accurately predicted using our two-mass, two-impulse model, *2*) impact forces, regardless of foot strike mechanics, can be accurately quantified from lower-limb motion and a fixed anatomical mass ($0.08m_b$), and *3*) runners maintain similar loading rates ($\Delta F_{vertical}/\Delta time$) across footwear conditions by altering foot strike angle to regulate the duration of impact.

NEW & NOTEWORTHY Here, we validate a two-mass, two-impulse model of running vertical ground reaction forces across four footwear thickness conditions (barefoot, minimal, thin, thick). Our model allows the impact portion of the impulse to be extracted from measured total ground reaction force-time patterns using motion data from the ankle. The gait adjustments observed across footwear conditions revealed that runners maintained similar loading rates across footwear conditions by altering foot strike angles to regulate the duration of impact.

barefoot running; effective mass; impact forces; shoes; spring-mass model; two-mass model

INTRODUCTION

The action-reaction forces between a runner's foot and the ground determine basic functional outcomes; they also inform the design of shoe and other interventions that modify or accommodate them. Basic outcomes include bodily motion, running performance, musculoskeletal stresses, loading rates, and the incidence of overuse injury. Interventions include running shoes, orthotics, prosthetics, and synthetic running surfaces. Although hundreds of studies have measured running ground reaction force-time patterns, their mechanical basis has been difficult to identify for a variety of reasons. These include the anatomical complexity of the musculoskeletal system, variable neuromuscular activation of muscle-tendon units involved, and highly dynamic contractile conditions that affect muscle force generation at the cross-bridge, fiber, and tissue levels. Consequently, a quantitative understanding of the factors responsible for the variability introduced in the force-time patterns by footwear and other foot-ground interface interventions is not available.

A long-standing observation in the running biomechanics literature is that shoe cushioning fails to decrease the magnitude of the early, localized, rising-edge force peak (26) typically present on the overall force-time impulse (i.e., the force-time integral; Fig. 1). This counterintuitive result, termed the "impact force anomaly," is at odds with expected attenuation effects (29) and is not observed in nonrunning footwear cushioning tests. Material testing of footwear (9, 17, 29) and non-weight-bearing impact tests on shod individuals (1, 18) consistently demonstrate the expected attenuation effects. Similarly, musculoskeletal and mechanical models consistently predict that impact forces should be attenuated by shoe cushioning (21, 25, 35, 36). Additionally, subjective self-reports of runners indicate that impacts feel softer in more heavily cushioned shoes (22, 31). Nonetheless, the expected mechanical effects of cushioning are consistently deemed to be absent from force plate data acquired from individuals running in differently cushioned shoes (2, 3, 9, 13, 14, 17, 23, 24, 29). Most of these studies report no change in the magnitude of the localized force peak present along the rising edge of the measured force-time impulse. However, some studies actually report greater rising-edge force peaks in more heavily cushioned shoes (2, 3).

Address for reprint requests and other correspondence: P. G. Weyand, Locomotor Performance Laboratory, Dept. of Applied Physiology & Wellness, Southern Methodist University, 5538 Dyer St., Suite 105, Dallas, Texas 75206 (e-mail: pweyand@smu.edu).

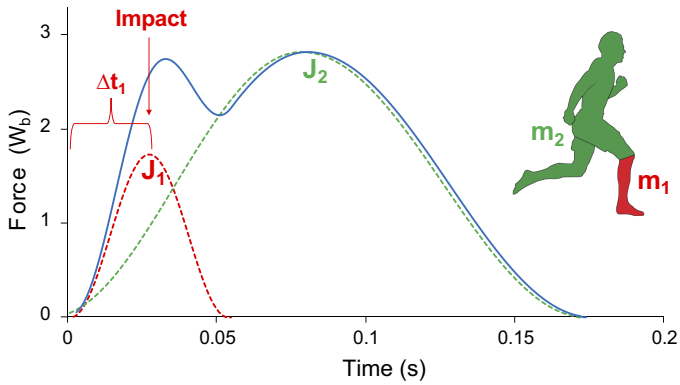

Fig. 1. Two-mass model linkage between bodily motion and running ground reaction forces. Impulse J_1 corresponds to the impact of the lower limb mass m_1 with the ground (dashed red line). Δt_1 is the deceleration time interval of m_1. Impulse J_2 corresponds to the motion of the remainder of the body's mass, m_2 (dashed green line). The sum of the impulse curves provides the total ground reaction force-time pattern (solid blue line). W_b, body weight.

A number of explanations have been proposed for the shoe-cushioning impact force anomaly (29). The leading theory is that runners adjust some combination of their pre-impact lower-limb motion, foot strike orientation, and the stiffness of their ankle and knee joints upon impact (i.e., "muscle tuning," per Refs. 3, 25, 27, and 36). These explanations are fully plausible, as gait kinematic changes before and during impact are commonly observed across different shoe cushioning conditions (2, 4, 15, 30). In contrast, Shorten and Mientjes (29) have proposed that the force anomaly is an artifact resulting from incorrect quantification of the impact event itself. Through spatial and frequency analyses, these investigators conclude that the rising edge of force-time impulse represents the summed force contributions from the body's entire mass. Although fully consistent with Newton's law of acceleration, this suggestion is at odds with common mechanical interpretations of the waveform's rising edge (2, 5, 11, 12, 19). Generally, the early portion of the waveform is attributed to a small, distal fraction of the body's mass termed an "effective" mass that is not specifically identified but that is deemed to stop abruptly on surface contact (12, 27).

The explanation of running force-time patterns provided by our recently introduced two-mass, two-impulse model (6, 7) may explain the force anomaly while elucidating running impact mechanics more generally. The model is based on an impulse momentum expression of Newton's law of acceleration and requires very limited, stride-specific data (contact time, aerial time, ankle acceleration) to predict the full force-time pattern for any given footfall. A strength of the model is that the two impulses comprising the total ground reaction force are quantified from motion data using classic force-motion relationships. This model attribute should theoretically allow gait and impact mechanics across different footwear and other conditions to be measured and predicted per the illustration in Fig. 1. Our model partitions the body's mass (m_b) into two discrete anatomical components: a constant lower-limb mass fraction (foot and shank, $m_1 = 0.08m_b$) (28) and the remainder of the body's mass ($m_2 = 0.92m_b$). Prior validation on 500 force-time impulses acquired across a nearly fourfold speed range (3.0 to 11.2 m/s) in standardized footwear supported the model's theoretical basis (7). The average goodness of fit achieved approached unity ($r^2 = 0.95$) with a mean error of prediction of only 0.17 ± 0.010 W_b (W_b is body weight).

Here, we hypothesized that running ground reaction force-time patterns across different footwear conditions can be predicted by the motion of the two anatomical mass components in our model. We tested this possibility across four shoe-sole thickness conditions ranging from a zero, barefoot condition to a relatively thick-soled running shoe with a 34-mm heel. The present hypothesis is based on prior results indicating that the slight delays in the rising-edge force peaks, such as those consistently observed with additional cushioning (2, 3, 9, 13, 14, 17, 23, 24, 29), are sufficient to permit substantially larger force contributions from the more proximal portions of the body's mass (m_2 and J_2 in Fig. 1). In theory, the inevitable covariation that footwear introduces in lower-limb gait motion, foot strike orientation, and landing stiffness should not confound our test. Rather, the model's force-motion linkage should quantify and predict their summed, simultaneous effects on measured force-time patterns. Empirical support for our hypothesis could aide interpretations of the musculoskeletal and gait adjustments observed across different footwear surface conditions. More directly, our hypothesis test has the potential to advance the currently incomplete understanding of running impact forces (3) and provide a practical tool for assessing the mechanical effects of footwear, orthotics, prosthetics, and synthetic running surfaces.

METHODS

Experimental design. We evaluated the ability of our motion-based two-mass model to predict landing and total vertical ground reaction forces across different footwear conditions using two approaches. Our primary test was an experimental intervention that tested the model under four footwear conditions commonly chosen by contemporary runners. Footwear conditions that were deemed most likely to introduce foot strike and landing mechanics variability in addition to introducing material effects on impact mechanics were chosen to maximize the rigor of the model test. The chosen footwear conditions administered were barefoot (i.e., no shoes), a minimal sole (Vibram FiveFinger KSO; Vibram, Concord, MA), a thin-soled racing flat (NikeZoom Waffle Racer VII; Nike, Beaverton, OR), and a relatively thick-soled jogging shoe (AsicsGel Cumulus-14; Asics, Kobe, Japan). The respective footwear conditions are illustrated in Fig. 2; corresponding footwear masses, heel, and forefoot thicknesses appear in Table 1.

Our second test utilized the two-mass model to predict the effects shoe cushioning should theoretically have on running ground reaction force-time patterns. We accomplished this by incorporating the effects of shoe cushioning on impact durations in vitro (29) into the timing of the impact event under typical running footfall conditions in vivo (Δt_1; Fig. 1). For this test, all running conditions and model inputs other than impact timing (i.e., lower-limb velocity, contact time, and aerial time) were held constant. We hypothesized that prolonging the impact period would cause the localized force peak on the rising edge of the total force time pattern to be *1*) delayed in timing and *2*) increased in magnitude.

Two-mass model. The fundamental principle of the two-mass model (7) is that the vertical ground reaction force waveform is composed of the sum of two impulses due to the acceleration of the lower limb (m_1) during the impact interval and the simultaneous acceleration of the rest of the body (m_2) during the total contact interval (Fig. 1). Impulse J_1 corresponds to the acceleration a_1 of lower limb mass m_1 during impact:

Fig. 2. Footwear conditions and sole thickness designations. *A*: barefoot. *B*: minimal. *C*: thin. *D*: thick.

$$J_1 = F_{1avg}(2\Delta t_1) = (m_1 a_1 + m_1 g)(2\Delta t_1), \quad (1)$$

where F_{1avg} is the average force of impulse J_1 during the impact interval $2\Delta t_1$, $m_1 = 8\%$ of total body mass m_b (28), and g is the acceleration due to gravity ($g = +9.8$ m/s^2). Impulse J_2 corresponds to the acceleration a_2 of mass m_2 during contact:

$$J_2 = F_{2avg}(t_c) = (m_2 a_2 + m_2 g)(t_c), \quad (2)$$

where F_{2avg} is the average force of impulse J_2 during the contact time interval t_c and $m_2 = 92\%$ of total body mass m_b. The total impulse J_T during contact is

$$J_T = J_1 + J_2. \quad (3)$$

The total stance-averaged vertical force is

$$F_{Tavg} = m_b g \frac{t_c + t_a}{t_c}, \quad (4)$$

where t_c and t_a are contact and aerial times and m_b is the total body mass. The total impulse can be calculated from F_{Tavg} and t_c:

$$J_T = F_{Tavg} t_c. \quad (5)$$

The acceleration a_1 due to the impact of lower limb mass m_1 is determined from the vertical velocity Δv_1 of the ankle marker slowing to zero over the time interval Δt_1:

$$a_1 = \frac{\Delta v_1}{\Delta t_1}. \quad (6)$$

Minor fluctuations in the ankle marker at the lowest position during impact can cause variability in the velocity-time profile. To eliminate this variability, a threshold of -0.25 ms and a projection to 0.0 ms is used for Δt_1 measurements. From *Eq. 1*, the average force F_{1avg} of m_1 during impact is

$$F_{1avg} = m_1(a_1 + g). \quad (7)$$

Impulse J_1 of m_1 during the total impact interval $2\Delta t_1$ is

$$J_1 = F_{1avg}(2\Delta t_1). \quad (8)$$

Table 1. *Shoe parameters for each footwear condition*

Footwear Condition	Barefoot	Minimal	Thin	Thick
Brand	None	Vibram	Nike	Asics
Mass, g	0	159	190	331
Heel height, mm	0	5	13	34
Ball height, mm	0	3	11	21

Values provided are for men's North American size 9 shoes.

Impulse J_2 is determined from impulse J_1 and total impulse J_T as

$$J_2 = J_T - J_1. \quad (9)$$

The average force F_{2avg} of m_2 during the contact interval t_c is then

$$F_{2avg} = \frac{J_2}{t_c}. \quad (10)$$

Acceleration a_2 of mass m_2 can be determined from F_{2avg} using *Eq. 2*:

$$a_2 = \frac{F_{2avg}}{m_2} - g. \quad (11)$$

The ground reaction force curves *F(t)* for J_1 and J_2 are a result of nonlinear elastic collisions and are each modeled using a bell-shaped curve function during the impact interval and contact interval, as described by Clark et al. (7).

Subjects. Eight healthy, physically active subjects participated in this study: three women (76.6 ± 14.2 kg) and five men (86.6 ± 14.7 kg) who were between 18 and 35 yr of age. All were running regularly through some form of physical activity at the time of the study, but they were not recreational or competitive runners. All subjects volunteered and provided written, informed consent in accordance with the requirements of the Southern Methodist University Institutional Review Board, which approved the study.

Data acquisition. Custom-instrumented force treadmill and motion capture equipment was used to acquire kinematic and kinetic parameters for each of the footwear conditions. A force instrumented treadmill (AMTI, Watertown, MA) capable of reaching speeds of >20 m/s was used to collect vertical ground reaction force data at 1,000 Hz. Simultaneous 1,000-Hz motion capture data with 0.7-mm resolution were acquired for 3.5 s during each trial using three Fastec Imaging HiSpec 2G cameras (Mikrotron, Unterschleissheim, Germany). Force and motion data were filtered with a low-pass, fourth-order, zero-phase-shift Butterworth filter with a cutoff frequency of 25 Hz. Subjects wore reflective markers placed on the lateral aspect of the right heel and forefoot that were affixed to the respective shoes or skin. Reflective markers were also placed on the lateral aspect of the joint axis of rotation for the right ankle, knee, and hip. All video data were processed using MATLAB software (MathWorks, Natick, MA) with custom digitization routines (16). The position-time data for the ankle marker were used to determine impact impulse (J_1) timing from the time elapsing between initial foot-ground contact and the time at which the ankle marker reached a vertical velocity of zero, or Δt_1. Contact and aerial times were determined from the time during which the measured force exceeded a 40-N threshold.

Per existing literature convention, foot angles upon impact were quantified from the angle between foot and ground at touchdown as follows: negative for rear-foot strikes and positive for forefoot strikes. For this purpose, a neutral or zero condition standing baseline reference was acquired by having each subject stand while a single-frame video file was recorded. Foot angles during running trials were quantified in accordance with the deviation from the standing reference "zero" condition established for each subject.

A minimum of three to six right footfalls were acquired from each trial completed by subjects at each speed under each footwear condition (Fig. 3). Two subjects were unable to successfully complete the 7.0 m/s trial. Two hundred and seventy-five footfalls were ultimately acquired and analyzed for their force-time pattern characteristics. Footwear condition data for each subject were acquired during two test sessions. Within each session, subjects completed two of the four footwear conditions at random. Prior to protocol administration, subjects were habituated to each footwear condition by walking on a treadmill at a slow pace for 5 min and running for 10 s or more at a jogging speed <4.0 m/s. Protocol test speeds of 4.0 and 7.0 m/s were completed in ascending order.

Measured step-by-step force-time patterns from single trials at 4.0 and 7.0 m/s appear in Fig. 3, *A* and *D*, respectively. Two-mass model-generated force-time patterns for the steps from the right limb for the respective trials appear in Fig. 3, *B* and *C*, for the 4.0 m/s trial and in Fig. 3, *E* and *F* for the 7.0 m/s trial.

Data analysis. Modeled versus measured force-time patterns were compared for each of the eight footwear-speed trial conditions as follows. Model waveforms were generated empirically from the existing form of the two-mass model (7) using the following measured inputs: body mass (m_b), contact time (t_c), the aerial time (t_a) following the footfall, the vertical velocity of the ankle marker at touchdown (Δv_1), and the time elapsing between the first instant of surface contact and the time at which the ankle marker vertical velocity equaled zero (Δt_1). Agreement between measured and model-predicted force-time patterns on a total of 275 measured footfalls was subsequently assessed using the r^2 goodness-of-fit and the root mean square error (RMSE) statistic per Clark and colleagues (6–8). Because the force-time pattern variability across footwear conditions was expected to occur predominantly along the rising edge of force-time patterns, we also performed r^2 and RMSE statistical analysis on the first half of the waveforms only (50% of t_c) for comparison to the full (100% of t_c) waveform values ($n = 275$).

In addition to the analysis performed on the 275 individual footfalls acquired, trial mean values for the measured model inputs from sequential footfalls of the right limb for each subject under each experimental condition were also determined. We did so to illustrate differences across the eight experimental conditions in brief, representative form.

We had two expectations for the performance of our two-mass model across the four footwear conditions tested. First, we expected that neither r^2 goodness of fit nor root mean square error (RMSE) trial-mean values would differ across footwear conditions at either protocol speed (1-way ANOVAs, $\alpha = 0.05$). Second, we postulated that the overall performance of the model across footwear conditions would be equivalent to that previously reported across a broad range of speeds in standardized footwear (7): specifically, respective overall values of $r^2 \geq 0.95$ and RMSE ≤ 0.20 W_b.

Lower limb surface impact velocities. To assess the influence of running velocity on the vertical velocity of the limb at surface contact (Δv_1) at and beyond the range of speeds in our protocol, we evaluated the Δv_1 versus speed relationship from kinematic data acquired on a separate cohort ($n = 35$) of nonspecialized runners who completed treadmill trials at speeds from 3.0 to 9.0 m/s in standardized racing flats (Nike Zoom Waffle Racer VII). We expected that Δv_1 values would *1*) increase systematically with running velocity across this broad range of speeds and *2*) not be affected by footwear condition at either of the two specific speeds in our protocol.

Modeling the isolated effects of shoe cushioning on force-time patterns. Force-time patterns with soft and firm cushioning were generated for a hypothetical subject ($m_b = 80$ kg) during heel-toe intermediate speed running. Typical running stride parameters for contact time ($t_c = 0.20$ s), aerial time ($t_a = 0.15$ s), and lower limb impact velocity ($\Delta v_1 = 1.25$ m/s) were held constant across both conditions. The timing of *impact impulse 1* (Δt_1) across the two conditions differed as follows; firm-cushioned Δt_1 was assigned 0.025 s, whereas the respective Δt_1 value for the soft-cushioned condition was 0.030 s. These Δt_1 inputs resulted in a relatively higher acceleration value of $a_1 = 50$ m/s^2 for the firm-cushioned versus a value of $a_1 = 42$ m/s^2 for the soft-cushioned condition (*Eq. 6*).

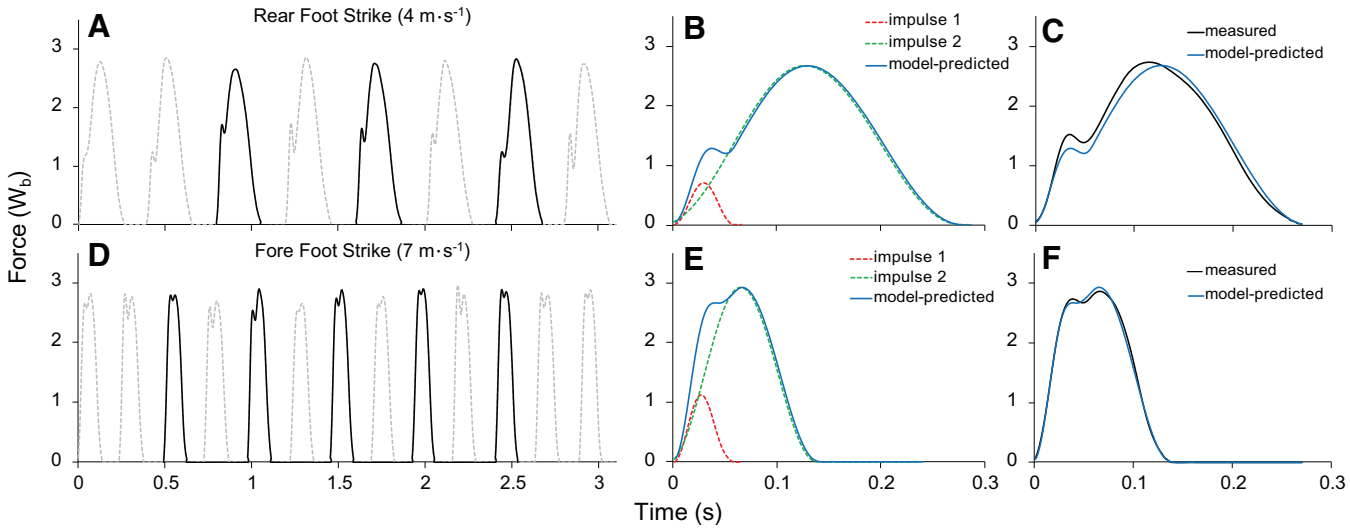

Fig. 3. Measured and modeled force-time patterns from moderate and fast protocol trials. Data were acquired and modeled for right leg footfalls (continuous line segments) and subsequent aerial intervals, as illustrated. *A*: rear foot strike at 4 m/s in the minimal footwear condition with right leg *footfalls 3*, *5*, and *7*. *B* and *E*: average values from the right leg footfalls and corresponding kinematics were used as input parameters to generate a trial-averaged *impulse 1* (dashed red line) and trial-averaged *impulse 2* (dashed green line), which were summed to obtain the trial-averaged model-predicted force waveform (solid blue line). *C* and *F*: model-predicted waveform (solid blue line) and measured average force waveform (solid black line) for the right leg footfalls analyzed for these respective trials. *D*: forefoot strike at 7 m/s in the thin footwear condition with right leg *footfalls 3*, *5*, *7*, *9*, and *11*. W_b, body weight.

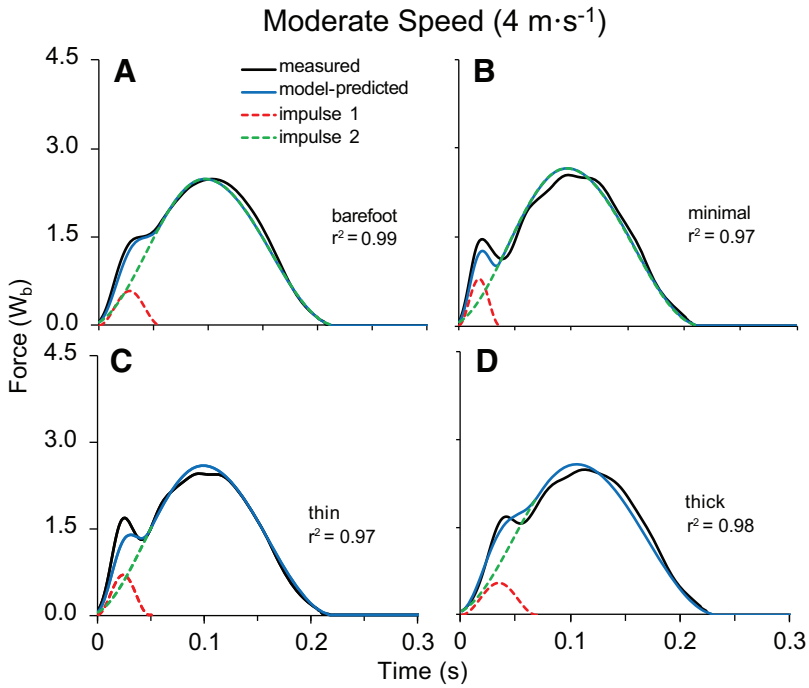

Fig. 4. Vertical ground reaction force-time impulse waveforms at 4 m/s for each footwear condition from a representative subject. The 1st (dashed red line) and 2nd impulse (dashed green line) are summed to provide the model-predicted total force-time waveform (solid blue line). Model-generated force-time waveforms (solid blue line) were compared with trial-averaged vertical ground reaction force waveforms (solid black line) using the r^2 goodness of fit statistic for each condition. *A*: barefoot. *B*: minimal. *C*: thin. *D*: thick. W_b, body weight.

RESULTS

Representative force-time patterns across footwear conditions. Model-predicted versus measured force-time patterns across footwear conditions for individual subjects running at 4.0 and 7.0 m/s appear in Figs. 4 and 5, respectively, as multistep averages. As illustrated, model predicted force-time patterns across the footwear conditions at both speeds matched the measured patterns closely. The considerable footwear condition variability present along the rising edge of the total force-time patterns at both speeds was accurately predicted by the summed contributions of impulses J_1 and J_2 of the model. Model impulse summation successfully predicted the slope of the rising edge as well as localized rising-edge force peaks that differed by roughly one-third in timing and by more than twofold in magnitude across the eight different trial conditions.

At both protocol speeds, the total force-time patterns from the barefoot condition differed somewhat from the three footwear

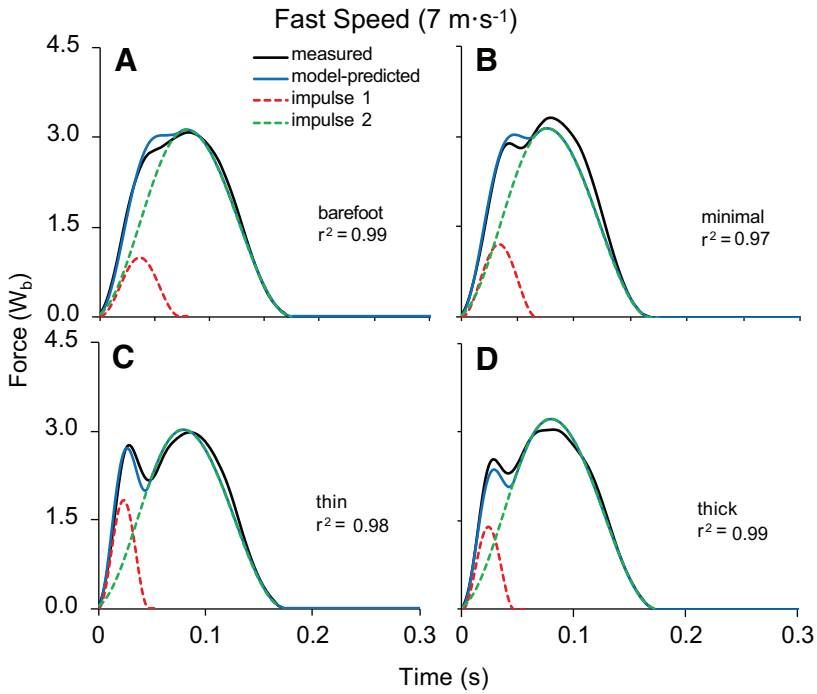

Fig. 5. Vertical ground reaction force-time waveforms at 7 m/s for each footwear condition from a representative subject. The 1st (dashed red line) and 2nd (dashed green line) impulses are summed to determine the model-predicted total force-time waveform (solid blue line). Model-generated force-time waveforms (solid blue line) were compared with trial-averaged vertical ground reaction force waveforms (solid black line) using the r^2 goodness of fit statistic for each condition. *A*: barefoot. *B*: minimal. *C*: thin. *D*: thick. W_b, body weight.

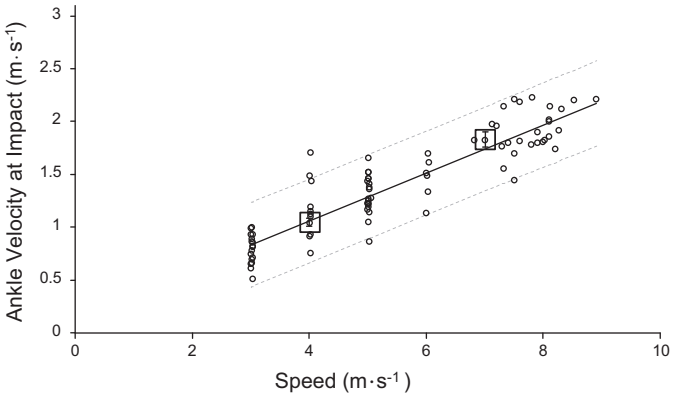

Fig. 6. Lower limb impact velocities vs. running speed. Vertical velocities of the ankle marker at impact (Δv_1) from 82 trials across running speeds from 3 to 9 m/s from 35 subjects running in standardized footwear (○), corresponding trend line (solid line) and 95% prediction interval (dashed lines). The Δv_1 values (means ± SE) across footwear conditions for the cohort of 8 subjects at 4 and 7 m/s (□).

conditions in that the rising edge of the total force-time pattern lacked a distinct, localized force peak.

Lower limb pre-impact velocities versus running speed. The Δv_1 versus speed linear best-fit relationship obtained from our separate cohort of 35 subjects running in standardized-footwear (thin condition) appears in Fig. 6 (open circles). As illustrated, the overall mean Δv_1 values (means ± SE) of our footwear subjects across all four conditions at both 4.0 (1.05 ± 0.04 m/s) and 7.0 m/s (1.83 ± 0.07 m/s) closely conformed to those of our separate, larger cohort of subjects running in standardized footwear at the same speeds. At both protocol speeds, the mean Δv_1 values of our footwear-condition subjects agreed with the best-fit normative value to within 0.15 m/s or less.

The influence of footwear condition on the Δv_1 means at each protocol speed was negligible, as the four condition means were nearly identical to one another in both cases.

Force-time patterns across footwear conditions. The total force-time patterns and corresponding impact impulse J_1 contributions are illustrated in Fig. 7 as ensemble averages from all of the footfalls analyzed at both 4.0 and 7.0 m/s. For both protocol speeds the ensemble-averaged J_1 impact impulse was essentially invariant in magnitude across footwear conditions but differed somewhat in duration and, therefore, peak force. At both 4.0 and 7.0 m/s the impact impulse duration in the barefoot condition was longer and the J_1 impact peak force lower than in each of the three footwear conditions (Fig. 7, *C* and *D*). At the faster protocol speed of 7.0 m/s there was an inverse relationship between the thickness of the shoe sole and the duration of the impact event; the thicker the sole material interface between the foot and the running surface, the briefer the average duration of the impact interval. Additionally, at 7.0 m/s for both the barefoot and minimal footwear conditions, the extended duration of the impact interval coincided with a greater peak force on the ensemble-averaged total force-time pattern (Fig. 7*B*).

Foot and ankle impact mechanics across footwear conditions. Across footwear conditions at both speeds, the mean foot angle at touchdown exhibited a relationship to shoe sole thickness that was largely inverse in nature (Fig. 8, *A* and *B*). The less thick the interface between the foot and ground, the more positive the foot angle at touchdown. At the faster protocol speed of 7.0 m/s, at which the incoming limb velocities Δv_1 and impact impulses J_1 were nearly twice as great, subjects landed with more positive foot angles in each of the four respective footwear conditions. Therefore, the most positive foot angle of +14° was observed for the condition that combined the

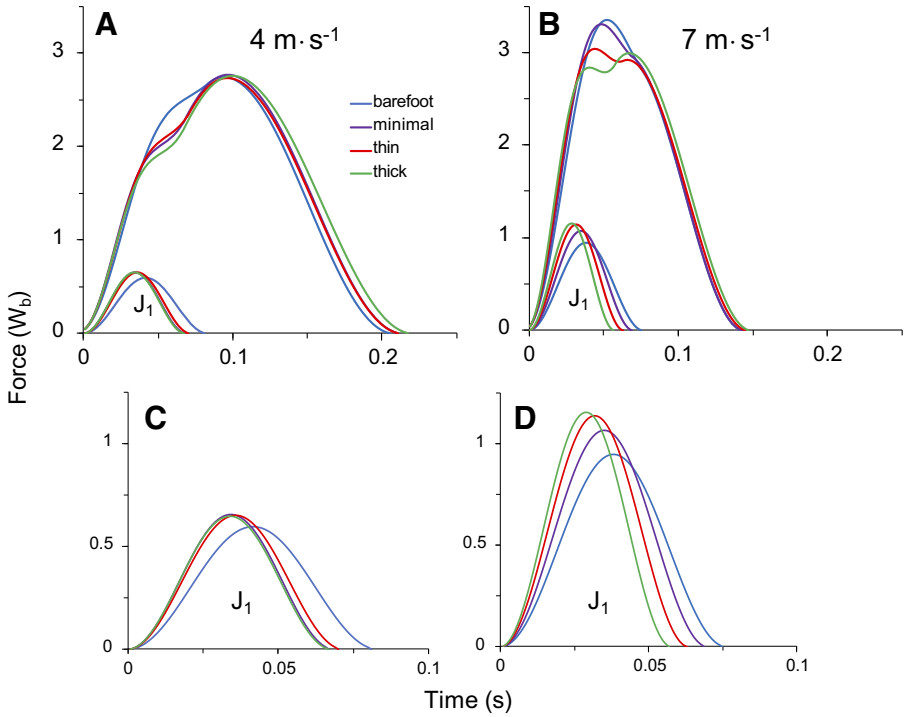

Fig. 7. Ensemble-averaged, model-predicted impact (J_1) and total vertical ground reaction force-time waveforms for the 4 footwear conditions at each protocol speed. *A* and *B*: model-predicted forces and corresponding impulse J_1 curves for each footwear condition were averaged for all subjects and trials at 4 (*A*) and 7 m/s (*B*). *C* and *D*: impulse J_1 curves are rescaled for greater clarity. W_b, body weight.

greatest impact impulse with the least shoe cushioning, i.e., 7.0 m/s barefoot.

The relationship between foot angle at touchdown and the duration of the impact was positive (Fig. 8*B*) at both protocol speeds. The more positive the foot angle at touchdown, the longer the duration of the impact event. At the slower speed of 4.0 m/s at which incoming limb velocities were slower, the condition times to the impact impulse peak Δt_1 ranged from a minimum of 0.034 s in the thick footwear conditions to a maximum of 0.041s in the barefoot condition. At 7.0 m/s, at which incoming limb velocities were greater, the times to the impact impulse peak Δt_1 ranged from a minimum of 0.028 s for the thick condition to a maximum of 0.038 s for the barefoot condition.

Model-predicted versus measured force-time pattern agreement. The agreement between the model-generated force-time versus measured force-time pattern averages for each of the eight protocol trial conditions appear in Table 2 for goodness-of-fit (r^2) and Table 3 for the individual error of prediction (RMSE). The overall goodness-of-fit mean approached unity at $r^2 = 0.96 \pm 0.004$ (Table 2), whereas the mean error of prediction was 0.17 ± 0.010 W_b (Table 3). Neither statistic varied across the footwear conditions at the respective protocol speeds ($P > 0.05$), as assessed by one-way ANOVA.

The r^2 and RMSE values for the first half (50% of t_c) of force-time patterns from individual footfalls were nearly identical to the those for the full waveforms [first half: $r^2 = 0.94 \pm 0.004$, RMSE $= 0.20 \pm 0.006$; full waveforms: $r^2 = 0.95 \pm 0.002$, RMSE $= 0.19 \pm 0.005$, $n = 275$] indicating that the model predicted the more variable rising edge of the impulse with similar accuracy to the overall force-time patterns.

Model-predicted isolated effects of shoe cushioning on force-time patterns. Two-mass model-predicted effects of cushioning-induced prolongation in *impulse 1* timing (Δt_1) on the total ground reaction force waveform appear in Fig. 9, *A* and *B*. The prolongation of Δt_1 by 0.005 s from 0.025 to 0.030 s while holding all other runner, gait, and model factors constant resulted in a reduction in the slope of the rising edge of the total force-time impulse. However, as hypothesized, increasing Δt_1 increased the magnitude of the localized force peak by almost 200 N on the rising edge per the figure illustration. The 0.005-s prolongation of Δt_1 was sufficient to double the force contributions made by impulse J_2 to the total impulse at the delayed time of the localized, rising-edge force peak. Consequently, the localized rising-edge force peak in the simulated soft-cushioned condition was greater in magnitude despite the reduction in the magnitude of the J_1 impact impulse force peak.

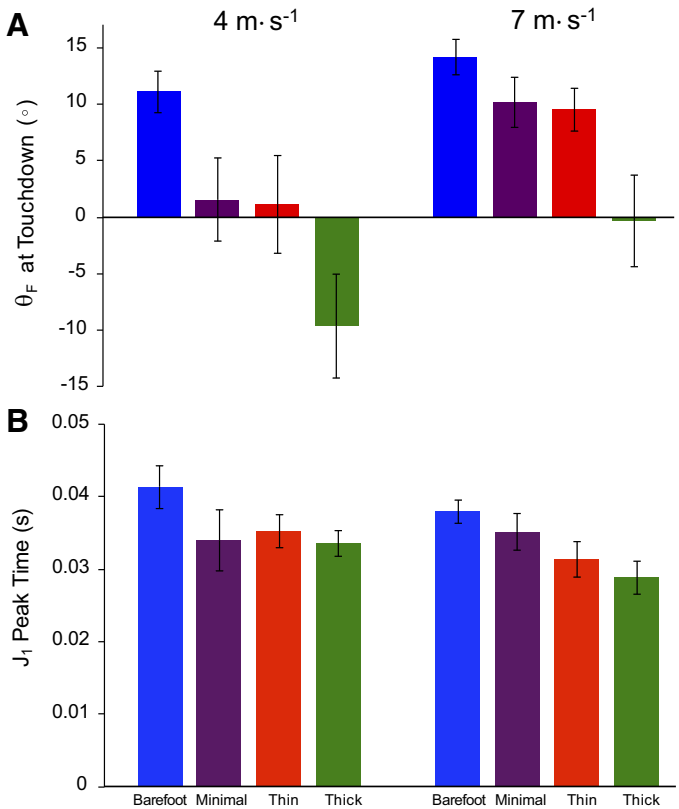

Fig. 8. Lower limb impact mechanics across footwear conditions. *A*: foot angles (θ_F) at impact for each footwear condition were averaged (means ± SE) for all subjects for both the moderate (4.0 m/s) and fast (7.0 m/s) protocol running speed (note: negative values are rear foot strike angles, and positive values are forefoot strike angles; 0° corresponds to a flat foot landing). *B*: impulse J_1 deceleration time (Δt_1; means ± SE) during impact for each footwear condition at the protocol running speed.

DISCUSSION

As hypothesized, our two-mass model successfully predicted vertical ground reaction force-time patterns across the four footwear conditions tested at each of our two protocol speeds. Although running ground reaction forces have been examined across footwear conditions at considerable length, the apparent absence of cushioning effects seemed to defy mechanical theory and quantitative explanation. The present results indicate that footwear effects can, in fact, be fully explained using classic force-motion relationships. Here, when doing so with the few stride-specific inputs our two-mass model requires, the force-time patterns we predicted accounted for an average of 95–96% of the pattern variability present within the footfalls analyzed across footwear conditions.

Achieving close fits to measured data via some form of mechanical modeling that relies upon iterative post-facto refinement, simulation, or other optimization techniques is not uncommon. However, the present agreement was achieved with directly measured inputs for each of the 275 individual footfall force-time patterns analyzed and without any refinement or optimization of the a priori form of our model (7). Accordingly, the classic force-motion relationships in the model appear to be fully capable of simultaneously quantifying the effects of footground cushioning, foot strike mechanics, and joint and limb landing stiffness from precision motion data. Additionally, our modeling test identified how shoe cushioning effects can be obscured by conventional interpretations of the total force-time waveform pattern.

One basic implication of our results is that shoe cushioning can attenuate impact forces, as mechanical theory (29) and intuition have long suggested it should.

Landing and impact mechanics: a tale of two impulses. The accuracy and conciseness of the quantitative explanation offered here for footwear effects on running ground reaction forces prompts an immediate question: why were these effects not previously identified? The mechanical issues in question have been studied at considerable length for roughly four

Table 2. *Trial-averaged r^2 values across footwear conditions*

Speed, m/s	Barefoot	Minimal	Thin	Thick	Average
4.0	0.98 ± 0.006	0.96 ± 0.010	0.98 ± 0.004	0.98 ± 0.005	0.97 ± 0.003
7.0	0.92 ± 0.020	0.93 ± 0.020	0.97 ± 0.009	0.97 ± 0.005	0.95 ± 0.008
Total	0.95 ± 0.011	0.95 ± 0.011	0.97 ± 0.004	0.98 ± 0.003	0.96 ± 0.004

Values are means ± SE.

decades using a variety of experimental and theoretical approaches (1–3, 9, 12–14, 17–19, 23–25, 29). Through virtually all of the prior work on this issue, the critical factor obscuring footwear effects and thereby impeding mechanical understanding of running ground reaction forces has been the contribution of the non-impact portion of the body's mass. In our model, the substantial contributions of the non-impacting mass m_2 (impulse J_2) to the total force-time impulse appear in Figs. 1, 3, 4, and 5. As illustrated, the contributions of the non-impacting mass m_2 begin at the instant of touchdown and increase in a direct, time-dependent manner. These contributions are sufficient to equal or exceed half of the total impulse during the early potion of the contact period generally conceptualized as the impact period.

The obscuring effect that the non-impact mass and impulse can have on the total force-time impulses under softer-cushioned footwear conditions results from three simultaneous, interdependent phenomena that are not present in material (9, 17, 29) and non-weight-bearing tests (1, 18) of shoe cushioning effects. The first of these phenomena is a slight delay in the time to the impact force peak (Δt_1), the second is a modest reduction in the impact force peak, and the third is the increased force contribution of the body's nonimpacting mass (m_2) at the delayed time of the impact peak. In combination, these three factors obscure the impact attenuation effect of shoe cushioning on the overall force-time waveform patterns, as illustrated by the example in Fig. 9. In this theoretical example that holds the limb's impact velocity and total J_1 impulse constant, an impact attenuation effect that reduces the J_1 force peak from roughly 770 to 660 N simultaneously extends the time to the J_1 peak, Δt_1, by 5 ms. This temporal delay doubles the force contribution from mass m_2 at the time of the localized force peak on the rising edge of the total force-time waveform, increasing J_2 force contributions from roughly 750 to 1200 N. The specific quantitative contributions of these three interdependent phenomena will vary across different running speeds, foot-ground contact times, incoming limb velocities, impact durations, and cushioning-introduced impact prolongation. However, the overall effects in Fig. 9 accurately represent the integrated, combined effects of cushioning on the total force-time impulse.

A noteworthy outcome of the quantitative example illustrated in Fig. 9 is that the localized, rising-edge force peak is actually greater in the condition in which the impact force peak is smaller due to the cushioning-induced attenuation. In this regard, our theoretical outcome is completely consistent with the many shoe cushioning results reported in the literature over the last four decades (2, 3, 9, 13, 14, 17, 23, 24, 29). These studies vary somewhat in the relative magnitudes of the localized force peak along the rising edge of the force-time impulse in more heavily cushioned shoes; some report rising-edge force peaks that are slightly less (20), with some slightly greater (3, 13), whereas most report no significant differences (2, 9, 14, 23, 24). However, these studies are fully consistent in reporting that the rising-edge force peak occurs at a later post-impact time in more heavily cushioned shoes. Per the time course of the J_2 impulses illustrated here and elsewhere, delays of even several milliseconds in the timing of the J_1 impulse peak substantially increase the force contributed by the body's non-impacting mass both at the time of the impact peak and more so at the time of the localized rising-edge peak on the total force-time impulse waveform.

Quantitative implications of the mechanics of landing and impact. Several insights are provided by the ability of the two-mass model to predict the force-time patterns across our experimental footwear test conditions, particularly along the highly variable impulse rising edge. Most importantly, our model fully supports and indeed quantifies the force summation effects Shorten and Mientjes (29) concluded must be present in the early portion of the impulse. Our analysis, like theirs, demonstrates that Newtonian interpretations of the impulse are not only correct but also necessary for a quantitative understanding of force-time patterns measured from force platforms. Therefore, the widespread practice of quantifying impact mechanics from the rising edge of the total force-time waveform measured is problematic in two significant respects. First, the attribution of the early portion of the total impulse to a small fraction of the body's mass violates classic Newtonian mechanics. Consequently, the anatomically unclear effective masses often quantified via this practice lack valid physical and mechanical interpretations. Second, the localized rising-edge of the force-time pattern should not be used to quantify the timing of running impact forces. The more subtle mechanical effect introduced by the impulse contribution of the body's non-impacting mass, m_2, is the slight but inevitable timing delay between the actual impact force peak J_1 and the time at which a localized force

Table 3. *Trial-averaged RMSE values across footwear conditions*

Speed, m/s	Barefoot	Minimal	Thin	Thick	Average
4.0	0.14 ± 0.021	0.16 ± 0.026	0.14 ± 0.014	0.12 ± 0.012	0.14 ± 0.009
7.0	0.27 ± 0.039	0.26 ± 0.033	0.18 ± 0.030	0.17 ± 0.013	0.22 ± 0.017
Total	0.19 ± 0.027	0.20 ± 0.024	0.15 ± 0.016	0.14 ± 0.010	0.17 ± 0.010

Root mean square error (RMSE) values are means ± SE expressed units of the body's weight.

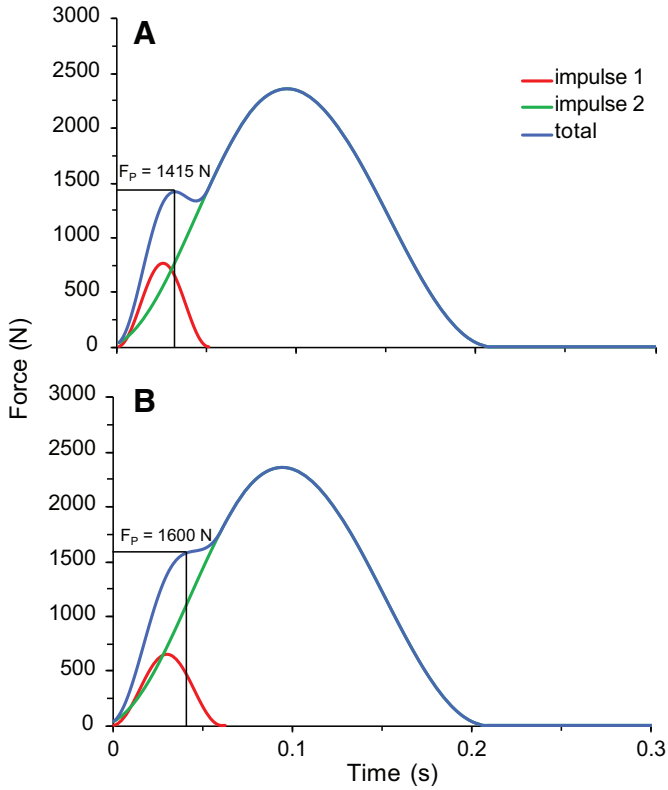

Fig. 9. Schematic illustration of altered impulse J_1 timing (Δt_I) on the rising edge of the total force-time pattern. *A*: Δt_I = 0.025 s. *B*: Δt_I = 0.030 s. Across *A* and *B*, all model variables except for impact impulse timing were held constant for an intermediate running speed as follows: subject mass (m_b) was 80 kg, contact time (t_c) was 0.20 s, aerial time (t_a) was 0.15 s, and lower limb impact velocity (Δv_1) was 1.25 m/s.

peak appears on the rising edge of the full waveform (Figs. 1, 4, 5).

Finally, our quantification of the importance of the body's non-impacting mass to the total force-time waveform addresses several observations for which a mechanical explanation had not previously been available. A first is the apparent discrepancy between the substantially greater reductions in shock as measured from accelerometers mounted on the tibia versus the relatively modest reductions in force-time, rising-edge force "impact" peaks (10) after runners modify their landings to be "softer" upon verbal instruction. More fundamentally, the contributions of the non-impacting mass m_2 explain why cushioning effects are consistently present in material tests (9, 17, 29), modeling exercises that hold all noncushioning effects constant (21, 25, 35, 36), and non-weight-bearing tests that eliminate the gravitational loading contributions of the non-impact portion of the body's mass (1, 18). In each of the aforementioned test circumstances, the contributions of the non-impacting mass are either absent or preclude the time-dependent quantification necessary to correctly model the mechanical effects of shoes that are present during running.

Foot strike selection regulates impact forces and limb loading rates. The literature on running impact forces is extensive and includes dozens of studies assessing the influence of footwear, foot strike mechanics, running speed, and other factors. Nearly all of the prior literature conclusions have been based on inferences drawn from the total force-time patterns that did not isolate the impact event as implicitly assumed (2, 3, 5, 10, 11, 14, 19, 23–25). Although prior practice is understandable in the absence of a direct method for impact force quantification, the predictive accuracy achieved by our model here, particularly along the highly variable total impulse rising edge, indicates that we have correctly quantified the impact impulse. In this regard, our model's decomposition of the rising edge of the total force-time impulse into discrete impact and non-impact portions provides a basis for interpreting foot strike and limb-landing adaptations to footwear conditions that has not been previously available (3). An important distinction versus prior analyses is avoiding the complicating and potentially confounding assumption that the distal portion of the body's mass that is abruptly decelerated upon impact differs for forefoot versus rear foot impacts (19, 27). In contrast, the recognition that the lower limb's mass does not vary with foot strike allows the impact impulse to be quantified using classic force-motion relationships. Accordingly, the only variables required to do so are the mass of the lower limb, its pre-impact vertical velocity, and the time to reach a vertical velocity of zero after initial impact.

An immediate capability that concise quantification of impact forces provides is insight into the gait features that runners can and cannot modify when impacting the surface. Given that the anatomical mass of the lower limb is obviously constant, runners could theoretically adjust impact forces by altering the pre-impact velocity of the contacting limb (Δv_1), the time course of deceleration after impact (Δt_I), or both. Our data indicate that our subjects modified impact timing without altering pre-impact limb velocities in the different footwear conditions tested. Why do runners utilize only one of two theoretical mechanisms available to them for impact attenuation?

Two aspects of our pre-impact limb velocity data suggest that altering this variable is not a viable option for adjusting impact forces. The first is how invariant pre-impact velocities were across the four heterogeneous footwear conditions assessed at each of our two protocol speeds. The average variation in pre-impact velocities across the different footwear conditions was 3.6% or less of the overall Δv_1 mean at each of our two protocol speeds. In contrast, the between-speed Δv_1 means differed by more than 50%. The second is the close conformation of the Δv_1 means for our footwear subjects to the values observed on a large cohort of athletic subjects running in standardized footwear across a broad range of speeds (Fig. 6). As illustrated, the overall means of our eight footwear subjects at 4.0 and 7.0 m/s agreed with the best-fit Δv_1 versus speed relationship for the standardized footwear (thin condition) cohort of 35 subjects to within 0.03 and 2.6%, respectively. The level of agreement observed from these independent populations supports a basic coupling between limb pre-impact velocities and running speed. This conclusion is well supported by earlier investigations (7, 8) revealing that maximizing limb pre-impact velocities is a mechanical strategy athletes use to maximize sprint-running speeds.

In contrast to limb impact velocities, runners did modify Δt_I impact durations to a moderate extent across footwear conditions at both protocol speeds (Figs. 7 and 8). At the faster protocol speed involving impact impulses that were substantially larger, there was an inverse relationship between impact duration and shoe thickness (Fig. 7, *B* and *D*); the thinner the shoe sole interface, the more runners opted to prolong the duration of the impact period. A similar but less pronounced

pattern of impact duration regulation across footwear thickness was also observed at the slower speed. The pattern may have been slightly less consistent at the slower speed because the impact impulses at this speed were only half as large (Fig. 7, *A* and *C*). Nonetheless, at our moderate protocol speed of 4.0 m/s also, runners prolonged the impact period in the barefoot condition that offered zero cushioning in comparison to the three footwear conditions.

The consistent relationships between the angle of the foot at touchdown (θ_F), footwear thickness, and impact duration identify the control strategy runners used to modify their impact mechanics. Across both footwear condition and speed, our data indicate that runners adopted more positive foot strike angles as a strategy to prolong impact durations and reduce limb loading rates (Figs. 7 and 8). Across footwear conditions at both speeds, the more limited the material thickness between the foot and surface, the more positive the foot angle runners selected before impact and the more prolonged their impact durations. The trend across our two protocol speeds conformed to the same overall pattern; runners adopted more positive foot strike angles at the faster speed that involved greater impact forces than they did at the slower one. The outcome of impact duration modification via foot strike-mediated Δt_I regulation was that for each of our two test speeds, the rising edges of force-time impulses and, therefore, also the limb-loading rates were nearly identical regardless of the presence or absence of cushioning and its relative thickness.

Many earlier studies have reported the tendency for runners to adopt more positive foot angles (i.e., more pronounced forefoot landings) on impact when running barefoot or in minimal thickness shoes (3, 4, 17, 19, 30). Our results here parallel these earlier findings and in the basic context of impact mechanics provide a consistent mechanical explanation for them. Adopting progressively more positive foot angles (θ_F) before impact is a means by which the impact duration can be extended and thereby reduce limb-loading rates and impact force peaks (Figs. 7 and 8). The consistency with which runners altered impact duration inversely with shoe thickness at running velocities with different incoming velocities offers a remarkably direct interpretation of foot strike landing angle modification. Runners adjust foot strike mechanics as needed to substitute musculoskeletal cushioning for shoe cushioning when the latter is limited or absent. The more shoe cushioning available to yield during the impact period, the more willing runners were to land on or near the rear portion of their foot. In this regard, our mechanical analysis of impact and landing supports intuition as well as long-standing literature suggestions of a less quantitative nature (3, 4, 13, 17, 19, 30, 34) and the cushioning sensation reports of runners (22, 31). Runners avoid impact landings on their heels when little or no cushioning is present, particularly when running on firm surfaces.

Concluding remarks. The quantitative understanding of the force-motion relationships involved in human running that we have validated here across footwear conditions and previously across running speed (7) has broad potential application. Although footwear condition was the experimental intervention implemented here, our two-mass, two-impulse model could also be used to investigate the limb surface mechanical perturbations introduced by orthotics, running prostheses, and surface stiffness. More clinically focused applications targeting load-related overuse injuries and rehabilitation are also possible. The ability to independently quantify the impact portion of the total ground reaction force allows the effectiveness of gait retraining for impact force reduction (10) to be assessed directly rather than inferred incorrectly from the total force-time impulse measures that include non-impact forces. Impact assessments could be based either on precision kinematic data per our methods here or on acceleration data from sensors mounted on the lower limb (10, 32, 33).

We close by noting that our methods make it possible to compare the in vitro mechanical properties of running shoes with their in vivo mechanical performance. We do so with the caution that the individual variability in the impact-related modifications runners adopt in different shoes mandates individual in vivo testing for shoe performance assessments to be fully valid.

ACKNOWLEDGMENTS

We thank the participants for their time and effort in volunteering for the study.

GRANTS

This work was supported in part by a Fairess Simmons Fellowship to A. B. Udofa as well as a US Army Medical and Materiel Command award (W81XWH-12-2-0013) to P. G. Weyand.

DISCLOSURES

P. G. Weyand, L. J. Ryan, and K. P. Clark are the inventors of US Patent No. 8363891, which is owned by Southern Methodist University and contains scientific content related to that presented in this article. The patent is licensed to SoleForce, in which the three aforementioned individuals are equity partners. A. B. Udofa does not has any conflicts of interest, financial or otherwise, to disclose.

AUTHOR CONTRIBUTIONS

A.B.U., K.P.C., L.J.R., and P.G.W. conceived and designed research; A.B.U., K.P.C., and L.J.R. performed experiments; A.B.U., K.P.C., L.J.R., and P.G.W. analyzed data; A.B.U., K.P.C., L.J.R., and P.G.W. interpreted results of experiments; A.B.U., K.P.C., L.J.R., and P.G.W. prepared figures; A.B.U. and P.G.W. drafted manuscript; A.B.U., K.P.C., L.J.R., and P.G.W. edited and revised manuscript; A.B.U., K.P.C., L.J.R., and P.G.W. approved final version of manuscript.

REFERENCES

1. **Aerts P, De Clercq D.** Deformation characteristics of the heel region of the shod foot during a simulated heel strike: the effect of varying midsole hardness. *J Sports Sci* 11: 449–461, 1993. doi:10.1080/02640419308730011.
2. **Addison BJ, Lieberman DE.** Tradeoffs between impact loading rate, vertical impulse and effective mass for walkers and heel strike runners wearing footwear of varying stiffness. *J Biomech* 48: 1318–1324, 2015. doi:10.1016/j.jbiomech.2015.01.029.
3. **Baltich J, Maurer C, Nigg BM.** Increased vertical impact forces and altered running mechanics with softer midsole shoes. *PLoS One* 10: e0125196, 2015. doi:10.1371/journal.pone.0125196.
4. **Chambon N, Delattre N, Guéguen N, Berton E, Rao G.** Is midsole thickness a key parameter for the running pattern? *Gait Posture* 40: 58–63, 2014. doi:10.1016/j.gaitpost.2014.02.005.
5. **Chi KJ, Schmitt D.** Mechanical energy and effective foot mass during impact loading of walking and running. *J Biomech* 38: 1387–1395, 2005. doi:10.1016/j.jbiomech.2004.06.020.
6. **Clark KP, Ryan LJ, Weyand PG.** Foot speed, foot-strike and footwear: linking gait mechanics and running ground reaction forces. *J Exp Biol* 217: 2037–2040, 2014. doi:10.1242/jeb.099523.
7. **Clark KP, Ryan LJ, Weyand PG.** A general relationship links gait mechanics and running ground reaction forces. *J Exp Biol* 220: 247–258, 2017. doi:10.1242/jeb.138057.
8. **Clark KP, Weyand PG.** Are running speeds maximized with simple-spring stance mechanics? *J Appl Physiol (1985)* 117: 604–615, 2014. doi:10.1152/japplphysiol.00174.2014.

9. **Clarke TE, Frederick EC, Cooper LB.** Effects of shoe cushioning upon ground reaction forces in running. *Int J Sports Med* 4: 247–251, 1983. doi:10.1055/s-2008-1026043.
10. **Crowell HP, Davis IS.** Gait retraining to reduce lower extremity loading in runners. *Clin Biomech (Bristol, Avon)* 26: 78–83, 2011. doi:10.1016/j.clinbiomech.2010.09.003.
11. **Denoth J.** Load on the locomotor system and modeling. In: *Biomechanics of Running Shoes*, edited by Nigg BM. Champaign, IL: Human Kinetics Publishers, 1986, p. 63–116.
12. **Derrick TR.** The effects of knee contact angle on impact forces and accelerations. *Med Sci Sports Exerc* 36: 832–837, 2004. doi:10.1249/01.MSS.0000126779.65353.CB.
13. **DeWit B, De Clercq D, Lenoir M.** The effect of varying midsole hardness on impact forces and foot motion during foot contact in running. *J Appl Biomech* 11: 395–406, 1995. doi:10.1123/jab.11.4.395.
14. **Hamill J, Russell EM, Gruber AH, Miller R.** Impact characteristics in shod and barefoot running. *Footwear Sci* 3: 33–40, 2011. doi:10.1080/19424280.2010.542187.
15. **Hardin EC, van den Bogert AJ, Hamill J.** Kinematic adaptations during running: effects of footwear, surface, and duration. *Med Sci Sports Exerc* 36: 838–844, 2004. doi:10.1249/01.MSS.0000126605.65966.40.
16. **Hedrick TL.** Software techniques for two- and three-dimensional kinematic measurements of biological and biomimetic systems. *Bioinspir Biomim* 3: 034001, 2008. doi:10.1088/1748-3182/3/3/034001.
17. **Komi PV, Gollhofer A, Schmidtbleicher D, Frick U.** Interaction between man and shoe in running: considerations for a more comprehensive measurement approach. *Int J Sports Med* 8: 196–202, 1987. doi:10.1055/s-2008-1025655.
18. **Lafortune MA, Hennig EM, Lake MJ.** Dominant role of interface over knee angle for cushioning impact loading and regulating initial leg stiffness. *J Biomech* 29: 1523–1529, 1996. doi:10.1016/S0021-9290(96)80003-0.
19. **Lieberman DE, Venkadesan M, Werbel WA, Daoud AI, D'Andrea S, Davis IS, Mang'eni RO, Pitsiladis Y.** Foot strike patterns and collision forces in habitually barefoot versus shod runners. *Nature* 463: 531–535, 2010. doi:10.1038/nature08723.
20. **Logan S, Hunter I, J Ty Hopkins JT, Feland JB, Parcell AC.** Ground reaction force differences between running shoes, racing flats, and distance spikes in runners. *J Sports Sci Med* 9: 147–153, 2010.
21. **Ly QH, Alaoui A, Erlicher S, Baly L.** Towards a footwear design tool: influence of shoe midsole properties and ground stiffness on the impact force during running. *J Biomech* 43: 310–317, 2010. doi:10.1016/j.jbiomech.2009.08.029.
22. **Milani TL, Hennig EM, Lafortune MA.** Perceptual and biomechanical variables for running in identical shoe constructions with varying midsole hardness. *Clin Biomech (Bristol, Avon)* 12: 294–300, 1997. doi:10.1016/S0268-0033(97)00008-9.
23. **Nigg BM, Bahlsen HA, Luethi SM, Stokes S.** The influence of running velocity and midsole hardness on external impact forces in heel-toe running. *J Biomech* 20: 951–959, 1987. doi:10.1016/0021-9290(87)90324-1.
24. **Nigg BM, Herzog W, Read LJ.** Effect of viscoelastic shoe insoles on vertical impact forces in heel-toe running. *Am J Sports Med* 16: 70–76, 1988. doi:10.1177/036354658801600113.
25. **Nigg BM, Liu W.** The effect of muscle stiffness and damping on simulated impact force peaks during running. *J Biomech* 32: 849–856, 1999. doi:10.1016/S0021-9290(99)00048-2.
26. **Nigg BM.** *Impact Forces. Biomechanics of Sport Shoes*. Calgary, AB, Canada: Topline Printing, 2010, p. 1–44.
27. **Nigg BM, Mohr M, Nigg SR.** Muscle tuning and preferred movement path—a paradigm shift. *Current Issues Sport Sci* 2: 1–12, 2017. doi:10.15203/CISS_2017.007.
28. **Plagenhoef S, Evans FG, Abdelnour T.** Anatomical data for analyzing human motion. *Res Q Exerc Sport* 54: 169–178, 1983. doi:10.1080/02701367.1983.10605290.
29. **Shorten M, Mientjes MI.** The 'heel impact' force peak during running is neither 'heel' nor 'impact' and does not quantify shoe cushioning effects. *Footwear Sci* 3: 41–58, 2011. doi:10.1080/19424280.2010.542186.
30. **Squadrone R, Gallozzi C.** Biomechanical and physiological comparison of barefoot and two shod conditions in experienced barefoot runners. *J Sports Med Phys Fitness* 49: 6–13, 2009.
31. **Sterzing T, Schweiger D, Ding R, Cheung JT, Brauner T.** Influence of rearfoot and forefoot midsole hardness onbiomechanical and perception variables during heel-toe running. *Footwear Sci* 5: 71–79, 2013. doi:10.1080/19424280.2012.757810.
32. **Thompson M, Seegmiller J, McGowan CP.** Impact accelerations of barefoot and shod running. *Int J Sports Med* 37: 364–368, 2016. doi:10.1055/s-0035-1569344.
33. **Udofa AB, Ryan LJ, Weyand PG.** Impact forces during running: loaded questions, sensible outcomes. IEEE 13th International Conference on Wearable and Implantable Body Sensor Networks. San Francisco, CA, June 14–17, 2016, p. 371–376. doi:10.1109/BSN.2016.7516290.
34. **Wakeling JM, Pascual SA, Nigg BM.** Altering muscle activity in the lower extremities by running with different shoes. *Med Sci Sports Exerc* 34: 1529–1532, 2002. doi:10.1097/00005768-200209000-00021.
35. **Wright IC, Neptune RR, van Den Bogert AJ, Nigg BM.** Passive regulation of impact forces in heel-toe running. *Clin Biomech (Bristol, Avon)* 13: 521–531, 1998. doi:10.1016/S0268-0033(98)00025-4.
36. **Zadpoor AA, Nikooyan AA.** Modeling muscle activity to study the effects of footwear on the impact forces and vibrations of the human body during running. *J Biomech* 43: 186–193, 2010. doi:10.1016/j.jbiomech.2009.09.028.